UNIVERSIDADE NOVA DE LISBOA
FACULDADE DE CIÊNCIAS E TECNOLOGIA

MARIA DO CARMO HENRIQUES LANÇA

ELECTRICAL AGEING STUDIES OF POLYMERIC INSULATION FOR POWER CABLES

(ESTUDO DO ENVELHECIMENTO ELÉCTRICO DO ISOLANTE POLIMÉRICO DE CABOS ELÉCTRICOS)

Dissertação apresentada para obtenção do Grau de Doutor em Engenharia Física – Física Aplicada pela Universidade Nova de Lisboa, Faculdade de Ciências e Tecnologia.

LISBOA
2002

To the late Dilip Das Gupta

and

À memória de minha mãe,
(In memory of my mother)
Maria da Conceição

Acknowledgements

It is not an easy task to thank all and forget none of the many that help me to do and conclude this work. There is always the danger of forgetting some. So I start by thanking those that I might have forgotten to mention and deserve to have their names here.

First, Professor Marat Mendes, my Portuguese supervisor who was always available to help me workwise, and also for his personal kindness and support in all the difficult moments.

The late Dr. Dilip Das Gupta, my British supervisor, for accepting to supervise the research work carried out at Bangor and for all the months that I stayed there. For his suggestions, ideas and keeping me on the right track and also for his personal support. Unfortunately Dilip left us before the conclusion of this thesis and he was sorely missed during the later stages of the writing.

To Professor Eugen Neagu for the many hours spend around the setup in the laboratory (for discovering what was wrong with the electrometer), for the enlightening discussions and ideas. Also for all the helpful experience of polymeric insulators, thank you.

All in my research group in Secção de Materiais Electroactivos of Departamento de Ciência dos Materiais da Faculdade de Ciências e Tecnologia da Universidade Nova de Lisboa:
Carlos Dias for the time spent helping with some experiments, and for his availability to answer any of my questions,
Professor Maria Amália Bento, Professor José Marat-Mendes, Carlos Dias, Rui Igreja and Paulo Inácio for helping to ease my teaching load.
Our secretary Dina, who brighten the days with her good mood.
Our technicians, Rui Costa and Miguel Moreira, who carried out some of the routine tasks of the electrical ageing of polymers.

I am also grateful to everybody I met in the laboratory of Professor Das Gupta in Bangor.
To Pablo Marin-Franch for teaching me my way around the labs.
To Walter Sakamoto, especially for helping me to perform the medium frequency DRS measurements with the lock-in amplifier and for keeping me in touch with the Portuguese language.
To Albert Rees with all his technical knowledge always available to give a helping hand or to find someone that could do it.
A special thanks to Claudia Castellani and Yener Altunbas for their friendship, all the encouraging words and nice dinners making me feel part of their family. And to all the others that helped me and made me feel at home. And last but not the least to my friends Teresa Marat-Mendes and Luísa Moreno.

To Dr. Paulo Scarpa, sadly deceased, for his thesis that helped me to start to understand the meaning of electrical ageing and polymeric insulation. For being always available to do some measurements and answer my many questions.

I do not want to forget the place where this work started, in Professor Robert Hill's laboratory at Kings College in London, where I had the pleasure of working with Professor Len Dissado (now at Leicester University) on the fractal nature of water trees. I am also grateful to John Alison and Leslie Askew for helping during my stay there.

I am also very grateful to Professor John Fothergill and John Houlgreave at Leicester University for lending me the first modified Cigré cells that I used for ageing. Also once more to Professor Len Dissado, Dr. Kaori Fukunaga, Alex See and Will Peasgood for the PEA measurements and discussion of results.

I would like to thank Fundação Calouste Gulbenkian for the financial support that allowed me to travel to the University of Bangor.

I am in debt to Eng. Francisco Pedroso of General Cable, CelCat, who has provided us with the polyester films for pressing and who has always been always available to sort out any problems.

Thanks are due to Borealis, which supplied LDPE and XLPE pellets for sample preparation.

Warm thanks to my friends for listening and bearing with me at all my troubled and difficult moments. Thank you to Paulo Ivo Teixeira for helping to correct the English. And especially to my friend José Esteves for all the help with Linux and availability to solve any small or big computer stuff problem.

Finally thanks to my family, my father Higino and my aunt Fernanda. Especially to those whose company I no longer share, my mother Maria da Conceição and my aunt Benilde and my uncle Manuel, with "saudades".

Resumo

Os polímeros têm sido extensivamente usados como isolantes em cabos eléctricos. O polietileno, primeiro polietileno de baixa densidade e mais recentemente na sua forma reticulada, é um dos isolantes mais comuns em cabos eléctricos de média e alta tensão. Este dieléctrico sofre de envelhecimento eléctrico sob diferentes formas, tais como arborescências de água e eléctricas e por fim ruptura dieléctrica. O último processo leva a dispendiosas falhas dos cabos eléctricos. Muitos trabalhos de investigação têm sido dedicados a este assunto e, apesar do progresso feito, os resultados são muitas vezes contraditórios e difíceis de reproduzir. Qualquer nova informação sobre este problema é um passo em frente na prevenção da falha dos cabos e na aumento do seu tempo de vida útil.

O objectivo desta tese é relacionar dois aspectos diferentes do envelhecimento eléctrico: dano localizado e mudanças nas propriedades de volume do polietileno. Para tentar alcançar este objectivo diferentes técnicas experimentais tiveram de ser usadas. O dano localisado apresenta-se sob a forma de arborescências de água (*water trees*) e canais de ruptura dieléctrica, uma vez que arborescências eléctricas (*electrical trees*) não foram observadas no decurso deste trabalho. Os métodos usados neste estudo foram FTIR, determinação da dimensão fractal de arborescências de água e estatística da ruptura dieléctrica. As modificações das propriedades eléctricas e dieléctricas de volume foram obtidas, principalmente, por DRS, FTSDC e PEA. A partir dos resultados de FTIR foi possível encontrar produtos de oxidação (sendo os principais acetonas e iões carboxilato) e quebra de cadeias. Os valores estimados para a dimensão fractal revelam como responsável o mesmo mecanismo microscópico para as arborescências de água (pelo menos para as envelhecidas a diferentes frequências e temperaturas). A estatística da ruptura dieléctrica mostra a importância do fabrico e processamento do isolante, uma vez que ruptura ocorrida durante o período inicial é maioritariamente dependente dos defeitos existentes antes do envelhecimento. A comparação entre os resultados de DRS, FTSDC e PEA revela o papel desempenhado pela carga espacial no envelhecimento para períodos mais longos. Os dois diferentes aspectos (envelhecimento localizado e em volume) são difíceis de relacionar porque o primeiro tem um caracter estocástico. Contudo a presença de carga espacial encontrada nos estudos de volume pode ser vista como um dos factores responsável pelo início da destruição localisada.

Summary

Polymers have been widely used as electrical insulators in power cables. Polyethylene, initially low density and more recently crosslinked, are one of the more commonly used insulators in medium and high voltage power cables. They suffer electrical ageing in different forms, such as water treeing, electrical treeing and finally dielectric breakdown. The last one leading to costly cable failure. Many research works have been developed on this subject despite of the progress made up to now, results are still sometimes contradictory and difficult to reproduce. Any new insight into this problem is a step further in preventing failure of the cables and increasing their useful lifetime.

The aim of this thesis was to relate ageing in two different aspects of electrical ageing: localised damage and changes in bulk properties of the polyethylene. For this different experimental techniques were used. Localised damage was water treeing and breakdown channels since no electrical trees were observed. The methods used for this study were FTIR, estimation of fractal dimension of water trees and statistics of dielectric breakdown. The changes of electric and dielectric bulk properties were accessed using mostly DRS, FTSDC and PEA. From the FTIR results it was possible to find oxidation products (mainly ketones and carboxylate ions) and chain scission. The values estimated for fractal dimension point to the same underlying microscopic mechanism for water treeing (at least for samples aged at different frequency and temperature). Breakdown statistics point to the important role of manufacture and processing of the insulator, since early breakdown is mostly dependent on defects resulting from these processes. A correlation between DRS, FTSDC and PEA shows the role played by space charge and trapping on ageing for longer times. The two different aspects (localised and bulk) are difficult to correlate because the first one has a stochastic behaviour. However the presence of space charge found in bulk studies can be regard as one of the initiator factors for localised damage.

Table of contents

List of figures

Chapter 2

Chapter 3

Chapter 6

Appendix B

List of tables

Chapter 2

Chapter 3

Chapter 4

Chapter 5

Chapter 6

Chapter 7

List of symbols and most commonly used acronyms

AC – alternating current

AFM – atomic force spectroscopy

C – capacitance

C_o – geometric capacitance

D - dielectric displacement or dielectric induction

DC – direct current

D_{cal} – calculated fractal dimension (similarity)

D_f – diffusion coefficient

D_q – generalised fractal dimension (of order q)

D_{WT} – water tree estimated fractal dimension (capacity)

D_{cal} – calculated value of the fractal dimension of a water tree image

DRS – dielectric relaxation spectroscopy

DSC – differential scanning calorimetry

E – electric field

E_a – activation energy

E_c – conduction band energy level

E_e – electron energy

E_F – Fermi energy level

E_g – band gap energy

E_L – local electric field

E_v – valence band energy level

$ESCA$ – electron spectroscopy for chemical analysis

G – conductance

F – free energy

FD – frequency domain

$FIDC$ – final isothermal discharging current

$FTIR$ – Fourier transform infrared red spectroscopy

$FTSDC$ – final thermally stimulated discharging current

G -conductance

$HDPE$ – high density polyethylene

I – current

IC – inter-cluster exchanges

ICC – isothermal charging current

IDC – isothermal discharging current

HF – high frequency

L – water tree length

ℓ - water tree length

$LDPE$ – low density polyethylene

LF – low frequency

LFD – low frequency dispersion

$MDPE$ – medium density polyethyelene

MF – medium frequency

$\overline{M}_n$ - number-average molecular weight

$\overline{M}_w$ - weight-average molecular weight

MWS – Maxwell-Wagner-Sillars

N_o – Avogadro's number

N_d – number of permanent dipoles

P – polarization

$P_F(t)$ - cumulative distribution function (probability of failure)

PD – partial discharges

PE – polyethylene

Q - charge

Q_c – charge accumulated during ICC

Q_d – charge released during total discharge

Q_{FIDC} – charge released during FIDC

Q_{FTSDC} – charge released during FTSDC

Q_{ICC} – charge accumulated during ICC

Q_{IDC} – charge released during IDC

QDC – quasi-DC

R - resistance

RT – room temperature

S – entropy

$SALS$ – small angle light scattering

$S(L)$ - total damage in a water tree

SEM – scanning electronic microscopy

SCLC – space charge limited current

T – temperature

T_i – charging temperature in isothermal current measurements and initial temperature in thermally stimulated measurements

TD – time domain

TFL – trap filled limit

T_g – glass transition temperature

T_m – melting transition temperature

T_{max} – maximum peak temperature for thermally stimulated measurements

TSC – thermally stimulated charging current

TSDC – thermally stimulated discharging current

U – internal energy

V – applied voltage

V_{TFL} – trapped filled limit

V_{tr} – transition voltage between ohmic and space charge limited conduction

XLPE – crosslinked polyethylene

WLF – Williams-Landel-Ferry

Z - impedance

a – shape parameter in Weibull statistics or
distance between neighbouring potential wells

d – sample thickness

d_f – fractal dimension

d_t – fractal dimension of a water tree

e – electron charge

f – frequency

$g(t)$ - probability density function

h – Planck's constant

$\hbar = h/2\pi$

$h(t)$ - hazard function

i – current

j – current density

k_B –Boltzmann constant

m_e^* – electron's effective mass

n – carrier concentration

n_t – number of traps

p – pressure

q – charge

t – time

$\tan\delta$ - dielectric loss

x - position

Φ – dielectric response function or dielectric decay function

Ψ – dielectric relaxation function or potential decay function

α – polarisability

β – heating rate or

width at half height of a peak

β_{PF} – Poole-Frenkel coefficient

χ – susceptibility

χ_s – static susceptibility

δ - angle between the electric field and the polarization

$\delta(x)$ - delta function

ε_r – dielectric constant or relative permittivity (sometimes also represented by ε)

ε_0 – permittivity of vacuum

ε_s – static permittivity (occurs at long time or low frequency)

ε_∞ – high frequency permittivity (occurs at short time and high frequency)

ε_{rs} – static dielectric constant (occurs at long time or low frequency)

$\varepsilon_{r\infty}$ – high frequency dielectric constant (occurs at short time and high frequency)

ϕ – work function

ϕ_m – metal work function

λ – wavelength

λ_D – Debye screening length

μ – mobility

μ_d – dipole moment

ν – frequency

θ – Bragg angle for X-ray diffraction or

ratio of number of electrons in conudction band to the number of traps

ρ – resistivity or

ρ_m – density

σ – conductivity

σ_s – surface conductivity

ω – angular frequency (sometimes also simply called frequency, however its relation to f is $\omega=2\pi f$)

τ – relaxation time

τ_{eq} – equivalent relaxation time for T_m in thermally stimulated measurements

τ_W – characteristic time to breakdown

Chapter 1. Introduction

"(...) science does not progress tidily"
E. Mendonza in History of physics
The word insulator comes from the latin "insula"
suggesting that it is isolated from its surroundings(...)
L.A. Dissado & J.C. Fothergill

According to the above statement a perfect insulator will be electrically completely isolated whatever is contained inside it, allowing no current to flow. Yet the perfect insulator does not exist and the work developed here studies a tiny part of the departures from perfection of one of the best insulating polymers (also the chemically most simple known): polyethylene.
For decades insulating polymers have been widely used in power cables. Initially low density polyethylene (LDPE) and later crosslinked polyethylene (XLPE) have been the most common insulators in medium and high voltage power cables. Electrical ageing of the insulation is inevitable and may in the long run give rise to costly cable failure. Understanding the ageing related phenomena is essential to achieve better quality materials that will provide a extended life time of the cables.

This work is an attempt to regard ageing from two different points of view: the local damage (represented by water treeing and breakdown channels) and the bulk ageing (represented by a change in bulk dielectric and electrical properties). Localised damaged is accessed by means of fast Fourier infrared spectroscopy (FTIR), breakdown statistics, fractal analysis of water trees, etc. The bulk ageing was studied either by dielectric relaxation spectroscopy (DRS), thermally stimulated discharge currents (TSDC) or pulsed electroacoustic (PEA)), etc. The task of relating these two aspects is a difficult one and can only be achieved for longer ageing times since initial ageing is dominated by breakdown from manufacture and processing defects and contaminants.

Although localised damage is the responsible for insulation failure by ultimate breakdown of the polymer, the material subject to electrical (and simultaneously thermal) ageing has its bulk properties changed by the stresses under work during the course of the time they are applied. Its expected that space charge is entering and/or appearing in the polymer enhancing chemical

and mechanical stresses that end up resulting in a permanent degradation of the material even if not leading directly to dielectric breakdown. Thus electric and dielectric bulk properties will change during ageing. Pre-existing traps and/or new traps will be filled with space charge that was able to diffuse in and properties such as dielectric constant and conductivity are liable to be affected.

One of the most puzzling phenomena in electrical ageing is water treeing (localised damage). It is the result of the degradation of the polymer under the effect of an alternate electric field and aqueous salts [Steennis90, Dissado92, Ross98, Crine98]. Since the first time it was detected nearly three decades ago, much work has been published showing that many different factors seem to affect water tree inception and growth, such as: temperature, mechanical stress, type and concentration of ionic salts, applied electric field (frequency and magnitude), polymer morphology and composition, etc. Revealing the complex nature of water tree mechanisms of inception and growth, conflicting and difficult to reproduce results have been reported either for field aged or laboratory accelerated aged specimens. This shows the importance of a good characterisation of sample properties prior to and after ageing. Many experimental techniques have been used: dielectric relaxation spectroscopy analysis (DRS) [Scarpa95, Das Gupta99], thermally stimulated depolarisation currents (TSDC) [Bamji93], laser intensity modulation method (LIMM) [Wübbenhorst98], pulsed electroacoustic spectroscopy (PEA) [Ohki98], differential scanning calorimetry (DSC), Fourier transform infrared spectroscopy (FTIR), depolarisation currents, etc. Many theoretical models have been proposed but none seems to fully explain inception and growth mechanisms. Over the last few years some progress has been made into finding a suitable theoretical model [Zeller87&91, Ross92&98, Xu94]. The experimental results and models point to a complex mechanism involving electro, mechano and chemical processes. In the laboratory special accelerated ageing techniques were developed. Nevertheless when comparing field and laboratory aged specimens the dominant mechanism in the later seems to be electro-mechanical while in the former the electro-chemical seems to dominate. In order to obtain better quantitative data, different characterisation methods must be used and also it is necessary to gather information from different experimental techniques.

The material under study was polyethylene, mainly low density polyethylene (LDPE) but also cross-linked polyethylene (XLPE). However the choice of polyethylene as one of the most

common insulators is by no means without controversy, quoting Shaw and Shaw [Shaw84]: "*From a material-science viewpoint the common use of polyethylene as an experimental treeing substrate material have been a disastrous mistake. (...) Crosslinked or not, the chemical and physical state of polyethylene is perhaps the more dependent on past history (...) than any other common polymer. Polyethylene not only has a multitude of chemical variations (...) but a large portofolio of crystalline habits, organisation and orientation. (...) the modulus of polyethylene can be made to vary experimentally over two orders of magnitude by control of the orientation and crystallinity alone*". The previous sentence reveals some of the difficulties found in studying the effect of ageing on this polymer. In order to overcome this a new experimental procedure proposed by Neagu [Neagu01] for high insulating polymers was used for the first time in the study of transport and trapping of charge in polyethylene. This procedure combines usual isothermal measurements of charge and discharge currents and non-isothermal measurements (called final thermally stimulated discharge currents – FTSDC). Also takes in account the residual charge that remains trapped at the end of the isothermal step by including a final discharge (FIDC) step that discharges completely the sample before the next run takes place.

The thesis is divided into two different parts. In the first part we have tried to give the reader a general view of the state of the art that however does not intend to be a complete description of all available information.

Chapter 2 is a brief review of polymer characteristics and properties focusing on polyethylene. Polymers are classified according to different features such as: origin, response to temperature (thermoplastic and thermoset polymer, chemistry of synthesis and structure). Still related with the polymeric structure are the bonds, morphology and crystallinity (amorphous and semi-crystalline polymers) that are briefly described. The mechanical properties and relaxation processes are also discussed. In the final part of the chapter specific polyethylene characteristics are presented.

In chapter 3 transport and trapping of charges in insulating materials are treated with the last part of the chapter focusing on polyethylene (this problem is addressed in greater detail during the discussion of FTSDC results in Chapter 7). The band theory for insulating polymers is introduced. A description of the existing theories for transport and conduction is given (carrier type, high and low field mechanisms are presented). Next transient and steady state currents and their relevance to identify some transport and trapping mechanisms are summarised. And as stated above the chapter ends by focusing on polyethylene.

For Chapter 4 the problem of dielectric relaxation is dealt in particularly with application to polyethylene. The dielectric response is presented in the time and frequency domains. Empirical models starting with Debye model are treated. The effect of temperature on the dielectric relaxation spectra is focused and the importance of dielectric data presentation in order to identify mechanism is reviewed. The main classes of dielectric solid materials according to their dielectric response are presented. Next physical models to explain the different observed behaviour are dealt with (especially Jonscher's universal law and Dissado-Hill cluster model). The relation between data from non-isothermal currents (TSDC) and dielectric relaxation spectrum is made. Finally published results of dielectric relaxation spectra of polyethylene are discussed.

As for Chapter 5 electrical ageing is presented with main attention on water treeing and a brief review on electrical treeing and dielectric breakdown. A space charge model for electrothermal ageing that allows lifetime estimation is presented.

The second part of this thesis begins with Chapter 6 and 7 where the experimental procedures followed and the results obtained during this research are presented.

Sample preparation and ageing and the different techniques used to characterise the unaged and (electrical and thermally) aged specimens are described in Chapter 6. Preparation of samples was made from pellets by hot pressing and disc-shaped specimens were obtained. These samples were submitted to different ageing conditions being always under planar electrode geometry where the electrodes were the solution of NaCl. Samples suffered electrical plus thermal ageing (also called AC or electrical ageing) at different temperatures and for different time periods (the applied AC field was mainly at 50 Hz with an amplitude of 6 kV/mm) or just thermal ageing (also called no-AC or thermal ageing)

In Chapter 7 the results of the measurements made are presented and discussed. The characterisation of unaged samples was made using microscopy (optical, SEM, AFM), DSC, surface potential measurements and X-ray diffraction. Comparison between unaged and aged samples (AC and no-AC ageing) was made by dielectric relaxation spectroscopy in the frequency range of 10^{-5} Hz to 10^{5} Hz. To cover this broad range three different measurements techniques were used: in the low frequency range (LF) – 10^{-5} Hz to 10^{-1} Hz – time domain measurements were performed; for the medium frequency range (MF) – 10^{-1} Hz to 10^{2} Hz – measurements were performed using a lock-in amplifier and in the high frequency range (HF) – 10^{2} Hz to 10^{5} Hz – a RLC General Radio Bridge 1621 was used. Isothermal charge and discharge currents and the non-isothermal discharge currents (FTSDC) allowed mainly to

distinguish some differences between electrical plus thermal ageing and just thermal ageing since unaged samples were difficult to analyse. The PEA technique helped to obtained the space charge profile of the samples (unaged, AC and no-AC aged samples). Some of the samples showing water trees were dyed with methylene blue and used (together with some other samples from other authors) to estimate the fractal dimension of water trees. The chemical changes were studied by FTIR and some evidence of oxidation was found for aged samples. A breakdown statistics using the two-parameter Weibull function was made.

Finally in Chapter 8 some possible conclusions are made. Two different mechanisms seem to be playing a major role in the ageing process of the samples studied in this work: diffusion and oxidation. Some suggestions for further work are also presented.

Chapter 2. Polyethylene: polymer properties

Polymer: from the Greek "many-membered"

In this chapter a brief review of polymer characteristics is presented. Special emphasis will be given to an electrical insulator polymeric material named polyethylene (PE) that also has many other applications. Electrical and dielectric properties will be discussed in greater detail in subsequent chapters.

2.1 Polymers

In the 1920s H. Staudinger[1] proposed the *"macromolecular hypothesis"* giving rise to one of the most important type of materials now used in everyday life and also in industry.

Strictly speaking, a polymer is any large molecule (long chain macromolecule) composed of any number of smaller units (the *"mers"* or monomers). According to this definition any ionic crystal, such as NaCl, could be a polymer. Yet this name is restricted to materials where monomers are linked by covalent bonds. A few examples of this kind of bonds are [Rosen93]:

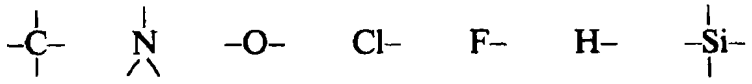

(see also Table 3.1).

The name of the polymer is usually the name of the composing monomer plus the prefix *poly*. Polyethylene is the polymer resulting from the monomer ethylene (polyethene is the ICI trade name for PE):

ethylene polyethylene

The long chain structure of the macromolecules gives the polymers distinct and variable properties. The degree of polymerisation, n (also called chain length and representing the number of units in the macromolecule), is in the range 10^3-10^5 granting also high average molecular weight. In a polymer there is a distribution of molecular weights and only an average molecular weight can be define, for instance the number-average molecular weight is:

---

[1] Nobel prize's winner in 1953 for his pioneer work on polymers.

$$\overline{M}_n = \frac{\sum M_x n_x}{N}, \tag{2.1}$$

and the weight-average molecular weight is:

$$\overline{M}_w = \frac{\sum w_x M_x}{\sum w_x}, \tag{2.2}$$

n_x is the number of moles of the x-mer with molecular weight M_x, $w_x = n_x M_x$ is the total weight of the x-mer and $N = \sum n_x$ the total number of moles in the sample.

The length of the main chain can exceed 1 μm. Flexibility and interaction of the chains together with polar group interactions (dipoles) define the mechanical and electrical properties of polymers. Many physical properties show a change at a critical (average weight) number of chain atoms around 1000. Practically all polymers are good electrical insulators[2] because they have large band gaps (see 3.2), low dielectric constant and dielectric loss in a wide range of frequencies (see 4.8). Combining the good insulator characteristics and mechanical properties, polymers are ideal to be used as insulating material in electrical appliances, such as power cables.

2.1.1 Types of polymers

Polymers can be classified according to different criteria and a brief summary is given.

a) Origin

Natural – some polymers are produced by nature, examples are natural rubber, nucleic acids and cellulose.

Natural modified – natural polymers that have been modified in order to improve their properties for human use, such as vulcanised rubber and derived cellulose.

Synthetic – Completely artificially produced, one of the simplest is polyethylene.

b) Response to temperature

Thermoplastics – Some polymers soften when heated. If a mechanical stress is applied they will flow. After cooling their characteristics are reversibly recovered.

Thermosets – These polymers become soft on heating. However when cooled the process is not reversible and the initial characteristics are not recovered.

[2] Conducting polymers are a more recent field of application for polymers. They are specially developed to become conductors.

c) Chemistry of synthesis

Addition or chain reaction– In addition polymerisation the monomer molecules are added to the polymer chains. The unit molecule is not broken and the polymer has the same chemical formula as the monomer. The reaction involves the opening of a double bond.

Vinyl monomers (where C=C is present) produce vinyl polymers by addition reaction. Polyethylene (also a hydrocarbon polymer since it is made only of C and H atoms) is one of such kind:

$$n\ CH_2{=}\ CH_2 \longrightarrow (—CH_2—CH_2—)_n.$$

Other vinyl monomers are propylene and vinyl chloride which give rise to polypropylene and poly(vinyl chloride), respectively.

Polyether is another polymer formed by addition but this time from an opening-ring reaction. The ethylene oxide ring opens to originate polyether, which contains carbon and oxygen atoms in its backbone.

Condensation or step reaction – Polymers are formed from an organic condensation reaction where a small molecule (usually water) is also produced. Intervening monomers are multifunctional (have more than one reactive group per molecule). Polyester and polyamide (nylon-6,6) are polymers obtained in such a way.

d) Structure

Linear – The chain molecules are strictly linear. High density polyethylene (HDPE) is a polymer prepared specially to have almost linear chains (1 to 5 CH_3 branches per 1000 carbon atoms).

Branched – Main chains exhibit ramifications that can appear during polymerisation. In polyethylene branching can occur when a hydrogen atom from a monomer or from a polymer molecule is transferred to a growing chain radical. Vinyl polymers in general contain one branch for every 10^4 monomer units in the chain (they are essentially linear). Low-density polyethylene (LDPE) has 15 to 30 CH_3 per 1000 carbon atoms. *Short* branches are several units long while *long* branches can be as long as the main chain. Branching can have a large effect on polymer properties. It lowers density and crystallinity (compare LDPE and HDPE in Table 2.3) and increases the number of weak points in the chains.

Crosslinked – Long polymeric chains can extend until they cross with other chains. When all chains are interconnected in three dimensions a network polymer appears. In a crosslinked polymer the molecular weight (average weight of the main chain in a polymer) becomes very

large and the material is a thermoset. Some properties change, for instance, they are less crystalline and their Young modulus is proportional to the degree of crosslinking (fraction of covalent bonds that participate in crosslinking) [Dissado92].

Crosslinking can arise in two ways. One possibility is during polymer manufacture if tri- or higher order functional monomers are used. The other is by chemical reactions in existing macromolecules (curing). This can be achieved by adding a catalyst (usually a peroxide), using radiation or a chemical hardener.

For example, XLPE (cross-linked polyethylene) is obtained during extrusion of polyethylene by adding a catalyst to the initial mixture, the more often used are dicumyl peroxide (described in more detail below) and silane.

If the polymer consists of one kind of monomers they are called homopolymers. Heteropolymers can be made of more than one type of monomers. If two different monomers are present they are called copolymers (if three different monomers are present they are named terpolymers).

Copolymers are classified according to the way monomers are distributed in the chains. A copolymer with monomers A and B distributed in a random fashion along the backbone is called random copolymers.

ABAABABBBAAB

Block copolymers have continuous blocks of the same unit.

AAAABBBBBAAAABBBBBAAAA

Both examples show linear polymers, a graft copolymer has always branched chains:

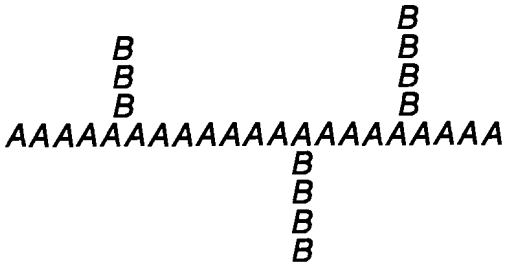

2.1.2 Bonds and structure

In a polymer the atoms are kept together by different kinds of bonding. The main type is the *covalent bond* (sharing of electrons between the atoms) that joins the atoms in the polymeric chain. Secondary interactions (bonds) are:

hydrogen bonds due to a dipolar moment between hydrogen and oxygen –also chlorine and fluorine- atoms from different molecules;

dipole interactions arise when dipole moments appear between atoms with an unequal share of electrons (a hydrogen bond is a stronger dipolar interaction where the dipolar moment is higher);

ionic interactions between ions and

van der Waals resulting from temporary dipoles created by uneven distributions of charges in non polar atoms, for instance between carbon atoms belonging to different macromolecules.

In Table 2.1 [Rosen93] typical values characteristic of these bonds can be seen.

Table 2.1 –Bond parameters [Rosen93]

Bond type	Interatomic distance (nm)	Dissociation energy (eV)
Primary covalent	0.1-0.2	50-200
Hydrogen bond	0.2-0.3	3-7
Dipole interaction	0.2-0.3	1.5-3
Van der Waals	0.3-0.5	0.5-2
Ionic	0.2-0.3	10-20

As concerns the spatial arrangement one should distinguish between configurations (only by bond breaking it is possible to change the configuration) and conformation (different conformations correspond to rotation of atoms around single bonds). The geometric distribution of the atoms in the macromolecule (or any molecule) is such that it minimises the energy. In polyethylene the chain is arranged in a zigzag fashion with the carbon atoms in the backbone and the hydrogen atoms on either side corresponding to a trans conformation. In other vinyl polymers with more than one kind of different substituent groups attached to the backbone the spatial arrangement can be classified according to the way these groups are distributed (tacticity or stereoregularity). There are different stereoisomers: isotatic (identical atoms or groups are on the some side of the chain); syndiotactic (different atoms or groups alternate along the plane of the chain) and atatic (if the different atoms or groups are randomly distributed). Stereoregularity tends to increase crystallinity.

2.1.3 Morphology and crystallinity

The presence of very long molecular chains makes it more difficult to achieve the conditions for a 100% crystalline material. The regularity of the chain is very important to the ability to

form crystals. Linear molecules are much easier to align and arrange spatially in a regular manner. In the example referred in 2.1.2 isotactic vinyl polymers are more likely to be crystalline than atactic polymers. Branching and crosslinking are also factors that decrease crystallinity. Long side groups appearing on the backbone make the packing of the macromolecules more difficult. Also the intermolecular forces have to be strong enough to overcome thermal disorder. There are completely amorphous polymers but a completely crystalline one has never been produced. In wholly amorphous polymers the chains are arranged in a random manner presenting a "ball-like" shape. As a material in the glass phase they look transparent. A fully crystalline polymer is much more difficult to obtain but nowadays polymers with almost 100% crystallinity have been made[3]. If it existed it would look completely opaque. The majority of polymers are semicrystalline and usually look milky. The polymer is composed of small crystalline regions (crystallites) and amorphous regions.

Crystalline regions may be formed from sheets, long fibres or superstructures. A first model developed was the *fringed micelle model.* However thermodynamically this model is unlikely to happen on a large scale. This together with new experimental evidence has led to the development of the *lamellae model.* Most of the polymeric materials will have crystalline regions were the long chains are folded to form sheets which are called lamellae. These look like small ribbons. Typically their dimensions are of 10 μm wide, 1 μm long and 10 nm thick. The chains can fold and reenter the lamella in a regular or irregular (switchboard) manner or can cross from lamella to lamella or even end in the amorphous region in between (see Figure 2.1). During primary crystallisation twisted lamellae grow from nuclei in a star-like fashion forming larger structures known as spherulites (Figure 2.2). They show a Maltese cross pattern when viewed under polarised light (see photograph of PE in Figure 2.5). Usually their radius is around 10 μm but can be large enough to be seen to the naked eye. They are space filling polyhedra and between the twisted lamellae there exists amorphous material and other lamellae resulting from secondary crystallisation.

[3] Compared with a metal were the defect concentration is on the order of ppm, it is not possible to have a totally crystalline polymer where the defect concentration is at least around 1%.

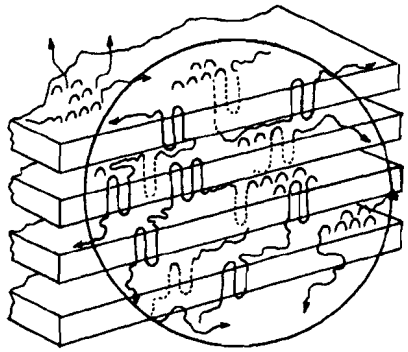

Figure 2.1 – Several lamellae showing alignment, folding and reentering of chains with the amorphous region in between [Bartnikas83].

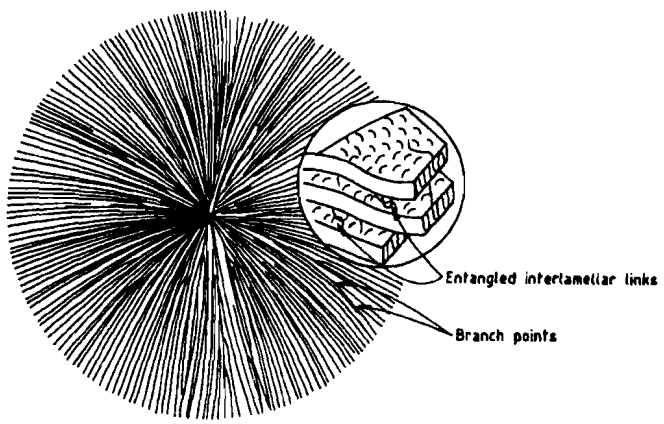

Figure 2.2 – Spherulite grown from a nucleus with many lamellae (like a sea urchin) [Dissado92].

The degree of crystallinity (% of crystalline volume or mass present in polymer) is usually between 5-50% [Blythe79]. It depends on thermo-mechanical history, branching and crosslinking, stereoregularity and copolymerisation. If a melted material is rapidly cooled or quenched it will have insufficient time to form the crystallites and will be less crystalline then a slowly cooled similar melt. If a polymer is stretched the chains will tend to align and the degree of crystallinity will increase.

Crystallinity greatly influences the polymer properties specially the mechanical properties. Density for instance can be considered a good measure of the degree of crystallinity. A denser polymer is more crystalline. Since in crystalline regions the molecules are more closely packed, crystallinity tends to increase strength and rigidity. Also electrical and optical properties can be modified. It has already been stated that a totally amorphous polymer is transparent, a semi-crystalline one looks milky and one almost entirely crystalline is opaque (opaque character can also be due to the introduction of a new phase, such as a filler). Table

2.3 illustrates property changes for different types of polyethylene (including degree of crystallinity).

Some experimental techniques to characterise the crystalline content of a polymer are density measurements (as stated before), infrared and Raman spectroscopy, differential scanning calorimetry (DSC), X-ray diffraction and small angle light scattering (SALS). For morphology studies several microscopy techniques have been used: optical, scanning electron microscopy (SEM), transmission electron microscopy (TEM), atomic force microscopy (AFM), etc.

2.1.4 Mechanical properties

These properties are mostly determined by density and in turn molecular length and number and length of side chains determine density. Many polymer applications use their unique mechanical properties (elasticity, viscosity, etc.). The rheological[4] behaviour of polymers is difficult to explain and unusual when compared with other types of materials. It is also strongly dependent on temperature and time of the applied stress. As an example, the Hooke´s law of elasticity is often not verified (only for small stresses it is verified). When a yield point is reached slippage of chain results in an incomplete recovery. Finally at the ultimate stress fracture occurs. Some values for PE can be seen in Table 2.3. Different types of rheological behaviour are:

a) Viscous flow – associated with irreversible slippage of molecular chains;

b) Rubberlike elasticity – the material shows a complete recovery after mechanical deformation (rapid molecular movements are occurring);

c) Viscoelasticity – the material has an elastic behaviour because it is able to recover from the mechanical deformation but it shows the deformation is dependent on the time the stress is applied so that it also shows creeps;

d) Hookean elasticity – the stress and the strain show a linear relationship (related to bond stretching and rotation).

Polymers are viscoelastic materials.

Two simple phenomenological models have been used to explain creep and relaxation behaviour based on coupling elastic springs and viscous damping. The Maxwell model is based on springs and damping cylinders in series while the Kelvin-Voigt model uses a parallel

[4] Rheology is the study of deformation and flow in materials.

configuration of the same elements. Molecular theories try to explain this kind of behaviour on the basis of the molecular structure of polymers.

The factors affecting mechanical properties are:

i) Interaction between the macromolecules;

ii) Flexibility of chains – with associated molecular motions (motion of branch points, rotation of side groups, crankshaft motion, segmental motion and motion of crystallite features);

iii) Spacing of polar groups.

2.1.5 Relaxation processes in polymers

Besides the first order melting transition it is well know that polymers exhibit other transitions. They are usually visible both in the mechanical and the dielectric relaxation spectra of polymers (see Figure 7.7, a DSC spectrum of the LDPE samples prepared during this work). Some of the relaxations appearing in the mechanical spectra will not show up in the dielectric spectra if no dipoles are associated with that particular mechanism. Mechanisms for the same transition can be different according to their mechanical or dielectric character. For an isochronal plot (constant frequency) transitions are classified from the highest temperature to the lowest using the Greek alphabet letters α, β, γ and δ, etc. (see Figure 2.3). In Table 2.2 a more complete labelling of the relaxation processes is presented. The polymer can show just some of these transitions and not all of them depending, for instance on the degree of crystallinity. NMR studies have also proved to be very helpful for understanding the underlying physical mechanisms causing each relaxation.

Table 2.2 – Relaxation peaks notation [adpated from Boyd85a]

Number of processes	T_{max} ⟵ **(isochronal)** ⟵ T_{min}			
3 (semicrystalline)	α (α_c)	β (α_a)	γ	δ
2 (amorphous)		α (α_a)	β	γ

An important second order transition happens when the polymer behaviour changes from glass to rubber and is called glass transition at temperature T_g (a second-order transition). For semicrystalline polymers it is associated with the β process (also labelled α_a – *a* for amorphous - and α can also be called α_c – *c* for crystalline). In amorphous polymers it is

related to the α transition (the one occurring at higher temperature[5]). This kind of transition is also studied by measuring the changes in some thermodynamic properties with temperature, such as density, heat capacity, etc. Density measurements have revealed that below T_g a temperature change will not change the density while above T_g an increase in temperature will decrease the density. Below T_g there is motion of individual atoms and small groups of atoms, no large-scale cooperative motion exist. Above T_g the motions become of the liquid type.

In low crystalline polymers (amorphous) the α (α_a) transition is well defined. This feature is typical of the glass transition, which is a cooperative phenomenon corresponding to micro-brownian motion of the chains. It can be associated with a kind of crankshaft motion where the tails of the chains remain in the same position. Also it was described as damped diffusion of conformational changes along the chains [Schönhals97]. It is expected that both intermolecular and intramolecular interactions will contribute. The β relaxation it is not yet well understood. It can be related to fluctuations of localised parts of the main chain or to rotational fluctuations of the side groups or parts of them.

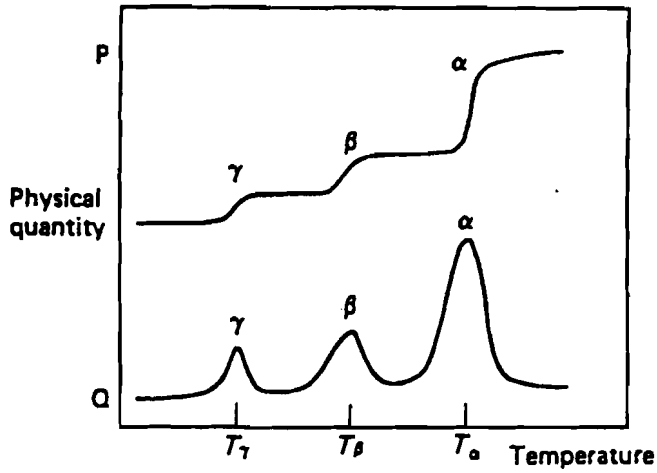

Figure 2.3 – Schematic diagram of phase transitions in semicrystalline polymers. It can be applied to both dielectric and mechanical spectra [Hall89]. For instance, P and Q can be, respectively, the real and imaginary components of the permittivity (dielectric measurements) or of the shear compliance (mechanical measurements).

For semicrystalline polymers, according to [Hedvig77] and [Boyd97] the α transition occurs in the crystalline regions of the polymer while the β transition occurs in the amorphous region. The γ peak is also associated with the amorphous region and is assumed to be a kind

[5] The higher temperature α transition of semicrystalline polymers disappears in amorphous ones. The first one showing up is in reality correspondent to the β (or α_a) transitions observed in semi-crystalline polymers.

of local crankshaft mechanism, in the main chain [Hedvig77] or more probably a kink followed by a crankshaft rotation [Boyd85b and Das Gupta94]. It possesses the properties of a sub-glass relaxation.

A discussion of the glass transition for polyethylene is given below (2.2.4).

2.2 Polyethylene

Polyethylene has previously been used as a good example to illustrate some of the characteristic properties of polymers. It was first produced by accident at ICI (Imperial Chemical Industry, ltd., England). As stated above polyethylene is obtained from ethylene by addition polymerisation. It belongs to the hydrocarbon and vinyl polymers. Also different types of PE have been mentioned. Table 2.3 shows the major characteristics of some of these. They differ mainly in the degree of branching and crosslinking, which change some of their properties. XLPE used nowadays as medium and high voltage power cable insulator and LDPE (low density, side-branched, free radical or high pressure polyethylene) will be discussed in detail. MDPE (medium density polyethylene) and HDPE (high density, linear or low pressure polyethylene) are also used for cables but, due to their cost, less often.

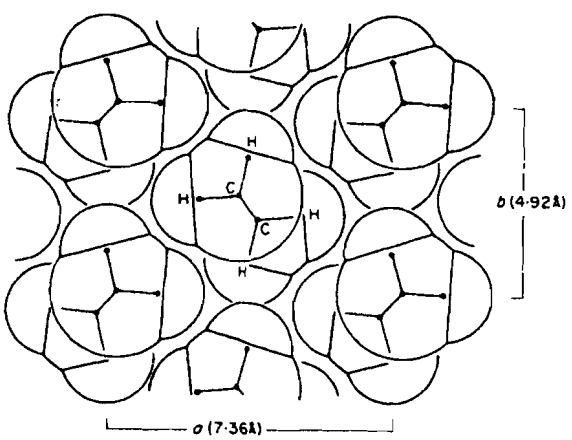

Figure 2.4 – Schematic representation of the unit cell of crystalline polyethylene at 20°C [McCrum67]. The c-axis is perpendicular to the plane.

2.2.1 General properties

Polyethylene has long macromolecules $(CH_2–CH_2)_n$ with methyl groups $–CH_3$ or vinyl groups $(CH=CH_2)$ as chain's ends. The PE macromolecule assumes a trans zigzag shape that has the lowest energy configuration. The typical length of C–C single bonds is 1.54 Å and the C–C–C angle is 109.5° (the tetrahedral bond angle). In the crystalline phase the molecules assume extended or helical conformation and lie parallel to each other. X-ray diffraction

measurements found that at 20 °C the unit cell is orthorhombic with dimensions 7.36 Å × 4.92 Å × 2.54 Å with a volume of 9.2×10^{-29} m^3 [Dissado92]. The unit cell contains two monomers with relative molecular mass of 56.1 (Figure 2.4). This results in a specific volume of 0.987×10^{-3} m^3kg^{-1} for the crystalline regions.

As was stated earlier the chains are grouped into crystalline lamellae whose dimension are dependent on the manufacture conditions (typical values are mentioned in 2.1.3). The c-axis of the orthorhombic cell will be perpendicular to the plane of the lamellae. The lamellae will group into spherulites of sizes ≈3 to ≈700 μm. Figure 2.5 shows a polarised light microphotography of press-moulded low density polyethylene (pressed in our laboratory).

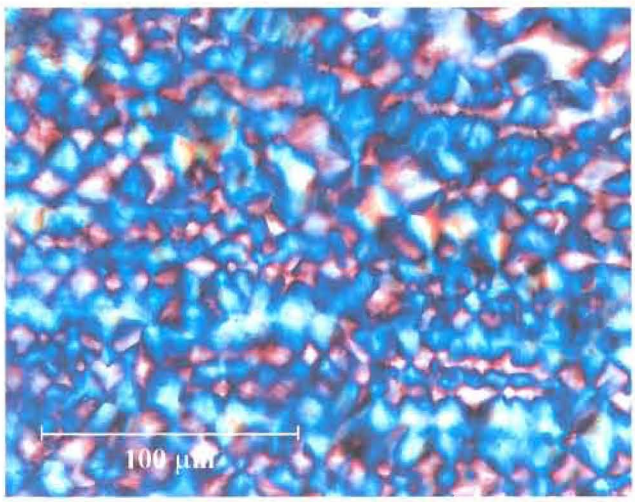

Figure 2.5– Optical microphotography obtained with reflected polarised light of microtomed low density polyethylene (the characteristic Maltese cross pattern of the spherulites is visible).

2.2.2 LDPE and XLPE

Low density polyethylene is a thermoplastic while XLPE is a thermoset (due to crosslinking). The operational temperature of the former is 70°C while for the later it has been increased to 90°C.

a) LDPE can be polymerised at pressures of 1000 to 3000 atm and temperatures as high as 250 °C. Traces of oxygen, peroxides (benzoyl, diethyl), hydroperoxides and azo compounds are used as initiators and benzene and chlorobenzene as solvents. Water or other liquids can be added to absorb the heat of reaction. LDPE is very inert chemically and it does not dissolve in any solvent at room temperature but at higher temperatures can be dissolved, e. g., by benzene and carbon tetrachloride. Also has a good resistance to acids and alkalis.

The physical properties depend greatly on molecular weight, long and short side-branching. Short-chain branching affects the degree of crystallinity and consequently the density

(implying that properties such as stiffness, tear strength, hardness, chemical resistance, yield point will increase with decreasing number of short branches while toughness and permeability, for instance, will decrease). Long-chains will change, per example, tensile and impact strength, resistance to environmental stress cracking.

Table 2.3 – Some properties of different forms of polyethylene
(Data from [Bilmeyer84, Das Gupta94, Goodfellow00, Rosen93 and Steennis90])

PE	LDPE	MDPE	HDPE	XLPE
Density (g/cm^3)	0.91-0.94	0.926-0.94	0.95-0.97	0.92
Average molecular length	1500-1530		7000-14000	
Number of side chains (per 1000 chain atoms)	20-40	5-15	1-5	———
Length of side chains (number of atoms)	2-5		<4	
Crystallinity(%)	42-55	54-63	64-90	
Crystalline melting point(^oC)	110-120	120-130	135	120
Glass transition (^oC)	0			-35
Mechanical properties				
Hardness-Rockwell (D shore)	41-46	50-60	60-70	
Young modulus(MPa)	200-400	170-380	600-1500	100
Yield strength (MPa)	10-20	10-25	25-50	20
Ultimate strength(MPa)	15-25		25-55	
Elongation to fracture (%)	400-700		100-600	
Flexural modulus (MPa)	34-410	410-800	700-1800	
Thermal properties				
Thermal conductivity (W/K-m)	0.33	0.4	0.45-0.52	0.3
Linear thermal expansion coefficient (10^{-6} K)	320		100-200	320

Table 2.3 – Some properties of different of different forms of polyethylene

(continued from previous page)

PE	LDPE	MDPE	HDPE	XLPE
Electric and dielectric properties				
Dielectric constant (1 MHz)	2.2-2.35	2.25-2.35*	2.3-2.4	2.4
tan δ at 1 MHz (10^{-4})	2	2*	10	10
Dielectric strength (kV/mm)	75		100	50
Volume resistivity (Ωcm)	10^{15}-10^{18}	10^{15}-10^{18}	10^{15}-10^{18}	10^{16}
Surface resistivity (Ωcm^{-1})	10^{13}		10^{13}	
Optical properties				
Refractive index	1.51	1.52	1.54	
Transmittance (%)	4-50	4-50	10-50	

*measured at 1 kHz

b) XLPE

Crosslinking is usually obtained by adding a catalyst, e.g. dicumyl peroxide. In cable manufacture the crosslinking agent is added to the polymer compound and after extrusion the application of high temperature and pressure will initiate the reaction. Usually the peroxide will generate two free radicals that will in turn originate acetophenone and methyl radicals. The former removes hydrogen from the polyethylene chain and produces methane and carbon radicals. These radicals will give rise to radicals in the polymer chain and cumyl alcohol. Finally the carbon radicals from different chains will react resulting in crosslinking. Sometimes steam is used at temperatures of 200 to 220 °C, this is called steam curing. This technique creates many voids and is being replaced gradually by dry curing which uses hot hydrogen. Cooling can be performed either using water (dry-curing wet-cooling) or gas (dry-curing dry-cooling). Two of the more important residual products are acetophenone and cumyl alcohol (that will diffuse out with time with diffusion rate depending on temperature gradient and barriers). Another crosslinking process uses silane where the amount of by-products is much smaller. See Table 2.4 for a comparison of the curing processes.

2.2.3 Voids, cavities and water in unaged polyethylene

Following Steennis definition [Steennis90], voids are filled with gases and cavities with liquids and/or solids. During manufacture of either LDPE or XLPE films or even power cables amorphous regions will gather water, impurities and residual products (such as crosslinking products for XLPE) or added products to increase the lifetime of the cable (antioxidants or tree retardants). Polar substances (e.g. water) can cluster in the voids creating cavities if supersaturation occurs. In XLPE the size of smaller voids and cavities is of the order of interlamellar regions. Largest voids are around 10 μm, however voids as large as 500 μm have been detected. Most of the voids will be filled with water or gases if steam-curing is used. On the other hand there are also microvoids (typically in the range 10 to 100 nm)[6] that together with voids will increase the specific volume. Because of molecular motion due to thermal fluctuations in the nanometer range (<3 nm) it is possible that there is space continuously appearing and disappearing.

Like many polymers polyethylene is considered hydrophobic yet some water will always be found. Some localised oxidation together with the presence of defects and impurities can result in water absorption. XLPE at 20 °C absorbs less than 100 ppm [Steennis90]. The water can accumulate in existing microvoids or newly produced voids.

Table 2.4 – XLPE void characteristics for different curing methods [Steennis90]

Curing method	**Void concentration (number/mm^3)**	**Maximum void size (μm)**	**Void volume/ PE volume (%)**
Steam	10^5-10^6	30	0.7 – 7
Dry	10^3-6.10^4	15	0.0007 – 0.4
Silane (one-shot)	≈10^4	15	≈0.07
Uncured	≈10^5	13	≈0.005

[6] Dissado&Fotthergill [Dissado92] raise the question *"when do microvoids become voids?"*.

2.2.4 Relaxation processes in polyethylene

Both the mechanical and dielectric spectra of LDPE exhibit α, β and γ relaxations in similar temperature and frequency range. The dielectric loss peaks are attributed to small concentration of residual carbonyl groups attached to the backbone chain. The mechanical spectra can be seen in Figure 2.6. It is worthwhile to refer that the peak position does not seem to change significantly for the different types of PE. In Chapter 4 (4.10), dielectric spectrum and the corresponding transitions will be discussed in greater detail. Here the possible mechanisms involved in each relaxation process will be briefly presented.

The α transition appears at temperatures above room temperature (as can be seen in Figure 2.6, at 1 Hz is around 50 °C). The dielectric α process is associated with the crystalline part of polyethylene and the mechanical one is transferred to the amorphous region but it requires the presence of a crystal fraction. This peak is only detected when the X-ray diffraction pattern shows sharp lines (which are identified with the crystallographic planes of the orthorhombic cell) and also higher peaks for increased crystallinity. The peak temperature is dependent on the method of crystallisation, the thermal history of the sample and on side-branch concentration. In [Boyd85b] the α transition is explained as a relaxation of the amorphous part due to translational mobility in the crystalline part.

Near 0 °C the β peak appears. It is more intense the higher the amorphous percentage. Also peak height is dependent on side branching and could be a relaxation of part of the molecule containing side branches. Temperature does not affect the peak because since the side-branches content is low and they will move independently of each other. From thermally stimulated depolarisation current measurements a split of β in two different peaks has been observed. According to Hedvig (see [Hedvig77] and 4.10) polyethylene possesses two different amorphous phases.

A γ peak appears circa –120 °C. Its magnitude depends only on density but their temperature and shape do not vary. It is associated to a local motion maybe followed by local crankshaft motion.

Activation energies calculated from isochronal spectra at different temperatures found in the literature are presented in Table 2.5.

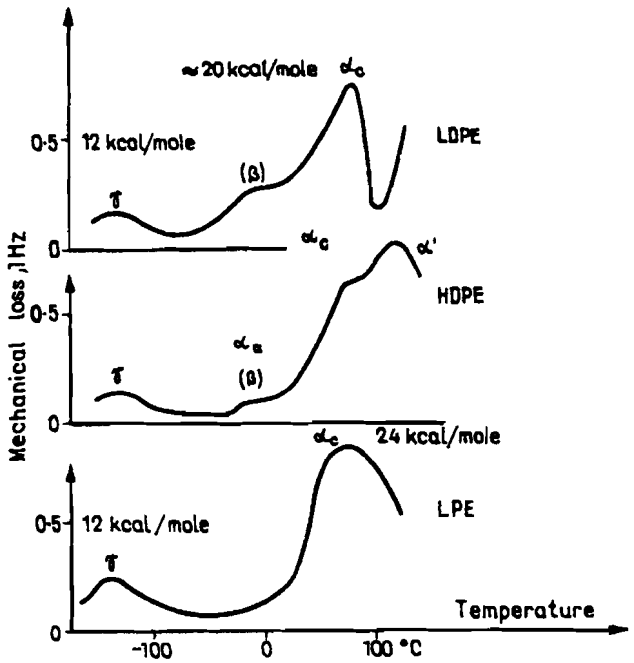

Figure 2.6 – Mechanical spectra measured at 1 Hz for LDPE, HDPE and LPE (linear polyethylene[7]), after [Hedvig77]. The activation energies in kcal/mol are shown for the three peaks.

Table 2.5 – Activation energies (kcal/mol) after [McCrum67].

Process	Dielectric	Mechanical
α	28	25
β (from different authors)	16-38	16-38
γ	11	11-15

Finding the glass transition in polyethylene has given rise to many discussions. In their book McCrum et. al [McCrum67] ended the discussion about T_g with this statement: "*It is by no means certain that the assignment of a T_g in polyethylene is a meaningful activity*".

More recently, β (α_a) has been recognised as the glass transition [Boyd85a, 85b and 97] which seem to agree too with some of the initial arguments. In [McCrum67] such arguments place T_g in the regions just below 0 °C and include a specific volume change with temperature

[7] LPE is prepared with the Phillips catalyst and has a high density of 0.96g/cm^3, high crystalline content (97%), very few side branches (<1 per 1000 carbon atoms) and melting point of 140 °C.

(a knee is seen), the empirical rule gives $0.5 < \frac{T_g}{T_m} < 0.67$ which for T_m = 115 °C leads to $-80^o C < T_g < -10^o C$ and are all in agreement with the choice of β as the glass transition.

Chapter 3. Charge transport and trapping mechanisms in insulators

The low conductivity of PE arises from extremely low carrier mobility and a paucity of carriers which may become localised within the structure

D.K. Das Gupta

3.1 Introduction

To obtain good insulators it is essential to be able to understand the mechanisms of charge transport and trapping in these materials. This includes identifying the type and origin of the charge carriers and to know their concentrations and mobilities. This task is not an easy one and in spite of the progress made it is still far from a satisfactory outcome.

According to the material (superconductor, conductor, semiconductor or insulator), electrical conductivity is a property for which one of the largest variation in magnitude is found, as can be observed in Figure 3.1 – (a). The best-known polymeric insulators are polyethylene (PE), polystyrene (PS), polyethylene terephtalate (PET or polyester) and polytetrafluoroethylene (PTFE or teflon) and fall at the low-conductivity end.

The conductivity depends on the type of the carrier (characterised by its charge, $q_i(E,T,A,X)$, mobility μ_i (E,T,A,X) and concentration $n_i(E,T,A,X)$):

$$\sigma = \sum_i \sigma_i = \sum_i \left| n_i q_i \mu_i \right| \tag{3.1}$$

where E is the electric field, T is the temperature, A are the environmental conditions and X indicates the direction [Das Gupta97].

The carrier types are electrons, holes, ions and polarons[8] but usually one carrier dominates. The large span of conductivities can only result from changes in mobility or concentration. In Figure 3.1 – (b) the chart of mobilities for different materials shows a much smaller variation than the one found for the conductivity (Figure 3.1 – (a)). The concentration of carriers is able to vary from nearly zero to more than one per atom (~10^{29} m^{-3}) as can be deduced from the band theory [Dissado92]. Consequently concentration ends up to be the main responsible for the wide spread of the conductivity range.

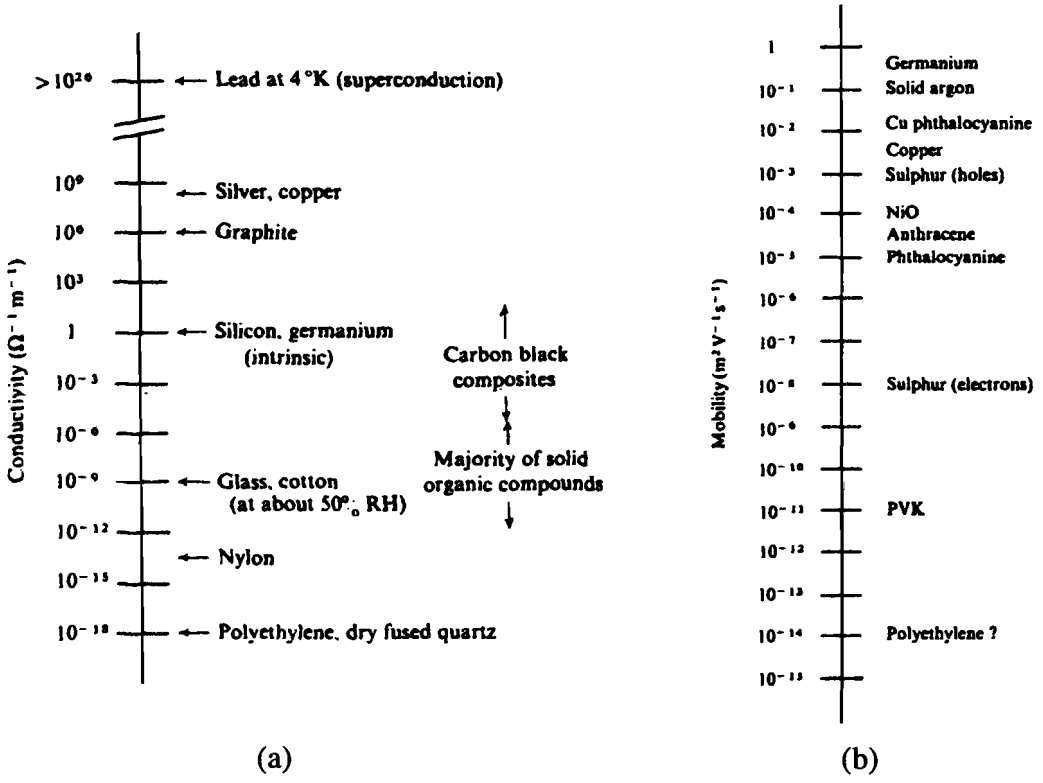

Figure 3.1 – Chart of typical conductivities (a) and mobilities (b) [Blythe79].

The currents measured for high insulators are very small but can help to identify the mechanism of carrier transport. Remarkably difficult is to identify the type of carriers and traps [Wintle99]. Important can be the type of interfaces (injection and blocking at electrodes) and trapping and detrapping parameters (energy and detrapping times). Contributing to conductivity are intrinsic properties of the materials but a relevant role can be played by the concentration and nature of defects (structural and chemical). In very good insulators impurities are often the origin of carriers and traps, resulting in low mobilities and concentrations. For instance the low conductivity of polyethylene is a consequence of the low mobility and concentration of carriers that can remain trapped for long times (accordingly with the quotation at the beginning of this chapter).

3.2 Band theory

Isolated atoms and small molecules have well defined energy levels for the electrons known as orbitals. When a large number of atoms interact, such as in condensed matter, a much more complex structure arises and the energy levels can be so close together that they overlap

[8] A polaron is a charge surrounded by a polarised region (from a distortion caused by the presence of the charge itself).The transport of the carrier must be accompanied by the transport of the polarisation.

forming bands. There are some energy levels that are not allowed and give rise to forbidden band gaps. For electrons the occupancy of a state obeys the Fermi-Dirac statistics and the probability that a given state of energy E_e is occupied is given by

$$P(E)=\frac{1}{1+e^{\frac{E_e-E_F}{k_BT}}}, \tag{3.2}$$

where E_F is called the Fermi energy. At absolute zero the electrons occupy the lowest energy levels and E_F corresponds to the highest occupied level (can be regarded as the chemical potential of the electrons). As is depicted in Figure 3.2 the lowest band is fully occupied (first that lies below the Fermy energy) and is called the valence band (energy E_v)[9]. The highest band (first above the Fermi energy) it is known as the conduction band (energy E_c). If the last occupied band (conduction) is not completely filled the material is a conductor (like it happens for metals). In the case the conduction band is empty the material can be either a semiconductor or an insulator[10] depending on the energy gap between the two bands[11] (valence and conduction). Usually, a semiconductor will have a band gap (energy E_g) between ~0.2 to 2.0 eV and an insulator has $E_g > 2$ eV. When two different materials are put in contact the Fermi level defines what kind of contact is formed (e. g., ohmic or blocking) and changes occur in the band structure at the interface in order that the Fermi levels of the two materials become coincident.

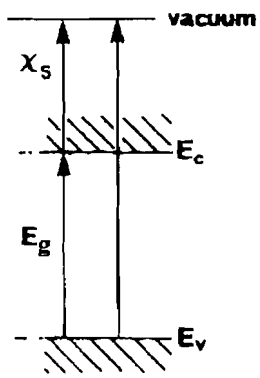

Figure 3.2 – Diagram showing the relative position of the conduction and valence bands (the highest energy bands occupied). The gap energy, E_g, is the difference between the bottom of the conduction band energy (E_c) and the bottom of the valence band (E_v). The electron affinity is χ_s and E_c and E_v are measured using as reference the vacuum level [Wintle83].

[9] These energies are relative and measured using a reference, the vacuum level, that corresponds to the energy of an electron at rest at infinity.

[10] It must be noticed that the distinction between a semiconductor and an insulator is not very sharp.

Table 3.1 – Binding energies for some covalent bonds common in polymers [Dissado92].

Bond	Binding energy (eV)
C – C	3.8
C = C	7.0
C – H	4.5
C – F	4.7
C – Cl	3.5
C – O	3.7
C = O	5.6
O – O	2.3
N – H	4.5
N – O	2.6
H – H	1.5

The kind of bonds between the atoms constituting a material defines the electric behaviour of the materials. For instance, all insulators are materials with covalent bonds and an even number of valence electrons. Almost all polymers fall into this class and albeit they have very large molecules, the intra-molecular bonding is covalent and van der Waals forces dominate between molecules. Typically the secondary bonds have a binding energy less than 0.5 eV while the covalent bonds are much stronger (as shown by the examples in Table 3.1).

Theoretical model calculations for the energy levels where first successfully applied to crystalline materials. For polymers, which are amorphous or semi-crystalline, similar models where used but less successfully. Many calculations focused on polyethylene because it is the simplest polymer (theoretical calculations and experimental results for PE bands are presented in 3.7). The ideal dielectric band structure is illustrated in Figure 3.3 – (a), showing well-defined edges for the bands. In a real polymer the molecular arrangement is irregular leading to less sharpen band edges. But besides this structural disorder there are localised chemical or structural defects (such as impurities, oxidation products, dangling bonds, amorphous/crystalline interfaces, etc.) resulting in states in the forbidden gap. These states are localised near the defect (see Figure 3.3 – (b)) and are called traps. Acceptors (electron traps) are located below the conduction band while donors (hole traps) are situated slightly above the valence band. The time that a carrier spends trapped in localised states depends on the depth of the trap (the energy needed to remove the carrier), temperature, electric field, etc.

[11] When the gap between conduction and valence band is very small, electrons can easily be excited to the conduction band.

The trapping time strongly conditions the mobility and as a consequence the conductivity, as will be discussed in more detail below.

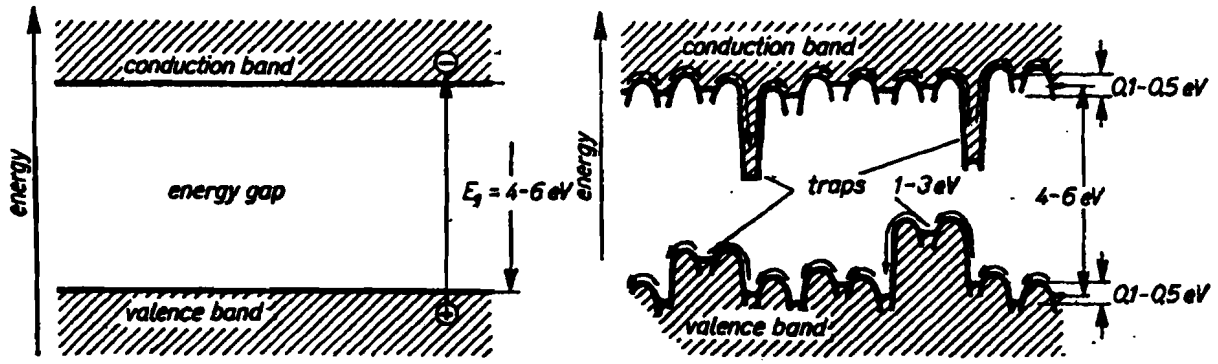

Figure 3.3 – Schematic representation of the energy levels of an insulator, (a) – ideal dielectric and (b) – more realistic model for a polymer [Hilczer86].

Either by hopping or tunnelling the charge carriers can be able to escape from one trapping centre to another. The distance between trapping is critical to allow this kind of conduction. The closer the traps are to each other the more probable is the transfer. In Figure 3.4 schematically represented by squares are the localised states. In the centre of the band gap the density of traps is low and also the overlapping between the trapping sites (squares). Near the conduction and valence bands the density is high enough to allow hopping (or tunnelling). As consequence the mobility follows the trend indicated in Figure 3.4, decreasing sharply and giving rise to a mobility edge (gap) that controls mobility instead of the carrier density that decreases much slower.

When the localised states are so close that the overlap produces almost a continuous region (band) these states are called extended states (Anderson) and another conduction mechanism can result (see [Blaise01] and 3.3.2.1).

3.3 Conduction and transport

The transport mechanism can be classified according to the type of carriers (ions, electrons or holes and polarons) and the value of the applied electric field (high and low field effects). The characteristics of the material such as chemical composition and morphology will impose the availability of one type of carriers and usually one kind dominates. However factors like temperature, electrodes (material and configuration) and ambient conditions (pressure, humidity and atmospheric gases) can be important.

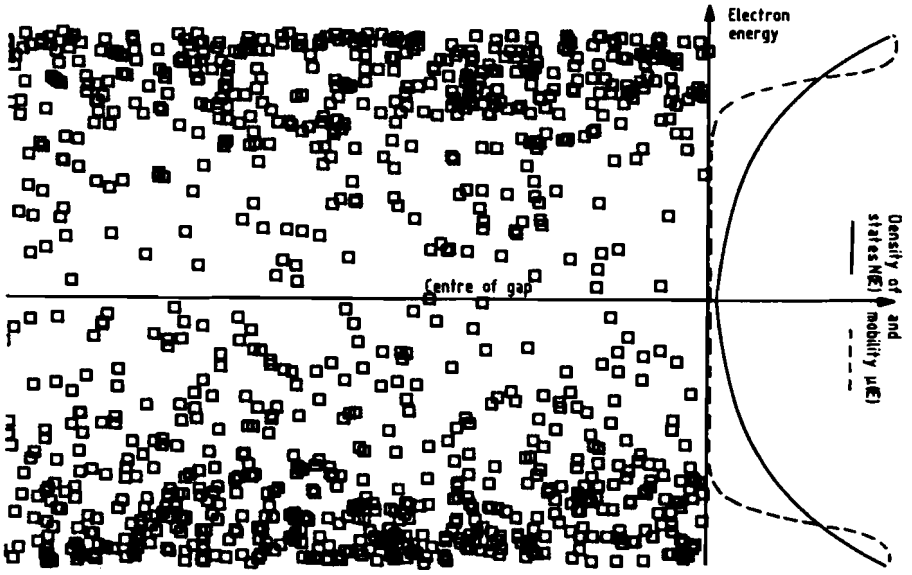

Figure 3.4 – Representation of electron localised states (squares) in the band gap for a non-crystalline material. The density of states and the mobility as a function of the electron energy is sketched on the right end side [Dissado92].

In large band gap insulators (8 to 10 eV), like polyethylene, the concentration of free intrinsic carriers is very small and most of the free charge carriers are the result of impurities. However for a given polymer it is difficult not only to identify the carriers but also to know the mechanism involved. The identification of a single mechanism is not possible by the usual measurements done to quantify the effect of electric field and temperature. Moreover, most of the times more than one mechanism can be active at the same time.

3.3.1 Carrier type

As stated above in 3.1 the main types of carriers are ions (including the proton) and electrons (including holes) and also the polaron. Only the first two will be briefly described here. For an insulating material the conductivity can be due to electrons (and/or holes), ions or both. It should be emphasised that it is difficult to find out the carrier type (this impairs, many times, distinction between electronic and ionic conduction).

3.3.1.1 Ionic conduction

It is expected that almost any small or medium size molecule would be able to cross almost any polymer film. As a consequence small ions could pass through if the electrostatic forces could be considered negligible [Wintle83]. However these interactions are quite important and give rise to traps for ions.

Concentration of ions, which are irrelevant when other properties are concerned, can influence significantly the electrical properties of an insulating polymer. The ions can have two different origins [Dissado92]. *Intrinsic ionic conductivity* exists if the ions (ionic groups) are a product of the dissociation of the polymeric main-chain or side-groups and electrons/protons are transferred from one chain to another (which are bound together by hydrogen bonds). The intrinsic conductivity is expected to be almost non-existent below the glass transition and to increase with temperature because the molecules need to assume favourable positions for the transfer to occur. On the other hand the *extrinsic ionic conductivity* arises from the presence of ionic impurities that do not belong to the chemical structure of the polymer. These ions can be the result of the manufacturing process (such as anti-oxidants and crosslinking by-products in XLPE), diffusion of ions and/or be products of oxidative processes occurring during ageing. The most common are: cations – H_3O^+, Na^+, K^+ and anions – OH^-, Cl^- and Br^-.

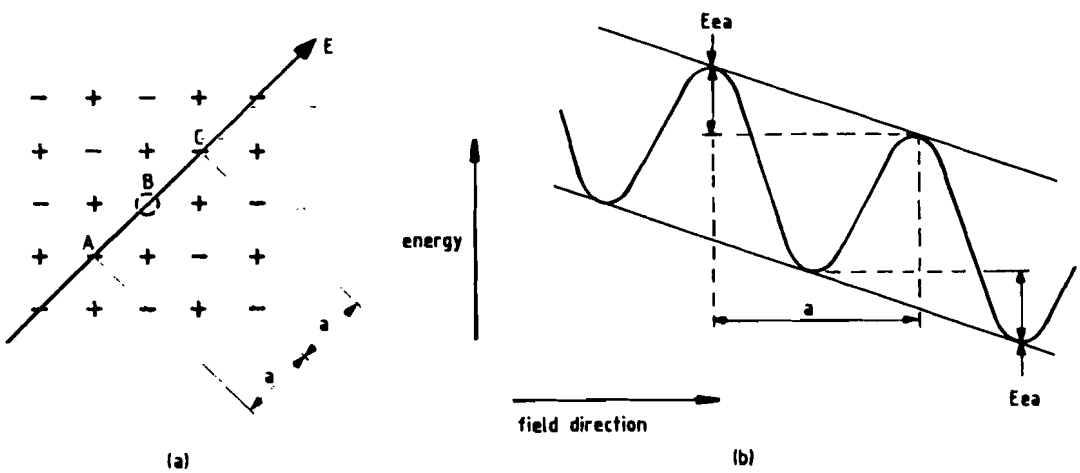

Figure 3.5 – The effect of the electric field on the lattice potential wells is seen. Figure (a) represents the direction of the electric field through a lattice vacancy (B) and (b) is seen the distortion caused by the electric field (lowering one side of the barrier while increasing the other side) [Dissado92].

The hopping theory was initially developed for the movement of vacancies in ionic crystals and included field dependent mobility and concentrations. In this type of material the conductivity would be due to the movement of a vacancy that could jump between the wells (thermally activated process). The presence of a field distorts the wells as can be observed in Figure 3.5. For hopping of ions, Mott and Gurney [Mott40] proposed a simple model, where the ions are in potential wells (lattice or structural defects, chemical impurities, etc.) and the

effect of the field is similar to the one for vacancies. This model will be described for low field in 3.3.2.1 and for high field in 3.3.2.2 below.

Table 3.2 summarises some important properties of ionic conduction. Contrary to electronic conductivity, the ionic conductivity is expected to increase when glass transition and melting point temperatures are crossed [Blythe79, Ieda84]. Extrinsic conductivity is expected to decrease with increasing pressure. In polymers used for insulation this kind of behaviour is observed suggesting that extrinsic conductivity can be important in these materials [Dissado92]. The concentration of ionic impurities would also affect conductivity. Usually in materials used as insulators, reduction of the impurities increases their resistance so that a careful preparation is very important for the quality of the insulators. Water absorption, which has a relatively high dielectric constant, generally leads to an enhancement of the conductivity.

Table 3.2 – Comparison between ionic and electronic conduction (based on a table presented by Ieda [Ieda84]).

Parameter	**Conduction**	
	Ions	***Electrons***
Mass transfer	Yes	No
Pressure	Decreased	Increased
Ionic impurities	Yes	
Temperature	Increased	Decreased
At glass transition ($T>T_g$)	Increased	Decreased
At melting point ($T>T_m$)	Increased	Decreased

3.3.1.2 Electronic conduction

Electron and hole transport is determined by the band structure. In materials with wide band gap, conduction is not likely to occur by free electrons in the conduction band or holes in the valence band. It is more probable that the conduction mechanism is dominated by hopping between traps and/or the extended states (or tunnelling for higher fields). Traps can also control intramolecular transport of carriers over the long main chain. Carriers may encounter traps at conformational defects (chain folds) or at polar groups (for instance, in PE it can be carbonyl groups).

Intermolecular transport has also to be taken into account for conduction of the carrier across the material. Thermally activated intermolecular hopping is a possible mechanism. It seems reasonable that electrons get attached to small molecules. Therefore an alternative to intermolecular transfer is percolation of carriers through the amorphous regions [Wintle99] which is restricted by the free volume within the polymer.

Mostly the intermolecular process will limit the conductivity. The values found for the intramolecular mobility ($>10^{-4}$ $m^2V^{-1}s^{-1}$) are higher than the ones for intermolecular transport ($10^{-7} - 10^{-14}$ $m^2V^{-1}s^{-1}$) [Dissado92]. For Teflon at room temperature the hole mobility is of the order of 10^{-16} $m^2V^{-1}s^{-1}$ and the electron mobility is even smaller [Hilczer86], and these values are near the ones obtained for intermolecular mobility. Considering a molecule as a miniature lattice, calculations were done for a long PE molecule (with a planar zig-zag configuration) predicted a hole mobility of the order of 10^{-9} $m^2V^{-1}s^{-1}$ and a band gap above 5 eV [Blythe79]. But the values of the mobility for PE are much lower than this one as will be presented in 3.7.

The crystallinity lowers the conductivity by introducing more amorphous/crystalline interfaces that act as strong traps due to Maxwell-Wigner-Sillars polarisation. The temperature rise leads to a decrease in mobility by reducing the mean free path. On the contrary the pressure increase will increase the overlap of the electronic functions and consequently the transport [Ieda84] (see also Table 3.2).

3.3.2 Electric field

The mechanisms leading to conduction and carrier transport are dependent on the field, among other factors. For field up to 10^6 to 10^7 V/m (low fields) the conductivity varies linearly with the electric field and the behaviour falls in the ohmic regime regardless of carrier type. For higher fields non-linear effects appear and consequently a super-ohmic response.

For bulk mechanisms the equations describing this behaviour are known (for a single carrier type). The current density, j, is the sum of the conduction, diffusion and displacement currents (one dimension):

$$j = \sigma E + qD_f \frac{\partial n}{\partial x} + \frac{\partial D}{\partial t}, \tag{3.3}$$

where σ is the conductivity, E the electric field, q is the carrier charge, D_f the diffusion coefficient, n the carrier concentration and D the dielectric displacement.

The convection current (due to charge transport) is the sum of the conduction and diffusion current

$$j = \sigma E + qD_f \frac{\partial n}{\partial x}, \tag{3.4}$$

other important equations are Poisson's and continuity equations.

3.3.2.1 Low field effects

For ohmic conduction the steady state current will be linearly dependent on the applied electric field, implying that the conductivity is field independent. It is also expected that conductivity is not dependent on electrode material and sample thickness being just a material characteristic. Yet it can be affected by factors such as ambient humidity or temperature. According to Equation (3.1) the linear dependence results in carrier concentration and mobility independents of the field. However in real polymers, inhomogeneities (including interfaces amorphous/crystalline and barriers adjacent to the electrodes) give rise to non-linear effects. Nevertheless to fields up to 10^6 Vm^{-1} the linearity holds in most polymers.

For a free trap model electrons contributing to the ohmic conductivity will behave in similar manner as free electrons in metals and semi-conductors. In the absence of an applied electric field, and due to thermal activation, the electrons experience a thermal energy with a zero net velocity. When an electric field is applied a force acts on the electrons and the average velocity is no longer zero (drift velocity). These drift velocities are usually 5 to 6 orders of magnitude lower than the average thermal velocities. The field is only able to disturb slightly the electrons. The mobility calculations give higher values than the typical ones found in insulating polymers. But, as seen above, the material has traps that immobilise the electrons reducing the number of carriers by a factor that can be as low as 10^{-10} to 10^{-6} [Dissado92].

For ions Mott & Gurney [Mott40] proposed a thermally activated hopping mechanism. As can be seen in Figure 3.5 the field lowers(raises) the barrier by $\mp 1/2aE$ (a is the spacing between two neighbouring wells) and the current density is given by:

$$j = j_o \exp\left\{\frac{-E_a}{k_B T}\right\} \sinh\left\{\frac{eaE}{2k_B T}\right\}, \tag{3.5}$$

Consequently a plot of $\log\frac{i}{E}$ vs. E will produce a straight line of slope $\frac{ea}{2k_B T}$ [Scarpa95].

This model provides very low mobilities in accordance with the experimental results for high insulating polymers.

Another proposed "hopping" mechanism involves jumping from the localised states (detrapping) into the extended states at the mobility edge. These carriers in the extended states are able to move like free carriers until they are re-trapped into the localised states. The

model, called multiple-trapping, describes conduction as the result of successive trapping-detrapping with the carrier jumping between trapped (localised states) and the extended states [Watson95, Blaise01]. The carrier mobility is controlled by the time it spends trapped.
Arrhenius temperature dependence is sometimes observed for ohmic response implying a probable change of carrier concentration and/or mobility with the temperature. Mobilities that are dependent on the concentration are related to hopping between localised states. And non-Arrhenius behaviour might be associated with variable range hopping [Wintle83].

3.3.2.2 High field effects

When the applied field is increased (>10^6 V/m) the voltage vs. current characteristic no longer has an ohmic behaviour. It becomes super-ohmic with the current increasing faster than the voltage. The mobility (and the conductivity) is (are) field dependent.
The high field effects can be divided in electrode and bulk effects:
a) Electrode effects

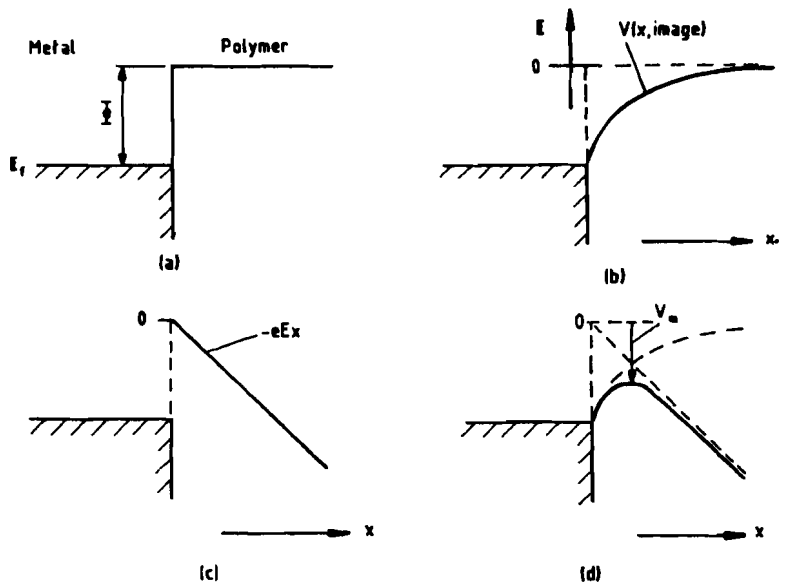

Figure 3.6 – Potential barrier at metal-polymer interface (electrode). (a) Total barrier, (b) effect of Coulombic image force included, (c) potential energy due to the electric field and (d) total barrier shape [Dissado92].

In a metal–polymer contact, such as the one occurring in samples with evaporated electrodes[12], the electrons must overcome a potential barrier so that they are able to enter the

[12] According to Wintle [Wintle83,99] this is the contact that gives rise to less "non-wanted" effects due to the type of contacts (mechanical, silver paint, colloidal graphite electrodes are some of the other ones mentioned).

polymer. In vacuum the barrier height is equal to the work function of the metal, ϕ_m. Since these barriers are high, thermal injection is very small. But the barrier is modified by the presence of an applied electric field (see Figure 3.6) increasing the probability of injection to occur. This mechanism, called Richardson-Schottky emission or *Schottky injection*, gives an injection density current dependent on the temperature and the electric field:

$$j \propto T^2 \exp\left(-\frac{\phi - \frac{e}{2}\sqrt{E/\pi\varepsilon_o\varepsilon_r}}{k_B T}\right) \tag{3.6}$$

A straight line is obtained for a Schottky plot of $\log(j/T^2)$ vs. $\sqrt{E}$.

For fields above 10^9V/m the potential barrier becomes thin and tunnelling is possible. This is known as the *Fowler-Nordheim injection* and the current density behaviour is obtained by quantum mechanics calculations,

$$j \propto E^2 \exp\left\{-\frac{4}{3}\sqrt{\frac{2m_e^*}{\hbar^2}}\frac{\phi^{2/3}}{eE}\right\} \tag{3.7}$$

where ϕ is the barrier height (see Figure 3.6 – (a)) and m_e^* is the electron effective mass. Tunnelling is independent of temperature, inversely proportional to the sample thickness and strongly dependent on the electrode material [Scarpa95]. It is also possible for hole injection to occur by tunnelling of electrons from the valence band.

b) Bulk effects

Space charge limited conduction (SCLC) appears when the electrode-polymer contact permits an easy injection of one carrier type that subsequently becomes trapped. A high concentration of charge in the material may build up, lowering the electric field. Charge concentration, type, mobility and easiness of injection from electrodes and traps' characteristic determine if the SCLC is the dominating mechanism. A simple model was developed by Mott and Gurney [Mott40] for a dielectric with no traps and no thermally generated carriers and ohmic electrodes. Electron injection is considered and diffusion current is neglected. The current density has just two components, one ohmic and another dependent on the square of the applied voltage, for a sample thickness of d:

$$j = n_o e\mu\frac{V}{d} + \frac{9\varepsilon_o\varepsilon_r\mu V^2}{8d^3} \tag{3.8}$$

this is known as the Mott-Gurney square law or the Child's law for solids. There is a transition voltage above which the SCLC regime predominates over the ohmic behaviour

$$V_{tr} = \frac{8e_o n d^2}{9\varepsilon_o \varepsilon_r}. \tag{3.9}$$

The existence of traps is taken into account including a factor θ that gives the proportion of electrons in the conduction band compared with the ones that remain trapped. The above equations are modified and the trap-limited SCLC is:

$$\begin{aligned} j &= \theta \frac{9\varepsilon_o \varepsilon_r \mu V^2}{8d^3} \\ V_{tr} &= \theta \frac{8en_o d^2}{9\varepsilon_o \varepsilon_r} \end{aligned} \tag{3.10}$$

θ can be very small ($10^{-6} - 10^{-10}$) [Dissado92].

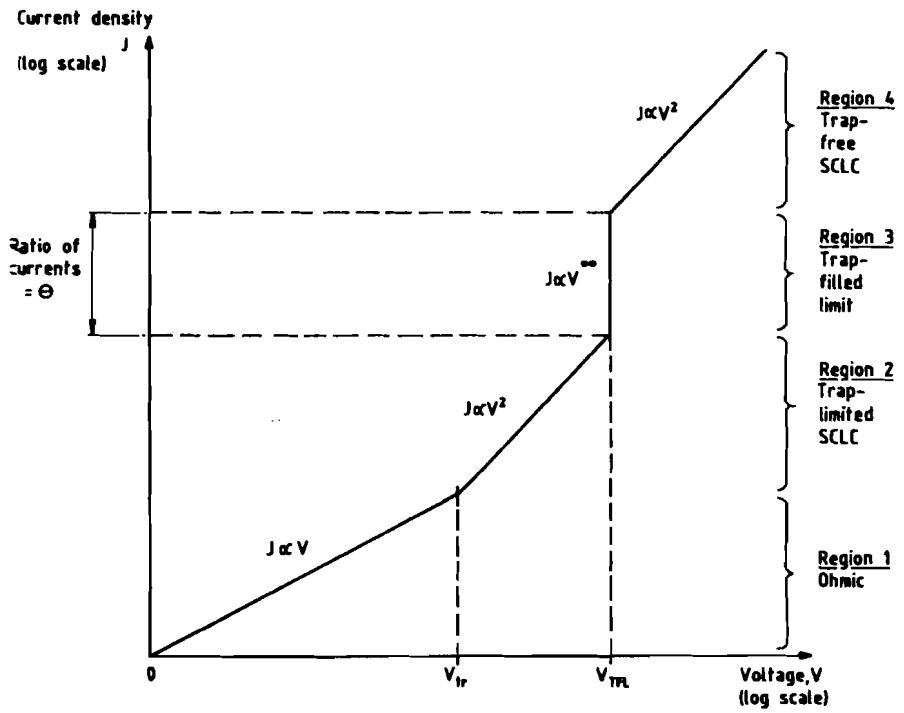

Figure 3.7 – Schematic representation of the different regimes of conduction [Dissado92].

At a sufficiently high field, charge injection is enough to approximately fill all the traps, this is the *trap-filled limit* (TFL). At this limit the factor θ changes from the very low values to close to unity and the current increases very fast (with a slope close to infinity). The trapped-filled limit voltage is:

$$V_{TFL} = \frac{en_t d^2}{2\varepsilon_o \varepsilon_r}, \tag{3.11}$$

where n_t is the number of traps. After the trap-free SCLC regime is dominant with a slope of two.

Figure 3.7 shows the characteristic of the four different regimes (ohmic, trap-limited SCLC, trap-filled limit and trap-free SCLC).

Hopping mechanisms can also be dominant at high fields. It has been described above that the electric field lowers the potential barriers in the direction of the electric field (3.3.1.1). For more mild fields the current is linear with the applied voltage. For high fields the mobility becomes an exponential of the field. The *Poole-Frenkel* mechanism is illustrated in Figure 3.8 – (a) and (b). In (a) is represented the simplest case with hopping from one potential well to the next, facilitated by the lowering of the barrier in the field direction. For (b) there is overlap of the potential wells allowing backward jumps. The Poole-Frenkel equations results in an exponential dependence of the conductivity considering no compensation of ionisation:

$$\sigma = \sigma_o \exp\left(\frac{\beta_{PF}\sqrt{E}}{2k_B T}\right), \tag{3.12}$$

where β_{PF} is the Poole-Frenkel coefficient (a characteristic of the material). Some improvements were made, such as the one by Onsager that added the effect of diffusion or the one taking into account the effect of Coulombic screening. A plot of log j or log σ vs. $\sqrt{E}$ gives a straight line. This is the same dependency observed for the Schottky emission and it makes experimentally difficult to distinguish between Poole-Frenkel and Schottky mechanism[13].

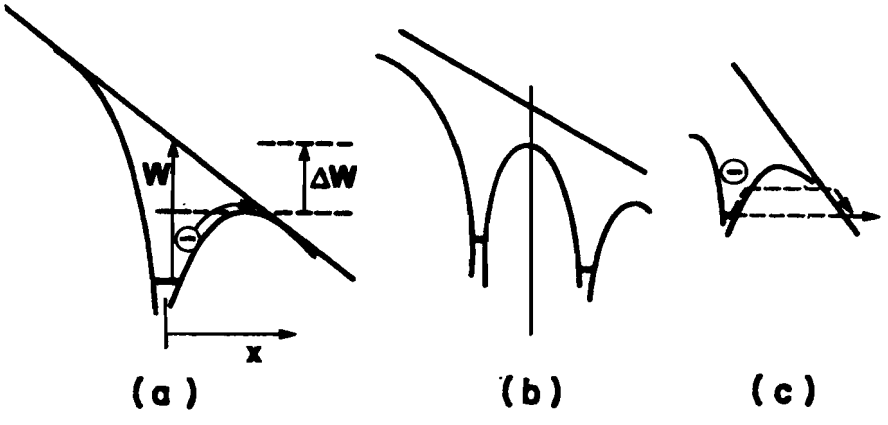

Figure 3.8 – Some high field models for bulk conduction. (a) One-center Poole-Frenkel, (b) multiple-overlap Poole-Frenkel and (c) tunnelling showing both simple tunnelling and a combination of thermal excitation with tunnelling [Wintle83].

[13] For bulk conduction, the Poole-Frenkel mechanism is the equivalent of the Schottky injection mechanism.

Tunnelling becomes probable for fields above 10^9 V/m or a combination of thermal excitation and tunnelling as is represented in Figure 3.8 – (c). The thermal promotion takes the carrier to an equi-energetic level of a neighbouring empty site. Mott refers to this mechanism as *variable range hopping* but Dissado & Fothergill [Dissado92] prefer to call it *thermally assisted tunnelling*.

3.4 Transient response

Subjected to a step voltage there is a charge transfer that gives rise to a decaying current until a (quasi) steady state is reached. Besides the very fast change of current there is a slow decaying current, that is called charging or absorption current, and it has two components, one transient due to relaxation processes, and another related to the steady state conduction. In high insulating polymers this steady state current can take a very long time to be reached (from hours to days) or can never be reached [Das Gupta97, Wintle99].

In a similar manner when the step voltage is removed a transient current (discharging or desorption) appears that tends to zero (the steady state component is no longer present).

For most of the processes the transient current obeys the Curie-von Schweidler[14] decaying power law (also discussed in 4.3 related with the dielectric relaxation response):

$$i(t) = Kt^{-n}. \tag{3.13}$$

The analysis of the charge and discharge currents can be useful on the identification and study of the mechanisms. The study of the influence of electric field, temperature, electrode material, sample thickness and the relation between the absorption and desorption currents together with the time dependence can help to identify the mechanism. In Table 3.3 is summarised the dependence according to the mechanism present.

Some times it is not easy to achieve reliable conclusions. Several mechanisms can be operative at the same time. Also in high insulators the currents are very low and sometimes do not reveal a specific influence. As is presented in our results discussed below in Chapter 7, the charge and discharge current registered are unable to reveal the presence of deep trapped charge that remains trapped for very long time.

[14] This relation is not valid at very short times where the inertial processes lead to a linear dependence of the current with time. Also $n < 1$ at infinitely long times would correspond to infinite total charge.

Table 3.3 – Transient currents behaviour with different experimental parameters (adapted from [Das Gupta76,97] & [Wintle73&83]).

Process	Electric field (E)	Thickness at constant field (d)	Electrode material	Temperature	Time dependence ($\propto t^{-n}$)	Relationship between charge and discharge transients
Dipolar reorientation (uniformly distributed in the bulk)	$\propto E$	Independent	Independent	Thermally activated (Arrehnius $T<T_g$ WLF* $T>T_g$)	$0 \le n \le 2$	Mirror images
Dipolar reorientation (surface polarisation)	$\propto E$	$\propto \frac{1}{d}$	Independent	Thermally activated	$0 \le n \le 2$	Mirror images
Maxwell-Wagner-Sillars interfacial polarisation	$\propto E$	$\propto \frac{1}{d}$	None	Related to conductance dependence	Exponential	Mirror images
Electrode polarisation	$\propto E$ (low field) and non-linear (high field)	Not specified	Strongly dependent through blocking parameter	Thermally activated $\propto \frac{1}{\sqrt{T}} \exp\left(-\frac{E_a}{k_B T}\right)$	Initially $n = 0.5$ followed by $n > 1$	Not clear
Charge injection forming trapped charge	Related to the mechanism that controls charge injection	Independent	Related to the mechanism that controls charge injection	Related to the mechanism that controls charge injection	$0 \le n \le 1$	Dissimilar
Tunneling injection	$\propto E$	$\propto \frac{1}{d}$	Strongly dependent	Independent	$0 \le n \le 2$	Mirror images
Hopping	$\propto E$	Independent	Independent	Thermally activated	$0 \le n \le 2$	Mirror images

* WLF = Williams-Landel-Ferry

3.5 Steady state response

In Equation (3.3) if $\frac{\partial D}{\partial t} = 0$ the steady state has been reached and it is expected that from that point on, the current density will be constant. How long it takes depends upon temperature, material, electric field, etc. As stated above (3.4) it may take between hours to days and it might never be reached. Some times it is difficult experimentally to ensure that it has been attained.

If following strictly the definition given by Equation (3.1), the conductivity will be a material characteristic for the specific experimental conditions (electric field, temperature, previous sample history, etc.). This only occurs if the carrier concentration and the mobilities are a characteristic of the material. However it happens many times that the carrier concentration and mobility are position dependent and cannot be measured. Also the conductivity of highly insulating polymers can vary for the same material, depending on sample preparation and conditioning. Any small change of impurities concentration, morphology, electric, thermal and environmental history influence the very low values of conductivity. Most of the times conductivity is used in a general way as $\frac{j}{E}$, without much care taken into assuring that steady state has been reached and not stating the specific experimental conditions under which the results were obtained[15].

The very low conductivity found in good insulators can be explained by the low values of carrier concentrations and mobilities. Concentration and mobilities depend upon external factors such as temperature and electric field and on the polymer properties such as morphology, chemical composition, degree of crystallinity, etc. According to Wintle [Wintle83], steady state conductivities in polymers range from 10^{-20} Sm^{-1} at room temperature to 10^{-14} Sm^{-1} at 120 °C and at glass transition there is a change in slope identical to one observed for free volume.

Experimentally it can be extremely difficult to measure the steady state currents. For high insulating materials the values to be measured are very small, as mentioned previously, the transient current may last for very long time and care has to be taken with surface currents.

The polymer morphology has also a great influence on the conductivity and can vary from sample to sample. Usually conductivity decreases with increasing molecular weight but tends

[15] This is one of the major problems when studying conduction on a very good insulator, such as polyethylene and has been addressed with some care in the course of the experimental work done here (see 6.4 and 7.3).

to increase with spherulite size and density. For ionic conductivity an increase occurs with crystallinity.

3.6 Surface conduction

Surface conduction can be of the same order of magnitude of bulk conduction if the insulating polymer surface is not dry or free of contaminants. Washing up the polymer surface with hexane removes impurities and reduces the surface conductivity (for results on polyethylene see [Sakamoto02]). For a dry and clean polymer the current on the superficie can be measured using an interdigital array as one of the electrodes. The conduction is highly dependent on humidity and electrical history of the sample (the electric field is strongly dependent on the external geometry). For typical polymers σ_s is in the range of 10^{-10} to 10^{-16} S. Oxidation plays also an important role because it helps water absorption. For a dry polyethylene whose surface is not clean the conductivity is below 10^{-9} S (comparable to the bulk conductivities)

For experiments on charge injection on the surface[16] in PET an estimate of the surface mobility give a value around 5×10^{-12} $m^2V^{-1}s^{-1}$ [Wintle99]. This is of the same order of bulk conductivity and can indicate ionic motion or shallow trapping of electrons.

Since only a brief insight was given here, for further reading good reviews are Wintle [Wintle83,99] and Das Gupta [DasGupta92].

3.7 Charge transport and trapping in polyethylene

The high insulating characteristics of polyethylene arise specially from the high band gap and the existence of deep traps with long trapping times, which results in very few carriers participating in the conduction process. In Figure 3.9 it is shown schematically the results from different experimental methods for the energy of the band gap and also the value of the work function ($\phi = 4.5$ eV). The band gap is near 9 eV and the mean free path for electrons in the conduction band is below 100 Å. This polymer has a slightly negative electron affinity [Wintle83]. Calculations on the probability of the conduction band to be occupied at 100 °C gave extremely low results, of the order of 10^{-60} [Dissado92].

[16] Possibly it is what happens during the preparation of the hot-pressed moulded samples used in this work (see Chapter 6 and 7).

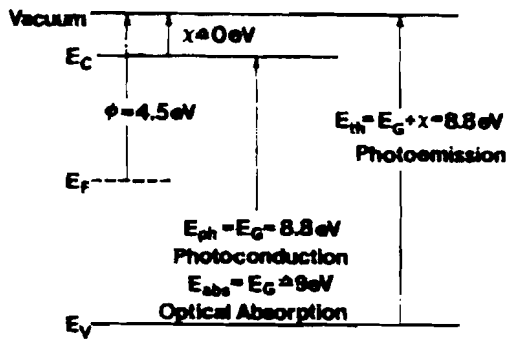

Figure 3.9 – Energy levels in polyethylene and band gap energies obtained from different experimental methods [Wintle83].

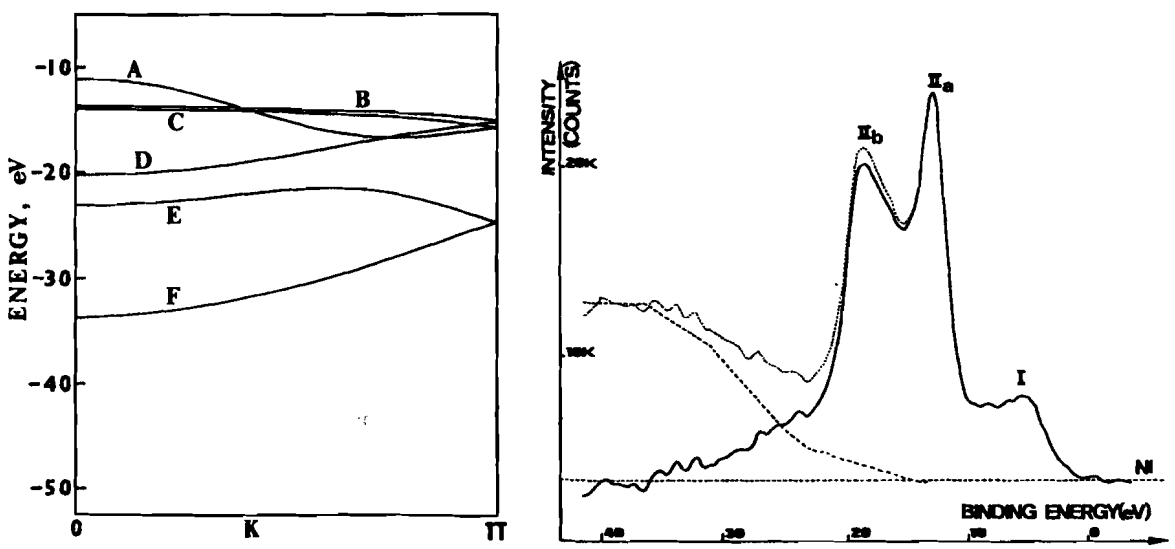

(a) (b)

Figure 3.10 – Band structure for polyethylene (a) from theoretical calculations [Wood72] and (b) from ESCA measurements where the solid line represents the corrected curve [Delhalle74]. The low energy peak (I) is signed to the ionisation from the four topmost bands (A, B, C and D). The double peak (II_a and II_b) correlate with the lower two bands (E and F).

Polyethylene is the simplest polymer and consequently the best to try to calculate theoretically the band structure. As was said previously the theory has not been very successful for the more complex polymeric systems but an illustrative result is presented in Figure 3.10 – (a). These calculations are compared with experimental results obtained with ESCA (Figure 3.10 – (b)). The lower broad peak (I) observed in ESCA can be decomposed into four components (at 4.9, 6.4, 7.8 and 9.0 eV) and is assigned to the ionisation of the four topmost bands (A, B, C and D in Figure 3.10 – (a)). The other more intense peaks (II_a and II_b), at respectively 13.2 and 18.8 eV, are assigned to the bands E and F (Figure 3.10 – (a)).

Carrier type has been difficult to identify and moreover little is known about trapping centres. Some features seem to suggest that electrons are the carriers with the mobility constrained by the time they spend trapped. However other features are in agreement with ionic conduction (conductivity increases as temperature is raised above the melting point).

The very small number of carriers available makes any small change in their number to have a considerable effect on conductivity. Conductivity appears to be an extrinsic phenomenon highly influenced by impurities. The experimental results show this influence with major problems in obtaining reproducible results and considerable differences between experiments performed by different research groups. Pélissou et al. [Pélissou88] and Ohki et al. [Ohki98] have found for conductivity at room temperature values of the order of 10^{-16} Sm^{-1}. According to [Wintle70&83] polyethylene mobility at 20 °C is around 10^{-14} to 10^{-16} $m^2V^{-1}s^{-1}$, similar to the results of [Fischer78, Pélissou88 & Hwangbo98]. On the other hand Taylor et al. [Taylor71] found a value higher than 2×10^{-18} $m^2V^{-1}s^{-1}$ at 40 °C for low fields. The value found in this work also agrees with the ones reported on literature (see Chapter 7).

From experimental results it is expected that the amorphous part will be more conductive. Work was done on polyethylene crystals, which revealed to be highly conductive suggesting that amorphous/crystalline interfaces have a important role on limiting conduction [Wintle83]. For measurements of TSC below room temperature dipolar reorientation is the main mechanism. Above room temperature the charging current is independent of sample thickness and electrode material but a non-linear response with the field sets in (even for low fields). Therefore dipoles can be ruled out for higher temperatures and it seems likely a space-charge mechanism with traps. Oxidised polyethylene presented an increase of the current with carbonyl content and oxidation increases conductivity. Impurities are also important for transport. Adding halogens (I_2 and Br_2) assisted electrons and holes to jump between chains with an increase of electron and hole mobilities [Ieda84]. The some author quotes X-ray induced TSC for polyethylene that reveal oxidation products, cross-links and impurities acting as carrier traps[17].

As for high field results, according to Wintle [Wintle99], it remains ambiguous and difficult to identify a dominant mechanism.

[17] For a more detailed review of thermally stimulated results for polyethylene see discussion of experimental results in 7.3.

Transient currents in low density polyethylene have been studied extensively by Das Gupta et al. [Das Gupta78] for commercial films. The results fitted well using the Curie-von Schweidler law for temperatures below –70°C. However above this temperature there is the onset of the steady state and this new contribution has to be taken into account. Based on temperature, electric field, electrode material and thickness dependence these authors conclude that below room temperature dipolar reorientation in the bulk is the dominant mechanism (related to reorientation of C=O groups). Above room temperature a charge carrier hopping is the most probable mechanism. No definitive identification of carrier type or traps was made.

A recent paper by Montanari et al. [Montanari01] attempts to study charge injection, transport and trapping in LDPE, XLPE and HDPE by combined analysis of transient current measurements with space charge experiments (PEA). The applied electric fields are usually higher than those used during the work presented here. For low fields the authors concluded that polyethylene has ohmic behaviour and probably ionic species are involved (such as stated also by Das Gupta et al. [Das Gupta78], however Taylor et al. point out to electronic conduction [Taylor71]). At higher fields it is suggested a modification of the SCLC, including heterocharges and a limited supply of charges from the electrodes, called by Montanari et al. [Montanari01] *space charge-assisted conduction*. At high fields both HDPE and XLPE current data follows the Schottky injection and SCLC law, while LDPE data cannot be fitted by neither. Mobilities were calculated for fields ≥ 30 kV/mm at 20 °C by different methods, with a values found for the steady state for: 10^{-14} – 10^{-15} $m^2V^{-1}s^{-1}$ (LDPE) and 10^{-16} – 10^{-17} $m^2V^{-1}s^{-1}$ (XLPE and HDPE). LDPE is also the one that shows higher conductivity but less amount of space charge. The same authors reported also traps depths of 0.80 to 1.07 eV. The higher values (deeper traps) found for HDPE and the lower ones for LDPE. These results would explain the higher mobilities found in the low density polyethylene.

In conclusion it is very difficult to study transport and trapping mechanisms in polyethylene. Results vary from sample to sample and are quite dependent on manufacture and conditioning. A careful control of the experimental conditions and a good knowledge of the sample under study (morphology, impurities content, etc.) is needed to be able to obtain information leading to characterise conduction in polyethylene.

Chapter 4. Dielectric relaxation

The essence of relaxation is the existence of disorder

A. K. Jonscher

4.1 Dipoles and charge carriers

Materials present charges that usually balance each other given an overall neutral system. If these charges are free carriers the presence of an electric field will produce a conduction current. On the other hand, if dipoles[18] exist they will induce a displacement current. Ideal insulators only show induction while ideal conductors only exhibit conduction. A dielectric is essentially an insulating system. In 1891 Maxwell [Maxwell91] has defined dielectric as a medium where conduction and induction takes place simultaneously.

A dipole is characterised by a dipole moment vector dependent on charge magnitude and distance between the two charges. If the dipoles are randomly oriented in a material the net dipole moment (sum of the individual dipole moments) is zero. When an electric field is applied the dielectric properties of the material (such as the dielectric constant, ε) determines the response (polarisation due to orientation of the dipoles in the field direction). Dielectric relaxation results from the non-instantaneous response of the dipoles.

For an electrostatic field the polarisation, P, is given by[19]:

$$\begin{aligned} P &= (\varepsilon_r - 1)\varepsilon_o E + \text{higher terms in } E \\ &= \varepsilon_o \chi E + \text{higher terms in } E \end{aligned}, \tag{4.1}$$

where ε_o is the dielectric permittivity of vacuum, χ is the medium susceptibility, ε_r the medium relative permittivity (or dielectric constant) and E the electric field. The higher terms in E are known as hyperpolarisation and usually they are not relevant.

The polarisation is the net dipole moment per unit volume and can be defined in terms of molecular/atomic/electronic properties

$$P = N_o \alpha E_L, \tag{4.2}$$

(α is the polarisability, N_0 is the Avogadro number and E_L the local electric field).

---

[18] A dipole consists of a positive and a negative charge of the same magnitude separated by a given distance.

[19] In this relation the medium is considered isotropic, if it was anisotropic both P and ε would have to be tensors. Also in this presentation it will be adopted a scalar notation since in most experimental applications this approximation will be valid (the medium is considered isotropic and also due to the planar configuration used a one-dimension approach can be used).

Polarisability for atoms can vary from 0.1 – 50 m^3 (lowest for noble gases and highest for group I elements) and for molecules the values are much higher. The polarisation at a microscopic (molecular) level can be divided in different components:

(i) electronic (induced) – the electric field is able to distort the electronic cloud around an atom. The frequency is very high and responsible for light refraction (10^{15} – 10^{18} Hz);

(ii) atomic (induced) – the electric field is able to displace the nuclei in a molecule or lattice (10^{12} – 10^{15} Hz)

(iii) orientational (permanent) – if the molecule already posses a dipole the electric field will align these dipoles (<10^{12} Hz).

Also polarisation arising from charge carriers is possible (even if it is rarely discussed in the related literature). Intermediate between free charges and dipoles, charges that are localised at sites (like the ones in a potential well) are able to hop to neighbouring sites. Hopping of charge carriers under certain conditions can originate a polarisation. The hopping cannot be distinguished from a dipole rotation and it influences the dielectric spectra at low frequencies. For instance ions in interstitial or vacancy sites move essentially by hopping. Also it is possible to give rise to a DC conductivity if there is possible paths to occur percolation (however the mobility is much lower than for free carriers). As well if the material is heterogeneous with regions of different dielectric constant a so-called Maxwell-Wagner-Sillars (MWS) polarisation can be formed by accumulation of charges at the interfaces. The carriers can also originate non-linear effects due to charge injection and removal.

4.2 Dipoles in a static field

As stated above under the influence of the electric field dipoles will tend to align and consequently condition the dielectric response. The total contribution for the dielectric response will arise from reorientation of permanent dipoles and from new induced dipoles.

Clausius and later Mossoti developed a local field approach for a "gas of dipoles" trying to quantify the influence of neighbouring dipoles. Debye using the Lorentz-Lorenz relation for the refractive index modified the original Clausius-Mossotti equation:

$$\frac{\varepsilon_s - 1}{\varepsilon_s + 2} - \frac{\varepsilon_\infty - 1}{\varepsilon_\infty + 2} = \frac{N_d \mu_d^{\,2}}{9\kappa_B T} \tag{4.3}$$

where ε_s is the static dielectric constant (representing the long time response) and ε_∞ is the high frequency dielectric constant (representing the instantaneous response), μ_d is the permanent dipolar moment and N_d is the number density of permanent dipoles.

Using the above equation for polyethylene (that can be seen as an assembly of $-CH_2$ units) it is possible to obtain for the high frequency relative permittivity a linear relation with the density , ρ_m [Blythe79]:

$$\varepsilon_\infty = 2.276 + 2.01(\rho_m - 920)\times 10^{-3} \tag{4.4}$$

which is in fair agreement with experimental evidence.

However this model could be further refined and Onsager adapted the Equation (4.3) for a condensed phase system with rigid non-associated molecules (successfully applied to liquid systems but still unrealistic for polymers):

$$\frac{\varepsilon_s - 1}{\varepsilon_s + 2} - \frac{\varepsilon_\infty - 1}{\varepsilon_\infty + 2} = \frac{3\varepsilon_s(\varepsilon_\infty + 2)}{(2\varepsilon_s + \varepsilon_\infty)(\varepsilon_s + 2)} \frac{N_d \mu_d^{\,2}}{9\kappa_B T} \tag{4.5}$$

Applying a statistical theory, the short range orientation interactions of neighbouring molecules were introduced by the Kirkwood correlation function. Frölich improved the previous model by developing a new general theory which could be applied successfully to polymers.

4.3 Dielectric response in time and frequency domains

The complex frequency dependent permittivity can be defined as:

$$\varepsilon(\omega) = \varepsilon'(\omega) - i\left(\varepsilon''(\omega) + \frac{\sigma}{\varepsilon_o \omega}\right)$$
$$\tan\delta = \frac{\varepsilon''}{\varepsilon'} = \frac{\text{energy dissipated per cycle}}{\text{energy stored per cycle}} \tag{4.8}$$

the contribution from free charge carriers (true DC conductivity) is represented by the last term in the first equation which is linearly dependent on the material characteristics (conductivity σ) and inversely on the frequency (ω). The real (ε') and imaginary (ε'') components of the permittivity represent the response of dipoles. The real component is related to a capacitive component of the current and the imaginary one with a resistive (lossy) component (see also 4.6). The later one is called the dielectric loss factor and $\tan\delta$ is known as the dielectric tangent or dissipation factor (the angle δ is the angle between the electric field and the polarisation vectors).

The displacement (dielectric induction) will reflect the contribution of the instantaneous free charges response and the delayed effect of dipoles,

$$D(t) = \varepsilon_o E(t) + P(t) \tag{4.9}$$

[20] ξ gives the deviation from two states been equally occupied.

It is assumed that the dielectric response obeys two considerations and a function $\Phi(t)$ [21], the dielectric response function, is defined:

(i) Casuality principle – $\Phi(t)=0$ for $t<0$

(ii) (Boltzmann) superposition principle (linearity) – the response of consecutive elementary excitations is the sum of the individual responses (this is valid for most systems if the excitation is kept below a certain limit). It was first discovered by Boltzmann for creep and stress relaxation in polymers.

$$P(t)=\varepsilon_o\int_{-\infty}^{+\infty}\Phi(\tau)E(t-\tau)d\tau \tag{4.10}$$

mathematically represents the convolution of the response function and the electric field. Physically it means that a dielectric has a memory of the past history with all the previous excitations contributing to the present polarisation.

Three specific field dependencies on time are commonly used in order to study the dielectric response:

(i) Delta function $E(t)=E_o\delta(0)$;

(ii) Step function $E(t)=\begin{cases}0 & t<0\\ E_o & t\geq 0\end{cases}$; (4.11)

(iii) Harmonic function $E(t)=E_o e^{i\omega t}$;

the easiest mathematical treatment is for the step function (ii), for which the polarisation becomes [Jonscher83]:

$$P(t)=\varepsilon_o E_o\int_0^t\Phi(\tau)d\tau. \tag{4.12}$$

Replacing in Equation (4.9), one gets,

$$D(t)=\varepsilon_o E_o\left\{H(t)+\int_0^t\Phi(\tau)d\tau\right\}, \tag{4.13}$$

($H(t)$ being the Heaviside function) and it follows for the current density flowing in the system:

$$j(t)=\frac{dD}{dt}+\sigma E_o=\varepsilon_o\frac{dE}{dt}+\frac{dP}{dt}+\sigma E_o=\varepsilon_o E_o\{\delta(t)+\Phi(t)\}+\sigma E_o \tag{4.14}$$

---

[21] Sometimes it is used another function called potential decay function (or dielectric relaxation function), $\Psi(t)$ [Daniel67]. The dielectric response function is the time derivative of this function.

It should be noted that the polarisation current represents the adjustment of the polarisable entities to the step field and it should go to zero at very long times. On the other hand, the steady state current (DC) is the continuous motion of free carriers from one electrode to the other.

The step function corresponds to the measurement of the dielectric constant (the so called time domain (TD) measurements) by measuring the discharge current. This situation can be treated as the sum of two step functions (according to the superposition principle), one E_o from $-\infty$ to $+\infty$ and the second a negative step function starting at t=0.

The frequency domain (FD) formalism is related to the time domain by Fourier transforms (appearing first in the convolution integral present in Equation 4.10). It is possible to write Equation (4.1), considering just the linear term:

$$P(\omega)=\varepsilon_o\chi(\omega)E(\omega) \tag{4.15}$$

Where the frequency dependent susceptibility, $\chi(\omega)$, is the Fourier transform of the response function,

$$\chi(\omega)=\chi'(\omega)-i\chi''(\omega)=\frac{\varepsilon(\omega)-\varepsilon_\infty}{\varepsilon_o}=\int_0^{+\infty}\Phi(t)e^{-i\omega t}dt$$

with

$$\chi'(\omega)=\int_0^{+\infty}\Phi(t)\cos(\omega t)dt \tag{4.16}$$

$$\chi''(\omega)=\int_0^{+\infty}\Phi(t)\sin(\omega t)dt$$

For zero time the real part of the susceptibility can have a value different from zero (representing the static value of the susceptibility) and the imaginary part has to be zero. Using reverse Fourier transforms it is possible to obtain the dielectric response function from either of the susceptibility components.

In measurements performed in time domain the currents obey the Curie-Weiss-von Schweidler law (also discussed in 3.4)

$$\Phi(t)\propto i(t)\propto t^{-n}. \tag{4.17}$$

A loss peak is observed in the log-log graph of current versus time as two straight lines with slopes $-n$ and $-(1+m)$ passing by a slope of -1 at the peak maximum. The response function representing the peak is [Jonscher83]:

$$\Phi(t)\propto i(t)\propto\frac{1}{(\omega t)^n+(\omega t)^{1+m}}, \tag{4.18}$$

For a Debye process there is an exponential decay (with slope -1) and for all other cases more than one process have to be considered to explain a non-exponential law.

From the current measurements under a step function it is possible to obtain an approximate expression for the imaginary permittivity developed by Hamon [Hamon52]. For a sample of geometrical capacitance C_o the current corresponding to the application of a step voltage (as in Equation (4.11-*ii*)) as stated before, obeys the Curie-Weiss-von Schweidler,

$$i(t) = Kt^{-n}. \tag{4.19}$$

(where K is a constant determined from the experiment). From Equation (4.14) and not considering the contributions from the delta-function and the DC conductivity, the response function is

$$\Phi(t) = \frac{K}{C_o V_o} t^{-n}, \tag{4.20}$$

and the imaginary susceptibility can be calculated from the last equation in (4.16)

$$\chi''(f) = \varepsilon''_r(f) = \frac{a}{C_o V_o} \frac{1}{2\pi f} i(0.1/f) = \frac{a}{C_o V_o} t i(t), \tag{4.21}$$

where $t = 0.1/f = \pi/5\omega$ and a is a constant that depends on the exponent n (expression valid for $0 < n < 2$). If $0 < n < 1$ then a is close to unity.

It is possible to deduce a similar approximation for the frequency derivative of the real component of the dielectric constant [Dias96]:

$$\frac{d\varepsilon'(\omega)}{d(\ln\omega)} \approx \frac{1}{C_o V_o} \frac{1}{\omega} i(t) \approx -\frac{2}{\pi} \varepsilon''(\omega) \quad \text{and } \omega t = 0.56146. \tag{4.22}$$

Finally the real and imaginary components are related by the Kramer-Kronig relations (consequence of the casuality principle):

$$\begin{aligned} \chi'(\omega) &= \frac{2}{\pi} \mathbf{P} \int_0^\infty \frac{x\chi''(x)}{x^2 - \omega^2} dx \\ \chi''(\omega) &= \frac{2\omega}{\pi} \mathbf{P} \int_0^\infty \frac{\chi''(x)}{x^2 - \omega^2} dx \end{aligned} \tag{4.23}$$

where **P** represents the Cauchy principal value (ignoring the imaginary contribution arising at the pole $x = \omega$). As a consequence the area under the loss (imaginary component of susceptibility) is related to the polarisation increment.

4.4 Debye model and related empirical models

4.4.1 Debye model

The physical model for non-interacting dipoles developed by Debye was characterised by a single relaxation time. Based on the superposition principle and on an exponential approach to

equilibrium, the theory results in an exponential dependence of the dielectric response function:

$$\Phi(t)=\frac{1}{\tau}e^{-t/\tau} \tag{4.24}$$

For a constant field (step function) the displacement is:

$$D(t)=\varepsilon_o E_o\left\{\varepsilon_\infty+(\varepsilon_s-\varepsilon_\infty)\left(1-e^{-\frac{t}{\tau}}\right)\right\} \tag{4.25}$$

However the most common function is the harmonic variation of the field (used experimentally in frequency domain measurements). For this variation of the electric field the permittivity is (Debye equations):

$$\varepsilon=\varepsilon_\infty+\frac{\varepsilon_s-\varepsilon_\infty}{1+i\omega\tau}=\begin{cases}\varepsilon'=\varepsilon_\infty+\dfrac{\varepsilon_s-\varepsilon_\infty}{1+(\omega\tau)^2}\\ \varepsilon''=\dfrac{(\varepsilon_s-\varepsilon_\infty)\omega\tau}{1+(\omega\tau)^2}\end{cases} \tag{4.26}$$

The imaginary part exhibits a symmetrical loss peak that has a maximum at $\omega_{max}\tau=1$ with amplitude $\varepsilon''_{max}=\dfrac{\varepsilon_s-\varepsilon_\infty}{2}$.

The Debye behaviour is observed in very few materials among which are the dilute solutions of large polar molecules in non-polar solvents [Daniel67]. Also [Jonscher83] reports another example of a ferroelectric single crystal of cesium dihydrogen phosphate (CsH_2PO_4)[22].

4.4.2 Distribution of relaxation times

Some dielectrics show a near-Debye behaviour exhibiting relaxation peaks that are still symmetric but broader and with lower loss maxima. At the other extreme are materials showing no loss peaks or very wide and distorted peaks. Examples of this response are many insulating materials, including pure polyethylene (for more details see 4.8).

One of the more simple approaches to explain the departure from the single relaxation time model is to consider the sum of several Debye processes with different relaxation times. In the limit there will be a distribution function of relaxation times, $g(\tau)$ [Williams97, Daniel67]:

[22] Presented as the best example of "ideal" Debye response found by this author.

$$\Phi(t) = \int_0^{+\infty} g(\tau)\frac{1}{\tau}e^{-t/\tau}d\tau$$
$$\varepsilon_s - \varepsilon_\infty = \int_0^{+\infty} g(\tau)d\tau \tag{4.27}$$

In a real material different relaxation times and a distribution of effective dipole strengths are observed since not all dipoles will be identical. Furthermore some rotations will be preferred to others depending not only on the rotating dipole but also on the surrounding environment. Hence this will lead to a distribution of relaxation times, meaning a distribution of activation energies and pre-exponential factors (for example, when there is an Arrhenius temperature activated process–see 4.5). Nevertheless a complete physical interpretation requires obtaining (and understanding) the distribution function of a specific material.

4.4.3 Related empirical models

In order to account for the departure from the ideal behaviour the Debye relations (Equation 1.26) were modified by introducing some empirical fitting parameters. One of the first presented was the one-parameter *Cole-Cole* function [Cole41]:

$$\varepsilon = \varepsilon_\infty + \frac{\varepsilon_s - \varepsilon_\infty}{1+(i\omega\tau)^\alpha} \quad 0<\alpha\leq 1 \tag{4.28}$$

with a symmetrical but broader loss peak with maximum at $\omega_{max}\tau = 1$ and amplitude $\varepsilon''_{max} = \frac{\varepsilon_s - \varepsilon_\infty}{2}\tan\frac{\alpha\pi}{4}$.

To include non-symmetrical peaks *Davidson-Cole* [Davidson51] proposed another one-parameter function:

$$\varepsilon = \varepsilon_\infty + \frac{\varepsilon_s - \varepsilon_\infty}{[1+(i\omega\tau)]^\beta} \quad 0<\beta\leq 1 \tag{4.29}$$

with maximum at $\omega_{max}\tau = \tan\frac{\pi}{2(1+\beta)}$.

Also in 1941 Fuoss and Kirkwood rewrote the imaginary part of the dielectric constant for the Debye model (Equation 4.26) as

$$\varepsilon'' = \varepsilon''_{max}\,\mathrm{sech}(\ln\omega\tau) \tag{4.30}$$

From this expression a parameter γ was introduced originating the symmetrical *Fuoss-Kirkwood* function only valid for the imaginary permittivity:

$$\varepsilon'' = \varepsilon''_{max}\,\mathrm{sech}(\gamma\ln\omega\tau) = 2\varepsilon''_{max}\frac{(\omega\tau)^\gamma}{1+(\omega\tau)^{2\gamma}} \quad 0<\gamma\leq 1 \tag{4.31}$$

Table 4.1 – Some empirical and physical models for dielectric relaxation [Jonscher83], [Scarpa95], [Havriliak97] and [Das Gupta99]*.

Model	Function	Parameters	
One parameter			
Debye	$\varepsilon'' \propto \frac{1}{\left(\frac{f}{f_P}\right)^{-1} + \left(\frac{f}{f_P}\right)}$	$\alpha = 1$	$\beta = 1$
Cole-Cole	$\varepsilon'' \propto \frac{1}{\left(\frac{f}{f_P}\right)^{-\alpha} + \left(\frac{f}{f_P}\right)^{\alpha}}$	$0 < \alpha < 1$	$\beta = 1$
Davidson-Cole	$\varepsilon'' \propto \frac{1}{\left(\frac{f}{f_P}\right)^{-1} + \left(\frac{f}{f_P}\right)^{\beta}}$	$\alpha = 1$	$0 < \beta < 1$
Fuoss-Kirkwood	$\varepsilon'' \propto \frac{2\left(\frac{f}{f_p}\right)^{\gamma}}{1+\left(\frac{f}{f_p}\right)^{\gamma}}$	$0 < \gamma < 1$ Gives only the imaginary part	At high and low frequency limits is equivalent to Cole-Cole
Two parameter			
Havriliak-Negami	$\varepsilon'' \propto \frac{1}{\left(\frac{f}{f_P}\right)^{-\alpha} + \left(\frac{f}{f_P}\right)^{\alpha\beta}}$	$0 \le \alpha$	$\alpha\beta < 1$
Jonscher/ Dissado-Hill (Dipolar peak)	$\varepsilon'' \propto \frac{1}{\left(\frac{f}{f_P}\right)^{-m} + \left(\frac{f}{f_P}\right)^{1-n}}$	$0 < m < 1$ $(m = \alpha)$	$0 < n < 1$ $(n = 1-\alpha\beta)$
Jonscher/ Dissado-Hill (QDC process)	$\varepsilon'' \propto f^{n_1-1}$ for $f << f_c$ $\varepsilon'' \propto f^{n_2-1}$ for $f >> f_c$	$0 < n_2 < 1$ (also used is $m = 1\text{-}n_2$)	$0 < n_1 < 1$ (also used is $n = n_1$)

* $\omega = 2\pi f$, f_p is the peak maximum frequency

with $\varepsilon''_{max} = \frac{\varepsilon_s - \varepsilon_\infty}{2}\gamma$. In the low and high frequency limits this expression becomes equivalent to the Cole-Cole function.

Based on a modification of the dielectric response function in Equation (4.24) Köhlrausch[23] (1854) and independently Williams and Watts [Williams70] proposed

$$\Phi(t) = t^{k-1} e^{-(t/\tau)^k} \tag{4.32}$$

this time domain function was converted to the frequency domain by Williams and Watts resulting in a non-symmetrical loss peak.

A more general approach is to consider a two-parameter function like the one of *Havriliak-Negami* convenient to represent the loss peak region [Havriliak66,97]

$$\varepsilon = \varepsilon_\infty + \frac{\varepsilon_s - \varepsilon_\infty}{\left[1 + (i\omega\tau)^\alpha\right]^\beta} \quad 0 \le \alpha \text{ and } 0 < \alpha\beta \le 1 \tag{4.33}$$

The influence of the two parameters in the shape of the loss peak could be seen isolated from each other on the first two models presented (Cole-Cole and Cole-Davidson). The α parameter influences both slopes of the peak (making it broader or sharper) while β changes only the high frequency slope (making the peak asymmetrical). Therefore α represents the peak width and β its skewness.

In Table 4.1 are represented some of the functions presented above[24] and also those resulting from the physical models of Jonscher and Dissado-Hill (which will be discussed later in 4.8).

4.5 Temperature dependence

The permittivity depends not only of frequency (or time) but also on the temperature[25] since the relaxation arises from a thermal activation over an energy barrier.

It is observed experimentally that the dielectric loss peaks can depend differently on temperature in accordance with the physical characteristics of the mechanism that gives rise to the transition. For the β or α_a loss peak (glass transition) the relaxation time (τ) dependency

[23] Called Kölhlraush or stretched exponential law, it was found by Kölhlraush for the charge decay in a Leiden flask.

[24] The functions are presented differently in a more suitable form for direct fitting of the experimental dielectric relaxation data.

[25] Permittivity can also depend on the pressure.

follows the Vogel-Fulcher-Tamman-Hesse (VFTH) equation [Schönhals97]

$$\tau \propto \tau_o \exp\left(\frac{A}{T-T_o}\right) \tag{4.34}$$

where A is related to the activation energy, T_o is called the ideal glass transition temperature or Vogel temperature and τ_o is the pre-exponential factor. This equation is equivalent to the Williams-Landel-Ferry (WLF) equation

$$\tau \propto \tau_{or} \exp\left(\frac{C_1(T-T_r)}{C_2+T-T_r}\right), \tag{4.35}$$

where T_r is a reference temperature and C_1 and $C_2=T_r-T_o$ are the WLF parameters.

For the γ transition the equation is Arrhenius-like

$$\tau \propto \tau_o \exp\left(\frac{E_a}{\kappa_B T}\right) \tag{4.36}$$

For a single relaxation time (Debye) and if the above equation (4.36) is considered the imaginary permittivity is

$$\varepsilon''(T) \propto (\varepsilon_s(T)-\varepsilon_\infty(T))\frac{\omega\tau_o \exp(E_a/\kappa_B T)}{1+\omega^2\tau^2_o \exp(2E_a/\kappa_B T)} \tag{4.37}$$

If ε_s and ε_∞ are temperature independent the activation energy can be obtained from the area under ε'' in $\log(1/T)$ graph and is inversely proportional to this area (and not related to the frequency). If the local field theories of Onsager, Frölich and Debye (see 4.2) are considered [McCrum67] then

$$\varepsilon_s(T)-\varepsilon_\infty(T)=\frac{B}{T}, \tag{4.38}$$

is a good approximation (B is a constant) and the relation between the area and the activation energy is maintained but not depends on the values of ε_s and ε_∞ at the temperature of the peak maximum.

If the relaxation process is of non-Debye type, it is usually found that the temperature dependence does not change much [Jonscher83].

4.6 Presentation of dielectric data

Dielectric data presentation is an important issue since it allows us to identify some relaxation processes and to classify a material according to its dielectric response. The graphs of real permittivity and dielectric loss with frequency and temperature should be enough to numerically calculate the distribution function. However experimental data is usually too incomplete and not precise enough to allow these calculations. Also in practice the materials

will show the sum of the presence of more than one dielectric process (it is typical for a graph of dielectric loss versus frequency or temperature to exhibit two or more dielectric loss peaks). So instead of calculating the distribution functions an attempted is made to identify the processes by using the empirical functions discussed in 4.4 and also Jonscher and Dissado-Hill functions (see 4.8).

Plotting of the data becomes essential in identifying the physical processes. First it is necessary to choose which variables are going to be plotted (capacitance, permittivity, conductivity, impedance, etc.). Since dielectric data is mathematically a complex variable it is usual to make plots in the complex plane besides the linear and log-log graphs of the real and imaginary components with frequency and temperature.

4.6.1 Parallel and series circuits

In experimental measurements the most common geometry of the samples is the thin parallel plane with area A and thickness d (with $A \gg d^2$). The geometric capacitance is given by $C_o = \frac{A}{d}\varepsilon_o$, for a dielectric with permittivity ε (and relative permittivity ε_r) the capacitance

$$C = C_o\varepsilon_r = \frac{A}{d}\varepsilon \tag{4.39}$$

As stated in 4.3 a complex dielectric constant can be defined and a complex capacitance is:

$$C(\omega) = C'(\omega) - iC''(\omega) = \frac{A}{d}[\varepsilon''(\omega) - i\varepsilon'(\omega)] \tag{4.40}$$

The two more simple equivalent circuits that can represent a dielectric material are the parallel and series ones for a pure capacitor and a pure resistance (equivalent circuits using passive elements).

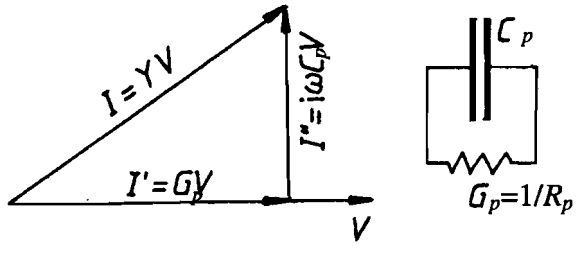

Figure 4.1 – Parallel circuit representing a dielectric material, G_p is the conductance and C_p the capacitance (both are frequency independent). The current I leads the voltage V (with a phase shift between the two). The admittance Y of the system is represented by the equivalent circuit on the right end side [Jonscher83].

For the parallel circuit it is more suitable to use a complex admittance (see Figure 4.1). This is the natural way to represent two parallel relaxation processes in which the voltage drives two currents [Jonscher83].

The admittance is related to the current and voltage and for a sinusoidal field (Z is the circuit impedance):

$$Y = \frac{I}{V} = \frac{1}{Z} = G_p + i\omega C_p \text{ and } \tan\delta = \frac{1}{\omega C_p R_p} \tag{4.41}$$

When two physical processes are acting in series, the natural presentation becomes the series circuit of Figure 4.2.

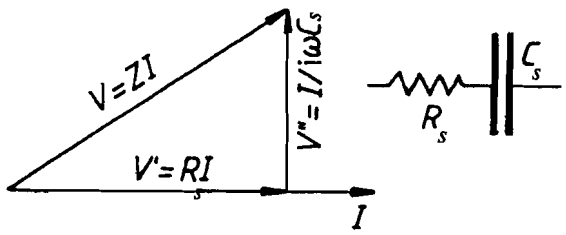

Figure 4.2 - Series circuit representing a dielectric material, R_s is the resistance and C_s the capacitance (both are frequency independent). The impedance Z of the system is represented by the equivalent circuit on the right-end side. The voltage V leads the current I (with a phase shift between the two) [Jonscher83].

For a sinusoidal field the impedance is:

$$Z = \frac{V}{I} = R_s + \frac{1}{i\omega C_s} \text{ and } \tan\delta = \omega C_s R_s \tag{4.42}$$

4.6.2 Cole-Cole plots

Since a complex representation was chosen for the permittivity, a plot in the complex plane was introduced by Cole and Cole [Cole41]. In this diagram the y-axis represents the imaginary component and the x-axis the real component of permittivity.

For a Debye process (single relaxation time) the plot is a semi-circle with radius $\frac{\varepsilon_s - \varepsilon_\infty}{2}$ and centre at $\left[\frac{\varepsilon_s + \varepsilon_\infty}{2}, 0\right]$, as can be seen Figure 4.3 – (a). Represented in Figure 4.3 – (b) is the Cole-Cole function, which is a depressed semi-circle with radius $\frac{\varepsilon_s - \varepsilon_\infty}{2}\text{cosec}\frac{\alpha\pi}{2}$ and centre

coordinates $\left[\frac{\varepsilon_s+\varepsilon_\infty}{2}, -\frac{\varepsilon_s-\varepsilon_\infty}{2}\operatorname{cotan}\frac{\alpha\pi}{2}\right]$. The parameter α is the tilt angle of the circular arc to the x-axis. For Cole-Davidson distribution the plot is no longer symmetrical, and the semi-circle is skewed. The parameter β is related to the tilt angle of the tangent to the x-axis $\left(\frac{(1-\beta)\pi}{2}\right)$.

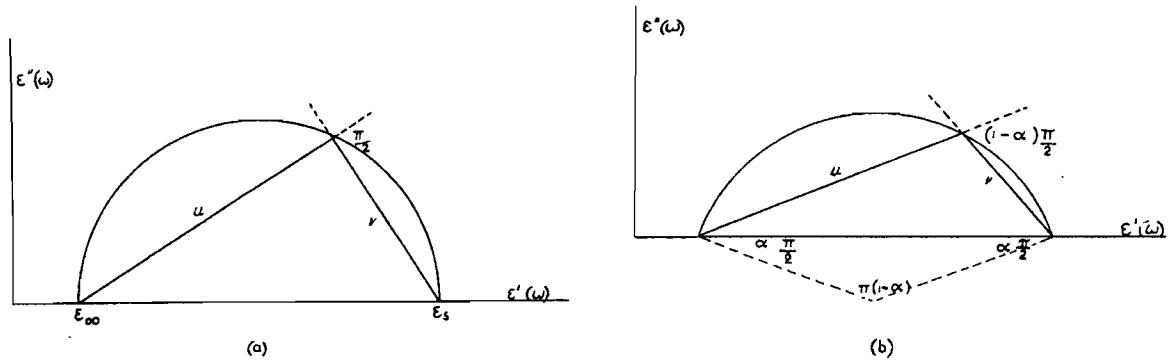

Figure 4.3 – (a) Debye process; (b) Cole-Cole distribution with parameter α [Daniel67].

4.6.3 Displaying dielectric relaxation data

Cole-Cole plots are useful when the steady conductivity is negligible. However when this component becomes important, Grant (1958) uses a complex plot of the conductivity,

$$\sigma(\omega)=\sigma'(\omega)+i\sigma''(\omega)=i\omega(\varepsilon''-i\varepsilon') \tag{4.43}$$

Besides the two simple circuits described above, it is possible to describe dielectric data as a combination of series and parallel circuits. Plotting the conductivity and the Cole-Cole graphs for the measured dielectric data can help to obtain the equivalent circuit that represents in a simplified manner the dielectric characteristics of the material under study. Figure 4.4 shows diagrams of complex permittivity and conductivity for same equivalent circuits. Interesting to see is the effect of the steady conductivity that distorts the permittivity plot and the effect of ε_∞ distorting the conductivity plot.

Jonscher [Jonscher83] proposes a slight different approach to the presentation of data. When the existence of a series combination of physical processes is suspected the complex impedance plot is suggested. For the parallel combination the complex admittance plot is used. These graphs together with the graph of susceptibility versus frequency are shown in Figure 4.5 for some equivalent circuits and the corresponding physical processes.

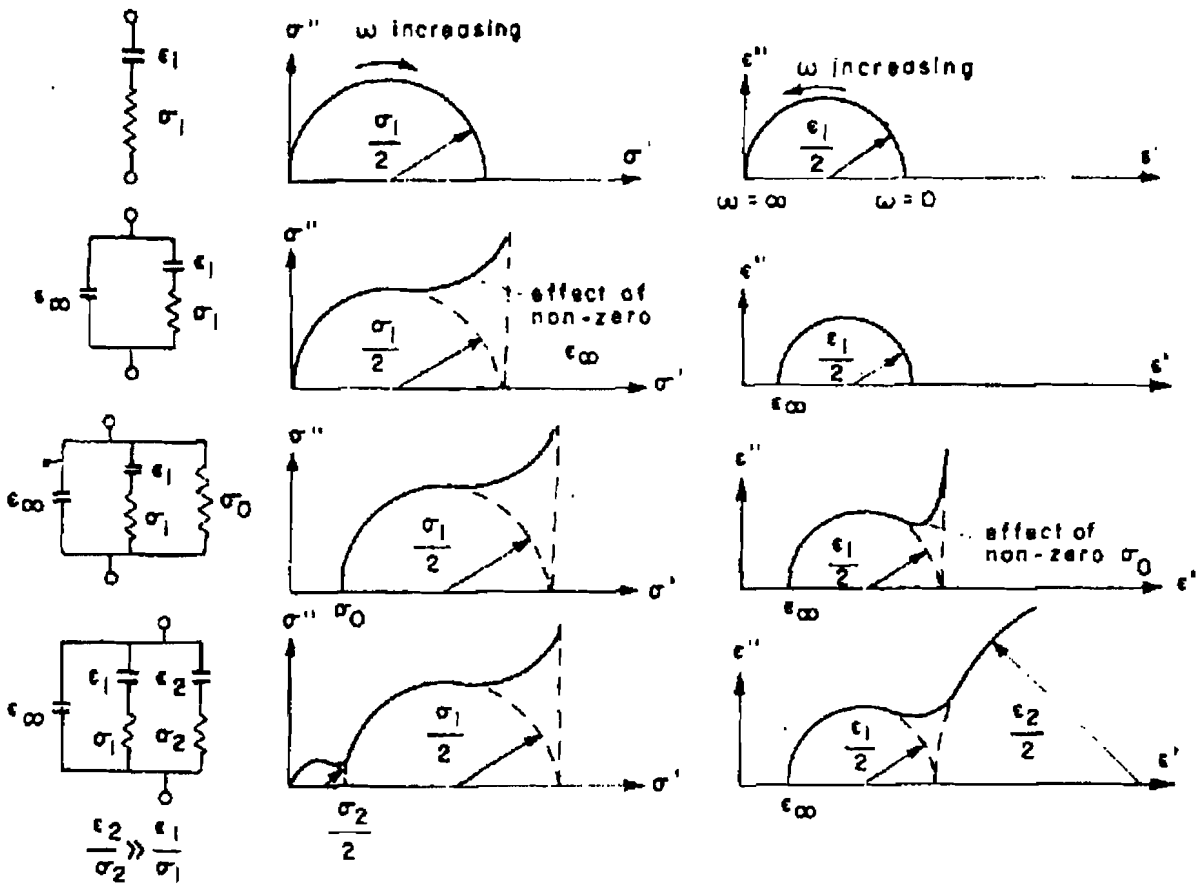

Figure 4.4 – Complex conductivity and permittivity (Cole-Cole) diagrams for four different equivalent circuits [Daniel67].

4.6.4 Temperature dependent graphs

The more complete way to represent the dielectric constant is to have three-dimensional plots of the real and imaginary dielectric constant (or of any of the other variables discussed above) as function of frequency and temperature.

Many times in practice instead of making measurements by changing the frequency at a fixed temperature the opposite is done and data is obtained at constant frequency with a sweep in temperature. Usually log $1/T$ is used because of the expected presence of activated processes.

If there is no major structural changes in the material the temperature dependence is not very strong. Under this assumption it is possible to obtain normalised curves from data obtained at different temperatures [Jonscher83].

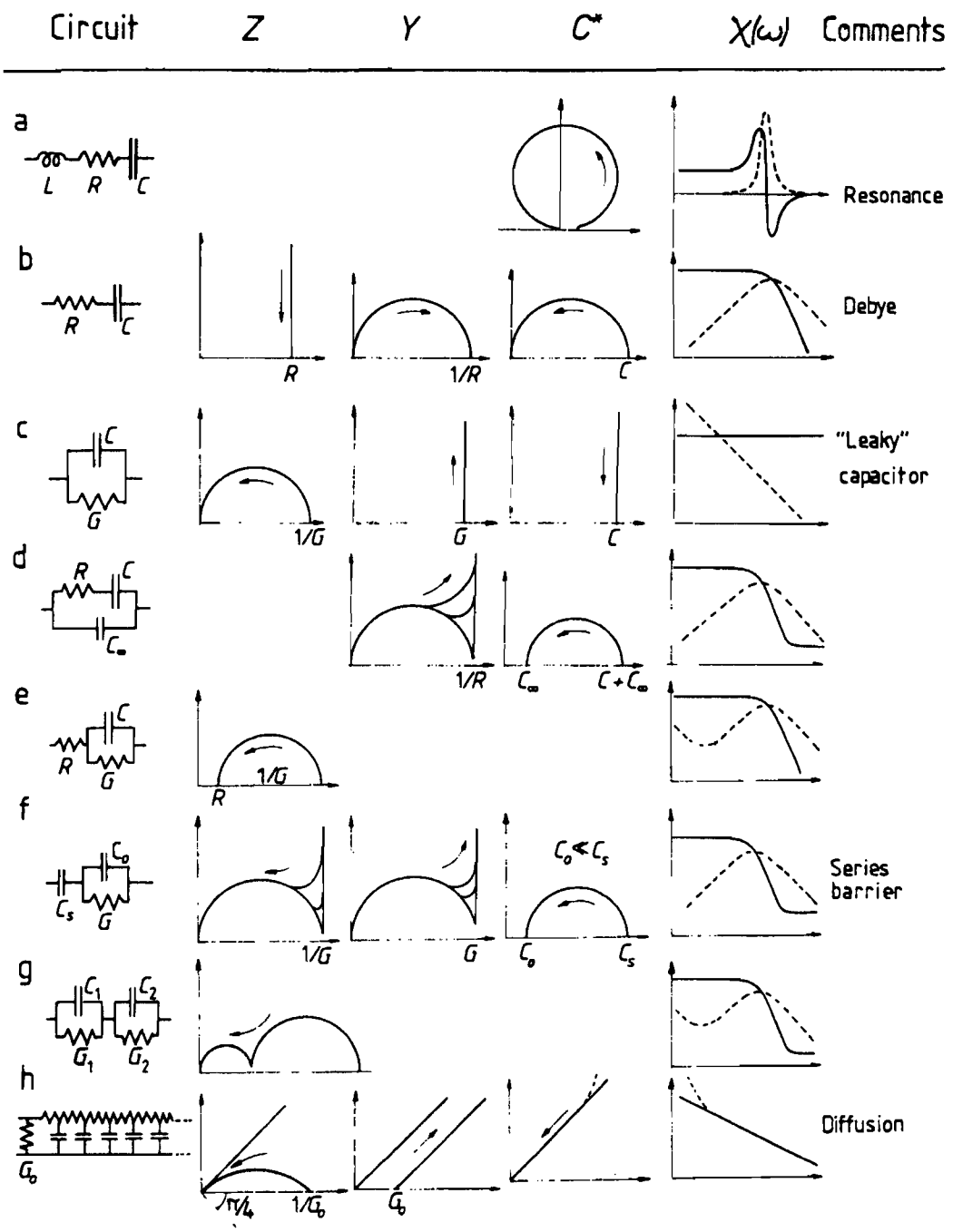

Figure 4.5 – Schematic representation of the properties of simple circuit combination of frequency independent elements. Arrows indicate the direction of growing frequency. When appropriate "Comments" refer to the simple physical significance of the various equivalent circuits [Jonscher83].

When plotting graphs of the log (dielectric loss) versus log ($1/T$) with constant frequency, important information can be obtained from the observed loss peaks: (*a*) the temperature maximum (relevant to find the relaxation time, meaning the pre-exponential factor of equations (4.34) to (4.36)); (*b*) the area below the loss peak (relevant to find the activation energy as explained in 4.5) and (*c*) the shape of the loss peak.

Another possibility to obtain the relevant parameters of Equations in 4.5 (4.34 to 4.36) is to fit the experimental data using the suitable temperature dependent equation [McCrum67].

4.7 Main classes of dielectric solid materials

A summary of the main types of dielectric response found in materials is seen in Table 4.2 with the expected frequency dependence of $\chi''(\omega)$ for the limits of high frequency (short time) and low frequency (long time).

Table 4.2 – Summary of the main types of dielectric response found in materials

	High-frequency	**Low-frequency**	**Loss peaks**	**Observations**
Dipoles	$\chi''(\omega) \propto \omega^{n-1}$	$\chi''(\omega) \propto \omega^{m}$	Yes	
Space charge peaks	$\chi''(\omega) \propto \omega^{n-1}$	$\chi''(\omega) \propto \omega^{m}$	Yes	Broader peaks and at lower frequencies than dipolar peaks
Carrier dominated	$\chi''(\omega) \propto \chi'(\omega) \propto \omega^{n_1-1}$	$\chi''(\omega) \propto \chi'(\omega) \propto \omega^{n_2-1}$	No	n_1 close to unity n_2 close to zero
DC conductivity		$\omega \to 0$: $\chi'(\omega) \to$ constant $\chi''(\omega) \propto \frac{\sigma_{DC}}{\omega}$	No	
Maxwell-Wagner-Sillars (interfacial)		$\chi''(\omega) \propto \omega^{-1}$ $\chi'(\omega) \propto \omega^{-2}$	Yes	Identical to space charge peaks at low frequency
Low-loss	$\chi''(\omega) \propto \chi'(\omega) \propto \omega^{n-1}$	$\chi''(\omega) \propto \chi'(\omega) \propto \omega^{n-1}$	No	n close to unity

A more detailed review of the dielectric relaxation responses is given below for the main types found in insulators:

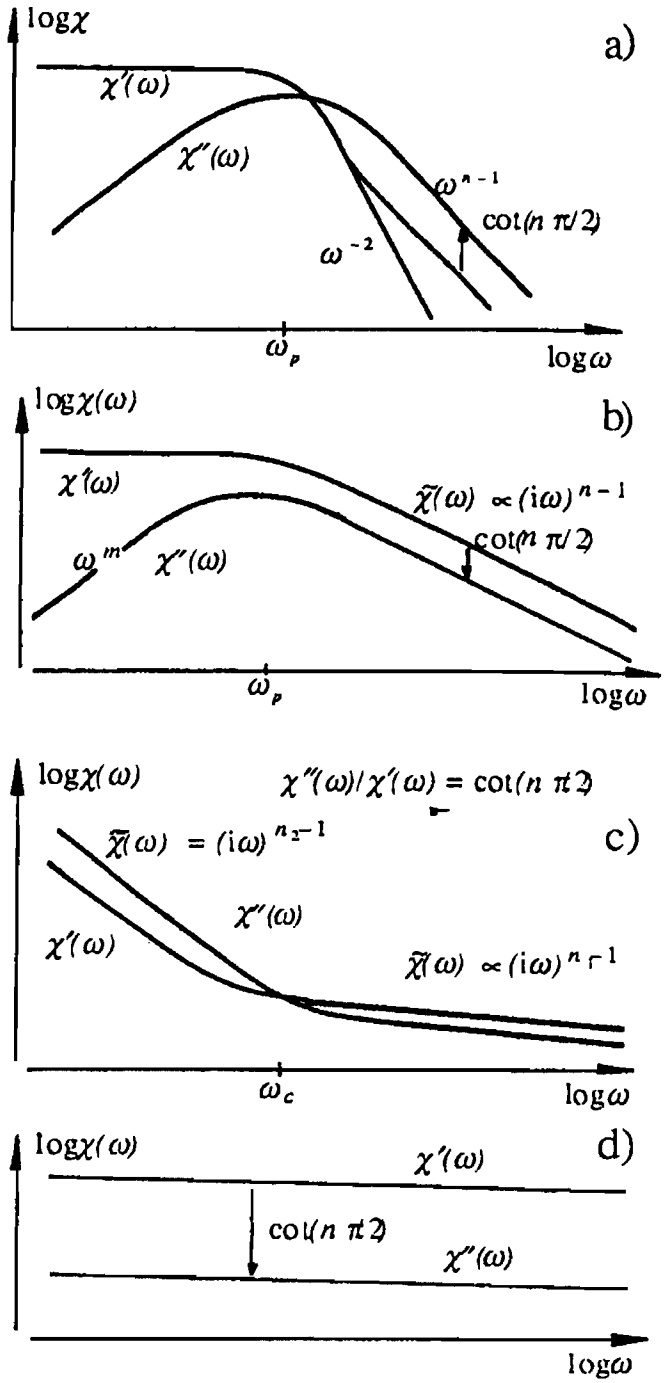

Figure 4.6 – Frequency dependencies of typical dielectric systems [Jonscher92]. Fractional power laws are observed for all systems represented at both low and high frequency limits. (a) Near-Debye (exponent –2 for χ' corresponds to true-Debye). (b) Broader and asymmetric loss peak. (c) Carrier dominated system. (d) "Flat-loss" in a low-loss material.

(a) Dipolar materials – near Debye behaviour

As stated before *true-Debye* behaviour is only observed in polar liquids. For solids only a single crystal ferroelectric obeys Debye relations in the frequency domain

$$\chi(\omega)=\varepsilon(\omega)-\varepsilon_{\infty}=\chi'(\omega)-i\chi''(\omega)\propto\frac{1}{1+i\omega\tau} \tag{4.44}$$

with the corresponding Laplace transform in the time domain

$$i(t)\propto\exp\left[-\frac{t}{\tau}\right]. \tag{4.45}$$

The related fractional power law for the high frequency limit is (see Figure 4.6-a)).

$$\chi'(\omega)\propto\omega^{-2} \tag{4.46}$$

Near-Debye loss peaks will have broader peaks and the high-frequency limit will follow a fractional power law

$$\chi(\omega)\propto(i\omega)^{n-1},\qquad \omega>>\omega_p \tag{4.47}$$

The exponent n is close to 0 and typically 0.1 or less. The components of the susceptibility, $\chi'(\omega)$ and $\chi''(\omega)$, follow the same law and are parallel in a log-log plot. Examples of materials presenting this kind of response are highly dilute dipolar systems in crystalline solids, highly pure p-n junctions and Schottky diodes, liquid like polymers and glasses above T_g.

(b) Dipolar materials – broader and asymmetric loss peaks

The response follows the relations in Table 4.2 for dipolar peaks (Jonscher and Dissado-Hill) for both high and low frequency. The exponents m, n are independent. The usual range of values for n is $0.5 < n < 0.9$ resulting in a much lower loss and flatter frequency dependence. Figure 4.6-b) represents the typical spectra in the FD for this kind of response. Materials showing this behaviour are, among others, polymers below T_g and many p-n junctions of medium and high impurity density.

The dipolar loss peak can be fitted by an empirical relation such as *Havriliak-Negami* (see Equation 4.33). The narrow range of frequencies limits the fitting accuracy.

(c) Carrier dominated systems – Low frequency dispersion (LFD)[26]

Instead of dipoles the material polarisation is dominated by ions or electrons. In these case the DRS spectra in FD shows no loss peaks (Figure 4.6-c)). At a characteristic frequency, ω_c, there is the change between two fractional power law regimes with different exponents,

$$\begin{aligned}\chi(\omega)&\propto(i\omega)^{n_1-1}\quad 0<n_1<1\quad \omega>\omega_c\\ \chi(\omega)&\propto(i\omega)^{n_2-1}\quad 0<n_2<1\quad \omega<\omega_c\end{aligned} \tag{4.48}$$

and

[26] Also called quasi-DC (QDC) as can be seen in 4.8.2.

$$\frac{\chi''(\omega)}{\chi'(\omega)} = \cot\frac{n\pi}{2}, \tag{4.49}$$

independent of frequency. Below ω_c, $\chi''(\omega) > \chi'(\omega)$ and the material has high value for the loss and the exponent is near 0. At ω_c a crossover between the components occurs and above this frequency the exponent is close to 1. Susceptibility increases towards lower frequencies without showing any saturation. Below and above ω_c the components of $\chi(\omega)$ are parallel in a log-log plot.

The sharp rise at low frequencies means that charge is being stored which is one of the differences from DC conductivity where no charge storage occurs. Also DC is characterised by a steady state distribution of charge and there is no change with time. For LFD the ratio $\chi'(\omega)/\chi''(\omega)$ is typically 0.01 to 0.1 and represents the fraction of stored energy. The DC limit can be hidden by LFD.

Examples of LFD responses are ionic and fast ionic conductors specially at high temperatures, hopping electronic system at the low frequency end, humid materials, interfacial Maxwell-Wagner-Sillars processes, etc.

(d) Flat loss of low loss dielectric materials

Finally in Figure 4.6-d) the low loss dielectric exhibits a single fractional power law with both components of susceptibility parallel in the log-log plot. It obeys the same equations (4.48) as in (c) with only one exponent n close to 1 and the susceptibility is nearly independent of frequency. Pure polyethylene has this type of response [Jonscher99a&01, McLachlan99]. However some materials deviate from this pattern. It is possible to find examples of flat loss which do not follow the universal power law and whose value of loss is comparatively high. Illustrative examples of systems showing flat loss are inorganic ceramics (ferroelectric ceramics), some pure polymers (PE and PVDF-α) and non-ionic glasses.

The different types of low loss responses are:

i) "Classical" type - the universal relations are obeyed (it is possible to determine ε_∞, an exponent n can be identified and ratio $\chi''(\omega)/\chi'(\omega)$ is frequency independent). The dielectric spectrum of pure PE and PE with different admixtures of graphite follows this trend;

ii) The real component of the susceptibility, $\chi'(\omega)$, cannot be determined since it is not possible to obtain a value for ε_∞. Nevertheless a constant slope is observed for $\varepsilon'(\omega)$ and the ratio $\varepsilon''(\omega)/\varepsilon'(\omega)$ is consistent with that slope (however $\varepsilon'(\omega)$ and $\varepsilon''(\omega)$ are not parallel).

iii) The log-log plot shows relatively flat loss behaviour but no power law can be obtained for $\varepsilon'(\omega)$ and $\varepsilon''(\omega)$. The values of $\varepsilon''(\omega)/\varepsilon'(\omega)$ can be comparably large and there is no ratio for $\chi''(\omega)/\chi'(\omega)$.

iv) A power law can be related to $\chi''(\omega)$ and $\chi'(\omega)$ but their ratio is not consistent with universal behaviour.

According to Jonscher [Jonscher92, 99] the dielectric spectra of a typical dielectric material will usually present the following response regions (Figure 4.7):

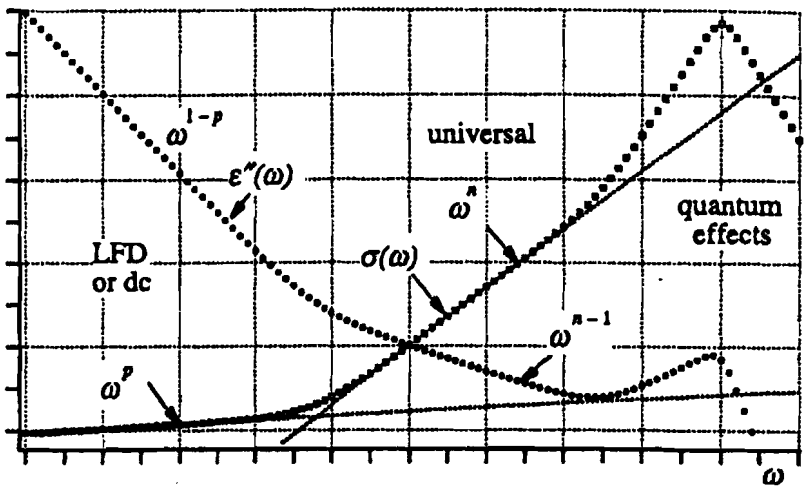

Figure 4.7 – Schematic representation of the dielectric spectrum of an ionic conductor [Jonscher99]. The log-log plot shows $\varepsilon''(\omega)$ and $\sigma'(\omega)=\omega\varepsilon''(\omega)$ and characteristic regions (1), (2) and (3).

(1) a low-frequency region that can be either dominated by DC conductivity or by LFD, presenting an Arrhenius behaviour;
(2) an intermediate region (from Hz to GHz) that may or may not present superimposed dipolar peaks. The temperature dependence will not be Arrhenius with a weak dependence on temperature and dominated by many-body interactions;
(3) the optical frequency region (GHz to THz) may also present loss peaks resulting from quantum transitions;
(4) sometimes at the top of region (3) a loss peak or saturation of conductivity may appear.

An alternative form to represent relaxation is time domain (TD) instead of frequency domain as was seen before (4.3). In Figure 4.8 the time response for the classes of materials discussed

above is shown. The experimental relation known as the stretched exponential law is also depicted in Figure 4.8 (see equation 4.32):

The short time response is similar for both dipolar and charge carriers but at long times the reservoir of dipoles is exhausted while the carriers have no limitation.

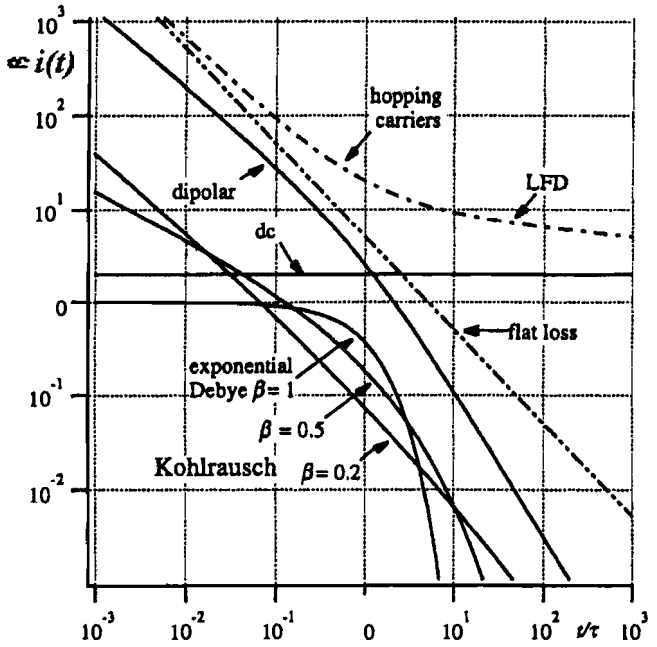

Figure 4.8 – Time domain response for the different types of dielectric materials [Jonscher99]. Represented are Debye, dipolar, DC, LFD, flat loss and also Kölhlrausch law(β is the *n* parameter of Equation 4.17).

4.8 Physical models

Besides the Debye model and the related distribution of relaxation times model other physical models have been proposed along the years (local field theories, distribution of hopping probabilities, interfacial Maxwell-Wagner-Sillars, etc.). However these models are unable to explain the wide variety of dielectric responses observed in different materials. Jonscher [Jonscher83, Jonscher92,97,99,99a&01] has proposed an "universal" model based on a very simple approach and Dissado and Hill [Dissado83,84&89] developed a model based on quantum mechanics. Both will be presented next.

4.8.1 Jonscher's Universal Law

From the analysis of experimental data of the dielectric spectra, Jonscher [Jonscher92, 99] has proposed a universal characteristic with the susceptibility spectra in the frequency domain following fractional power laws.

For dipolar materials, for instance, the power laws in the limits of high frequency (short time) and low frequency (long time) above and below a loss peak are:

$$\begin{aligned} \chi''(\omega) &= \cot\left(\frac{n\pi}{2}\right)\chi'(\omega) \propto \omega^{n-1} \qquad 0<n<1 \quad \omega >> \omega_p \\ \chi''(\omega) &= \tan\left(\frac{m\pi}{2}\right)[\chi'(0)-\chi'(\omega)] \propto \omega^{m} \qquad 0<m<1 \quad \omega << \omega_p \end{aligned} \tag{4.50}$$

ω_p is the loss peak frequency. The first relation corresponds to the falling part of the peak and the later to the rising. The corresponding relations in the time domain are:

$$\begin{aligned} i(t) &\propto t^{-n} \qquad t << \frac{\omega}{\omega_p} \\ i(t) &\propto t^{-m-1} \qquad t >> \frac{\omega}{\omega_p} \end{aligned} \tag{4.51}$$

The above equations are the Laplace transform of the frequency domain relations and also represent the well know Curie-Weiss-von Scheweidler law.

The following ratios are constant (depending only of the exponents n and m) and χ_s is the static susceptibility:

$$\begin{aligned} \frac{\chi''(\omega)}{\chi'(\omega)} &= \cot\left(\frac{n\pi}{2}\right) \qquad \omega >> \omega_P \\ \frac{\chi_s - \chi'(\omega)}{\chi''(\omega)} &= \tan\left(\frac{m\pi}{2}\right) \qquad \omega << \omega_P \end{aligned} \tag{4.52}$$

implying for the high frequency range a constant phase angle between the two components of $\chi(\omega)$.

In order to characterise the loss peak the Havriliak-Negami two parameter empirical relation can be used.

4.8.1.1 General description of "universal" fractional power law

Four parameters are needed to describe fully the "universal" dielectric response: the value of the characteristic frequency (ω_p for dipolar loss peaks and ω_c for carrier dominated systems), the amplitude of $\chi(\omega)$ and the exponents $m,n \in]0,1[$ (that determine the shape of the frequency response and time domain response[27]).

[27] The shape of response cannot be described with a single exponent.

Interactions are essential for the appearance of the universal character. Physically the consequence of the constant ratio $\frac{\chi''(\omega)}{\chi'(\omega)} = \cot\frac{n\pi}{2}$ (Equation 4.50) is a constant phase angle which in turn represents a energy criterion:

$$\frac{W_l}{W_s} = \cot\left(\frac{n\pi}{2}\right), \tag{4.53}$$

W_l is the energy lost per radian and W_s the energy stored at the loss peak. Jonscher[92] pointed out that this criterion is a direct consequence of Kramers-Kröning relations and independent of the physical mechanism. The limit $n\rightarrow 1$ conforms to low loss systems while $n\rightarrow 0$ to carrier dominated materials which are highly lossy systems. The energy criterion at microscopic level implies that the energy lost per reversal of every microscopic polarisation is independent of the rate of reversal. Considering that $\chi'(\omega)$ is directly related to the number of dipoles undergoing transitions then every dipole suffers the same amount of loss in every transition and the total macroscopic loss $\chi''(\omega)$ will be proportional to $\chi'(\omega)$.

4.8.1.2 Physical interpretation of universality

a) Dipolar materials

Jonscher [Jonscher97,99] has proposed a screening due to dipoles similar to that which happens with charge screening. It has been known for long time that the range of the coulombic field is limited by the screen made by charges on each other. A Debye screening length is calculated

$$\lambda_D = \frac{(\varepsilon k_B T)^{1/2}}{q^2 N^{1/2}}, \tag{4.54}$$

q is the particle charge and N the density of particles. A particle's electric field is almost completely shielded beyond a distance of a few λ_D and particles further way than this distance will not suffer the influence of this particle electric field. The number of particles within a sphere of radius λ_D is given by

$$\nu = \frac{4\pi}{3}(\varepsilon K_B T)^{3/2} q^{-3} N^{-1/2} \tag{4.55}$$

(it is interesting to observe that the number of particles (ν) increases with decreasing density (N)).

With dipoles the screening is much smaller than for charges but still large enough to influence relaxation. Considering dipoles (either molecular, ionic, induced atomic and ionic

polarisation) it is possible to define a dipolar screening radius (R_s) playing the same role as Debye screening length for charges:

$$R_s = r_1 \exp\left(\frac{\lambda_D^2}{\ell}\right) = \left(\frac{4\pi}{3}\right)^{-1/3} \exp\left(\frac{\varepsilon k_B T}{\mu^2 N}\right) \tag{4.56}$$

and the corresponding number of dipoles within the sphere of radius R_s

$$v_d = \frac{4}{3}\pi N R_s^3 = \exp\left(\frac{3\varepsilon k_B T}{\mu^2 N}\right) \tag{4.57}$$

r_1 is the radius of the sphere containing a simple dipole, ℓ is the dipole length and μ is the dipole moment ($\mu=q\ell$, q is the charge). Dipolar screening becomes effective at high densities [Jonscher97]. For distances longer than R_s the dipole is completely screened. The main physical parameters that determine v_d are temperature, dipole length and density. For instance below a critical value of density (N_1) v_d rises very fast.

If $v_d>>1$ ($N<< N_1$) the system is unscreened and dipoles will "see" each other over large distances. Individual dipoles will be unable to follow external fields and will give little contribution to polarisation. The dielectric spectra will be essentially flat. Low loss dielectrics with small density of dipoles will show this flat-loss response. The dipoles will form domains assuming the lowest possible energy (according to Jonscher [Jonscher99a] there is some form of piezoelectric coupling owed to the appearance of mechanical strain caused by the applied electric field).

For $v_d \approx 1$ ($N>>N_1$) the dipoles are almost completely screened and there is no interaction between them. The system behaves like independent dipoles and the relaxation spectra will show well-defined near-Debye peaks. For a complete screening the system is Debye-like and the relaxation is determined only by the probability of transition between the allowed orientations.

If there is partial screening dipole-dipole interaction extends to many dipoles and the field resulting from the dipoles is stronger than the external field. Dipole reorientations due to the external field become less probable and the system can be considered as more rigid. The loss peaks will become broader. The effect of screening will delay the response time of dipoles to external fields. For AC fields the screening is more effective for high frequencies (the dipoles have less time to react to the applied field) and loss peaks will also become asymmetric with sharper rise at low frequencies.

b) Carrier dominated systems

In order to explain the LFD response described in 4.7-c) Jonscher [Jonscher92] proposed a mechanism involving electrochemical processes. In this kind of relaxation response there will be a constant and relatively high loss per reversal. A possible model is based on the reversal of position by two ions. Assuming that an intermediate neutral compound is formed

$$A^+ + B^- \leftrightarrow AB \tag{4.58}$$

and immediately dissociated, resulting in the dissipation of energy (see Figure 4.9), this mechanism is able to explain the storage of large charge densities without giving rise to relatively high electric fields.

4.8.2 Physical model: Dissado-Hill cluster model

Dissado and Hill proposed a quantum perturbation theory considering condensed matter ordered into an array of spatially limited regions forming clusters [Dissado83&84]. These clusters are formed of individual microscopic units. The cluster array possesses a partial long range regularity, with limits corresponding, respectively, to the perfect regular and coupled superlattice and to a cluster gas with total absence of coupling.

An intermediate entity is formed and immediately dissociated with the corresponding energy loss.

Relaxation occurs as a response to an external influence (an external electric field) and results from a non-instantaneous reorganisation of the positions and orientations of the molecules, atoms or ions. It only occurs in systems possessing some structural disorder. First coupled local motions will take place originating intra-cluster displacements. Next weakly coupled inter-cluster motions will follow. In this ways a model extending from the microscopic to the macroscopic scale gives rise to different behaviour resulting in the observed two power laws [Dissado83].

The cluster model, developed by Dissado and Hill, was first applied to dipolar systems [Dissado83] and afterwards to charge carriers [Dissado84].

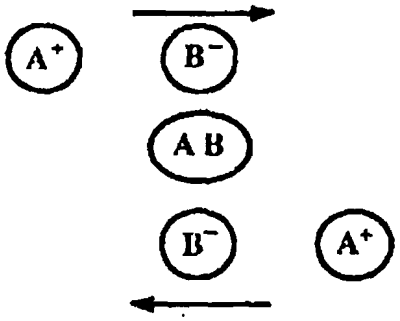

Figure 4.9 – The electrochemical model with interchange of position of two ions [Jonscher92].

4.8.2.1 Dipolar systems

As stated above a power law dependence was found experimentally for the high and low frequency limits of typical dipolar loss peaks (see also 4.8.1).

An expression for susceptibility was obtained considering that a perturbation was applied at zero time consisting of a number of structural displacements equivalent to local dipole rotations and causing potential surfaces to change. The complex susceptibility for all the frequency range will be a gaussian hypergeometric function. Initially independent dipole motions are generated and progress into correlated displacement involving larger and larger number of individual units. In the limits of high and low frequency two different power law regimes appear (intra-cluster and inter-cluster motions) resulting in the following equations:

$$\begin{aligned} &\chi'(\omega) \propto \chi''(\omega) \propto \omega^{n-1} && 0<n<1 \quad \omega > \omega_p \\ &\chi''(\omega) \propto \chi_s - a\chi'(\omega) \propto \omega^m && 0<m<1 \quad \omega < \omega_p \end{aligned} \tag{4.59}$$

where a is a constant. For the high frequency limit the ratio of the imaginary and real components of susceptibility is constant as is seen in Equation 4.52 and represented in Figure 4.6-(a).

a) Intra-cluster motions – For a perturbation applied at zero time the relaxation starts by motions of local independent dipoles. The motions become correlated and covering an increasing number of dipole sites. The spatial growth of the local fluctuations give rise to clusters and the intra-cluster motions originate a regime proportional to t^{-n}, $0<n<1$, resulting from the contribution per site to the dipolar displacement. The parameter n is a measure of the degree of structural ordering or cluster binding energy (with Debye limit of local independent and unclustered dipoles corresponding to $n = 0$ and for $n = 1$ a completely correlated cluster relaxing as a single body). Intra-cluster motions happen first and correspond to shorter times

(and higher frequencies in the dielectric spectra). The susceptibility is proportional to ω^{n-1} resulting from a equation similar to the one for damped oscillators

b) Inter-cluster motions – as the relaxation progresses at the critical time τ_p (or frequency, ω_p) a new power law regime appears. However the coupled motions will change continuously from cluster mode to inter-cluster motions. Near edge dipoles will interact with a neighbouring cluster causing changes in cluster size or structure that will be compensated by changes in other near by clusters. Dissado and Hill [Dissado83] called these changes inter-cluster exchanges (IC). The IC results from diffuse boundaries between the clusters and is considered a perturbation that alters the array structure. A local distribution of clusters will be produced and a new power law regime will appear with a parameter m, representing the degree of ordering in the array of clusters. Contrary to intra-cluster motions there is no damping factor and the susceptibility is proportional to ω^m, $0 < m < 1$. The limit of $m = 0$ represents a very highly ordered structure (near superlattice state) and for $m = 1$ the cluster molecules or atoms are almost unbound along the IC coordinate and there is a wide spread distribution of clusters (high disorder).

The indices n and m are a coarse measure but able to characterise the morphology of the material. Even if a certain degree of disorder exists in the material there must be present some organisation at different levels, corresponding to different size scales ranging from microscopic to macroscopic. A good example is a semi-crystalline polymer with a molecular arrangement of side-group orientations originating in chain folding in the crystalline regions. This arrangement results in crystalline lamella organised into spherulites (with amorphous and crystalline parts present) that determine the macroscopic structure of the polymer. This structural arrangement affects the relaxation rate, amplitude and shape of the loss peak and consequently the values of the exponents n and m.

Clusters are defined according to the class of materials under study. For instance, a material doped with a small amount of impurities will have its original structure distorted. The impurity centre will constitute a complex or grouping with properties different from the pure host and the impurity and this complex will form the cluster. An IC will correspond to a displacement of the impurity to a lattice site causing a local strain that is easily carried to another cluster. Another example is the topological imperfections in a crystal. For low content of impurities the system will be very little distorted and near Debye behaviour (n=0, m=1). A

planar imperfection will produce a change in the dipole moment similar to dipolar side-group rotation. These imperfect planes are identified with the cluster. And an IC will be caused by the exchange of dipole orientation with another cluster. It is accepted for this type of material n to approach unity because the regularity in the cluster is high. While m will be less than 0.5 since the crystalline regularity is strong and the range of cluster structures is limited.

As the two examples above illustrate, the pairs of indices n, m will correspond to different classes of materials [from Dissado84]:

(i) $n=0$, $m=1$ – Debye limit of an ideal liquid with independent cluster constituents and ideal transport;

(ii) $n=1$, $m=0$ – ideal crystal with no internal relaxation and zero loss. It acts like an unique entity for an external rotation;

(iii) $n \to 0, m \to 1$ – real liquids (pure liquids and solutions) with weakly bonded clusters and a wide spread distribution,

(iv) $n \cong \frac{1}{2}, m \cong \frac{1}{2}$ – fluids (plastics, waxes and viscous liquids) with clusters with a restricted range of structures and an intermediate average form;

(v) Solids

(a) $n \to 0, m \to 1$ – interstitial impurities and ferroelectrics;

(b) $n \to 1, m \to 0$ – topographical impurities in imperfectly crystallised materials, glasses and vitreous polymers;

4.8.2.2 Charge carriers systems

The dielectric relaxation behaviour for carrier dominated dielectrics is characterised by two power law regimes with the absence of loss peaks[28]. Jonscher has identified this kind of response and named it low frequency dispersion (LFD), as described in 4.8.1. It is also known as quasi-DC (QDC) [Dissado89], because the low frequency dependence is similar to DC conduction. QDC can be easily confused with DC behaviour. As stated above, Jonscher described the LFD in terms of hopping of charge carriers. Also Dissado and Hill [Dissado84] propose a similar process where a mechanically rigid lattice forming binding sites for ions and molecules is considered. If the system has a low occupation level then charge transport may occur by hopping with many available possible paths. On the other hand if the sites have high levels of occupancy the number of empty sites and in consequence the number of paths are

[28] Sometimes loss peaks can be present as was referred above.

reduced. A material exhibiting a QDC response can be seen as composed of clusters with the perfect lattice structure distorted close to the cluster boundary.

Contrary to dipolar systems, when the electric charge is confined to finite size clusters (such as pores) the long time behaviour exhibits a different regime with susceptibility diverging at low frequencies (see Equation 4.60). Susceptibility in the total frequency range is still represented by a gaussian hypergeometric function but m has been replaced by $-m$ [29]. The high and low frequency regimes are given by:

$$\begin{aligned} \chi'(\omega) &\propto \chi''(\omega) \propto \omega^{n-1} \quad 0<n<1 \quad \omega > \omega_c \\ \chi''(\omega) &\propto \chi''(\omega) \propto \omega^{-m} \quad 0<m<1 \quad \omega < \omega_c \end{aligned} \tag{4.60}$$

For a system in equilibrium the carriers will be in potential wells vibrating around an equilibrium position and phonon-like motions can exist. Irregularities caused by ion-ion repulsion or imperfections in inter-site distance displace the vibration centres. For vibrational modes with wavelength less than a critical value ζ_c, the motion of carriers within the cluster is cooperative (the site where a carrier is able to move to is determined by the occupation of neighbouring sites). When an electrical field is applied, ions (or other carriers) will hop to sites at lower potential, either in the same cluster or between different clusters, and the system becomes polarised. These two modes of inter-cluster and intra-cluster motion are discussed below:

a) Intra-cluster motions – for a distance less than ζ_c the charge dislocation occurs in the cluster that also becomes polarised. Related to this critical distance is ω_c dividing the relaxation dispersion in two different power law regimes. Intra-cluster motions dominate in the high frequency region and the index n will reflect the internal degree of organisation of the clusters. For highly ordered clusters showing an almost regular arrangement, n will be close to unity and the carriers motion will be highly correlated with rigidly displacing groups. If n approaches zero the clusters are highly irregular and the mobile charges are nearly independent. The limit of $n = 0$ relates to DC conductivity with completely free carriers.

b) Inter-cluster motions – For a distance greater than ζ_c the charge hops to an available site in a different cluster. Its motion is no longer correlated with the donor cluster but with the acceptor. There is effective charge transference resulting in the ionisation of the donor cluster

[29] $n=n_1$ *and* $m=1-n_2$ (see Table 4.1 and 4.8.1).

and also in a charged acceptor cluster. In a macroscopic scale the sample is characterised by an array of clusters (distributed from completely charged with either all sites occupied or unoccupied to neutral clusters with an average site occupancy). The hopping transport is expansion and contraction of ionised clusters. The low frequency region is determined by the inter-cluster hopping and the index m defines the average of the effective displacement ($m = 0$ unity displacement and $m = 1$ to infinity). Small values of m correspond to a highly regular distribution of cluster, with each cluster almost identical to the others. While large values of m are associated with a broad distribution of cluster structures with charge carried over long paths.

An example of LFD response are hydrogen-bond systems with the cluster polarisation arising by successive transfer of protons between hydrogen bonds. In this case maximum value of n should be around 0.6 and m of the order 0.8 – 0.9. Imposed on the QDC spectra there is a subsidiary loss peak. If there is paths where no recombination occurs a loss peak is possible to appear. For the loss peak the high frequency tail shows an index n related to the dipole structure (also with the inter-cluster regularity of the hydrogen bonding structure) and at low frequencies the index m shows the distribution of cluster array (which has the same value as the LFD m index).

At very low frequencies the ions may become free from the inter-cluster paths and DC conductivity will arise. QDC will be observed as a noise of DC. Only systems without blocking electrodes or structural domains not connected to the electrodes will show a DC behaviour. To identify true DC if m is close to unity it is necessary to verify if the real susceptibility is constant or not.

4.8.2.3 Fractal character of dielectric relaxation

The fractal behaviour is a fundamental feature of relaxation in real materials. For the dielectric relaxation Dissado & Hill [Dissado89] have shown that the cluster model is the consequence of two types of self-similarity. Each level of self-similarity is related with the two limiting power law dependencies observed in the cluster model. The fractal model is developed based on deterministic fractal circuits, which are exactly solvable and are idealised models for percolation systems. The Sierpinski carpet electrode consists of a conducting block in which an electrolyte is contained in square cylindrical pore channels and separated from the electrodes by a thin layer of the same electrolyte. Each pore acts as a transmission line and the total equivalent circuit is composed of a series of elements made of a resistance and a

capacitance in parallel. Moreover each pore itself can be thought of as constituted of another level of Sierpinski gaskets. Giving rise to the low frequency behaviour the pore system can be disposed in a way that their cross-sections on the outer surfaces form a fractal system. The other self-similarity, efficient at high frequencies, arises from the longitudinal pore system. In physical terms the fractal behaviour is due to an efficient exploration of the fractal lattice (in a cluster all possible paths intervene in the relaxation process) and the existence of self-similarity in connections between different clusters.

For the bound dipole case the circuit model can be seen as composed of irreducible series sub-circuits corresponding to individual dipoles. At high frequencies it can be regarded as dynamic connections along complex paths in space, while the low frequency power law is the effect of progressive connection of dipole motions forming a "chemical" path interrupted by non-connected contacts (steric hindrances, structural strains, etc.) or as brownian motion originating an instantaneous distribution of clusters.

Percolation can occur for the quasi-mobile carrier systems originating conduction. The high frequency behaviour appears when a mobile charge, looking for a counter-charge to recombine, is unable to efficiently explore the fractal matrix (the charge does not travel over all possible paths in the cluster). As for low frequency it can be considered as fast recombination in large connected clusters that eliminate this connections. In these systems traps can be regarded as clusters with larger clusters responding faster than small ones due to higher screening and weaker binding energy.

4.8.3 A probabilistic model

Relaxation is a stochastic process and some probabilistic models were proposed. A stochastic hopping model was presented by Niklasson [Niklasson87]. Another probabilistic model for dipolar systems was developed by Weron and collaborators [Weron91,93&01] and it will be presented in this brief discussion. Weron's model is a pure mathematical model based on disordered systems probabilistic relaxation response.

As stated previously (4.4.2) a way to modified Debye's independent dipole theory is to consider a distribution of relaxation times where each degree of freedom is independent and is associated with a characteristic relaxation time τ_i and $g(\tau)$ is a weight distribution. The relaxation function will be:

$$\Psi(t) = \int_0^\infty g(\tau)\exp(-t/\tau)d\tau \tag{4.61}$$

Weron's model intends to (i) derive the universal dielectric response from a simple analytical form obtained from the relaxation equation and (ii) in the limits of long and short times the response function has to agree with the empirical functions that fit the experimental data (fractional power law).

Susceptibility is related to the response function by a Fourier transform.

$$\chi(\omega)=\int_0^\infty e^{-i\omega t}\Phi(t)dt=-\int_0^\infty e^{-i\omega t}\frac{d\Psi(t)}{dt}dt \qquad (4.62)$$

The universal model of Jonscher was taken into account assuming two different stochastic mechanisms (also, as Dissado and Hill model, revealed a hierarchy of self-similar (fractal) processes). The first one is identified with the internal dynamics of the imperfections ("defects") in the clusters considering both the dipoles and environment. The second one is related to the macroscopic response from the interacting component clusters.

So that based on the existence of those two different stochastic (fractal) mechanisms the probabilistic model assumes two different transition times. One is the transition moment of the dipole related to waiting time for a reorientation to occur. The other has to do with the effect of screening and the screening adjustment time is described by the dissipation time. The total time is the sum of the first two. When a single probabilistic mechanism is considered the relaxation function will tend to be the stretched exponential (see Equation 4.32). An important assumption is that a dipole does not necessary changes its initial position with probability 1 (if not the resulting relaxation function was limited to the Williams-Watts function).

Table 4.3 – Power-law response from Weron's probabilistic model [Weron93].

Parameter γ	$\gamma=\alpha$	$\gamma>\alpha$
Properties of the relaxation function or potential decay function $\Psi(0)$	$\Psi(0)=1$ monotonically decreasing	
	$\Psi(t)\xrightarrow[t\to\infty]{}0$	$\Psi(t)\xrightarrow[t\to\infty]{}\Psi(\infty)$
Limiting properties of the response function $\Phi(t)$	$\Phi(t)\propto\begin{cases}(At)^{-n} & \text{as } At\ll 1\\ (At)^{-m-1} & \text{as } At\gg 1\end{cases}$	
Form of the power law coefficients n, m	$n=1-\alpha$	
	$m=\alpha/\kappa$	$m=\gamma-\alpha$
Properties of the power law coefficients n, m	$0<n<1$ since $0<\alpha<1$	
	$m>0$ since $k>0$, $\alpha>0$ $m>1$ for $k>\alpha$	$m>0$ since $\gamma>\alpha$, $\alpha>0$ $m>1$ for $\gamma<1+\alpha$

Derived from the model the general relaxation equation is:

$$\frac{d\Psi(t)}{dt} = -\alpha A(At)^{\alpha-1}\left[1-\exp\left(-\frac{(At)^{-\gamma}}{k}\right)\right]\Psi(t) \tag{4.63}$$

Conclusions are summarised in Table 4.3 and Table 4.4. The relaxation function is determined from parameters $0<\alpha<1$, $\gamma\geq\alpha$, $A,k>0$. A relation is found between α and γ and m and n from Jonscher's "universal" law and also Dissado-Hill cluster model.

Table 4.4 – Special cases of empirical functions [Weron93].

Parameter γ	$\gamma=\alpha$	$\gamma>\alpha$
Typical experimental observations	$1-n\leq m<1$	
	$\alpha<k\leq 1$	$2\alpha\leq\gamma<1+\alpha$
Less typical experimental observations	$0<m<1-n$	
	$k>1$	$\alpha<\gamma<2\alpha$
Cole-Cole response	$m=1-n$	
	$k=1$	$\gamma=2\alpha$
Cole- Davidson response	$0<n<1, m\rightarrow 1$	
	$k\rightarrow\alpha$	$\gamma\rightarrow 1+\alpha$
Broadened Debye response	$n\rightarrow 0, m\rightarrow 1$	
	$\alpha\rightarrow 1, k\rightarrow 1$	$\alpha\rightarrow 1, \gamma\rightarrow 2$
Flat loss response	$n\rightarrow 1, m\rightarrow 0$	
	$\alpha\rightarrow 0, k>0$	$\alpha\rightarrow 0, \gamma\rightarrow 0$

4.9 Correlation between TSDC measurements and dielectric measurements

From TSDC peak data is possible to calculate an equivalent frequency. If the isochronal dielectric relaxation spectrum is acquired at this frequency a loss peak will appear at the same temperature as the one in the TSDC plot. The equivalent frequency can be estimated from the relation $\omega\tau=1$ (Debye) and the equations defining the maximum TSDC peak (see [Vandershueren79]).

For an Arrhenius dependence the equivalent frequency is given by [Turnhout80, Vanderschueren79]

$$f_{eq} = \frac{1}{2\pi}\frac{\beta E_a}{k_B T_{\max}^2} \tag{4.64}$$

(where f_{eq} is the equivalent frequency, β the heating rate, E_a the activation energy and T_{max} the peak temperature).

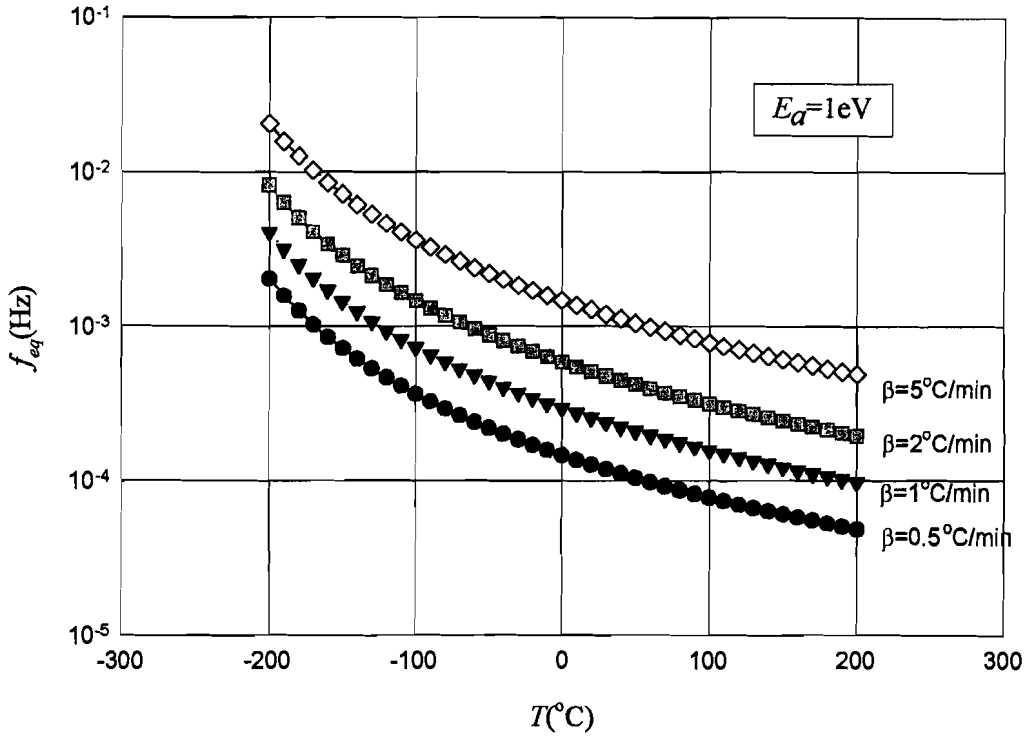

Figure 4.10 – Variation of equivalent frequency with temperature for different heating rates.

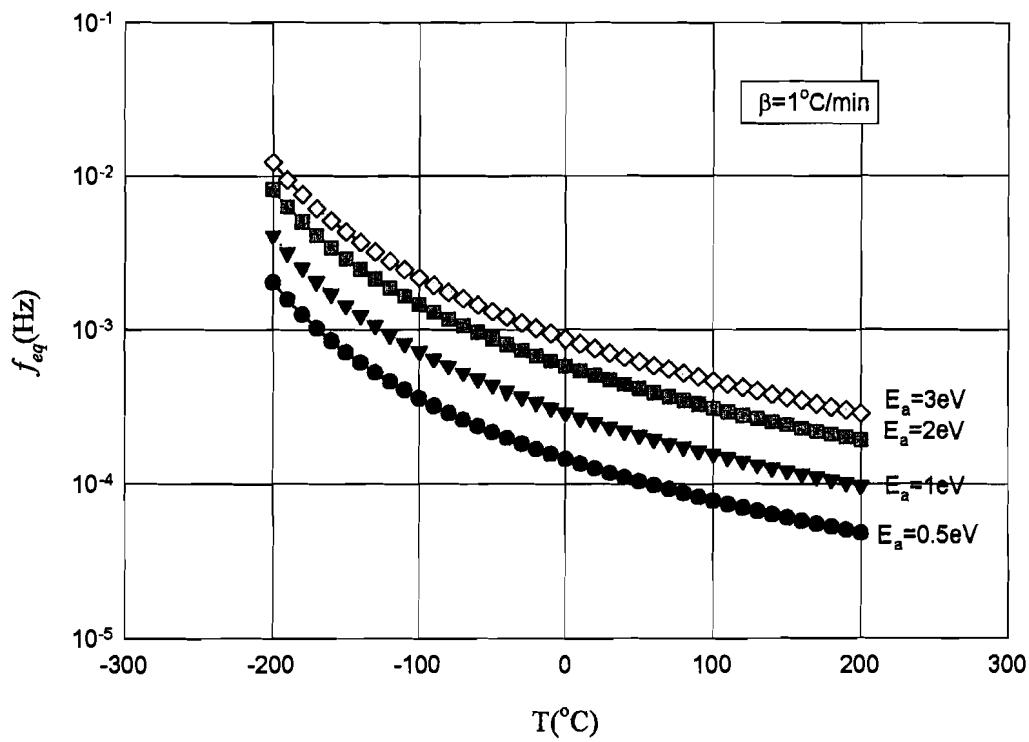

Figure 4.11 - Variation of equivalent frequency with temperature for different activation energies.

In Figures 4.10 and 4.11 is seen the influence of the peak temperature on the value of the equivalent frequency (typical values of the heating rate and activation energy were used). For a shift in the peak temperature between –200°C and +200°C and considering a heating rate of β = 1 °C/min and a activation energy of 1 eV (Figure 4.10), the frequency changes by nearly two decades. If β is larger the span is less pronounced but still cover more than one decade (compare 1 °C/min with 5 °C/min). When different values for the activation energy are used in the calculations the variation is smaller for higher values of E_a (Figure 4.11). As an example, if 0 °C is assumed as the peak temperature it is seen that the frequency changes over 1 decade for β varying between 0.5 °C/min to 5 °C/min (Figure 4.10). Changing the activation energy is similar to change the heating rate as can be seen in Figure 4.11.

In order to determine from TSDC results the complex dielectric constant as function of temperature (isochronal plot), Turnhout [Turnhout80] extended Hamon approximation. The formula derived is a first order approximation valid for an Arrhenius dependence with constant activation energy (considering a single relaxation time):

$$\varepsilon_0 E\varepsilon''\left[f_{eq}(T),T\right] \cong 1.47\frac{k_B T^2}{\beta E_a} j(T), \tag{4.65}$$

E is the applied electric field and $j(T)$ is the current density at temperature T.

As can be seen the frequency changes with temperature. However this variation in frequency can often be neglected and allows to use $f_{eq}(T_{max})$ instead of $f_{eq}(T)$ and a plot of ε'' versus temperature at constant frequency ($f_{eq}(T)$) is obtained.

It is also possible to obtain the isothermal dielectric constant-frequency plots. However it is more restrict since it is necessary to make more initial assumptions (p. ex., for the polarisation) and to determine more parameters.

4.10 Dielectric relaxation processes in polyethylene: a review of experimental results

Polyethylene as a very good insulator material shows low values for the dielectric constant (in [Phillips83] for LDPE typical values are ε'=2.25-2.35 and tan $\delta \approx 10^{-4}$ at 1 kHz). The dipolar moment of the C-H groups is 0.1 D and ε_0-ε_∞=10^{-2} and $\varepsilon''(max) \approx 10^{-6}$ which is not detectable . Nevertheless when comparing the dielectric data with IR (infrared) data it is possible to establish that the dielectric properties of pure polyethylene are predominantly due to the presence of carbonyl groups caused by oxidation. Present are also peroxy and hydroperoxy groups consequence not just of oxidation but also from polar additives [Scarpa95]. Oxidation will happen at defects and can give rise to very high Maxwell-Wagner-Sillars polarization. Injection of charge carriers from electrodes and their localisation in the polymer together with

impurities (such as ions) contribute also to the dielectric relaxation giving rise to space charge peaks.

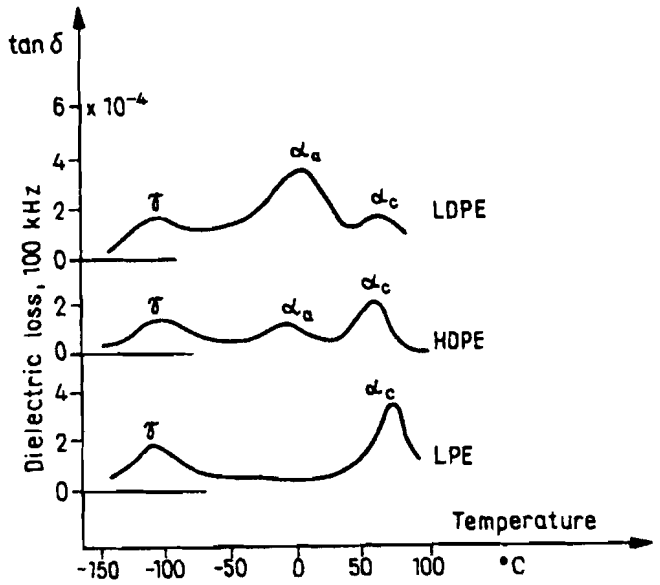

Figure 4.12 – Dielectric isochronal data for different forms of polyethylene [Hedvig77].

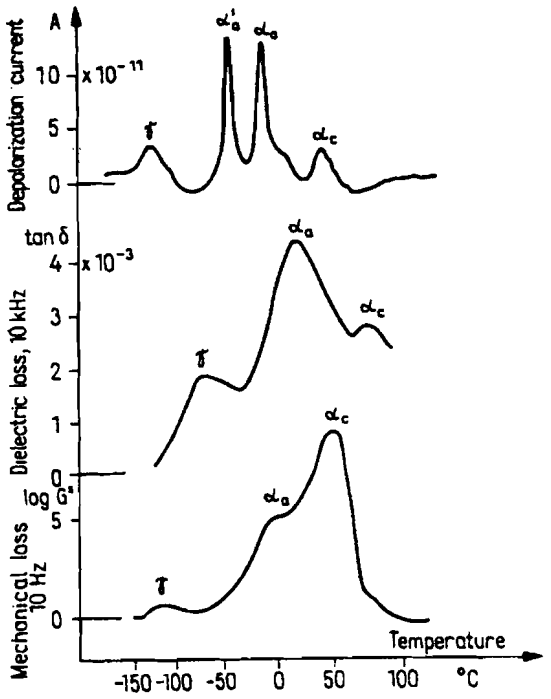

Figure 4.13 – Comparing TSDC, dielectric e mechanical spectra of low density polyethylene [Hedvig77].

Usually dielectric measurements in polyethylene are made by slightly oxidising the polymer. In Figure 4.12 spectra for different polyethylene forms are presented. For LDPE the three typical relaxations of semicrystalline polymers appear. In HDPE the relaxation α_a (or

β) connected with the amorphous phase is much lower, while in LPE has disappear because HDPE and even more LPE show a high degree of crystallinity [Boyd97]. In other results from Graff et al. [Graff94] a small β peak is visible for LPE. The α_c (or α) loss peak appears above room temperature around 50-70 °C (see Figures 2.6, 4.12. and 4.13). The β loss peak appear near 0 °C and corresponds to the glass transition (T_g), finally the γ peak appears below –100 °C. In Figure 4.13 there is a split in the β peak implying the existence of two different amorphous phases.

Dielectric data presented in Table 4.5 and Table 4.6 are taken from literature and does not intend to be an exhaustive collection of all the available results.

Table 4.5 – Dielectric loss peak temperatures T(K) from literature for oxidised LDPE.

		T(K)			
Peak	**Frequency (Hz)**	**[Ashcraft76]**	**[Graff94]**	**[Hedvig77]**	**[Barrie66]**
α	10^5	341	344	337	353
	10^4	328	325	358	
	10^3	306	307		
	10^2	293	297		
	10^1		290		
β	10^5	288	290	280	
	10^4	277	282	291	283
	10^3	273	274		
	10^2	263			
γ	10^5	200	183	168	183
	10^4	184	170	199	
	10^3	172	156		
	10^2	160	151		
	10^1	151			

As stated in Chapter 2, the dielectric and NMR α (α_c) transition occur in the crystalline part while the mechanical one in the amorphous but requiring the presence of a crystalline phase. Even if activation energies are similar for the dielectric and mechanical α relaxations, the mechanical one is broader. This means that the corresponding relaxation time is higher for the mechanical process. The relaxation times of the peak are dependent on lamellae thickness The dielectric peak is quite sharp on the isothermal plots and the process must involve almost a single relaxation time. The mechanism proposed involve a 180° rotation (twist) of the main chain advancing c/2 [Boyd85b] with all chains participating. A dipole perpendicular to the

main chain (e.g., carbonyl group) will also rotate 180° (see Figure 4.14). In polyethylene the chain will rotate 180° and will advance 0.127 nm. The mechanical relaxation results from the accumulated translational motion ending in deformation of the amorphous region between the lamellae.

Table 4.6 – Activation energies for the dielectric loss peaks of PE from dielectric data.

Peak	Activation energy (eV)	Reference
γ	0.75	[Ashcraft76]
	0.5	[Graff94]
	0.5	[McCrum67]
β	2.2	[Ashcraft76]
	2.5	[Graff94]
	0.7 – 1.6	[McCrum67]
α	1.1	[Ashcraft76]
	1.2	[Graff94]
	1.2	[McCrum67]

The glass transition α_a (or β) is a broad peak and the sharpness in the isochronal plots is inversely proportional to the activation energies. Dielectric constant maximum will increase with increasing temperature but the presence of long chain branches does not affect the relaxation. The mechanism is not very well understood but probably is related to segmental motion in the chains. Heat capacity measurements have made clear that this relaxation is the glass transition.

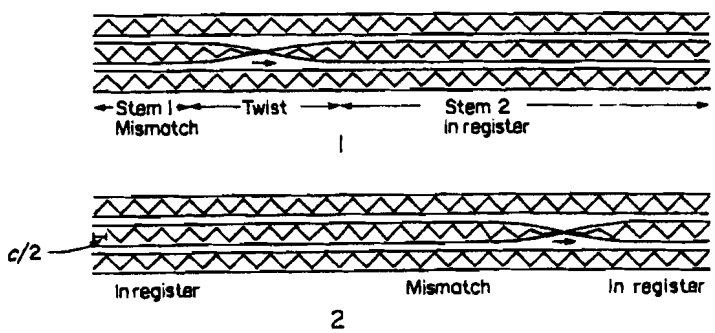

Figure 4.14 – Propagation of a smooth twist along the chain [Boyd85b]. The chain will end in crystallographic register by a c/2 advance.

The glass transition obeys a Vogel-Fucher-Tammannn-Hesse dependency (as seen in Equation 4.34) and T_o is usually 30 to 70 °C below T_g.

Finally the γ relaxation is a localised process with the character of a sub-glass transition. It occurs in the amorphous region and is very sensitive to morphological changes. It has an

Arrhenius dependence with temperature (see Equation 4.36) and a low activation energy. The process must be localised corresponding to a short molecular motion and initially a crankshaft motion was proposed. However the required energies were higher than the ones calculated experimentally. More recently a mechanism consisting of a localised kink or kink inversion was presented. At high enough temperatures the β and γ relaxation peaks can merge together[30].

[30] Just from mechanical measurements was reported by some authors [Papir71] a fourth peak (δ) at very low temperature (below –200 °C).

Chapter 5. Electrical ageing of insulating polymers

Come what may, time and the hour
runs through the roughest day.
William Shakespeare

Ageing either physical or chemical of any material is unavoidable. For an insulator different electrical ageing phenomena can occur enhanced by the presence of the electric field. The ultimate consequence is the failure of insulating characteristics. The main purpose of the scientist and engineer is, nevertheless, understand and if possible predict and reduce electrical ageing with ultimate consequence the increase of material lifetime. For an insulator polymer, such as polyethylene, three main ageing processes are observed: water treeing, electrical treeing and dielectric breakdown. Even before any of those phenomena appear the polymer is suffering electrical ageing. This chapter will not discuss this initial ageing but the major electrical ageing processes and will focus mainly on water treeing.

5.1 Water treeing

Water trees are permanent localised damage with the appearance of hydrophilic diffuse ramified structures with size ranging from a few microns up to 1 mm. They appear under the effect of an alternate high electric field[31] and aqueous salts in different polymers. Even if they are not a direct cause of dielectric rupture, their presence reduces the breakdown strength considerably. Furthermore they can be initiation sites for the more dangerous electrical trees and subsequent dielectric breakdown.

Since the first time they were detected three decades ago, much work has been published showing that many different factors affect water tree inception and growth. These parameters are such as: temperature, mechanical stress, type and concentration of ionic salts, applied electric field (frequency and amplitude), polymer morphology and composition, etc. [good reviews on this phenomenon are Shaw84, Steennis90, Disssado92 and more recently Ross98]. Revealing the complex nature of water tree mechanisms (both inception and growth), conflicting and difficult to reproduce results have been reported either for field aged or laboratory accelerated aged specimens.

---

[31] DC tree growth has also been reported (see 5.1.3-b).

The wet water trees are visible to the naked eye as small brownish spots, they collapse when dried and reappear by rewetting. If observed under an optical microscope, either wet or dyed, they are bush-like structures resembling treetops (see Figures 5.1 and 5.4). Two kinds of water trees are known, *vented trees* initiated at the polymer's interface and *bow-tie trees* starting in the bulk. The former type is much more dangerous for the insulation than the later.

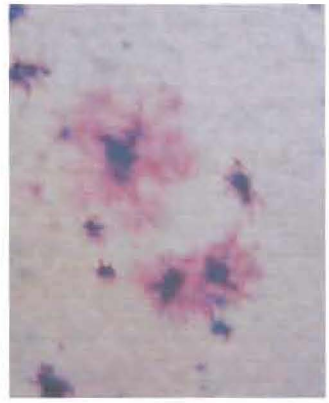

Figure 5.1 – Optical microscope photograph of methylene blue dyed vented trees (laboratory aged in a plane-plane geometry).

5.1.1 Morphology

Even after many published studies water tree morphology it is still under debate. Some consensus has been reached in the micrometer scale but it remains uncertain on the nanometer range. Frequently the water-treed polymer has to suffer some kind of treatment in order to observe the trees. This is a problem when trying to determine the lowest range structure because the tree can be modified by these treatments and artefacts can be created.

The overall shape of water trees is well known by optical microscopy of wet and dyed specimens. It is common to use staining techniques to render the tree permanently visible and also to better distinguish tree features. Several techniques have been developed but methylene blue dyeing is very common[32]. As stated by [Ross98] methylene blue is a redox indicator applied in its oxidised state for staining. The solution is buffered with a carbonate solution to prevent discoloration. After staining the methylene blue is still in its oxidised state. Staining is not a chemical process it is a diffusion mechanism with subsequent clustering of the dye in the water tree. The process can enlarge the observed tree structure but will not cause chemical changes.

[32] For details on methylene blue staining using the procedure by Siemens see Appendix A.

In observations with transmittance optical microscopy at lower magnifications (around ×100) the stained tree can be seen spreading in the general direction of the field. Usually it looks like connected branched channels.

Studies at higher magnification (including SEM studies) revealed that voids with diameter in the micron range are present in polyethylene either aged or unaged. In the treed region Shaw and Shaw [Shaw84] reported the presence of voids ranging from 0.1 to 30 μm with a numerical density of 10^5 to 10^7 mm^{-3} (while for untreed region is 10^3 to 10^6 mm^{-3}). In the tip of the water trees voids are rare while approaching the bulk of the tree the density increases. According to [Steennis90] applying higher electric fields (≈30 kV/mm) micro-channels of diameter around 1 μm are formed connecting the microvoids. At the tip in the nanometer range no channels were found. For instance, [Shinozaki91] has used laser scanning confocal optical microscopy and dyed the samples using a fluorescent dye and from serial sectioning a 3D image of bow-tie trees was reconstructed with focusing step of 1 μm. These authors observed discrete microcavities emerging with a uniform distribution along the tree and forming presumably continuous filaments. However the dye was not uniformly distributed suggesting that some diffusion paths are easier. The filament followed interlamella paths[33]. Trees are able to deform adjacent lamella [Dissado92]. In order to be observed by SEM, LDPE samples were sectioned by freeze fracture and oxygen plasma etched [King93]. Depending on ageing conditions trees showed voids or channels. Etching attacks strongly the treed regions revealing existing oxidation in these regions (presence of esters, ketones or carboxylate groups). [Moreau93] used fluorescence microscopy after dyeing the polymer with rhodamine (both XLPE cables and laboratory-aged specimens). Olley et al. [Olley92&95] developed a special technique for polymer etching for TEM and SEM studies. The presence of elongated channels and voids was detected. It is not clear if these units are connected or not. Also some damaged could be seen ahead of the tree tip. TEM showed finger-like structures of 0.2 μm probably parts of channels enhanced by the etching. The surrounding polymer is filled with small disconnected voids.

For higher resolutions discussion is still open [Ross98]. Besides the micrometer disconnected voids it is not know if the tree is formed of microchannels, tracks and/or microvoids. Cross et al. [Cross84] reported no connection between voids by helium transport. SEM studies were

[33] It is well know that water trees grow in the amorphous region between lamellae.

unable to find connections around the 50 nm range (order of the lamella dimension). However water transport can happen by permeation by hydrated sites and hopping of water molecules from one site to the other. TEM results show the presence of nanometer tracks different of surrounding PE due to oxidation. These would allow water transport while preventing helium to diffuse.

In conclusion water trees have a higher void density at micrometer scale than the polymer. They appear to be composed of disconnected microvoids in μm scale, between these voids the water and ions diffuse probably by the presence of hydrophilic tracks composed of pores in the nm range. However the structures allowing water diffusion between disconnected voids is still under debate. It seems to be present oxidised sites granting water transport. The techniques used need sample preparation that can cause artefacts influencing the results. Some features of water trees morphology are dependent on the ageing conditions as well as was found for length and density.

5.1.2 Characteristics

Contrary to what was initially expected water treed polymer still constitute an insulating material. Measurements made by Ross et al. [Ross89] in water trees previously saturated in water showed that the dielectric constant was 2.26 and the loss factor at 50 Hz was $\approx 20\times10^{-4}$. The water treed polymer has reduced breakdown strength. However the presence of a water tree crossing the entire insulation does not mean immediate dielectric breakdown under the usual service conditions in cables, i.e. with an electric field < 2 kV/mm. Also it has been detected electrical trees starting from water trees. This happens when the water tree crosses a point of enhancement of the local electric field such as an impurity or a void. In some experiments it was reported that the loss factor of the treed polymer was increased while others found no relation. No low magnitude partial discharges were detected during water tree growth.

In polyethylene the overall direction of propagation of water trees follow mainly the local electric field lines of the unaffected polymer. As will be referred in greater detail in 5.1.4, some typical products of polyolefins oxidation were found by infrared analysis (carboxylates, ketones, etc.). Also metal ions are present in trees.

5.1.3 Factors affecting initiation and growth processes

One of the major problems for fully understanding water treeing mechanisms lies in the many experimental parameters upon which the phenomenon is dependent. Furthermore it is difficult to know and/or control experimentally all the variables acting on water trees. As a consequence the experimental results for laboratory accelerated ageing and even field aged cables have proved to be conflicting and difficult to reproduce. As stated in the beginning of this chapter, temperature, mechanical stress, type and concentration of ionic salts, applied electric field (frequency and amplitude), polymer morphology and composition, etc., influence both inception and propagation of water trees. Also bow-tie and vented trees can be differently influenced by the same parameter.

As pointed out by Shaw and Shaw [Shaw84], the number of water trees (related to the initiation process) and the length (related to growth) have been widely used as a quantitative way to access the influence of different parameters.

a) Polymer morphology

Starting to consider the polymer itself, polyethylene, it is known that its characteristics are highly dependent on past history. Processing and manufacture can change chemically and physically the polymer. For example, introducing contaminants, creating defects and also thermal treatment can result in differences in properties such as crystallinity, spherulite size and number. The influence of ageing geometry is relevant as analyse of water trees aged in laboratory shows. Even comparing between different cables aged under similar service conditions may lead to distinct conclusions.

In their review [Shaw84] account for several experiments revealing the influence of morphology. Nevertheless [Steennis90] and [Dissado92] conclude that density, crystallinity and melt flow index hardly affect water treeing. For vented trees, Dissado et al. [Dissado92] emphasise the importance of molecular defects near the surface providing good initiation sites together with flexibility in the surface chain structure facilitating solvation of hydrated ions. Since water treeing propagates preferential along stacks of lamella with a common alignment then it is expected to depend upon molecular weight and polymer softness. Fan et al. [Fan96] showed that for larger and fewer spherulites the trees grow faster when it is possible to find more aligned lamella. In [Ross98] and [Crine98] the importance of polymer morphology is also discussed. For instance, heat treatment, such as annealing, can change the growth rate by causing longitudinal extension of lamella.

b) Electric field

Electric field is one of the factors that it is better known how it affects water treeing. For electric field strength it is certain it increases both the number and length of trees [Steennis90]. Regarding frequency, an increase will cause tree growth rate to increase until a maximum is reached (around 4 to 8 kHz, but values differs from work to work) followed by a decrease for higher values of frequency. An exponential relation between tree length and number of cycles (instead of frequency) has been found and associated with fatigue mechanisms [Crine98].

It is interesting to note that some laboratory experiments were able to grow water trees under DC voltage but very few and at a high electric stress. Their shape was different from the ones grown under AC.

c) Temperature

Dependence on temperature is more complex and contradictory results have been found. According to [Steennis90] for experiments at constant temperature an optimum growth rate is reached between 30 and 50 °C. For temperatures higher than 50 °C it was observed that water trees concentration increases but length decreases. Published results are different when temperature was cycled, some claim no effect while others have observed an increase in number and length [Dissado92]. If a temperature gradient is imposed on the sample there are reported results of a rise in number of bow-tie trees [Steennis90].

c) Additives, contaminants and tree-retardants

As is known XLPE has replaced LDPE as a cable insulator because it showed less water trees. Contrary to this decrease being related to the morphology it is related with the presence of a by-product of crosslinking, acetophenone. Therefore additives, contaminants, etc. can also affect treeing. Another example is antioxidants added during manufacture in order to prevent oxidation that reduces mechanical strength and flexibility but can sometimes enhance water trees.

In order to retard water treeing the polymer can be modified or chemical additives can be incorporated or even both [Steennis90]. The modifications to the polymer are defended by the groups that support the electro-mechanical theory for water trees, while the ones believing in the electro-chemical, model suggest chemical additives [Dissado92]. Both approaches have had some success, which confirms the complex nature of water treeing. Commercial materials are available such as tree-retardant polyethylene (TRPE) that is a blended polymer containing

low molecular weight polymers of a tree retardant functionality (oligomers). Another retardant material is the tree-retardant crosslinked polyethylene (TRXL) which has a different chemical functionality grafted to the main chain of the polyethylene molecule. Tree-retardant additives are added to the insulation when the cables are manufactured. The additives used are such as acetophenone and antioxidants, which also inhibit electrical treeing.

d) Humidity and ionic content

Another important parameter is humidity, for values below 70% of relative humidity hardly any water trees grow. And for humidity increase there is a corresponding increase in the number of trees. Experiments using different salt solutions have shown that water treeing is more enhanced in a solution of $CuSO_4$ than in NaCl. The increase of the ionic concentration (conductivity) leads to a higher growth rate for the trees [Dissado92]. However very high concentration have the opposite effect, because according to [Dissado92] it leads more easily to terminal reactions while for [Steennis90] it decreases the presence of oxygen. Studies on electrode material showed that Pt and Cu electrodes exhibit higher treeing than Al, Fe and Pb probably due to lower oxygen content in the solution. If the pH is increased also the growth rate of vented trees increases.

e) Mechanical stress

Mechanical stress can be present in cables either resulting from manufacture or from laying out the cables (according to calculations, pressure can be of 1 to 8 MPa). It is seen that water trees prefer to grow along the frozen-in mechanical stresses and not along the electric field gradient [Ross98]. Applying uniform hydrostatic pressure results in more but shorter trees [Shaw84]. Mechanical stress also aligns lamella and as stated before growth will be enhanced.

For an almost complete and controlled experimental study Crine [Crine98] has chosen at least 7 parameters: oxygen content, solution (ions and water), material properties, voltage (electric field amplitude and frequency), temperature and mechanical stress. Using Taguchi's method at least 16 different experiments had to be performed to reach some reliable conclusions [Crine00].

5.1.4 Oxidation and FTIR analysis

Since 1982 many authors have claimed the importance of electroxidation in water tree inception and propagation [Ross98]. However others consider that oxidation plays no major

role in water treeing [Bulinski98, Crine98]. The most common tool used to access the presence of oxidation products has been FTIR and especially μ-FTIR.

Table 5.1 – Literature survey of FTIR results found in electrical ageing studies of polyethylene (mainly low-density and crosslinked polyethylene).

Chemical species	Chemical formula	Band (cm^{-1})	Reference	Observation
Sulphates	SO_4^{-2}	625 and 1130	[Garton87]	Antioxidants
		1150	[Ross92]	Calcium sulphates $CaSO_4$
		1140	[Ross92]	HCl gas test (to distinguish from hydroxilic groups, silicon oxides which have also absorption near 1100 cm^{-1}
		600 and 1100	[Steennis90]	
Ether and alchool	RCOCR' ROH	600, 1100, 1160, 3550 and 3600	[Steennis90]	
Vynil bond	C=C	850-1000	[Bulinski98]	
		1630	[Gupta90]	
Carboxy-lates	COO^-	1013, 1044, 1425 and 1580	[Ross92]	First 2 probably due to CH_3 rocking and last 2 to symmetrical and antisymmetrical streching of CO, respectively.
		1575 and 1610	[Garton87]	
		1590	[Xu94]	Lies behind water absorption at 1640 cm^{-1}.
		1585	[Bulinski98]	With HCl gas test shifts to acid carboxylic at 1711 cm^{-1}.
		1585-1600	[Bulinski98]	
		1570, 1600, and 1720	[Steennis90]	
		1000 and 1200	[Steennis90]	Interaction of carboxylates with water

Table 5.1 – Literature survey of FTIR results found in electrical ageing studies of polyethylene (mainly low-density and crosslinked polyethylene)(continued).

Chemical species	Chemical formula	Band (cm^{-1})	Reference	Observation
Carbonyl	C=O	1150, 1710 and 1720	[Steennis90]	
		1538 and 1818	[Gupta90]	Shifts to 1590 with SF_4 treatment
		1725	[Garton87]	
Hydroxyl	OH^-	3400		
		3616-3645	[Steennis90]	Free hydroxil OH^-
Metal ions		1130	[Steennis90]	
Water	H_2O	1640 and 3400	[Garton87]	
		1640	[Bulinski98]	
Carboxylic acid	R-COOH	1712	[Bulinski98]	
Ketones	RC=OR'	1713	[Das Gupta90]	
		1718	[Garton87]	
		1720	[Bulinski98]	
Acetophe-none		1725	[Garton87]	
Aldehydes	RC=OH	1725	[Garton87]	
		1735	[Bulinski98]	
Esters	RC=OOR'	1740	[Garton87]	
		1742	[Bulinski87]	
		1740	[Das Gupta90]	From anti-oxidants.

In Table 5.1 is summarised the data from a literature survey of FTIR studies of oxidation products in electrically aged polyethylene (mainly on LDPE and XLPE). The experimental data available up to now show a variety of different results. This is once more related to different ageing conditions stressing the importance of many different factors affecting water treeing and the difficulty in knowing and controlling them.

Oxidation in polyolefins has been widely studied. For instance thermal oxidation occurs at temperatures above 50 °C resulting in chain scission [Xu94]. And there is formation of carbon double bonds (C=C), peroxides (R-OO-R´), hydroperoxides (R-OOH) and alcohols (ROH). Also formed are carbonyl (C=O) groups giving rise to ketones (R-CO-R´), aldehydes (R-COH), esters (R-COO-R´) and carboxylic acids (R-COOH). For electroxidation less is known but carboxylates seem to be, in most cases studied, one of the main products while ketones dominate in thermal oxidation. For a quantitative sum up of characteristic oxidation products see Table 5.2.

Table 5.2 – Distribution of the more important products according to the oxidation conditions [Xu94].

Oxidation Conditions/Products	**Ketones (%)**	**Carboxylates (%)**	**Carboxylic acids (%)**
Electrical + H_2O + ions	0	90-100	0
Thermal + H_2O + ions	70	30	0
Thermal (in air)	82	0	18
Photo (in air)	43	0	57

As is pointed out in the review by Xu et al. [Xu94] FTIR results are highly variable for laboratory ageing and more consistent for field aged cables. However it is always detected carboxylates, ketones and sulphate ions (probably from antioxidants or semi-conducting layers). Garton et al. [Garton87] concluded that field aged XLPE cables with water trees showed significant traces of oxidation. Also it was proposed that the ionic contaminants together with temperature effects would act as catalysts for oxidative processes. Though for polyethylene aged in the laboratory under higher stress conditions, Garton et al. verified that the mechanical factors are more important than chemical ageing. On another published work [Das Gupta90] found for laboratory ageing of XLPE, with and without antioxidants, an increase of carbonyl content and a reduction of oxidative stability. Also evidence of chain scission was observed. With the help of a derivation reaction it was also found carboxylates in

the aged samples. An important study has been made by the Kema group ([Steennis90], [Ross90, 92, 98]) combining different experimental techniques (μ-FTIR, HCl test, microscopy, etc.) to investigate electroxidation in polyethylene (mostly in service-aged cables). They have found evidence of oxidation products specially carboxylates and ketones. It was also detected chain scission and ion diffusion. Analysis of field aged and laboratory aged polyethylene showed that oxidation products present depend greatly on ageing conditions (as in Garton results [Garton87]). For service-aged cables carboxylates are usually the dominant products even if exceptions are encountered. However it is not the case for samples suffering accelerated ageing in laboratory. Based on these results an electrochemical and electrophysical model has been proposed. The electrochemical mechanism dominates for field ageing and the electrophysical for accelerated ageing as will be presented in detail in 5.1.5.

Bulinski et al. [Bulinski98, Crine98] have performed a thorough study on traces of oxidation in aged and unaged polyethylene. They have not found a clear influence of oxidation on the water treeing phenomenon. However if oxidation takes place in the surface then the overall volume of oxidation is very small compared to the total volume of a tree and it will be very difficult to obtain consistent results. Isothermal oxidative stability measurements confirm that oxidation is limited to the microcavities surface. Trees also show high concentration of metal and ionic contaminants resulting either from diffusion or even oxidation. Their presence would contribute to enhance more oxidation. Tests made in air and nitrogen atmosphere showed that vented tree initiation was not affected by oxygen presence while growth was increased. In some cases it was also found higher levels of oxidation in non-treed regions compared to areas showing water trees. Moreover thermally pre-oxidised samples would have less and smaller water trees. Based on these findings Bulinski and co-workers have concluded that oxidation alone cannot be responsible for water treeing and furthermore that it would not be the main mechanism.

5.1.5 Electro-mechano-chemical mechanisms: overview

Water treeing is a very complex process and many factors affect inception and growth mechanisms. Many different possible models have been suggested along the years. Earlier models were reviewed in [Shaw84] and [Steennis90] and more recently [Crine98] and [Ross98] have also published good reviews. First models were purely electrophysical (more often electromechanical) or electrochemical. Experimental evidence now points to a model involving all the three processes: electrical, mechanical and chemical. Also it must be kept in

mind that initiation and growth mechanisms have revealed different dependence on experimental factors. So it must imply different processes for the two steps. While for growth it is easier to gather information and some more or less complete models have been proposed, for initiation less is known.
Diffusion is an important mechanism since the presence of the electric field would increase the ingress of polar species into the polymer (water and ions). Formation and/or enlargement of microvoids either caused mechanically or chemically are present.

Among the first electrophysical models proposed are dielectrophoresis, electrostatic forces, partial discharge (now abandoned for lack of experimental evidence), electro-osmosis, electrostriction, electron bombardment, dielectric heating, environmental stress cracking (or environmental fatigue failure).

Addolall's [Abdolall82] and Henkel's [Henkel85] suggested separately models based on electrochemical mechanisms. The models were both based on free radicals electrochemical reactions but with different initiation steps. For Abdolall inception was caused by partial discharges while Henkel considered a reaction of water associated with a hydrophilic defect or contaminant. However partial discharge would require fields higher than the breakdown limit and the kind of initiation sites proposed by Henkel would result in too fast growth of the trees. In 1987 Garton [Garton87] adopted the same type of reactions with initiation caused by catalysed reactions occurring in the voids.

Due to the complexity of the phenomenon the suggested models had to involve a combination of different mechanisms. For instance, Zeller in 1987 [Zeller87] showed that the local field alone could not cause water treeing but suggested that it could cause electrochemical reactions leading to partial oxidation. These oxidised polar groups would be attached to the polymer macromolecules dragging water into the polymer matrix. Thermodynamic considerations showed that the water could condense giving rise to a microphase separation. The morphology of the tree would then be the result of this phase separation. An inverted micelle-like microvoid was formed with equilibrium between bound and free water, bound and dissociated ions and contractile pressure. This condensation enhances the local field at the front of the tree. According to [Dissado92] the AC field would force segmental motion and increase mechanical forces (still below the yield point) enough to increase free volume in

advance of tree boundary. This would help the diffusion of catalytic species and create new inception sites for oxidation.

More recently there is a debate between two different approaches. One considers more relevant the role of mechanical processes while the other points to chemical reactions as the main mechanism. However none of them exclude the combination of different types of mechanisms in the process of water treeing.

The authors defending the electromechanical approach claim that mechanical forces induced by the electric field would form water droplets. The pressure would increase and the local stress would break molecular bonds. This chain scission would end up creating cavities. The deformed water droplets suffered bond scission at the tips and new voids appeared giving rise to growth and eventually water trees were formed. Experimental evidence supporting this theory, as was referred in 5.1.4, was given by Bulinski et al. [Bulinski98] concluding that oxidation could not be the major responsible for treeing.

On the other hand there is models where electroxidation is the relevant process. Chemical reactions and especially oxidation with the help of water and ions cause local degradation. The high operating temperatures of cables or local heating will enhance some thermal oxidation that will favour bond breaking. However the initiation mechanism is not well understood. Water tree occurs in the amorphous regions and probably starts in pre-existing polar areas created during production and manufacture of the cables. Contaminants (for instance from the semiconductor layer) and residual catalysts can also act as polar sites.

A growth model was developed by the Kema group ([Steennis90] and [Ross92, 98]) which will be described below in some detail. According to this model water treeing consists of three major phenomena: oxidation, chain scission and diffusion combining electrical, mechanical and chemical mechanisms.
As can be seen Figure 5.2, ions have diffused in and are bonded to the polar groups in the polymer backbone formed when microcavities were created and/or enlarged. In cable aged tree diffusion is less significant than when stress is higher such as in water-needle tests. Diffusion is enhanced by the presence of the field (for instance by electro-osmosis or dielectrophoresis). The AC field permits the ingress of ions of opposite charges on different half-cycles and also allow water to diffuse through tracks (nanometer range) in the amorphous

part of the polymer. In these tracks water will move more easily than the larger hydrated ions. Oxidation occurs during growth, catalysed by the simultaneous effect of the presence of electric field, water and ions. Chain scission will result in enlargement of the tracks and may lead to void and channel formation (micrometer scale) with further increase of ionic diffusion. Subsequently through the tracks diffusion occurs ahead of the tip of the tree allowing further oxidation and treeing growth to proceed. As is seen in Figure 5.2 a water tree can be regarded as a salt (or ionomer) tree where hydrophilic groups are bonded to the polymer matrix (such as chemically bonded carboxylate salts or physically trapped inorganic ions). For field aged cables the more important oxidation products will be carboxylates while for higher stress configurations used in laboratory accelerated ageing carboxylate content is lower.

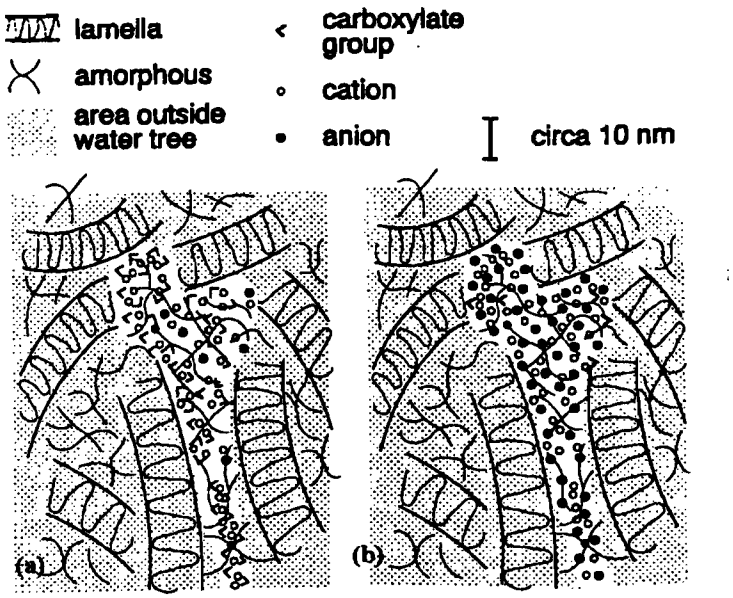

Figure 5.2 –Water tree structure (a) oxidation dominated – field aged cables; (b) diffusion dominated – needle test [Ross98].

Different reactions have been suggested for water treeing. As an example, one possible set of reactions is presented by Xu et al. based on the model of Kema's group [Xu94]. They have proposed for field aged cables a series of oxidative reactions divided in 5 steps:

a) Electrolysis of water

Water electrolysis can occur at very low potentials and currents. Reactions happen at the water/polymer interface. Products are oxygen, hydrogen peroxides and hydrogen peroxide radicals.

$$H_2O \xleftrightarrow[field]{} H^+ + OH^-$$

$$H^+ + e^- \xrightarrow[field]{} H^\bullet$$

$$4OH^- \xrightarrow[field]{} 2H_2O + O_2 + 4e^-$$

$$O_2 + e^- \longrightarrow O_2^{-\bullet}$$

$$O_2^{-\bullet} + H^+ \longrightarrow HO_2^\bullet$$

$$HO_2^\bullet + H^\bullet \longrightarrow H_2O_2$$

b) Initiation of degradation

Chain degradation catalysed by the electric field and ions of transition metals lead to the formation of chain radicals. Chain peroxides and peroxides radicals are produced (b and b').

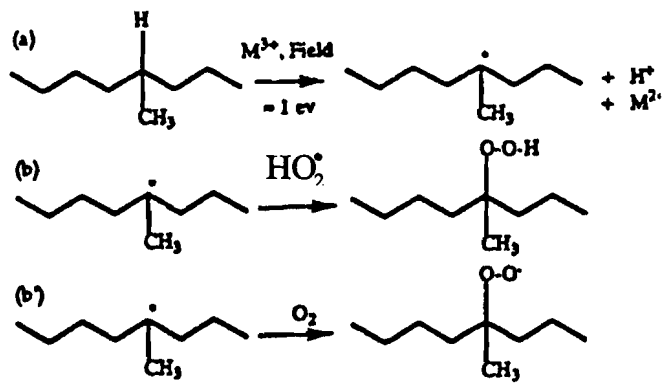

peroxide

peroxide radical

c) Catalysis of degradation by metal ions

Polymer chain peroxides and peroxide radicals perturb adjacent carbon-carbon bonds. Alkoxyl radicals will be formed.

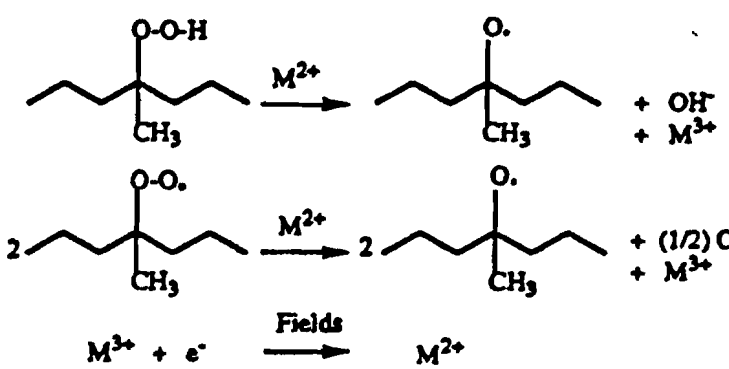

Alkoxyl radicals

d) Chain scission resulting in ketone and carboxylate ion formation

Chain alkoxyl radicals tend to form stable bonds by rearrangements. Adjacent carbon-carbon bonds can be broken. Ketones, chain scission and end-chain radicals appear. End chain radicals react to form carboxylate ions through intermediates such as aldehydes.

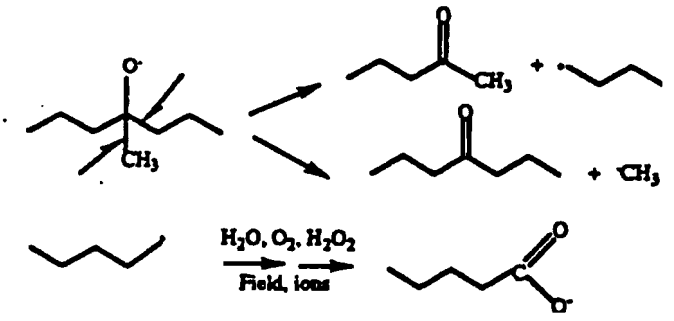

e) Conversion of ketones to carboxylates ions

Ketones can be converted to carboxylates by the action of the electric field

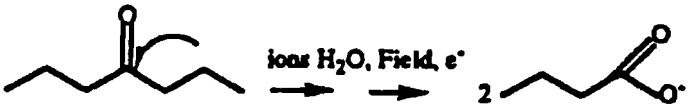

The set of reactions presented is just an example of possible reactions, for instance, in [Dissado92] different reactions are suggested.

In conclusion and quoting Crine: "Water treeing is a complex phenomenon tentatively explained (poorly) by several theories involving many parameters, with a lot of data, and for which we have a limited understanding of the synergistic effects between the various processes" [Crine98]. So even nowadays it is difficult to propose a totally satisfactory model for water treeing (for both inception and growth mechanisms). At present the available experimental data is contradictory and insufficient to provide enough basis for a complete theory. However some progress has been made and some conclusions can already be put forward as was presented above.

5.2 Electrical treeing

Electrical treeing will be briefly presented since no study on this phenomenon has been done during this work. Nevertheless it is a very important mechanism in electrical ageing. Its appearance will inevitably lead to breakdown after the electrical tree has crossed completely the insulation[34]. It has also been reported that water trees tips can become initiation sites for electrical trees.

[34] Even if not immediately.

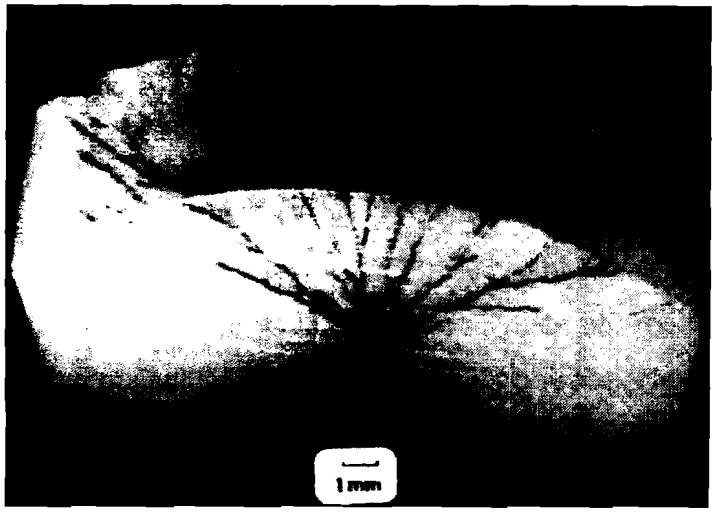

Figure 5.3 – Electrical tree grown in an XLPE cable during testing under DC voltage [Dissado92].

Electrical treeing is much better understood than water treeing. The main growth mechanism is partial discharges (PD). Initiation can take place at two different types of inhomogeneities where the electrical stress is higher. One is a solid interface, such as impurities (metallic particles, conducting contaminants) or structural irregularities that can enhance the electrical field [Dissado92]. The other is gas filled voids capable of originating PD leading to degradation. PD leaves charge on the cavity walls reducing the electric stress. Some charges will disappear either by recombination or charge transfer. The charge accumulation leads to the formation of a filamentary current with a very high current density and given rise to tree inception. On the other hand at impurities and interfaces the tree is initiated at sharp edges where the local electric field is higher. For laboratory experiences with metallic needle tips it was always present charge injection.

Like water trees they can be divided into vented and bow-tie trees. However unlike water trees the term vent agrees with the tree structure. Electrical trees are connected structures composed of channels (or tubes). The initial channel is a vent for the whole system and allows, in some cases, access to the external environment[35] (as the electrical tree in Figure 5.3 is an example).

The shape of the these trees dependent upon ageing conditions (electric field strength and frequency and polymer morphology) and can be divided into three types:

[35] The external environment can be the void or the semiconductor screen in cables.

a) Tree-like or branched – with channels showing diameters of ~30 μm for the larger branches to ~1 μm for the fine filamentary tubules. They appear for applied field, E_a, less than 5.4×10^8 Vm^{-1} if the frequency is 50 Hz.

b) Bush-type – very dense structures with a bush-like appearance. If these trees grow at 50 Hz the applied electrical field has to be 5.4×10^8 $Vm^{-1} < E_a < 6\times10^8$ Vm^{-1}.

c) Bush-branched – they are trees looking like bush trees but with one or more branches protruding from the bush boundary. If they appear at 50 Hz the applied electric field has to be higher than 6×10^8 Vm^{-1}.

The electrical trees are able to grow both under AC and DC voltage, voltage ramps, polarity reversal or impulses. In laboratory studies the most used configuration is a point-plane geometry using metal needles. Important parameters are nature of trapped gas, mechanical properties and morphology of the polymer in the bulk and at the interface [Mayoux97]. Regardless of AC or DC voltage the electrical trees show the same form[36]. The inception time for treeing is highly dependent on applied field, $t \propto E_a^{\,n}$, $5 < n < 20$ and is inversely proportional to frequency (experiments performed for an ageing time of 1 h gave $f^{1/3}$). The inception field under DC (slow ramp) can exceed the DC breakdown strength (space charge injected and trapped limits the local field). For large voids a minimum value for inception of the applied electric field is given by the partial discharge inception field.

In electrical treeing three different stages are observed [Dissado92]:

a) Inception stage;

b) Propagation or growth (divided in a initial fast growth and followed by slow fractal growth);

c) Runaway stage (leading towards breakdown).

After the tree has crossed the entire insulation breakdown is not always instantaneous (reported times to breakdown can be as high as 1h to 100h) [Dissado97a].

Like in water trees the shape of electrical trees implies a fractal character and a power law exists between the total damage (mass or volume) of the tree, $S(L)$, and tree length, L:

$$S(L) \propto L^{d_f} \tag{5.1}$$

[36] Once more contrary to water treeing mechanism that happens mainly under AC. The few reported experiments that successfully have grown water trees in DC results in very different shape from AC grown trees.

where d_t is the fractal dimension of the tree. For branch type trees, $1 < d_t < 2$ and bush or ball type, $2 \leq d_t \leq 3$.

As was stated above growth of electrical trees occurs through partial discharges in the gas-filled channels. For branch trees discharges happen intermittently covering the full length of the tree while for bush trees a large number of local discharges takes place over all the tree. These discharges cause localised damage producing a new channel extension to the tree.

A stochastic model has been proposed defining a local field dependent probability for a new extension to be formed (probability $\propto E^{\eta}$) and the field is calculated considering the tree as conductive [Niemeyer84, Wiesman86, David95].

Another model presented by Dissado et al. [Dissado97a] is the discharge avalanche model (DAM) evidencing the fractal character of the trees. The tree starts with the formation of a tubule that supports gas discharges. Propagation is impelled by discharges in the existing channels. To support the discharges the tubules walls have to be non-conducting. However discharges are a conducting extension of the initiating point. Damage is proportional to the number of ionisations occurring during avalanche. The physical mechanism(s) causing damage is (are) not exactly know but possible processes are: mechanical fracture in the electrostatic field of the space charge left by the partial discharges, bond breaking during the avalanche by thermal and other effects, bond breaking either by energy released during charge recombination or hot electrons produced in charge trapping. In this model field fluctuations produce the tree structure. The fluctuations are associated with space charge arising from the discharge avalanche itself.

Summarising, electrical trees are basically an ageing process driven by partial discharges. If they cross completely the insulation, they will end up giving rise to breakdown and failure of the insulation characteristics of the material.

5.3 Dielectric breakdown

Breakdown in an insulator material is always a destructive and irreversible process in which the material no longer possesses the insulating characteristics and his useful lifetime ends. It results in the formation of a breakdown channel crossing the polymer from one electrode to the other. This catastrophic process is caused by the electric field and is a thermal mechanism since damage consists of melting, carbonisation or vaporisation of the polymer (as can be observed in Figure 5.4).

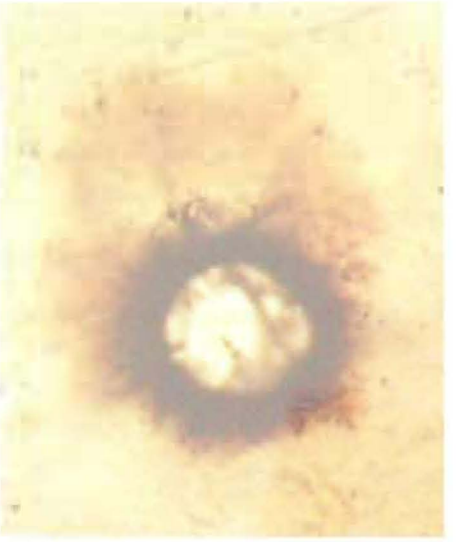

Figure 5.4 – Breakdown channel and water tree (wet, not dyed). It is visible the damage caused in the polymer by the breakdown. Interesting it was also the presence of the water tree (possibly the water tree has acted as an initiation for an electrical tree that end up originating a breakdown channel).

There are several phenomena leading to breakdown: thermal, electrochemical, electronic and partial discharges [Dissado92].

5.3.1 Thermal breakdown

Thermal breakdown takes place when the heat dissipated by the material cannot balance the generated heat. The temperature of the polymer increases (usually locally) and a critical value is reached. Conductivity rises exponentially by increased segmental motion in the region at high temperature. The current density is in turn increased causing further heating and the local temperature continues to augment. In this way a thermal runaway can happen giving rise to thermal instability. On the other hand the polymer can be physically damaged (for instance by melting). For localised thermal breakdown a filamentary breakdown path can be formed at a weak point in the material.

5.3.2 Electromechanical breakdown

Electrostatic attraction of the electrodes (electrostriction) causes a compressive stress. When the elasticity of the polymer is not enough to compensate the force, electromechanical breakdown occurs. Local heating can soft the polymer enhancing the electromechanical effect. The reduction in thickness increases the electric field and another breakdown mechanism can become active. Localised (filamentary) breakdown can take place at areas of

high stress. Shear stress can be active in these areas causing damage, which increases the local field that causes further damage.

In polyethylene the formation of soft spots by Joule heating has been observed without causing thermal breakdown [Dissado92]. However the consequent reduction of Young modulus lowers the breakdown strength and gives rise to electromechanical failure[37]. Electromechanical breakdown is more likely to occur in thinner specimens but it can also be part of the process of transforming partial discharges into electrical trees.

5.3.3 Electronic breakdown

Electrons are accelerated by the presence of the electric field and gain enough kinetic energy to cause local damage. Electronic breakdown can be divided into avalanche and Zener breakdown. The last one only occurs in semiconductors by electron tunnelling and requires high fields.

Impact ionisation or avalanche breakdown occurs when high energy electrons (accelerated by the field, injected from the cathode or by local fluctuations) can cause ionising collisions that generate ions and more electrons. This new electrons can in turn be accelerated and produce news collisions and more free carriers. By successive generation an avalanche process is created causing irreversible damage.

In polymers it is possible that electrons are captured in traps and the avalanche does not form. However in polyethylene the mobility can be high enough ($>10^{-4}$ $m^2V^{-1}s^{-1}$) to give rise to an avalanche breakdown. In thick insulators the field is not high enough for this mechanism to take place nevertheless very high local field can occur (for instance in a laboratory experiment using needle-plane configuration the field can be high near the electrode tip).

5.3.4 Partial discharge breakdown

Even the more sophisticated manufacturing and processing of polymers is unable to prevent gas-filled voids. Also voids can be introduced around defects or enlarged by additive diffusion, electromechanical forces or electrochemical effects (such as water trees). Their dimension can be as high as millimetres and go down to tens of nanometers. Below this value there is free volume which is a characteristic of the polymer and not a result of processing.

Void permittivity and breakdown strength are usually lower than the surrounding polymer. Also the local electric field is enhanced at the interface void/polymer in the field direction. If

[37] More than one effect can be combined to cause breakdown (in this case thermal and electromechanical).

the field is above a threshold value the gas can be ionised and the charge carriers are accelerated. Collision with the voids walls causes sparks and erodes the polymer. Nonetheless in free volume paths of tens of nanometers can exist making possible to accelerate free carriers and cause damage. The inception voltage for partial discharges in voids depends on the gas nature and pressure and void shape and size.

As was mentioned in 5.2, partial discharges can initiate and propagate electrical trees and finally breakdown occurs.

5.3.5 Stochastic nature of breakdown

Breakdown only occurs above a critical field. However breakdown does not take place immediately after a field above this critical value is applied. There is a statistical distribution of breakdown initiation times and also a statistical distribution of breakdown voltage that have an associated probability.

The stochastic nature of this process can have two different physical basis. One is spatial differences since breakdown is a local process depending on local conditions. The other is dynamic fluctuations caused by the constant changes in the local electric field.

5.4 The influence of trapped space charge in electrical ageing

Recently it has been proposed by Dissado et al. a model based on the effect of trapped space charge. It is assumed that ageing results from combined electrical and thermal stresses (electrical thermal life model). Rather than to relate ageing to defects resulting from manufacturing (macroscopic causes) this approach is made from the microscopic point of view and with trapped space charges assuming an important role[38]. A thermodynamic approach is considered with a reversible reaction taking the polymer from its initial state to electrical failure. The polymer is represented by moieties in initial state 1 (undeformed) and an activation energy barrier has to be overcome to reach the final state 2 (deformed). When a given fraction of moieties from the initial state have been converted to the final one it is accepted that the polymer electrical life has ended. The effect of the ageing is to form and/or enlarge voids by electromechanical stress. It is also assumed that the major contribution to the total time to breakdown, comes from the initiation time for microcraks or crazes to be formed and/or enlarged and not from the subsequent partial discharges (with electrical treeing formation and growth) and dielectric breakdown [Dissado95].

[38] This is more relevant for the extra-clean polymers that are being produced nowadays.

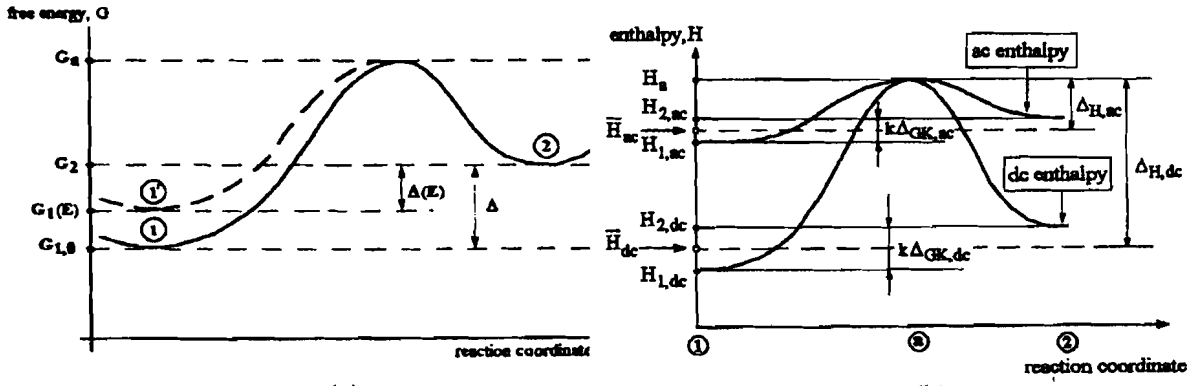

(a) (b)

Figure 5.5 – (a) Free energy diagram showing the effect of the applied field (space charge) in reducing the activation energy barrier [Dissado97]. (b) Effect of the applied voltage being DC or AC on the enthalpy of the reactants. The activated and the product states remain unchanged with the field for the DC regime but only the activated state remains unchanged for the AC [Mazzanti99].

The effect of trapped space charge is to reduce the activation barrier for the reaction to occur (see Figure 5.5 – (a)). There are electrostatic and electromechanical energies that arise from the enhanced local electric field of the space charges and these energies are more important at the boundary of the charge region. The model has many parameters but it is possible to assign a phenomenological meaning to them. They are all related to charge trapping and insulation degradation. It is also possible to predict a time for the formation of the microcracks (a lifetime for the insulation). The model also foresees thresholds for temperature and electric field.

The underlying physical description is different depending on whether DC or AC voltages are applied. However the electric field dependence is of the form $C'E^{4b}$ regardless of the frequency (C' is a constant related to polymer structure).

For DC the electromechanical stress generated by the presence of the space charge and the electric field ends up increasing the local strain and causes micro-creep [Dissado97]. Thus it is expected crazing and microvoid formation and coalescence. This results in the field dependence stated in the above paragraph and $C' \propto \frac{\alpha^2}{Y\varepsilon^4}$ (α is the electrostriction coefficient, Y the Young modulus and ε the dielectric permittivity).

When an AC field is applied the ageing is faster so a different mechanism must occur. In this case Maxwell stress are present giving a frequency dependence to some of the parameters [Mazzanti99] and adding new ones that can be also frequency dependent. However the dependence on $C'E^{4b}$ remains. The parameters related to the polymer structure remain unchanged. Those that are related to free energy differences (Gibbs[39], enthalpy and entropy) are affected by the amplitude and frequency of the electric field (for the influence on enthalpy see Figure 5.5 – (b)). The considerable reduction of the activation energy barrier in the AC regime is in good agreement with the expected greater harmfulness of the AC ageing compared with DC.

The model described above is not valid for nanovoids (diameter ≤ 10 nm) and it was recently modified to consider this feature. In this case elemental strain is responsible for the increase of pre-existing voids in the nanometer range [Dissado01]. The main difference is a field dependence of the form E^{2b} resulting from a new equation for the electromechanical energy and the role of the Young modulus is replaced by the bulk modulus [Mazzanti01]. From this thermal life model it is possible to calculate charge concentration in the voids which are in good agreement with the experimental results.

[39] The Gibbs free energy difference is not modified when going from DC to AC but the enthalpy is (see Figure 5.5 – (b)). The entropy variation for the DC voltage is also increased by 3 orders of magnitude for AC and can no longer be neglected.

Chapter 6. Experimental

6.1 Sample preparation and electrical ageing

6.1.1 Usual procedure

Films of low density polyethylene (LDPE) and cross-linked polyethylene (XLPE) were press moulded from pellets (Figures 6.1 and 6.2). Polyester (PET) discs had to be used in order to prevent polyethylene from adhering to the mould discs. The resulting pressed films of PE are around 10 cm in diameter and usually ≈ 200 μm thick. Pressing procedures were different for the two distinct polyethylene types.

The LDPE pressing process was carried out in 3 steps:

Heating up to 120 °C (or 140 °C) with no applied pressure; temperature kept at 120 °C (or 140 °C) for 5 min;

Pressure was applied gradually up to 250 bar; temperature kept at 120 °C (or 140 °C) for 50 min;

Cooling under pressure to room temperature (with the help of a water-coil).

The XLPE pellets contained dicumyl peroxide that catalysed the cross-linking process during the film manufacture. The pressing conditions were similar to LDPE except that the maximum temperature was 150 °C and the maximum pressure was applied quickly.

For ageing samples of diameter ≈ 30 – 35 mm and ≈ 200 μm thickness[40] were cut from the pressed films. Ageing was carried out in the laboratory using modified Cigré cells [Houlgreave92] as can be seen in Figure 6.3[41]. The basic configuration of a modified Cigré cell developed by Houlgreave et al. ([Houlgreave92, Fothergill93]) was chosen (see Figures 6.3 and 6.4). During ageing the cells were immersed in an insulator oil bath to ensure electrical insulation and also to keep the bath temperature constant. The planar samples were in contact with the aqueous solution. The solution acted as electrodes on both sides of the disc shaped samples (planar electrodes configuration).

Two different types of ageing processes were carried out: AC electrical ageing and thermal ageing in solution. For electrical ageing the samples were subjected to an applied AC field of 6 kV/mm at 50 Hz, (some additional experiments were made at a higher frequency ≅ 1 kHz)

---

[40] In addition some samples up to 1 mm thick were used in order to be microtomed.

[41] Many different configurations and geometries have been used in laboratory experiments for the electrical ageing of polymers (see Chapter 5).

at four different constant temperatures, respectively, room temperature[42] (RT), 35 °C, 40 °C and 50 °C. The aqueous solution was sodium chloride with concentration of 0.1 M or 1 M. The ageing time varied from 250 h up to a maximum of 2000 h . Thermal ageing took place under similar conditions except that no field was applied to the samples. These samples act as a reference for the single effect of immersing in solution at a given temperature for the same time as the electrically aged samples. A photograph of the thermal baths where the cells were immersed can be seen in Figure 6.5.

Figure 6.1-Press with controlled temperature used in the production of the polyethylene films.

Special safety care was taken since the experiments had to be run continuously for a long time (the longest ones for 2000 h) and it was necessary to build a Faraday cage. In order to apply the electric field an oil transformer coupled with a variable power amplifier (0 – 30 kV, 700 W, 50 Hz) was built (Figure 6.6). For the higher frequencies (≅ 1 kHz) a Trek HV power supply Model 610C was used. However a power limiting problem did not allow us to apply the field for a very long time and therefore most of the samples were aged under a frequency of 50 Hz.

[42] Room temperature samples could have no temperature control and then it could vary from 20 °C to 30 °C. Other samples were kept at constant temperature of 25 °C (RT in a Lisbon summer can be as high as 26–27 °C in the aqueous solution).

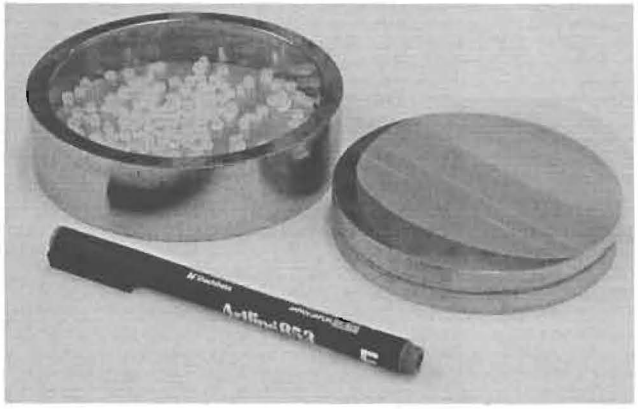

Figure 6.2- Mould used for the production of the polyethylene samples (LDPE pellets are visible).

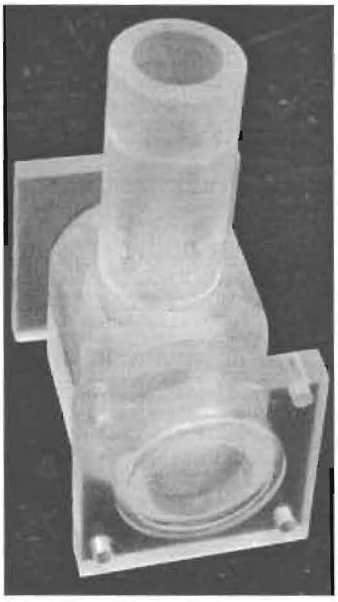

Figure 6.3- Modified Cigré cell (half a cell is seen).

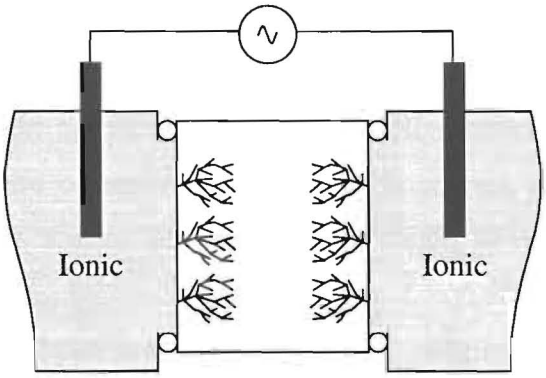

Figure 6.4 - Schematic representation of the modified Cigré cell.

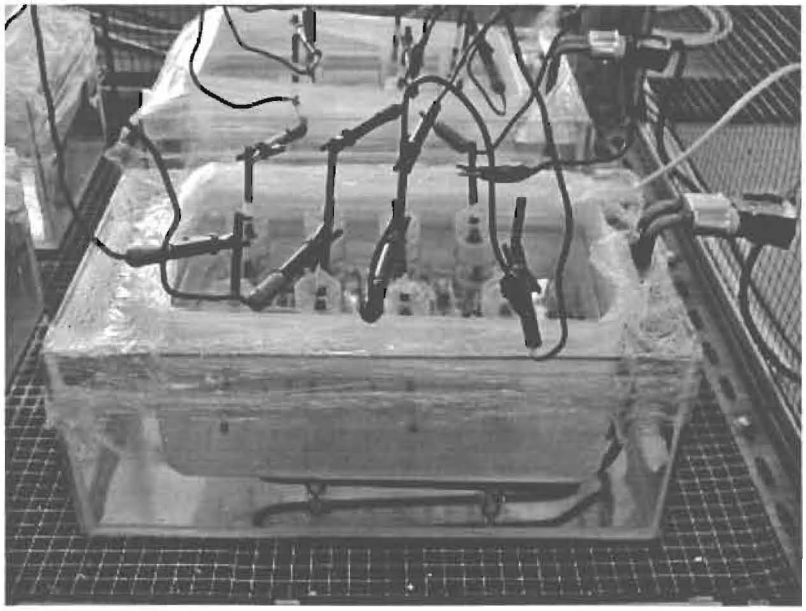

Figure 6.5 – Thermal bath with the ageing cells immersed.

6.1.2 Sample ageing for NMR studies (of pore dimension)

The ageing process of these samples was similar to that just presented. In order to increase initiation sites for water trees (and so the water tree density and the water content) the samples were sandblasted on one side prior to ageing. The configuration can be considered water-needle/planar instead of planar/planar as previously. All samples were aged at 40 °C, 6 kV/mm, 50 Hz in a solution of 0.1 or 1 M NaCl.

6.2 Analysis of the unaged polyethylene specimens

Some properties of the unaged polyethylene were studied (mostly low-density polyethylene but also some crosslinked polyethylene samples). Among the techniques used were optical/polarised light microscopy (Euromex ML 2000 microscope with reflected and transmitted light capabilities), scanning electron microscopy (Zeiss DSM-962) and atomic force microscopy (Nanoscope III AFM/STM with electric field and Kelvin probe). These techniques allowed the surface defects and spherulites to be investigated and with AFM images it was possible to obtain a value for the surface roughness by image analysis techniques.

Differential scanning calorimetry (Setaram DSC92) was employed to study melting point and glass transition temperatures. Two different scanning rates were used (1 and 5 °C/min).

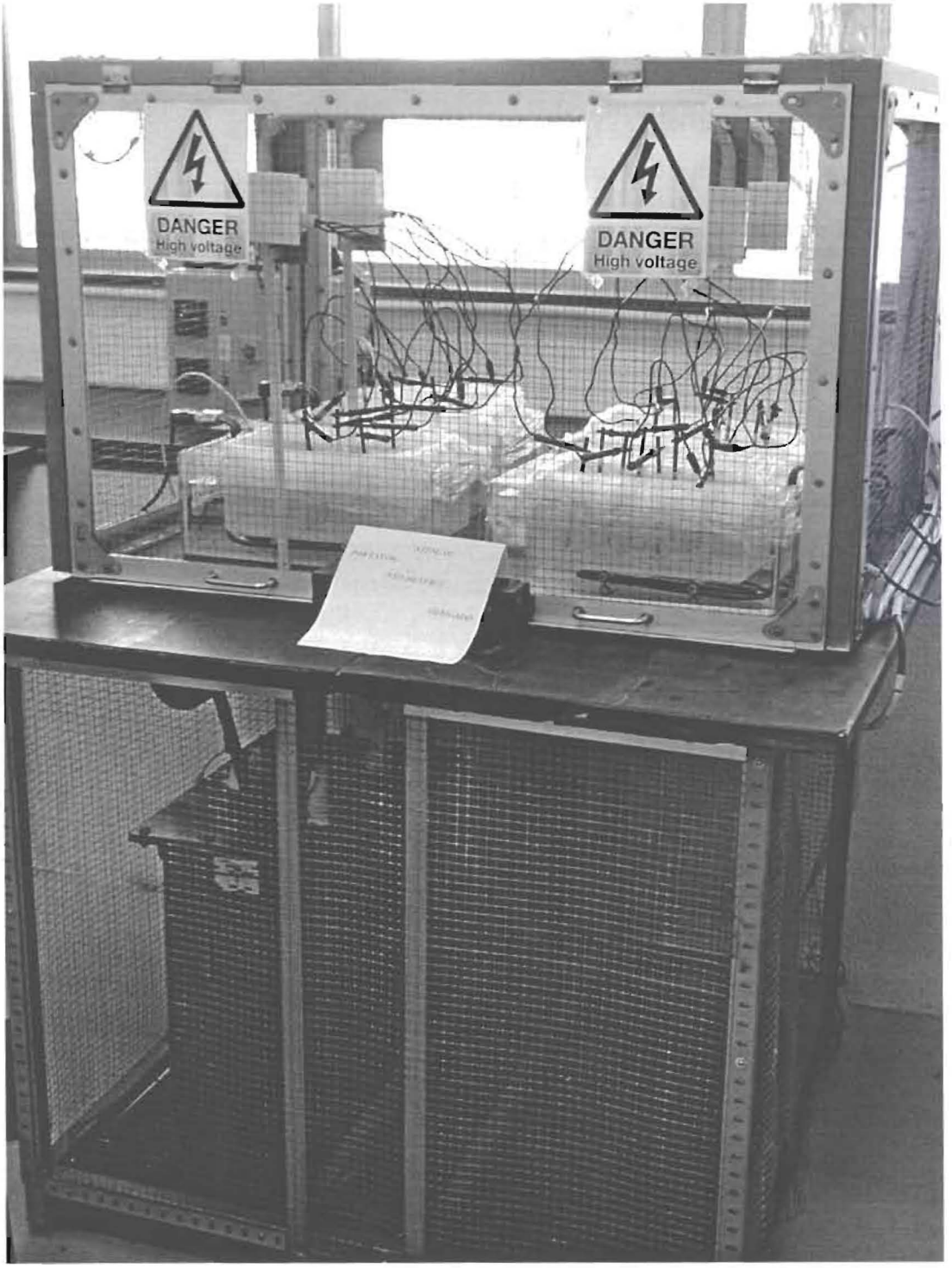

Figure 6.6 – Faraday cage and setup for the electrical ageing of PE. The cells immersed in the thermal bath can be seen inside the Faraday cage. On the lower part the oil transformer is visible.

Surface potential measurements were made in order to determine the presence of charges deposited during sample preparation. A Trek 6000B-7C electrostatic scan probe and a Trek 344-3 ESVM electrostatic voltmeter were used to measure the surface potential in different

positions (see Figure 6.7). The system allowed a line (one-dimensional) scanning of the sample and was coupled to a computer for data acquisition. Also the voltage decay was studied by performing measurements starting immediately after pressing until a week later (5 min, 72h and 1 week after pressing, respectively).

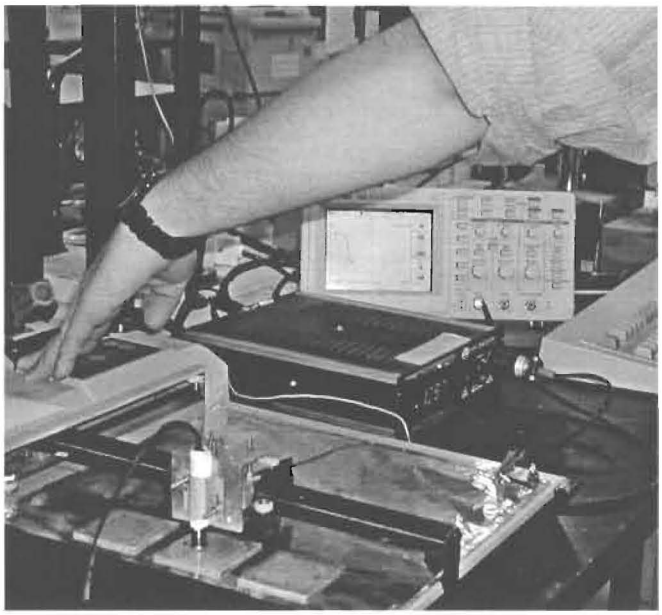

Figure 6.7 – Surface potential measurement apparatus.

X-ray diffraction (DRX–Rigaku DMAX III-C) allowed the estimation of the crystallinity and crystallite size. The crystalline percentage was calculated using the method of Nichols [Nichols54] based on calculation of the area of the three main peaks of polyethylene (corresponding to diffraction in planes (110), (200) and of the broad peak resulting from diffraction in the amorphous part). The background was subtracted and the areas of the three peaks obtained; the percentage of amorphous content, A, is calculated according to the formula:

$$A(\%) = 100\frac{xa}{xa + yb + zc}, \tag{6.1}$$

where a, b and c are, respectively, the areas of the amorphous, (110) and (200) peaks. The constants x, y and z are corrections factors for the polyethylene X-ray diffraction spectrum taking into account the atomic scattering factors, absorption, temperature and diffraction angle and their values are $x = 0.69$, $y = 1.00$ and $z = 1.43$ [Nichols54].

The crystallite size, d, was calculated using Scherrer´s method [Cullity78, Nath89, Das Gupta94]:

$$d = \frac{0.9\lambda}{\beta \cos\theta} \tag{6.2}$$

where λ is the wavelength of the X-ray beam (in this work Cu K_α radiation was used, which has $\lambda = 1.54$ Å), β is the full width at half height of the peak and θ is the Bragg angle.

6.3 Dielectric permittivity measurements

To cover the whole frequency range (10^{-5} Hz to 10^5 Hz) different measurement techniques had to be used. For the low frequency (LF) measurements ranging from 10^{-5} Hz to 10^{-1} Hz time domain measurements were performed. Samples were DC charged at 30 °C for 27 h with an applied electric field of 2 kV/mm using a Fluke HV-410B power supply. After switching off the applied voltage the sample was short-circuited and discharged through a 617 Keithley electrometer. The discharge current was recorded for 3 h (approximately 10^4s). Using the Hamon approximation (see Equation 4.21 in 4.3), it was possible to calculate the imaginary part of the dielectric constant. Another approximate equation can be deduced to obtain the real part of the permittivity [Dias96]:

$$\frac{d\varepsilon'(\omega)}{d(\ln\omega)} \approx -\frac{2}{\pi}\varepsilon''(\omega) \tag{6.3}$$

In the medium frequency range (MF) – 10^{-1} Hz to 10^2 Hz – measurements were performed using a lock-in amplifier (EG&G-7265). Applying an AC low voltage signal (V) at the measuring frequency both the real and imaginary dielectric constants could be obtained from the direct measurements of the two components of the current (i_x and i_y):

$$\varepsilon' = \frac{i_y}{\omega V C_0} \quad \text{and} \quad \varepsilon'' = \frac{i_x}{\omega V C_0} \tag{6.4}$$

Finally in the high frequency region (HF) – 10^2 Hz to 10^5 Hz – a RLC General Radio Bridge 1621 was used. The dielectric constant was calculated from the measured values of the capacitance, C_p, and the conductance, G_p (see 4.7.1):

$$\varepsilon' = \frac{C_p}{C_0} \quad \text{and} \quad \varepsilon'' = \frac{1}{R_p C_p \omega} = \frac{G_p}{C_0 \omega} \tag{6.5}$$

All the spectra were obtained at 30 °C under vacuum. Samples were aged for different times (500 h, 1000 h and 1500 h) and at different temperatures[43] (RT – room temperature[44], 35 °C and 40 °C). For the electrically aged samples an AC electric field of 6 kV/mm at a frequency

[43] The ageing temperature was kept constant throughout the ageing process (as stated in 6.1).

[44] Varying from 20 °C to 30 °C.

of 50Hz was applied. Another set of samples was thermally aged by being kept at the same temperature and for the same time but without applied electric field.

A remark should be made about experimental errors. According to Wintle et al. ([Wintle85] and [Wintle89]) edge effect corrections for disc electrodes on sheet dielectrics should be taken into account depending on the radius/thickness ratio of the samples. Based on Wintle calculations [Wintle89], the excess capacitance due to these effects was estimated for samples of 33 mm diameter and thickness around 200 μm, giving a value near 1.5% of the total capacitance. As the errors due to the inaccuracy of thickness and diameter measurements were near 10% (reflected also in a 10% error for the permittivity) it was considered unnecessary to apply the edge correction. The total error made in the measurement of the dielectric constant is never less than 10%. Probably an upper bound would point to a 20% error. There are a few experimental parameters for which the influence on the total error is difficult to quantify, such as temperature and pressure during the measurement. Since the values of ε'' are so low, they are near the resolution limit of the measuring devices, that even an error as high as this is an improvement on existing knowledge.

6.4 Isothermal charge and discharge currents and non-isothermal discharge currents

For high insulating polymers such as PE, space charge can remain trapped for very long times. After an experiment involving sample charging it is possible that a residual space charge remains and can even go undetected in discharge current measurements. However if a non-isothermal experiment is performed the influence of the remnant charge is visible. Consequently common TSDC measurements are highly affected even if conventional methods for isothermal charge and discharge measurements are sometimes unable to reveal the presence of this space charge in the sample. Therefore it is difficult to obtain reproducible results if care is not taken to control the remnant space charge. To overcome this problem, in this work a very recent procedure combining isothermal charge and discharge methods and non-isothermal measurements [Neagu01] was used and adapted for LDPE [Lança02]. This combined procedure is an improvement of the FTSDC (final thermally stimulated discharge current) method [Neagu99].

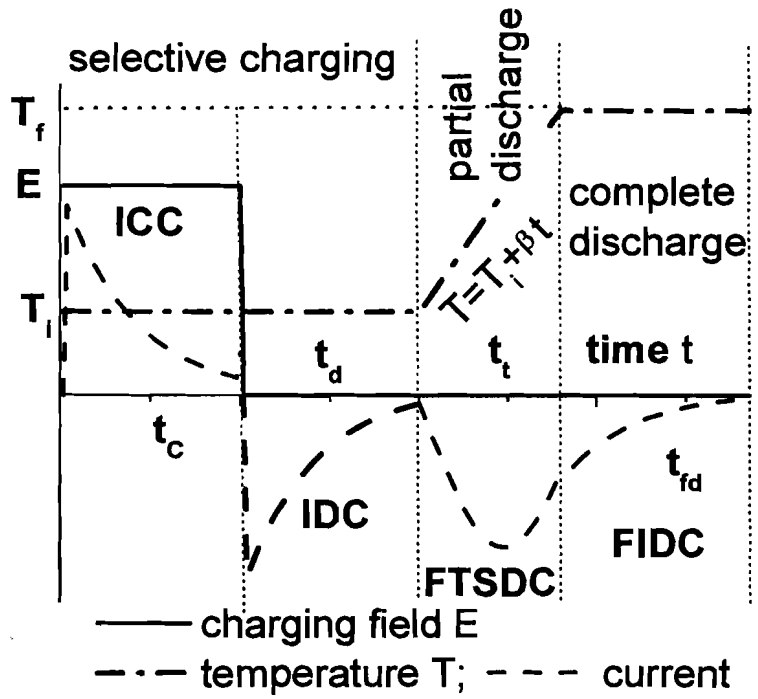

Figure 6.8 – Experimental procedure used to analyse space charge in LDPE. The four steps are schematically represented showing electric field, temperature and current. Selective charging corresponds to isothermal charging and discharging. Partial discharge proceeds during FTSDC. Almost complete discharge is only achieved during FIDC (schematics adapted from [Lança02]).

In order to ensure almost complete discharge of the sample a complete run of an experiment is composed of different steps (see Figure 6.8):

i) and *ii)* Isothermal DC charge and discharge currents measurement (ICC – isothermal charge current and IDC – isothermal discharge current). The sample is charged[45] at constant temperature (T_i) with a DC field (E) applied during time t_c and the ICC registered[46]. Then the field is switched off and the sample discharges during time t_d still at constant temperature T_i. and the *IDC* is recorded. This corresponds to selective charging of the sample.

iii) Non-isothermal discharge current measurement (FTSDC – final thermally stimulated discharge current) in which the sample is heated at a low constant rate β.

[45] HV power supply Ortec 456H.

[46] Currents were measured with Keithley electrometers models 617 and 6517A.

iv) Final isothermal discharge current measurements (FIDC) at the final temperature of *iii)* to allow a complete discharge of the sample, as much as possible, and the FIDC to be registered.

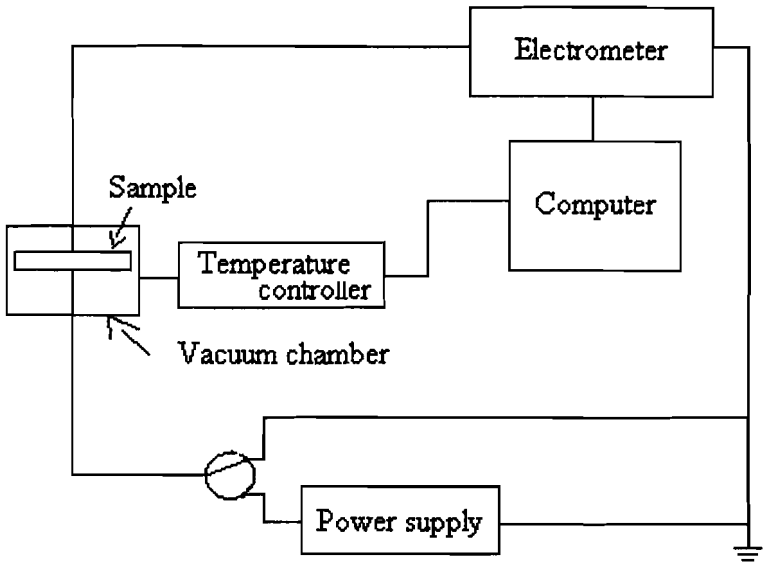

Figure 6.9 – Schematic representation of the experimental setup for combined isothermal charge, discharge current and non-isothermal discharge current measurements (FTSDC).

A careful selection of charge and discharge conditions (field amplitude, temperature and ratio of charge and discharge times) allow distinct features of space charge traps (activation energy and relaxation times) to be revealed in the following FTSDC. Finally the FIDC at the final temperature of FTSDC allow almost complete discharge of the sample. In this way the sample is conditioned so that prior history does not influence the next measurement impairing reproducibility and interpretation of results. The complete procedure is repeated in each run. Experiments following this full procedure are time consuming (particularly the FIDC step) but unfortunately unavoidable.

The first sample to be studied following this procedure was also used to establish the best parameters (field, temperature and charge/discharge times ratio) to be utilised for charging and discharging (selective charging) the following samples. A schematic representation of the experimental setup is seen on Figure 6.9. Aluminium electrodes with 33 mm diameter were vacuum deposited on both surfaces of the disc shaped samples. All experiments were performed under rotary pump vacuum.

Three different types of samples were used: *a)* thermally aged in solution (during 1500 h at 40 °C in 1M NaCl), *b)* electrically aged in solution (applied electric field of 6 kV/mm, 50 Hz during 1500 h at 40 °C in 1M NaCl) and *c)* unaged (just hot press moulded).

The method followed was implemented using samples of type *a)*, by a thorough test of the different conditions. For this sample charging and discharging temperatures of 2, 10, 20 and 30 °C were studied. Field intensity was also investigated and fields of 1, 2, 3, 4 and 5 kV/mm were applied. The influence of the ratio of charge and discharge times was also analysed. FTSDC was performed always at a heating rate of 1 °C/min from charging temperature up to 90 °C. This final temperature was kept during a long enough time in order to ensure almost complete discharge of the remnant space charge after each run (FIDC). Table 6.1 shows the history of measurements for a thermally aged sample.

A similar sequential procedure was followed for samples of type *b)* and *c)*, as can be seen in Tables 6.2 and 6.3.

The influence of rate of cooling (between two consecutive runs) was studied but it was difficult to achieve definitive conclusions.

6.5 Pulsed electroacoustic space charge profile measurements (PEA)

PEA allows us to obtain the depth profile of the space charge in the sample at high fields [Maeno88, Li94]. The measurements were performed in a setup developed at Kings College (University of London) and at the University of Leicester. The PEA cell used is suitable for sample with thickness of 100 to 300 μm [Alison98, 98a] and the LDPE samples used were 200 μm thick. A +400 V pulse of 5 ns duration was applied together with ±2.5 kV_{DC}. Measurements were performed at room temperature in air and three differently aged samples were used (unaged, electrically and thermally aged at 50 °C for 1500 h in a 1 M NaCl solution). The electrically aged specimen showed water trees and was measured dried and after 24 h immersion in distilled water (wet). The space charge profile was obtained from deconvolution of the voltage signal resulting from a piezoelectric sensor [Jereoense97]. The piezovoltage was measured at different times after application of the DC voltage (usually 0 h and 2 h later).

Table 6.1 – Measurement history of a thermally aged LDPE sample at 40 °C during 1500 h in 1M NaCl.

Run	Charge (ICC)	Discharge (IDC)	Final discharge (FIDC)@90 °C
1	2 kV/mm, 30 °C, 27h00	30 °C, 23h20	15h00
2	No charging[47]	–	–
3	2 kV/mm, 30 °C, 1h00	30 °C, 1h45	19h00
4	2 kV/mm, 30 °C, 3h00	30 °C, 3h00	40h00
5	2 kV/mm, 30 °C, 1h00	30 °C, 21h00	7h30
6	2 kV/mm, 30 °C, 1h00	30 °C, 3h00	32h00
7	2 kV/mm, 30 °C, 1h00	30 °C, 2h00	32h00
8	2 kV/mm, 30 °C, 1h00	30 °C, 2h00	14h30
9	4 kV/mm, 30 °C, 1h00	30 °C, 2h00	27h40
10	1 kV/mm, 30 °C, 1h00	30 °C, 2h00	18h00
11	3 kV/mm, 30 °C, 1h00	30 °C, 2h00	18h00
12	2 kV/mm, 20 °C, 1h00	20 °C, 2h00	14h00
13	3 kV/mm, 30 °C, 1h00	30 °C, 2h00	42h00
14	3 kV/mm, 30 °C, 1h00	30 °C, 2h00	24h00
15	5 kV/mm, 30 °C, 1h00	30 °C, 2h00	62h00
16	2 kV/mm, 10 °C, 1h00	10 °C, 2h00	42h00
17	2 kV/mm, 3 °C, 1h00	3 °C, 2h00	22h00
18	4 kV/mm, 2 °C, 1h00	2 °C, 1h00	19h00
19	2 kV/mm, 2°C, 1h00	2 °C, 3h00	–

[47] *No charging* is used to designate a run where just FTSDC was performed and, when a time value is seen in the fourth column, FIDC was also carried out.

Table 6.2 – Measurement history of an unaged sample

Run	Charge (ICC)	Discharge (IDC)	Final discharge (FIDC)@90 °C
1	2 kV/mm, 30 °C, 27h00	30 °C, 23h00	23h00
2	No charging	–	16h30
3	2 kV/mm, 2 °C, 1h00	2 °C, 2h00	16h30
4	4 kV/mm, 2 °C, 1h00	2 °C, 2h00	20h00
5	2 kV/mm, 2 °C, 1h00	2 °C, 3h00	16h00
6	2 kV/mm, 2 °C, 1h00	2 °C, 3h00	62h00
7	2 kV/mm, 2 °C, 1h00	2 °C, 3h00	62h30
8	4 kV/mm, 2 °C, 1h00	2 °C, 3h00	15h20
9	No charging	–	–
10	6 kV/mm, 2 °C, 1h00	2 °C, 3h00	13h45
11	Cooling and heating[48]	–	80 °C, 1h50
12	Cooling and heating	–	44h30
13	Cooling and heating	–	14h40
14	Cooling and heating	–	–
15	Cooling and heating	–	–
16	Cooling and heating	–	–

[48] *Cooling and heating* is used to designate a run were the sample was first cooled down from the previous FTSDC/FIDC maximum temperature (and the current was measured) and then heated (FTSDC). When a time value is seen in the fourth column, FIDC was also performed.

Table 6.3 – Measurement history of a sample aged at 40 °C, 1500 h, 1M NaCl, AC 6 kV/mm, 50 Hz.

Run	Charge (ICC)	Discharge (IDC)	Final discharge (FIDC)@90 °C
0	–	–	17h30
1	No charging	–	2h55
2	No charging	–	–
3	2 kV/mm, 2 °C, 1h00	2°C, 2h00	61h00
4	2 kV/mm, 2 °C, 1h00	2°C, 3h00	17h00
5	4 kV/mm, 2 °C, 1h00	2 °C, 2h00	14h15
6	2 kV/mm, 2 °C, 1h00	2 °C, 4h00	18h30
7	4 kV/mm, 2 °C, 1h00	2 °C, 4h00	14h25
8	No charging	–	–
9	4 kV/mm, 2 °C, 1h00	2 °C, 4h00	41h00
10	2 kV/mm, 2 °C, 1h00	2 °C, 4h00	34h00
11	4 kV/mm, 2 °C, 1h00	2 °C, 4h00	17h30
12	4 kV/mm, 2 °C, 1h00	2 °C, 2h00	40h00
13	4 kV/mm, 2 °C, 1h00	2 °C, 2h00	54h00
14	3 kV/mm, 2 °C, 1h00	2 °C, 4h00	15h00
15	3 kV/mm, 2 °C, 1h00	2 °C, 2h00	15h00
16	3 kV/mm, 2 °C, 1h00	2 °C, 2h00	20h30
17	3 kV/mm, 2 °C, 1h00	2 °C, 1h00	15h00
18	3 kV/mm, 2 °C, 1h00	2 °C, 1h00	56h00
19	3 kV/mm, 2 °C, 1h00	2 °C, 1h00	12h30
20	3 kV/mm, 2 °C, 1h00	2 °C, 1h00	45h00
21	3 kV/mm, 2 °C, 1h00	2 °C, 1h00	43h00
22	2 kV/mm, 30 °C, 1h00	30 °C, 2h00	38h30
23	Cooling and heating	–	–
24	Cooling and heating	–	–
24a	Cooling and heating	–	–

Table 6.3 – Measurement history of a sample aged at 40 °C, 1500 h, 1M NaCl, AC 6 kV/mm, 50 Hz (continued).

Run	Charge (ICC)	Discharge (IDC)	Final discharge (FIDC)@90 °C
25	3 kV/mm, 30 °C, 1h00	30 °C, 2 h00	18h00
26	Cooling and heating	–	–
26a	Cooling and heating	–	–
26b	Cooling and heating	–	–
27	4 kV/mm, 30 °C, 1h00	30 °C, 2h00	15h00
28	Cooling and heating	–	–
28a	Cooling and heating	–	–
29	Cooling and heating	–	–
29a	Cooling and heating	–	–
30	2 kV/mm, 2 °C, 1h00	2 °C, 2h00	22h00

6.6 Water treeing dyeing and counting

After ageing most of the samples will show small brownish spots, that are visible to the naked eye. If observed with the help of an optical microscope they can be easily identified as water trees. The water contained in the trees makes them visible because of the different refraction indexes of water and polymer. If the polymer is not kept in water in less than 24 h they will no long be visible (the water tree dries). Rewetting the samples (for approximately 24 h in distilled water) makes the trees visible again. In order to render them permanently visible the discs were methylene blue dyed using the technique developed by Siemens (see Appendix A).

Photographs of the dyed specimens were obtained by coupling an optical microscope with a photographic camera (usually enlarged ≅100× or 400×). From these photographs it was possible to count the number density and also the maximum size of water trees for the aged discs. This process is very time consuming and was done only for very few samples.

6.7 Fractal analyses of water trees

6.7.1 Water tree images: methylene blue and SEM microphotographs

For this study two types of images of water trees were analysed: methylene blue dyed and SEM images. The ramified aspect of water trees (being a growth process) suggest underlying fractal characteristics. Estimation of the fractal dimension may help to support the fractal hypothesis and also quantify the amount of damage within the tree[49].

(a) Methylene blue dyed water trees images

Some of the samples analysed were aged at Leicester University [Houlgreave92, Fothergill93] and others at Lisbon during this work. Both of them used pressed moulded LDPE disc-shaped samples and a modified Cigré ageing cell. Applied fields varied from 3.0 kV/mm to 11 kV/mm and frequencies from 50 Hz to 3 kHz. Photographs of the dyed water trees were digitised and an image process treatment was applied.

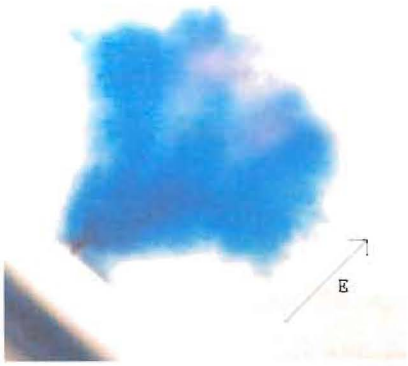

Figure 6.10 - Water tree grown (bush-like) in LDPE aged at 50 Hz (Leicester set). Photograph showing a water tree growing along the electric field direction, // (courtesy of Houlgreave and co-workers).

Figures 6.10 and 6.11 show typical examples of trees grown at different frequencies. The trees are bush like if grown at 50 Hz while at 1.16 kHz they have the shape of viscous fingers. Photographs were taken along two different directions, one perpendicular and the other parallel[50] to the electric ageing field, *E*. In this study it is better to identify these two different perspectives from the point of view of the photographed object rather than that of the

[49] For a brief introduction to some concepts of the fractal geometry see Appendix B.

[50] The disc-shaped samples were microtomed after ageing.

photographer. Therefore the photos taken along the direction perpendicular to the electric ageing field, where the water trees are observed along the growth direction of the applied field (and it is seen a cut perpendicular to the discs planar surface), will be described as "*parallel images*". And the photographs taken along the direction of the field, where the trees growth is observed along the direction perpendicular to the field (and where it is seen the planar surface of the discs), will be denoted by "*perpendicular images*". The difference between images along the direction of the applied field (parallel //) and perpendicular (⊥) can be seen in Figures 6.10 and 6.12.

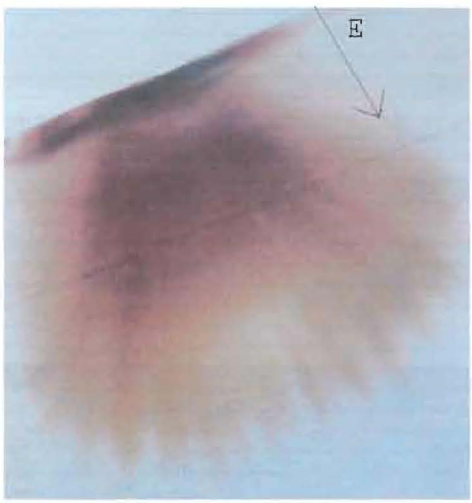

Figure 6.11 - Water tree grown (viscous finger) in LDPE aged at 1.16 kHz (Leicester set). Photograph showing a water tree growing along the electric field direction, //, or perpendicular to the films surface (courtesy of Houlgreave and co-workers).

(b) Scanning electron microscopy (SEM) images of the water trees

Samples from laboratory-aged 11 kV XLPE cable cores were also investigated (for details see [Olley92&95]). A special etching technique was developed by Olley et al. [Olley92] that is suitable for the SEM analysis of water trees. Special care was put into sample preparation because some procedures tend to destroy the connecting pathways. As shown in Figure 6.13, SEM allows the microstructure of the trees to be seen (order of magnitude down to a few μm). For the calculations some of the original photographs appearing in [Olley95] were used. Like the photographs of the methylene blue dyed samples they were also digitalized.

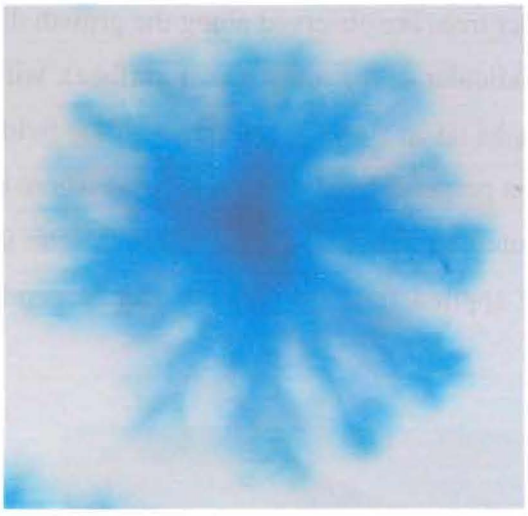

Figure 6.12- - Water tree grown in disc shaped LDPE aged at 50 Hz. Photograph showing a water tree growing perpendicularly to the electric field direction, ⊥, or parallel to the disc surface (courtesy of Houlgreave and co-workers,).

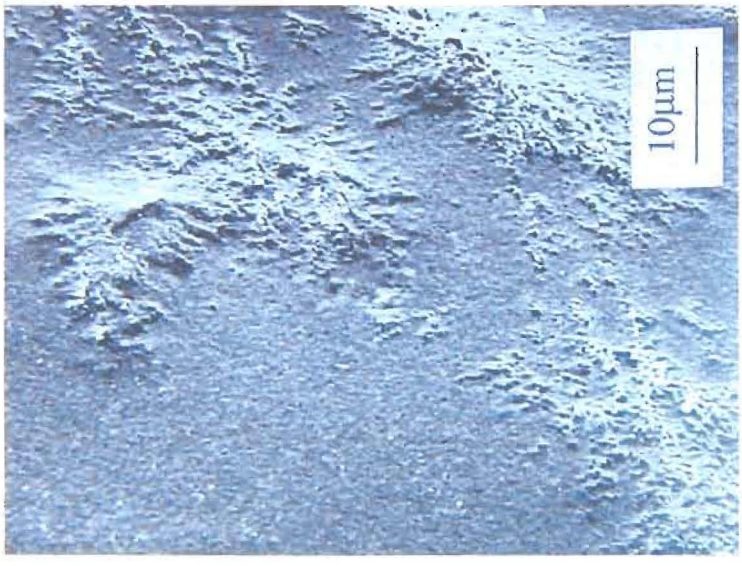

Figure 6.13- SEM image of water trees grown in XLPE cables (after Olley et al.[Olley95])

6.7.2 Image processing and estimation of the fractal dimension

A digitised image has to undergo a treatment chosen according to the purpose for which the image is to be used. The aim is to estimate the fractal dimension of the object shown in the image. It is necessary to distinguish the object from the surrounding background. In real images it is not easy to differentiate between object borders and other important features and to characterise correctly which parts belong or do not belong to the water tree. A large number of image treatment techniques have been developed and it can be a difficult task to know

which to apply to our specific problem. It is important to note that image treatment can influence the calculated value of the dimension (see [Huang94]). This is especially the case if the fractal dimension lies very near the Euclidean dimension in which the object is embedded.

(a) Methylene blue dyed water trees

The original photographs were in colour and were scanned using a colour scanner. Different scanning resolutions were used in order to figure out the influence of resolution in the calculated value of the fractal dimension. For our study the starting point is a colour image with a given resolution. The ideal final result is a binary image where each white pixel will represent the background and each black pixel the tree. First the image needs to be converted to greyscale. This is not very difficult since an RGB (red-green-blue) image can be converted to greyscale using available shareware packages[51] without much loss of information. The major problem is to convert the grey (or colour) image to a binary one. Several image techniques (filters) were tested to get the most faithful binary image. Among those are contrast stretching, histogram equalisation, median filter[52]. Some were applied to the colour image and other to the greyscale image [Lança96].

These photographs are either the result of the projection in a two dimensional space of the 3-D structure or the sectioning of the same 3-D structure of the water tree. According to Mandelbrot [Mandelbrot82], if the section is non-empty, for most fractals the fractal dimension D_{WT} of the 3-D water tree can be given by:

$$D_{WT} = D_{cal} + 1, \tag{6.6}$$

where D_{cal} is the estimated fractal dimension of the 2-D image. Kudo [Kudo98] has studied for electrical trees the relations between fractal dimensions estimated for the 2-D projection and for the real 3-D tree. If the structure is not very dense (fractal dimension less than 2) the projection has the same dimension as the parent tree. Both bush type electrical trees and water trees are very dense. Their projections can have a dimension of 2 (filling space completely), but the real tree dimension could actually be any value between 2 and 3. The real (3-D) electrical trees dimension has been estimated by sectioning and reconstruction of the whole tree from its sections. Kudo [Kudo98] showed that for electrical trees with projected fractal dimensions below about 1.65 the projected and sectioning fractal dimensions are the same. However when the projected fractal dimension is greater than 1.65 the sectioning fractal

[51] In this work two different packages were used: PBMplus by J. Poskanzer and Imagick by J. Cristy.

[52] For definitions of images treatment process see, for instance, [Haralick92].

dimension is increasingly higher than the projection, by a value that approaches 0.7 to 0.8 for the densest trees. When a substantial fraction of the structure is filled it can have a much larger value of the fractal dimension than the projection (because of the obscured structure). However, Equation (6.6) will also be used for projections. Adding 1 to the projected dimension gives an upper bound. Water trees have projected structures that also have a large part of the field filled in. It would therefore be expected that they will have a fractal dimension well above that of the projection, with $d_{proj} + 1$ being an upper bound, and $d_{proj} + 0.7$ possibly being a lower bound.

Three different processes were tried but only the last one gave acceptable and reproducible results. When the original image objects have well defined boundaries, good contrast and also a good resolution, a histogram of the distribution of colours or grey-tones shows sharp peaks. If this happens it is easy to distinguish between background and water trees and a simple threshold filter [Haralick92] can be then applied in order to get a binary image. For the images used, the peaks were not well defined and a more complex method had to be applied as will be explained later on. There are several different ways to define fractal dimension, as was stated before. In this work the capacity dimension is calculated using the box-counting numerical implementation. The algorithm employed was introduced by Liebovitch and Toth [Liebovitch90] and improved by Hou et al. [Hou92]. Calculations were performed using the computer implementation *fd3*[53]. A normalisation of coordinates was undertaken considering the maximum value of all the coordinates to imply no change in the aspect ratio. A series of thresholds were performed on the same image (varying from totally white to totally black binary images). For each of the threshold images a fractal dimension was calculated. First for a 2-D space (2-D fractal dimension D_2) and then for a 3-D space (3-D fractal dimension D_3) where the third dimension was the grey-tone or colour-level. A plot of D_3 vs. threshold level was made. D_3 starts with a value near 2, decreases and starts to increase until it again reaches a value similar to the initial one. So there is a minimum (looking at the images it corresponds to the threshold level value at which the tree-like shape starts to be "lost" in these plots). The minimum value of D_3 is thus the smallest fractal dimension for which the tree structure is retained. In Figure 6.14 typical graphs for the 3D and 2D vs. threshold level are presented. The minimum can be seen in Figure 6.14-(a) and for the same threshold level the corresponding fractal dimension is obtained from Figure 6.14-(b). However this minimum can

[53] *Fd3* is a shareware computer programme based on the box-counting algorithm and developed by Sarraile and Di Falco.

be very difficult to determine and for some tree images even impossible. But for those where the minimum is defined, the fractal dimension can be calculated. The fractal dimension of the three-dimensional water tree is calculated as $D_{cal}+1$ (see Equation 6.6).

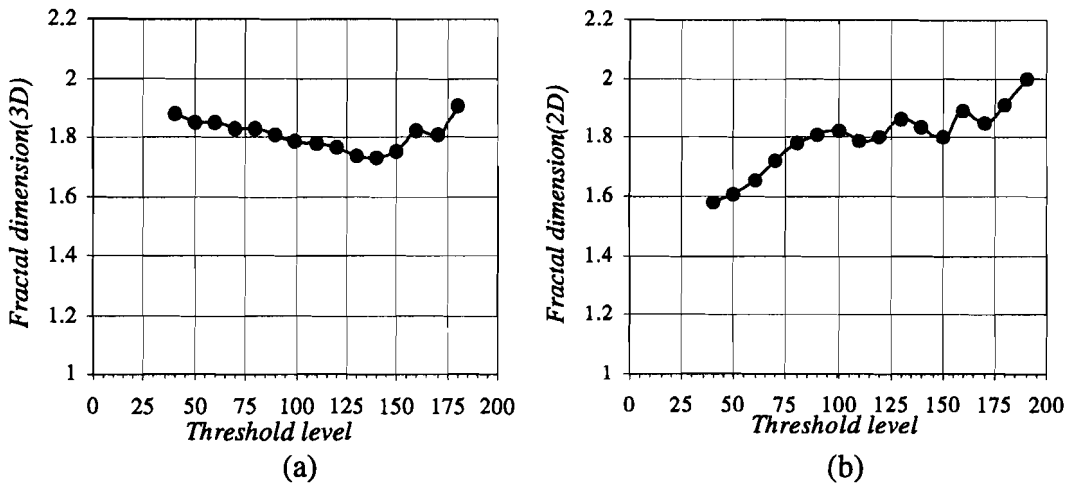

Figure 6.14 – Graph (a) shows the plot of the pseudo-fractal dimension (3D) as the threshold level (a minimum appears between threshold levels 130-140). From graph (b) the 2D fractal dimension (D_{cal}) is obtained by choosing the value corresponding to the same threshold level as the minimum in (a).

(b) SEM images

The available SEM images of the water trees are black and white photographs (see Figure 6.13). They are not 2-D projections but result from a planar cut through the polymer. In the digitised images the grey tone of each point can be related to the relief in the polymer surface. As a first attempt to estimate the fractal dimension a pseudo-fractal dimension was calculated. A three-dimensional space was considered by taking the third dimension as the grey tone. This dimension does not represent a true fractal dimension for the Euclidean (physical) space where the water tree grows.

6.8 Chemical changes in aged polyethylene

6.8.1 FTIR studies

Fast Fourier infrared spectrometry (FTIR) was used to detect chemical changes in the aged polymer. The study was carried out for both LDPE and XLPE films. In the electrically aged samples regions, revealing the presence of water trees, were analysed and compared with results from unaged specimens. A BioRad-FTS 165 FTIR spectrometer was used to obtain the

spectra. The number of scans was 100 and a resolution of 16 cm^{-1} had to be chosen because better resolutions would give rise to very noisy spectra. The lowest speed allowed by the equipment of 2.5 kHz was used. The noise was of the same order of magnitude as some of the oxidation relevant bands and made changes impossible to be detected. Initially in order to reduce noise samples were first cleaned in an ultrasonic bath. However no improvement was observed and the cleaning procedure was stopped.

6.8.2 NMR studies

For the NMR studies a Bruker AM250 spectrometer equipped with a 5 mm broadband probe without field/frequency control was used. To obtain a NMR signal samples (including unaged ones for comparison) were soaked in heavy water for 2 days. Samples were aged as described above (in 6.1.2) and details of NMR experiments are given in [Judenstein00].

6.9 Breakdown statistics

In many electrical ageing studies breakdown is almost inevitable, specially when involving planar thin samples even at relatively moderate electric fields. In the course of the ageing procedure some of the samples used in this work did suffer breakdown. Even if the experiments were not conceived to study breakdown but earlier stages of ageing, it can still be possible to gain some information about breakdown from the available data.

For dielectric breakdown time to failure the most common statistical treatment [Dissado92] is that using the two-parameter Weibull distribution [Weibull51]. The cumulative distribution function, giving the probability of failure of a sample at a given time, t, is:

$$P_F(t) = 1 - \exp\left[-\left(\frac{t}{\tau_W}\right)^a\right] \tag{6.7}$$

where a is known as the shape parameter (related to breakdown mechanism) and τ_W is the characteristic time to breakdown (determined by the deterministic breakdown mechanism or ageing mechanism)[54].

Also important is the probability density function:

$$g(t) = \frac{dP_F(t)}{dt} = \frac{a}{\tau_W}\left(\frac{t}{\tau_W}\right)^{a-1} \exp\left[-\left(\frac{t}{\tau_W}\right)^a\right], \tag{6.8}$$

[54] This time corresponds to $P_F(\tau_W) = 1 - \frac{1}{e} = 0.6321$ (with four significant figures).

and the hazard function:

$$h(t)=\frac{g(t)}{1-P_F(t)}=\frac{a}{\tau_W}\left(\frac{t}{\tau_W}\right)^{a-1}. \qquad (6.9)$$

To assess if experimental data can be correctly described by the Weibull distribution the usual technique is to plot the data on the so called Weibull probability paper. In this graph the x-axis is $\log(t)$, while the y-axis is assigned to $\log[-\ln(1-P_F(t))]$. If a straight line is approximately obtained the data can be fitted according to a Weibull distribution.

To build a Weibull plot from the experimental data (breakdown times) the main problem is to find $P_F(t)$. First the data points have to be sorted in ascending order and ranked accordingly from i=1 to r (number of samples that suffered breakdown). Then $P_F(t)$ is calculated using a suitable equation. The choice of this equation has been a matter of debate and depends upon the method chosen to estimate the two parameters. Furthermore the data can be censored or not (in the case of uncensored data all the aged samples will have suffered breakdown). However in most experiments not all the samples will have failed. In this study samples were removed at fixed times in order to do some measurements, meaning that from n samples that were used r have failed while n–r have not failed. So the data collected in this way is known as progressively-censored data.

The methods used for the estimation of the parameters are the least squares linear regression method and the maximum likelihood estimator [Johnson70]. Several techniques were compared for estimation accuracy, especially bias in the estimated parameters [Jacquelin96, Montanari97,97a&98]. For progressively-censored data the White method was recommended and simplified by Montanari et al. [Montanari98]. The White method is a weighted version of the least squares linear regression method [White69].

Samples aged at different temperatures (room temperature[55], 35 °C, 40 °C and 50 °C) were treated separately. Failure times were registered as well as ageing times for the samples that did not fail. The White method was used to construct the Weibull probability plots and estimate the two parameters (shape and characteristic time).

[55] An average temperature around 25 °C. The data analysed in this work was aged in a thermal bath at room temperature without temperature control.

Chapter 7. Results and discussion

7.1 Analysis of the unaged polymer morphology and composition characteristics

The unaged samples of polyethylene were analysed in order to establish some of the initial characteristics of the polymer prior to electrical or thermal ageing. A microscopic analysis was made using optical/polarised light microscopy, scanning electron microscopy (SEM) and atomic force microscopy (AFM) techniques. Differential scanning calorimetry (DSC) was employed to obtain calorimetric measurements and to identify possible characteristic transition temperatures. Surface potential analysis after disc sample processing allowed to assess the charge deposited during hot pressing and also its time decay. Finally X-ray diffraction was used to determine the polymer crystallinity[56].

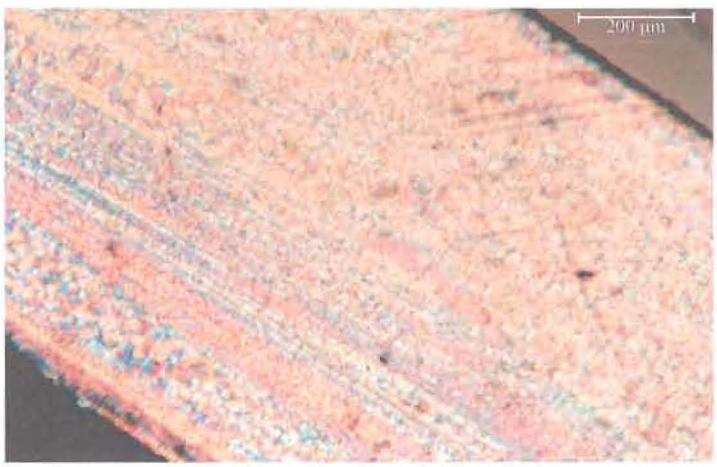

Figure 7.1 – Optical microphotography obtained under reflectance polarised light of a microtomed unaged LDPE sample (sample thickness ≅ 1 mm).

7.1.1 Optical microscopy

Figure 2.5 presented in 2.1.3 is a photograph obtained with a polarised light microscope and one can see the maltese-crosses characteristic of spherulites. Figure 7.1 shows a 1 mm thick microtomed unaged LDPE sample. It is visible the inhomogeneity of the sample structure, related primarily to the cooling conditions after hot pressing which were not uniform for both surfaces of the disc shaped films. Also the presence of different size spherulites is detected. At higher magnification it is more clearly seen the spherulites pattern (see Figure 7.2). As is known, ageing and especially water treeing occurs mostly at the interfaces of

[56] Other results are available (DRS, FTIR, FTSDC and PEA) but for comparison are presented together with the aged samples results.

crystalline/amorphous regions (see 5.1), so the distribution and size of spherulites is important in the ageing process. Another property that can be related to the presence of interfaces is crystallinity, which was studied using X-ray diffraction (see 7.1.6).

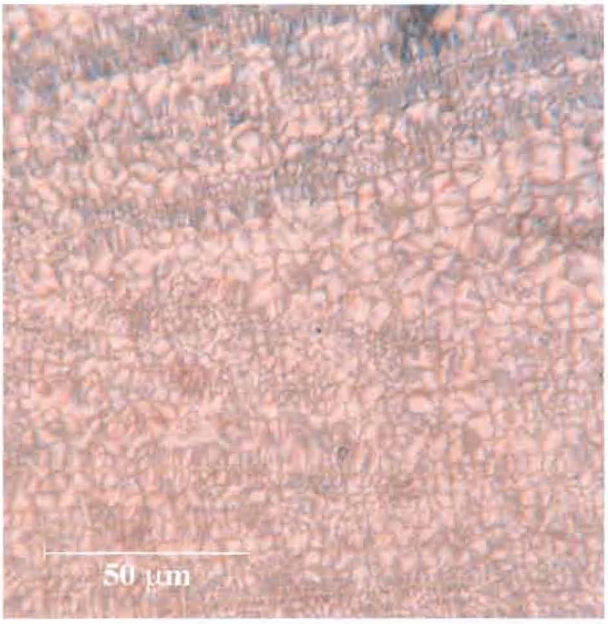

Figure 7.2 - Optical microphotography obtained under reflectance polarised light of the same microtomed sample as in Figure 7.1 at a higher magnification.

7.1.2 Scanning electron microscopy (SEM)

Two SEM microphotographs at different magnifications (×1000 and ×5000) are seen in Figure 7.3. The roughness (μm) of the surface is clearly observed exhibiting some regularity. Roughness at a different scale (nm) can be seen in AFM pictures (see 7.1.3 below).

7.1.3 Atomic force microscopy (AFM)

In Figures 7.4 to 7.6 some typical AFM photographs of unaged LDPE are shown. Different magnifications and scanning areas are represented and also a three-dimensional reconstruction of the surface for a square area of 10 ×10 μm^2.

The AFM analysis allowed us to calculate the surface roughness and a value between 2 to 3 nm was estimated. Comparison between roughness for the two surfaces of the disc shaped samples showed a slight difference. This seems to be related with the position on the press during hot pressing. As a consequence, one of the surfaces would have more irregularities and be more prone to water tree formation (and breakdown).

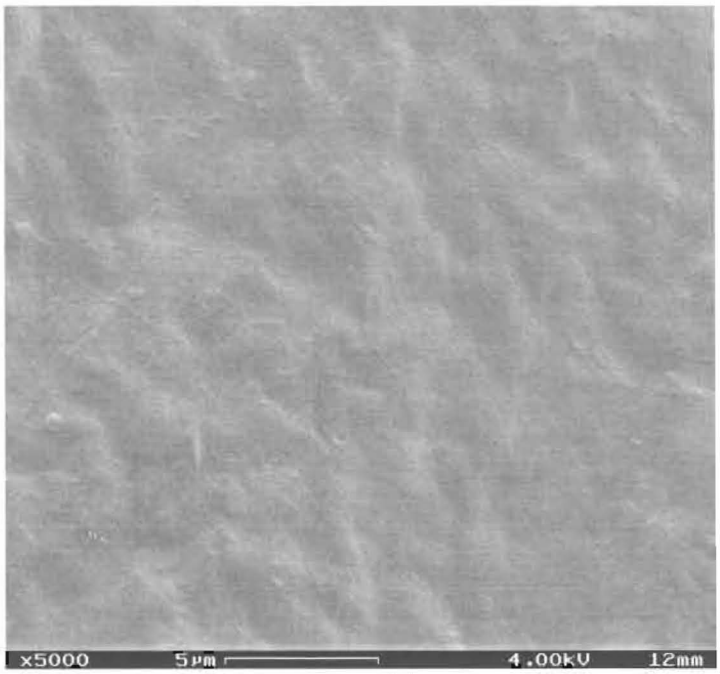

(a)

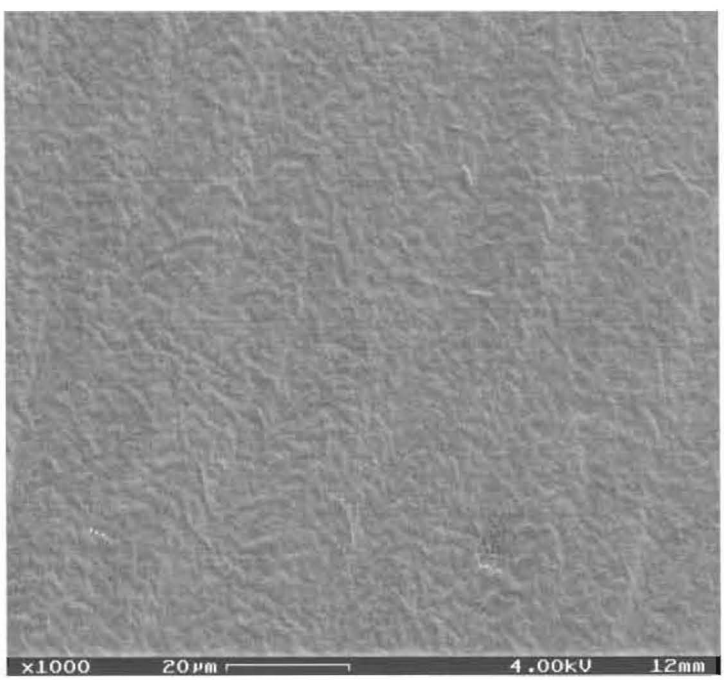

(b)

Figure 7.3 – SEM microphotographs of unaged LDPE. The images are × 5000 (a) and × 1000 (b) magnified.

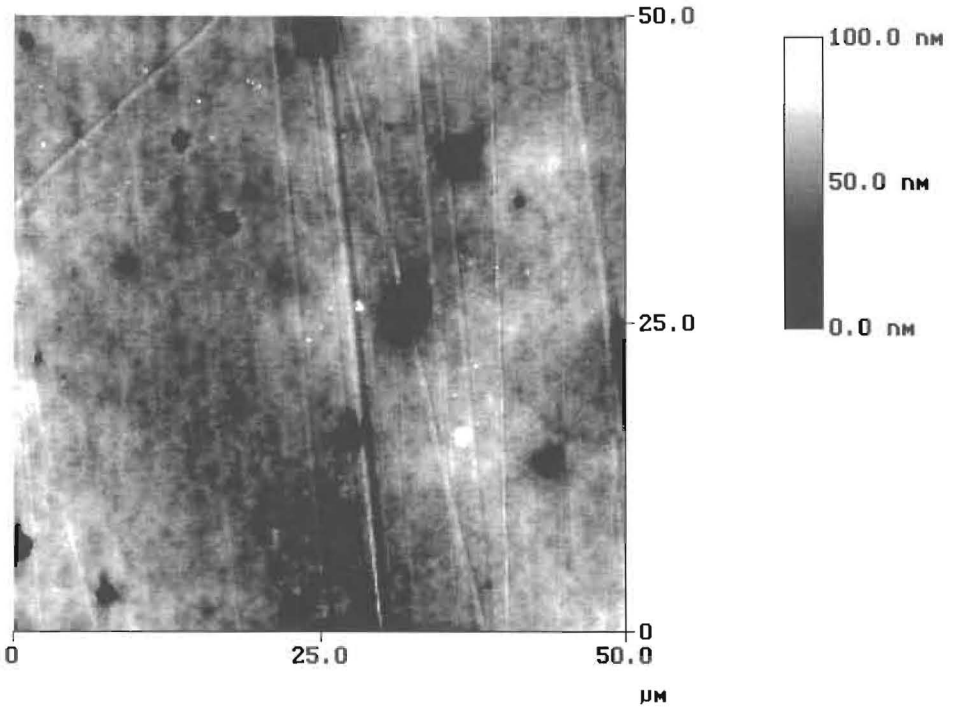

(a)

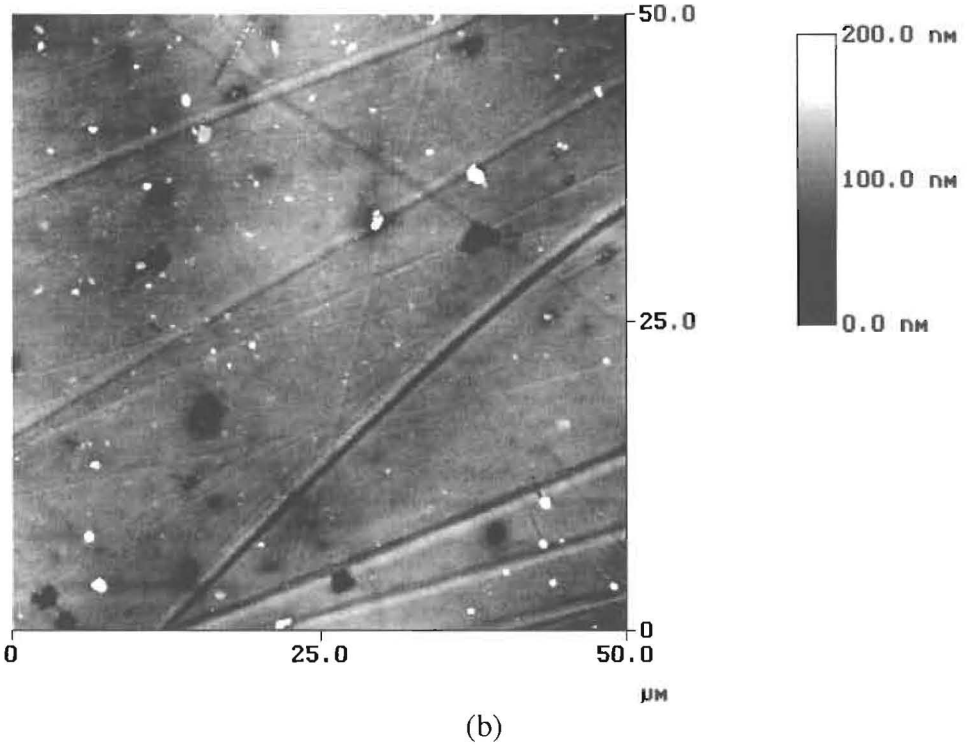

(b)

Figure 7.4 – AFM images of the surface of unaged LDPE. Microphotographs (a) and (b) were taken with different magnifications along the depth of the two opposite surfaces of the same disc shaped sample.

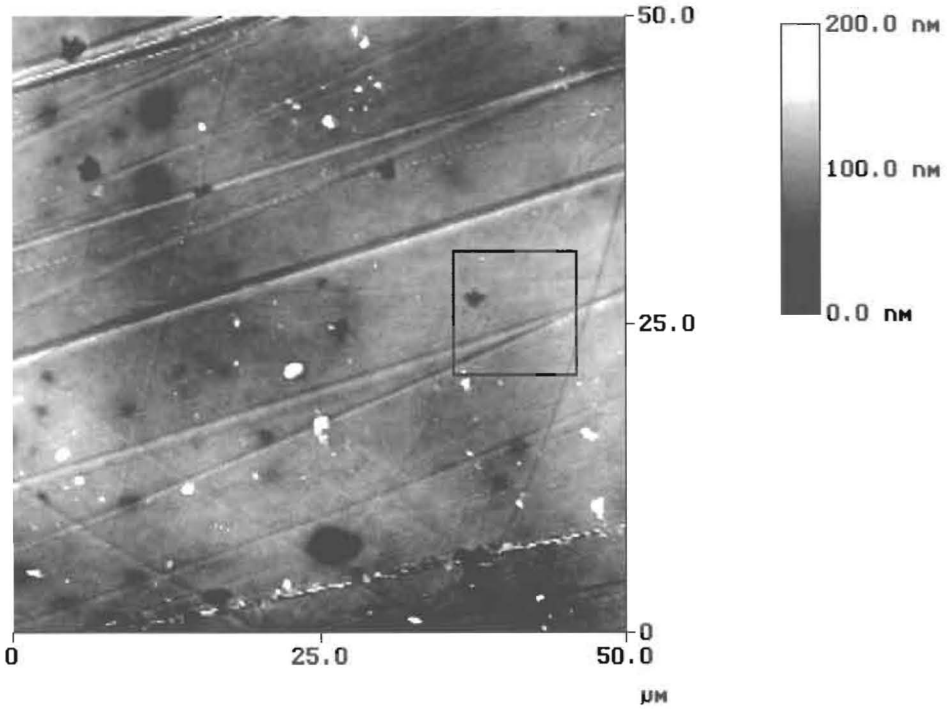

(a)

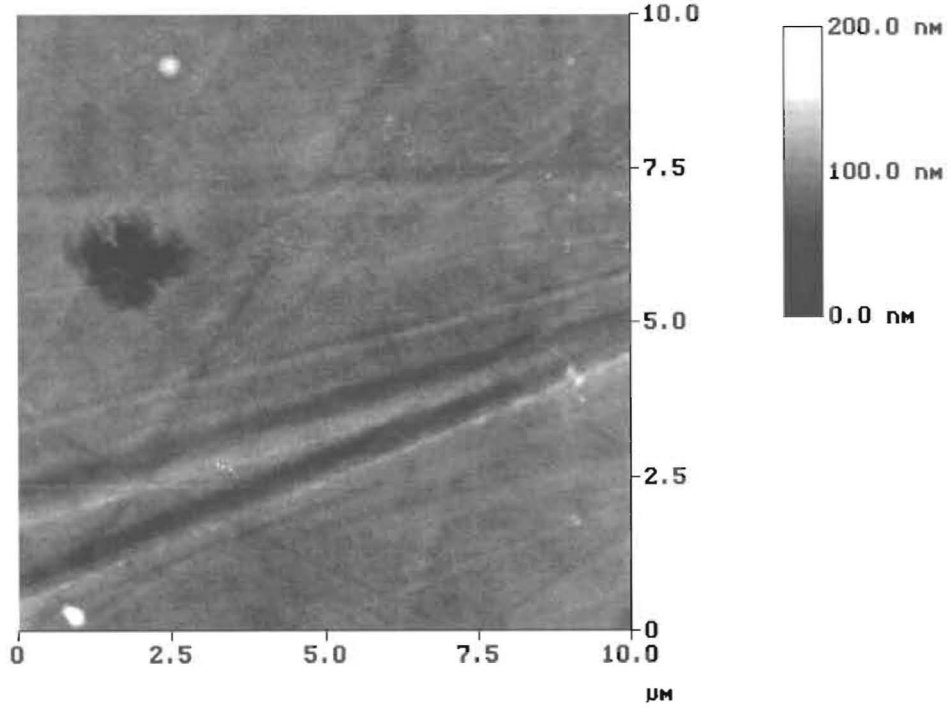

(b)

Figure 7.5 – AFM photographs of the same region of an unaged LDPE disc sample. The area marked as a square in part (a) is that observed at the higher magnification in part (b).

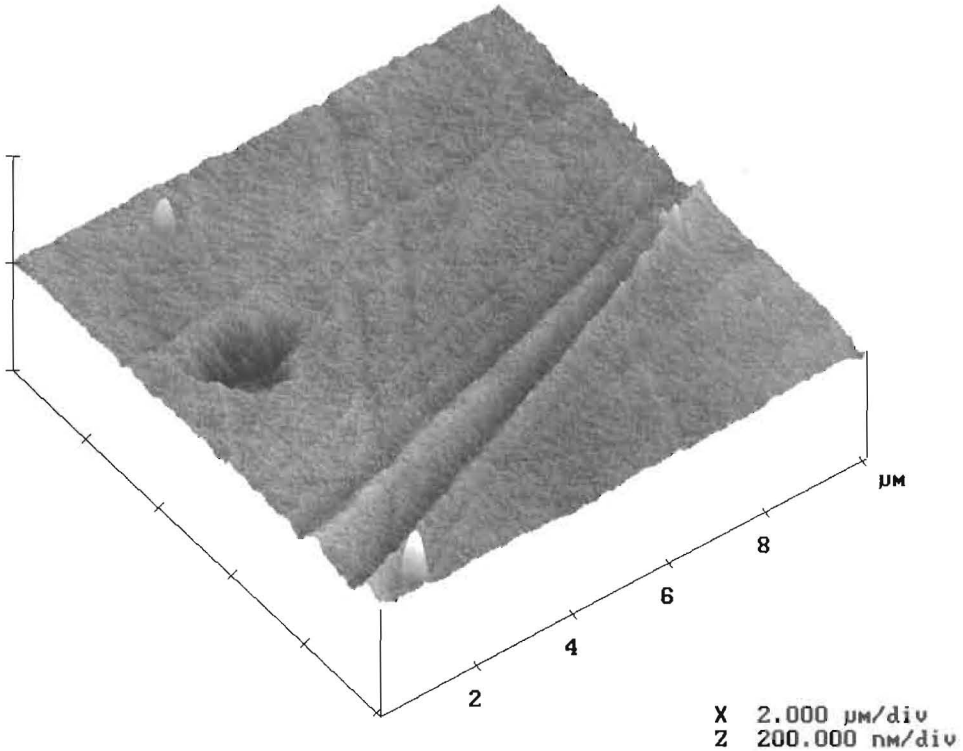

Figure 7.6 – Three-dimensional plot of the photograph in Figure 7.5 – (b).

7.1.4 Differential scanning calorimetry (DSC)

DSC was primarily used to characterise the melting point temperature and, if possible, the glass transition temperature. In Figure 7.7 are displayed typical DSC spectra (heating–the first performed–and cooling runs) obtained from unaged LDPE. Plots (a) and (b) correspond to a heating/cooling rate of 1 °C/min and 5 °C/min, respectively. Easily identified are the sharp peaks resulting from crystallisation (*A*) and melting (*B*). The position of peak *B* is ≅ 110 °C and the difference between its position in (a) and (b) is very small (less than 1°C). On the other hand crystallisation peak position changes significantly with heating rate. In plot (a) it is around 100 °C while in plot (b) it is approximately 90 °C. This change is not entirely due to the difference in rate but can also result from the system's thermal inertia [Höhne96]. The melting point obtained is in good agreement with the expected value (see Table 2.3).

A sharp peak *F* appears at 0°C in plot (b) and also a not well-defined asymmetrical peak at higher temperature (15°C) is seen in plot (a). The glass transition occurring in the amorphous region of LDPE, denoted as α_a or β, is known to be near this range of temperatures (see Chapter 2). A sharp peak is expected when the sample is annealed and a broader one when the sample is quenched [Höhne96] but the differences can also result from different heating rates. The cooling curves do not show any peak in this temperature region that may due to a too fast cooling for annealing to occur and the difference (peak) being too small to be observed. It

should be noticed that during heating, which was the first run performed on the sample, annealing is mainly a result of the sample preparation (hot pressing) and not of the DSC measurements conditions. Further measurements relate these peaks with the pressing procedure and they are probably due to structural changes but are not the glass transition.

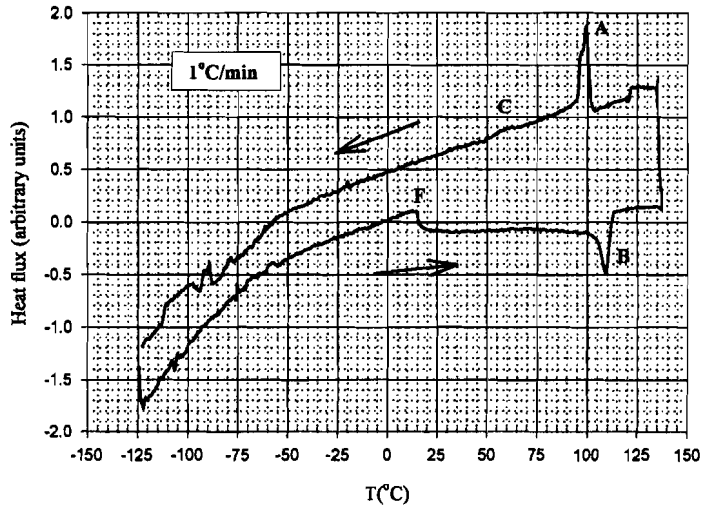

(a)

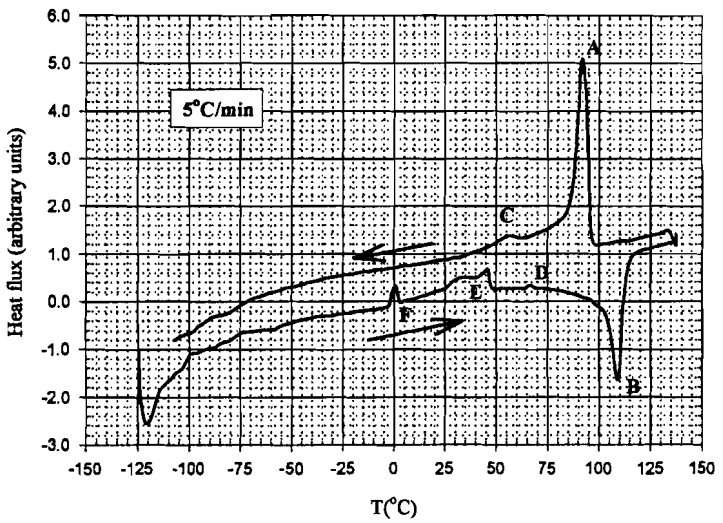

(b)

Figure 7.7 – DSC spectra for unaged LDPE; heating/cooling rate of 1°C/min (a) and of 5°C/min (b). The arrows show the direction of temperature change, so that the upper curve corresponds to sample cooling and the lower one to sample heating.

A small broad peak (*C*) around 55 – 60 °C is clearly visible in both plots during cooling and even a smaller peak (*D*) is visible in plot (b) during heating. *C* and *D* are probably related to the same mechanism. Finally a complex peak *E* is observed around 40 – 50 °C. It is possible that these peaks (*C*, *D* and *E*) are related to the α (or α_c) transition of the crystalline region of

the polymer. Also this peak is not seen during cooling which can be a consequence of too fast cooling that does not allow sufficient time for the crystals to grow.

As will be discussed below in 7.3, there were also observed in non-isothermal current measurements peaks at similar temperatures as *C, D* and *E*.

7.1.5 Surface potential measurements

Using an electrostatic probe the surface potential of unaged LDPE samples was measured in order to determine the presence of charges resulting from sample processing. Charge is expected to have been deposited essentially during the hot pressing procedure. These charges will accumulate predominantly at surface of the defects. In Figure 7.8 are seen four different scans made along the same direction (x axis on the graph) around 5 minutes after hot pressing of the sample was finished. This figure shows the distribution of the surface potential (charge) on the surface of the disc-shaped samples, which is not uniform. Figure 7.9 shows the surface potential decay with time since (immediately after) pressing until a week later. The decay of the potential is important for some of the surface regions with high potential values (*A* and *B*). However on *C*, which exhibits initially the highest potential, the decay is slower and at the end of a week the potential still has a high value.

Ageing, in the geometry used in this study with planar electrodes consisting of the aqueous solution, provides a route for charge decay. The higher temperatures and the AC field also enhance the decay process.

The initial stage of ageing must be dominated by the local electric field enhancement due to the presence of this charge. As will be seen in 7.8 this can be one of the reasons why some samples suffered breakdown in a very short time after the start of the AC ageing. And the same argument is also valid for water treeing initiation sites.

Suh et al. [Suh96] used FTIR and PEA measurements to investigate space charge in LDPE due to pressing conditions (temperature, time and backing film used). They concluded from FTIR measurements that when polyester is used as the backing film carbonyl groups from PET can be deposited on LDPE surface but no oxidation (with formation of carbonyl groups in polyethylene) was detected. These deposited carbonyl groups (small end chains from PET) could act as trapping centres. If the concentration was low, homocharge appeared in PEA measurements but when the concentration was higher it was heterocharge to be observed. Comparing with PEA results for the unaged LDPE (in 7.4), where only homocharge was observed, if this charge results from carbonyl groups, their concentration would be low.

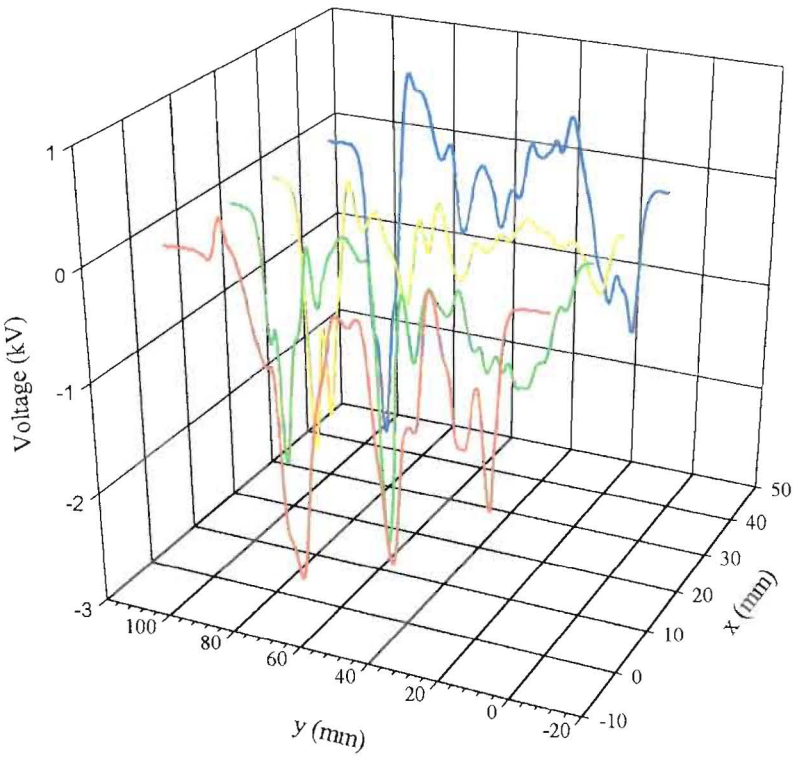

Figure 7.8 – Three-dimensional plot showing the surface potential of an unaged LDPE sample after hot pressing (no further treatment).

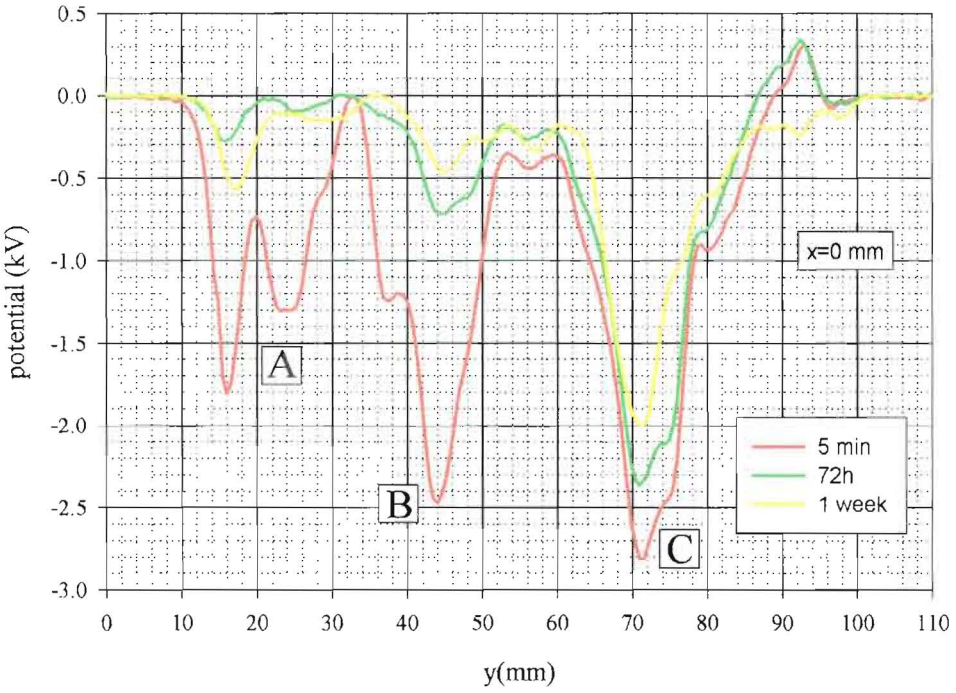

Figure 7.9 – Decay of the surface potential in the same sample as shown in previous figure.

Moreover our pressing temperature (120 or 140 °C) was relatively low compared to the 180 °C where the highest concentration of PET's carbonyl groups was observed by [Suh96].

However it is not sure that the homocharge observed in PEA is due to the C=O groups. Also from the analysis of FTIR results for unaged LDPE (see 7.7.1) it is difficult to ascertain if the typical carbonyl group of PET (at 1727 cm^{-1}) is observed or not. Nevertheless their contribution cannot be completely disregarded.

7.1.6 X-ray diffraction

The X-ray diffraction spectrum of polyethylene is shown in Figure 7.10. The two main peaks can be identified with diffraction on planes (110) and (200) [Billmeyer84]. A broad peak is expected from the contribution from the amorphous part [Nichols54]. Around 30° there is a very small third peak (210). When the diffraction angle studied goes up to 40° two more peaks could be seen. One of them is due to the Aluminium of the sample holder and appears at 38.5°. The other at ≅ 36° is attributed to diffraction on the plane (020) and is the third in intensity for the PE. Only the two first peaks (and the amorphous broad peak) were considered for crystallinity calculations because the other two have much smaller intensities.

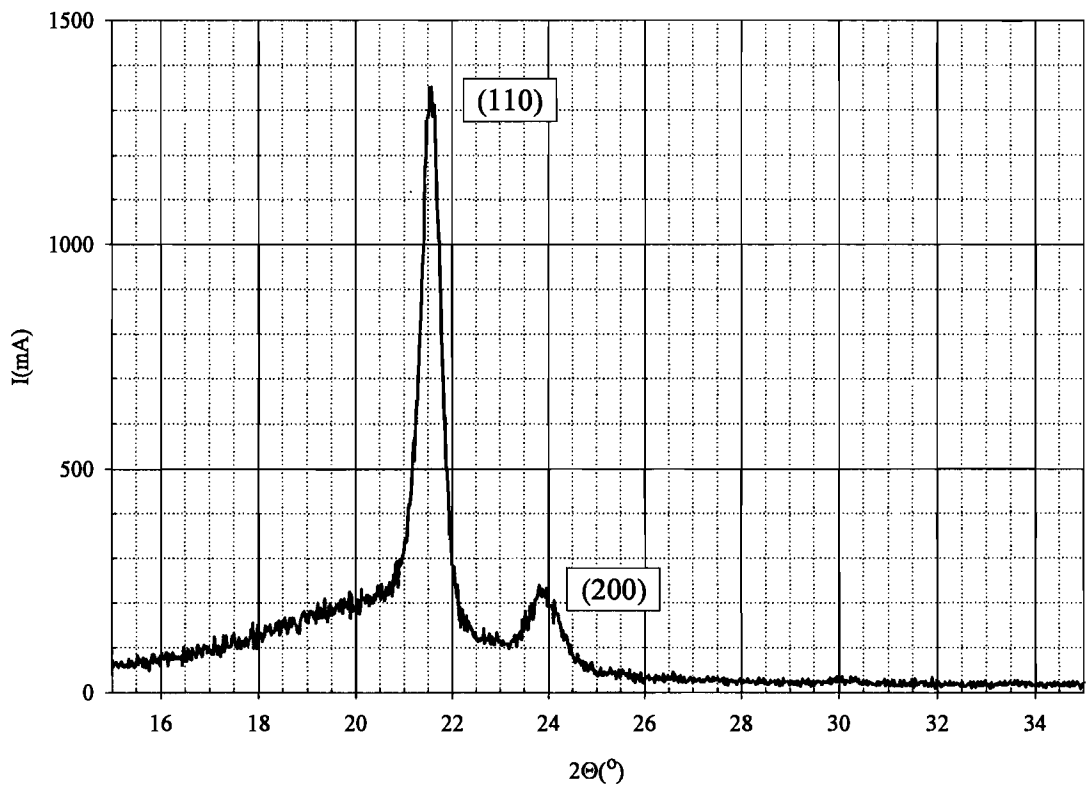

Figure 7.10 – X-ray difraction spectrum for an unaged sample of LDPE.

The maximum values of 2θ (θ is the Bragg angle) are seen in Table 7.1 for both LDPE and XLPE samples (the values in Das Gupta et. al [Das Gupta75] are 21.6° and 24.1°,

respectively). The broad peak is expected to have its maximum below the (110) peak maximum (at 19.5° according to [Noon73]). However due to the noise in the signal it is difficult to see the position of the amorphous peak maximum.

Taking for 2θ the interval between 15° and 35° after subtracting the background, the two main peaks ((110) and (200)) were fitted and their areas calculated. From these areas and the total area on the spectrum (minus the background) the amorphous peak area was calculated. Then the method in Nichols [Nichols54] was applied and the percentage of crystalline content was obtained (see 6.2).

Table 7.1 – Results for the two main diffraction peaks (110) and (200), crystallinity content and crystallite size for LDPE (three different samples: labelled LDPE *a*, *b* and *c*) and XLPE (two different samples: labelled XLPE *a* and *b*).

Sample	2θ (110) (°)	2θ (200) (°)	Crystallinity (%)	Crystallite size (Å)
LDPE a	21.4	23.6	60	185
LDPE b	21.5	23.8	60	170
LDPE c*	21.5	23.9	62	160
XLPE a	21.3	23.6	52	130
XLPE b	21.5	23.6	47	150

*thermally treated in air at 60 °C for 120h.

In Table 7.1 are also presented results for the crystallinity content and crystallite size for three LDPE samples (labelled LDPE *a*, *b* and *c*) and two XLPE samples (labelled XLPE *a* and *b*). For LDPE a value around 60%[57] was found in good agreement with those in [Nichols54][58]. The result obtained lies in the upper limit of the interval given in Table 2.3. However, as these samples are prepared by hot pressure and are cooled under pressure, it is possible that a pressure annealing process occurs giving rise to higher crystalline content than the one showed by LDPE prepared by other methods [Brooks99]. The higher value for crystallinity in LDPE *c* is a consequence of the thermal treatment after pressing (annealing in air at 60 °C for 120h). The other samples did not suffer any treatment after pressing. However it should be

[57] If no correction factors were used the result was near 50 %.

[58] However these authors do not state which kind of PE was used.

kept in mind that the calculation of the area and the background are not free from errors, which are difficult to quantify.

A smaller crystallinity content was found for XLPE (47 % and 52 %) as was expected (and is a result of the crosslinked structure). According to Dissado et al. [Dissado92] spherulites are expected in crosslinked thin film specimens produced by pressing moulds.

Crystallite size was calculated using Scherrer's method described in 6.2 and the values are of the same order of magnitude as those in [Noon73] and [Das Gupta75] for LDPE.

Crystallinity is an important parameter for ageing (see Chapter 5) since crystalline/amorphous interfaces play an important role by increasing the local electric field (including the accumulation of space charge ([Nath89, Dissado02, Mazzanti02]).

7.2 Dielectric relaxation spectroscopy

7.2.1 Results

An example of a typical graph of charging and discharging currents obtained using time-domain spectroscopy is presented in Figure 7.11 for a thermally aged LDPE sample. Since the polymer is a very good insulator the recorded current values are very small (down to 10^{-14}A) but within the same order of magnitude as the results presented by Das Gupta et al. [Das Gupta78]. Discharge current values agree quite well with the published data. However the charge current is slightly higher for the LDPE samples studied by Das Gupta et al. [Das Gupta78]. Those samples were commercial films while the LDPE samples in this work were press moulded from pellets with very few additives. More impurities (such as ions) can give rise to a DC conductivity component in the commercial films and may lead to the observed difference in the conduction current. Charge and discharge currents will be considered in detail below for some of the samples studied here (see 7.3).

All the data from the dielectric spectra presented, resulted from measurements made isothermally at 30 °C. The first two dielectric spectra observed present the imaginary part of the permittivity and show the effect of two different ageing parameters, temperature (Figure 7.12) and time (Figure 7.13) for electrically aged samples (also designated AC aged samples). As it was described in 6.1, samples exposed to thermal ageing only (also called no-AC aged samples) were also measured in order to analyse the ageing effects of samples immersion in solution (see Figure 7.14). Comparative plots of the dielectric loss vs. frequency are shown in

Figure 7.15. Results for individual samples are presented in Figures 7.16 to 7.24 (real and imaginary parts of the dielectric constant). This type of presentation was preferred to susceptibility plots, because determining ε_∞ was extremely difficult for some of the samples (even when it was possible, the errors involved were large).
Fitting to the experimental data was made using either the Jonscher universal law for loss peaks (similar to the empirical Havriliak-Negami function) or QDC (or flat loss) functions, see Table 4.1. Fitting parameters are shown in Table 7.4 further on.

Individual graphs were obtained using different measurement conditions according to frequency range (see 6.3 for details). The MF (medium frequency) measurements (made with the help of a lock-in amplifier) exhibit the largest errors, as can be seen by the scatter of experimental data points on the graphs of individual samples. Moreover measuring problems for the initial values of discharge current (shorter times, higher frequencies corresponding to 10^{-1} Hz decade) are encountered. To get better fittings some of the experimental points had to be disregarded. In some of the samples (such as those appearing in Figures 7.21 and 7.22) fittings with a very good correlation could be made. However for some of the others not so good fittings were obtained.

As was said previously, dielectric spectra in Figures 7.12 to 7.15 show a comparison of the results for the set of different ageing conditions studied (time, temperature and electrical or thermal ageing). Only fitting curves are presented in order to clearly illustrate the difference between different samples.

7.2.2 Discussion

Known spectra of TSDC for LDPE [Fischer76&76a] can help to find the position of probable dielectric loss peaks resulting from β and γ relaxations. From Equation (4.64) and from the Arrhenius equation Table 7.2 was obtained. Values of the temperature peaks maxima were collected from the literature (see footnote in the same table). All calculations for the loss peaks were made taking into account that dielectric measurements were performed at 30°C.
The data from Fischer was obtained from TSDC experiments and should be regarded as the most reliable. This table should be looked upon as an indication of the frequencies where probable loss peaks can appear and not as definite values (as the calculations made in 4.10 show).

Table 7.2 – Relation between TSDC peaks and the frequency of the loss peaks

Peak	TSDC peak temperature (°C)	Heating rate (β) (K/s)	Activation energy (eV)	Equivalent frequency (ν_{eq}) (10^{-3}Hz)	Dielectric loss peak frequency (at 30°C) (Hz)
γ	-135*	0.11*	0.4*	3.0	3.2×10^{7}
			0.5+	3.8	2.7×10^{5}
β	-28*	0.11*	0.3&	0.7	1.5×10^{-2}
			0.7*	1.7	9.5×10^{-1}
			1.0#	2.4	2.1×10^{1}
			2.5§	6.0	4.7×10^{7}

&no source, *[Fischer76]; +[McCrum67], #[Hilczer86] and §[Graff94]

As can be seen for the γ and β transitions a small variation in the activation energy, E_a, implies a variation in the loss peak frequency of one order of magnitude. No TSDC data was found for the α peak.

The data in Tables 4.5 and 4.6 can also be useful to find possible positions for the dielectric dipolar loss relaxation peaks for the isothermal data in this work (obtained at 30°C). The Arrehnius temperature dependence was assumed and results from estimations are presented in Table 7.3.

Table 7.3 – Possible frequency intervals for the position of dipolar loss peaks of LDPE in an isothermal plot at 30°C.

Peak	Frequency interval (Hz)
α	$[10^{2}, 7\times10^{2}]$
β	$[5\times10^{3}, 2\times10^{8}]$
γ	$> 2\times10^{9}$

An analysis of the spectra for the unaged sample (Figure 7.16) shows data very different from the results of McLachlan presented by Jonscher [Jonscher99a]. In those results the

polyethylene spectra follows Jonscher's universal law with a constant slope in the frequency range of 10^{-3} Hz to 10^{6} Hz. Except for the indication that it concerns very pure PE, no further information is given either about the polymer type, the measuring method or measuring temperature. In the spectra shown in Figure 7.16, three characteristic regions with loss peaks are clearly visible corresponding to the low frequency (LF), medium frequency (MF) and high frequency (HF) regions, respectively. The pellets from which the samples studied in this work were prepared are almost additive-free however with the presence of a small concentration of anti-oxidants (the value was not specified by Borealis). In addition the mould pressing process can also be responsible for the introduction of impurities and oxidation may also occur giving rise to both dipolar and space charge loss peaks (7.1.5).
Isochronal dielectric spectra especially for linear polyethylene (LPE)[59] slightly oxidised or chlorinated from Graff and Boyd ([Graff94] and [Boyd97]) show dipolar α and β peaks. [Ashcraft76] presents also some dielectric data for LPE and LDPE (slightly oxidised or chlorinated) revealing the presence of three main peaks (α, β and γ) and a weak δ peak at very low temperature. Also the measurements of Barrie et al. [Barrie66] show the presence of loss peaks in the LDPE spectra. For further details see 0.

It is also interesting to mention that the plots obtained are in some aspects similar to the ones obtained by Scarpa [Scarpa95] for XLPE (unaged and electrically aged in water) where the polymer was contaminated by impurities. However the LDPE samples analysed in the same work [Scarpa95] are clearly much more conductive following a typical QDC process. These specimens were obtained from commercial films and the presence of additives and contaminants seems to be high enough to make the polymer more conductive.

A parallel analysis of the data for LDPE aged under different conditions will also be made considering the three frequency regions. Observing the individual graphs for each sample (Figures 7.16 to 7.24Figure 7.16) it is seen that the changes in the real component of the permittivity are very small. However the results for the imaginary component show meaningful differences as is also perceived from the graphs presented in Figures 7.12 to 7.15.

[59] The difference between LDPE and oxidized LPE dielectric spectra will be mainly an enhancement of the α peak intensities (since LPE is much more crystalline than LDPE). Experimental evidence of this can be found in [Hedvig77].

Starting a more detailed analysis by the low frequency region (LF – 10^{-5} Hz to 10^{-1} Hz), Figure 7.13 compares different ageing times for electrically aged samples at 40 °C with the unaged LDPE. A broad low frequency peak is seen in the unaged specimen (maximum at $\approx 10^{-4}$ Hz). In the electrically aged LDPE for 500 h and 1000 h a shift in the peak is observed towards lower frequencies outside the measurement range (with a higher peak maximum and maximum frequency lying below 10^{-5} Hz). Yet for the 1500 h electrically aged samples (even for different temperatures as Figure 7.12 shows[60]) the increase towards lower frequency is no longer visible and ε'' is similar to the unaged sample. For thermally aged samples (Figures 7.14 and 7.15)[61] under similar temperature and time conditions no shift in peak position is seen and just an increase in its maximum is observed with increasing ageing time.

Loss peaks in this low frequency range are usually attributed to trapped space charge mostly resulting from Maxwell-Wagner-Sillars interfacial polarisation. For polyethylene a peak in the 10^{-4} Hz to 10^{-3} Hz interval can also result from dipoles (resulting, e.g., from the formation of free radicals) in addition to trapped space charge (such as ions) [Scarpa95]. For polymer samples subjected to thermal ageing the increase of the peak amplitude could arise from diffusion of space charge from the solution. The available trap sites would be occupied by the newly arrived charges and just the maximum would increase with no change in peak shape and position.

Looking at the 1000 h aged samples in Figure 7.15 there is a shift in the loss peak towards lower frequencies quite clear for electrically ageing compared with the thermal one. A maximum for the same ageing time in electrically aged XLPE with subsequent decrease with increasing ageing time was also observed in [Scarpa95]. When an AC electric field is present during ageing two different phenomena may be occurring simultaneously. First, diffusion (enhanced by the field) of space charge from the solution is occurring. At the same time the field also induces oxidation, giving rise to both oxidation products (such as ketones and carboxylates) and creating more space charge. The observed shift in the peak could be also due to two different effects. One caused by the presence of more ions and oxidation products that would make space charge to move more slowly. The other resulting from the creation of

[60] Ageing at room temperature shows at low frequency a remarked difference from the other two temperatures (35 °C and 40 °C). In order to explain this difference further data is needed and for the analysis presented here only the higher temperatures results were taken into account.

[61] For 500h thermally aged polymer the results obtained are not typical both in the LF and HF ranges. So analysis will just be focused on the other two ageing times (1000 h and 1500 h).

new trap sites by oxidation probably at the expenses of the existing ones. The pre-existing traps, since they are related to interfacial defects (cavities, impurities, carbonyl groups, etc.) would be favourable sites for oxidation.

It is interesting to note the similar responses of unaged and electrically aged for 1500 h. The number of available sites and reagents for oxidation to take place must be limited and the oxidation rate must initially be higher until the oxidation sites are becoming exhausted and then decrease. Moreover initially the local field needs enough space charge to accumulate in order to increase oxidation. As a consequence the dielectric spectra would show the highest values for the loss peak for a given time (around 1000 h). After this time diffusion would continue but the decrease in oxidation rate would give rise to fewer new traps.

If ageing is carried out for long enough time the traps will tend to be filled. New charges in the material will now move more freely and a decrease in the peak amplitude would occur. Two processes seem to be present when ageing happens in the presence of an AC electric field. One is diffusion, more enhanced by the field. The other is oxidation (which is not so significant for thermal ageing). Diffusion increases the low frequency peak present in the unaged material (10^{-4} – 10^{-3} Hz) without shifting the maximum (seen in the no-AC aged samples). On the other hand, the effect of the field is to shift the low frequency loss peak to frequencies below the measurement range (creation of new traps with longer relaxation times). At an advanced stage of ageing it is expected that, when all traps are filled and no new ones can any longer be created, the space charge will move freely and the polymer will become more conductive. As will be seen below in 7.3 no increase in conductivity is observed for the AC aged samples. Accordingly the electrical ageing is still at an intermediate stage where the traps at higher frequency (around 10^{-3} to 10^{-4} Hz) are disappearing and a clear shift in the peak towards lower frequencies is observed. For the 1500 h AC aged LDPE a peak in the measurement range no longer is visible and the response in the LF range becomes similar to that of the unaged polymer. Further confirmation of the occurence of oxidation in electrically aged polyethyene is given by FTIR analysis (see 7.7.1).

In Figures 7.25 and 7.26 Cole-Cole plots are presented for an unaged sample and an electrically aged for 1500 h (LF region only). In the plot for unaged LDPE two superimposed semi-circles (or depressed semi-circles) can be seen indicating the presence of two peaks in the dielectric relaxation spectra. Analysis of Figure 7.16 shows a broad peak in this region that may be composed of two individual peaks. Otherwise on the Cole-Cole plot of the AC aged sample (Figure 7.26) only one (depressed) semi-circle can be clearly seen and there is a sharp rise towards lower frequencies. All the graphs for other electrically aged specimens

reveal the appearance of this increase. This can be either due to DC conductivity (and it would show an asymptotic behaviour approaching infinity) or the beginning of a more intense peak with a maximum at a low frequency below the measurement range. However according to what was stated above the second hypothesis seems to be the more likely.
Figure 7.27 shows the equivalent circuits for unaged LDPE (a) and electrically aged: (b) and (c) assuming, respectively, two low frequency peaks and one low frequency peak with a superimposed DC conductivity.

The peak in the MF range can be attributed to impurities and anti-oxidants present in the material prior to ageing [Bamji91]. Oxidation products can also contribute to the peak (such as carboxylic groups) [Scarpa95]. A small contribution of the α dipolar loss peak could also be expected. Graff et al. [Graff94] found from measurements at 30 °C that the α peak frequency should be in the region 1 to 10 Hz. Yet for semicrystalline LDPE the α peak would be rather small because crystallinity is not very high and also the carbonyl dipoles choose preferably the amorphous fraction [Ashcraft76, Graff94]. As mentioned before some anti-oxidants were present in the LDPE pellets used to prepare the press moulded samples. Also the press moulding process can cause oxidation and introduce impurities into the films. Therefore the loss peak would be present even for unaged samples. From the graph in Figure 7.12, where the ageing temperature is varied for similar electrical ageing times, a slight reduction in the the peak amplitude is observed. This dependence on temperature reveals the presence of a diffusion process with species diffusing out of the polymer. Moreover, taking into account that the initial number of carbonyl groups must too be very small, the contribution of the α transition must be very small. Furthermore, if oxidation is very low (very few carbonyl groups) it is expected that the peak intensity would be too small to be detected. However when samples aged at similar temperatures are analysed (Figure 7.13 to 7.15) results are not consistent. It should be noted that the MF region measurements are the ones showing higher dispersion and consequently the largest errors. This scatter of the data makes fitting rather difficult and less reliable. Also it seems that the presence of the LF peak influences the fitted results for this region (which is more evident in Figure 7.22 that shows the highest value for LF loss peak maximum). However the influence of ageing on this region is much smaller than for the other frequencies ranges studied.

In the HF region of the spectrum (above 10^2 Hz) the unaged polyethylene (Figure 7.16) shows an increase due to a possible peak whose maximum lies near 10^5 Hz. According to Barrie [Barrie66] for highly pure LDPE there is a peak above 10^7 Hz (measurements performed at 30 °C) that can be attributed to an unresolved peak resulting from β and γ transitions (see also Table 7.2[62]). In XLPE samples studied by Scarpa [Scarpa95] a peak appears at this same frequency attributed to bound water but no connection can be made with the results presented here. The XLPE samples were measured in water and also no change is seen with ageing. In this work both electrically (Figure 7.13) and thermally (Figure 7.14) aged LDPE spectra[63] of the imaginary permittivity reveal changes in the HF peak with ageing. The maximum height of the peak seems to occur for the samples aged for 1000 h with a shift in the peak position. Contrary to the LF peak for both 1500 h aged samples (AC and no-AC) the peak has disappeared. This suggests that regardless of the electric field presence during ageing both peak position and maximum are affected. Nevertheless the AC field seems to cause a greater displacement of the peak position (once more it is clear when comparing 1000 h thermal and electrically aged specimens).

Reporting to the discussion on the LF region one has considered two different processes contributing to ageing, diffusion and oxidation. For the electrically aged specimens both maximum enhancement and peak shift could be explained by oxidation. The maximum would increase because oxidation leads to the formation of more dipoles (C=O). Variation of the peak position is more difficult to understand. Graff et al. [Graff94] in their discussion of dielectric β relaxation (a mechanism occurring in the amorphous region) point to the importance of the crystalline interface. In that paper the differences between the β peak strength and location for purely amorphous and semi-crystalline polymers are compared. Emphasis is given to the role played by the crystalline interfaces and also the connection of chains in the amorphous region to the crystal fraction. This leads to an immobilising effect resulting in a smaller peak but also in a shift to longer time (isothermal plot) or higher temperature (isochronal plot). The results presented for both LPE and LDPE (oxidised and chlorinated) by Graff et al. and Ashcraft at al. [Graff 94, Ashcraft76 and Boyd97] show this

[62] Barrie et al. [Barrie66] mention the contribution of the β transition to this peak which disagrees with what was expected from Fischer and Röhl's TSDC results [Fischer76, 76a] (calculations in Table 7.2). However as noted previously, any slight change of activation energy and heating rate will amount on a large change in the predicted peak frequency, as can be seen from the same table.

[63] The LDPE sample thermally aged for 500h was not considered.

effect. The isothermal plots of Figures 7.12 and 7.13 showing no peak for all the 1500h aged specimens (regardless of ageing temperature) would suggest also that the peak could have shifted to higher frequencies (shorter times), the change being probably due to a decrease in the interconnection between chains in the amorphous phase and in the crystalline regions. Considering that water treeing (and more generally oxidation) would happen preferentially at the amorphous/crystalline interface then chain scission resulting from oxidation would reduce the immobilising effect of chain interconnections between the two different regions. Furthermore the loss peak would be shifted to a higher frequency in an isothermal plot

Diffusion is also able to account for the differences arising from ageing, both thermal and electrical. The presence of the peak at a lower frequency than that reported [Barrie66] in the unaged films together with the presence of the MF peak indicate the presence of impurity ions initially in the samples. The ions would surround the existing dipoles and prevent them from moving faster and a screening effect could arise, and both maximum and peak position would be affected. If the ions tend to diffuse out with time then this blocking effect is reduced. If a field is present the diffusion effect would be enhanced and the shift and maximum would be affected. Competing diffusion and oxidation could originate the observed changes as was the case with the LF peak.

Table 7.4 – Fittting results for the dielectric spectra of LDPE samples (unaged and AC aged).

Sample	f(Hz)	Fit	a	fp	n	m	Comments
	LF	Peak	0.03	1×10^{-4}	0.66	0.18	Same data as
Unaged	MF	Peak	0.006	0.98	0	0.22	in Figure 7.16
	HF	Peak	6×10^{-4}	8×10^{4}	0	0.82	
	LF	QDC	1.6×10^{-6}	—	0	—	Same data as
RT	MF	Peak	0.006	0.019	0.29	0.66	in Figure 7.17
1500h	HF	Flat	1×10^{-4}	—	1(flat)	—	
	LF	Peak	0.028	6.4×10^{-5}	0.6	0	Same data as
35°C	MF	Peak	4.5×10^{-3}	2.1	0	0	in Figure 7.18
1500h	HF	Peak	2.5×10^{-4}	5.5×10^{-3}	0.8	1	
	LF	Peak	0.011	1×10^{-3}	0	0	Same data as
40°C	MF	Peak	6×10^{-3}	0.94	0.09	0	in Figure 7.19
1500h	HF	Flat	1×10^{-4}	—	0.9	—	
	LF	Peak	0.16	8.7×10^{-6}	0.53	0.45	Same data as
40°C	MF	Peak	7.1×10^{-3}	0.36	0.1	0.29	in Figure 7.20
1000h	HF	Peak	2.4×10^{-3}	1.2×10^{5}	1	0.71	
	LF	QDC	9.4×10^{-4}	—	0.65	—	Same data as
40°C		Peak	0.01	3.3×10^{-3}	0	1	in Figure 7.21
500h	LF+MF	Peak	0.019	0.13	0.3	0.7	
	HF	Peak	4.6×10^{-4}	6.4×10^{3}	0.7	1	
	LF	Peak	0.1	9.2×10^{-4}	0.5	0.02	Same data as
40°C-	MF	Peak	0.029	0.1	0	1	in Figure 7.22
1500h	HF	Flat	1×10^{-4}	—	1	—	
no AC							
	LF	Peak	0.12	4×10^{-4}	0.16	0.12	Same data as
40°C-	MF	Peak	9×10^{-3}	0.8	0	0.2	in Figure 7.23
1000h	HF	Peak	0.13	1×10^{6}	1	1	
no AC							
	LF	Peak	0.21	2.8×10^{-7}	0.6	0	Same data as
40°C-	MF	Peak	7.2×10^{-3}	1.5	0	0	inFigure 7.24
500h	HF	Flat	1.8×10^{-4}	—	0.88	—	
no AC							

QDC (LFD)
$$\varepsilon'' = af^{n-1} \tag{7.1}$$

Jonscher
$$\varepsilon'' = \frac{a}{\left(\frac{f}{f_p}\right)^{-m} + \left(\frac{f}{f_p}\right)^{1-n}} \tag{7.2}$$

Where a, n, m and f_p are fitting parameters as described in Table 4.1

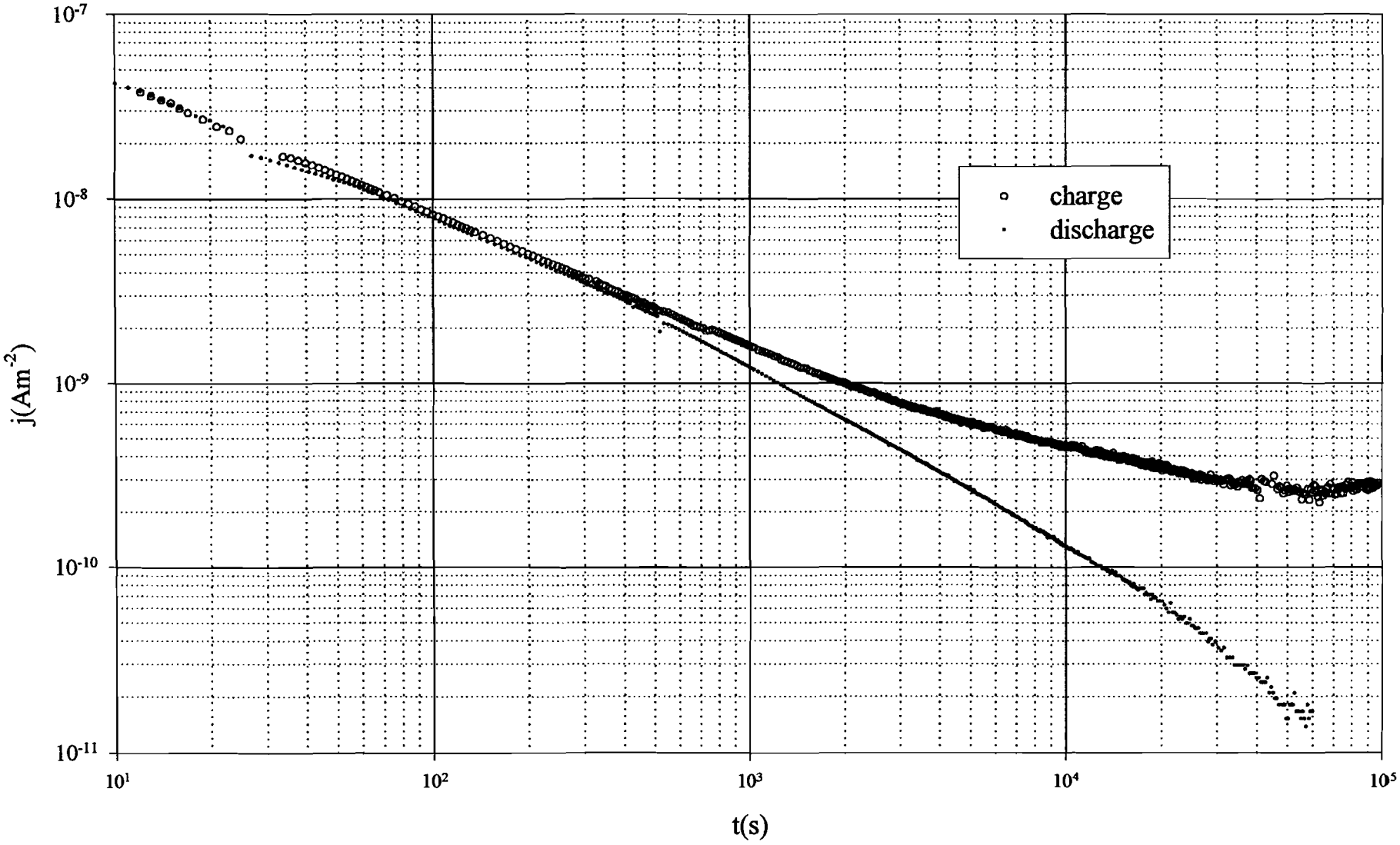

Figure 7.11 – Typical charge and discharge current curves for a LDPE sample (thermally aged sample at 40 °C for 1500 h in 1M NaCl – Charging conditions: 2 kV/mm, 27 h, 30 °C)

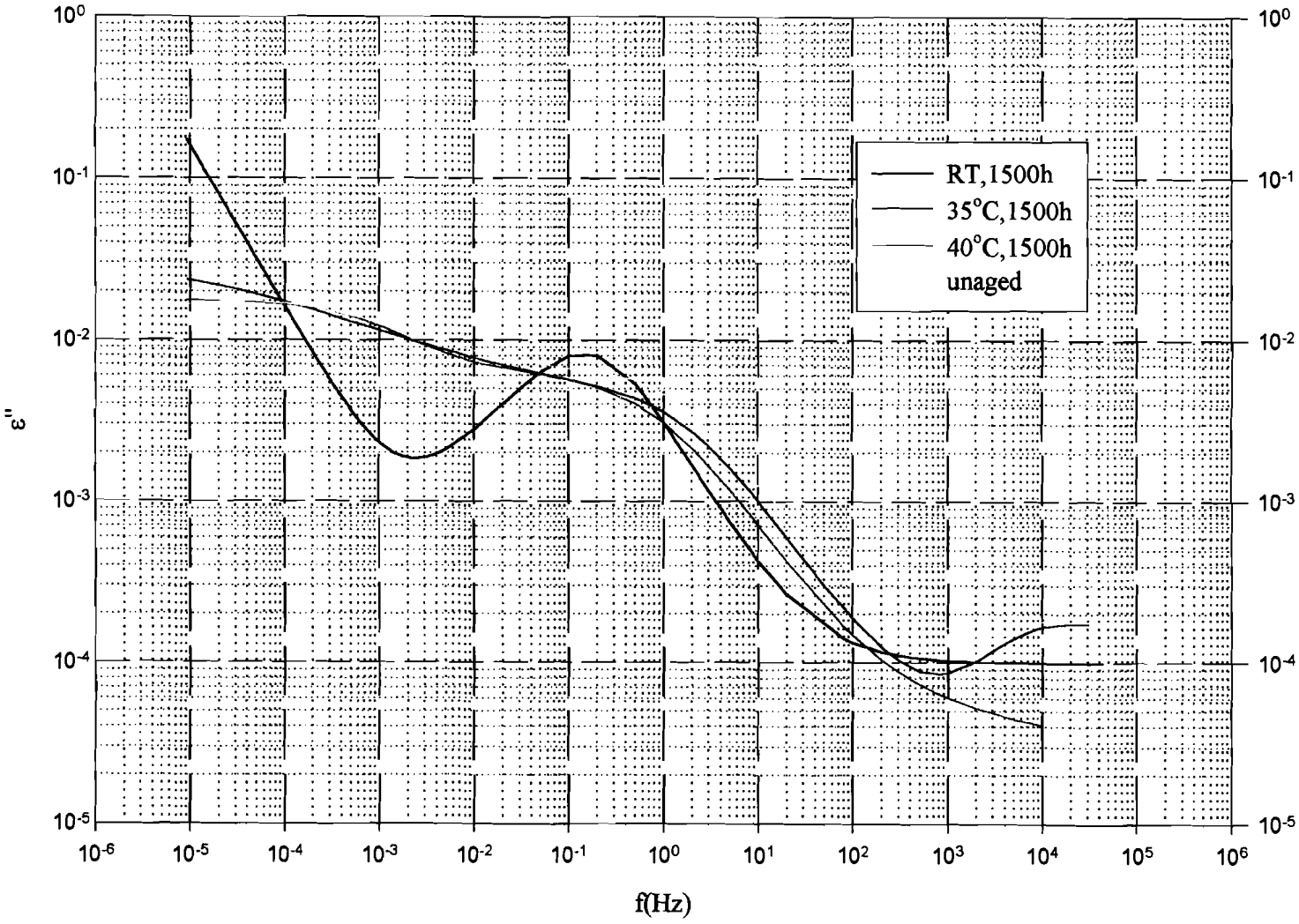

Figure 7.12- Dielectric spectra at 30 °C of LDPE for samples electrically aged (AC, 6 kV/mm, 50 Hz, 1M NaCl solution) for 1500 h at different temperatures.

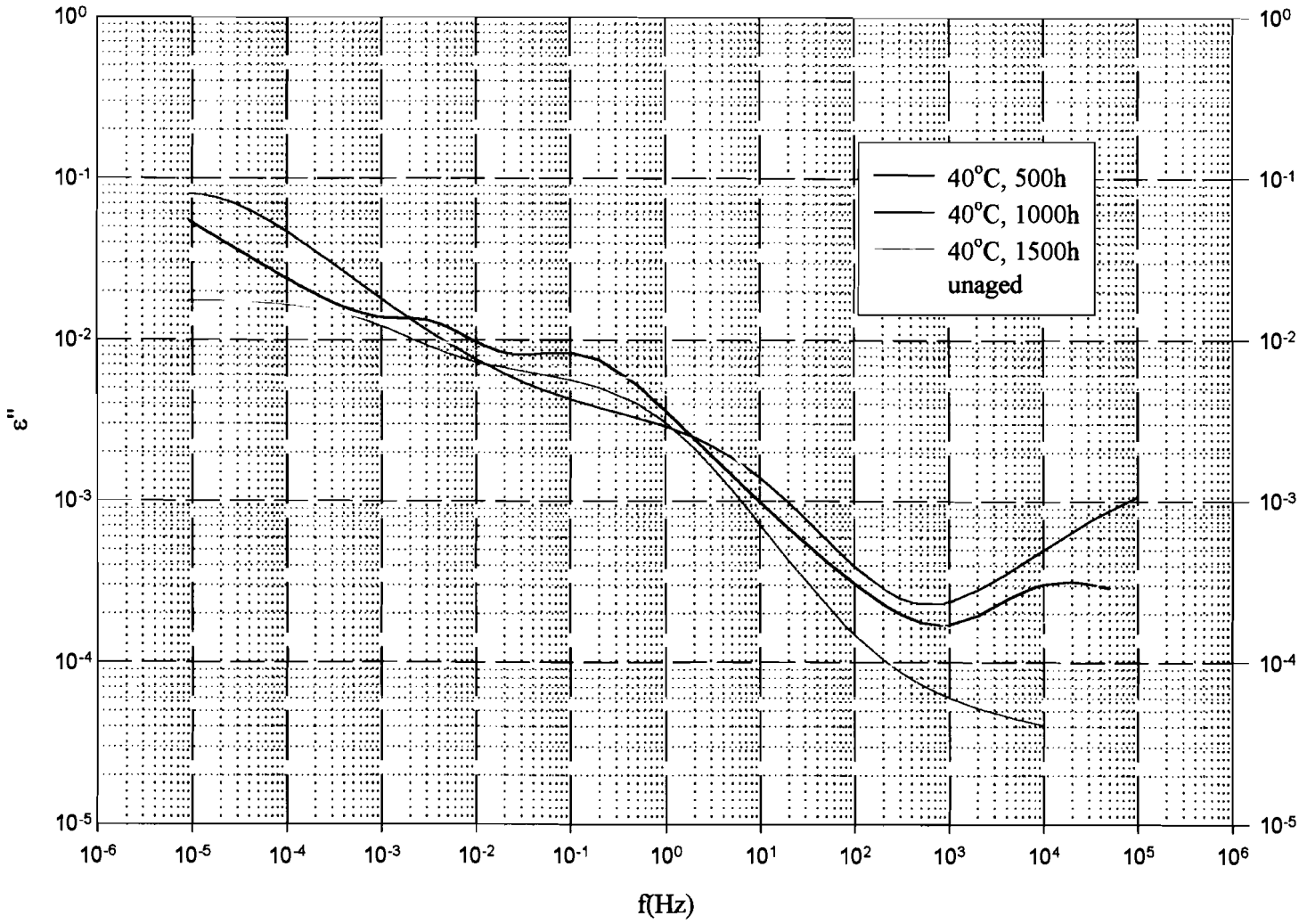

Figure 7.13- Dielectric spectra at 30 °C of LDPE for samples electrically aged (AC, 6 kV/mm, 50 Hz, 1M NaCl solution) at 40 °C for different ageing times.

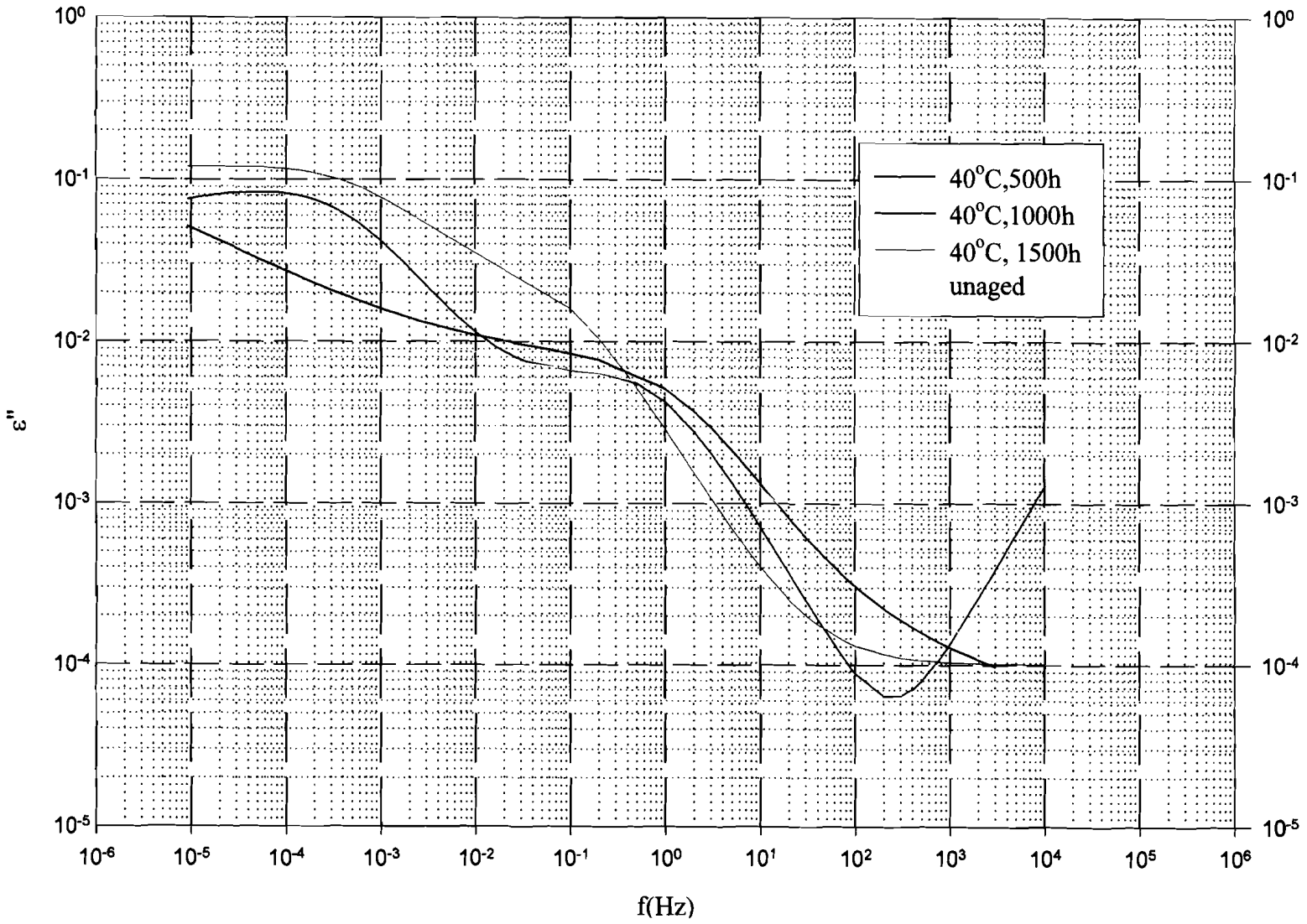

Figure 7.14 Dielectric spectra at 30 °C of LDPE for samples thermally aged (no AC, 1M NaCl solution) at 40 °C for different ageing times.

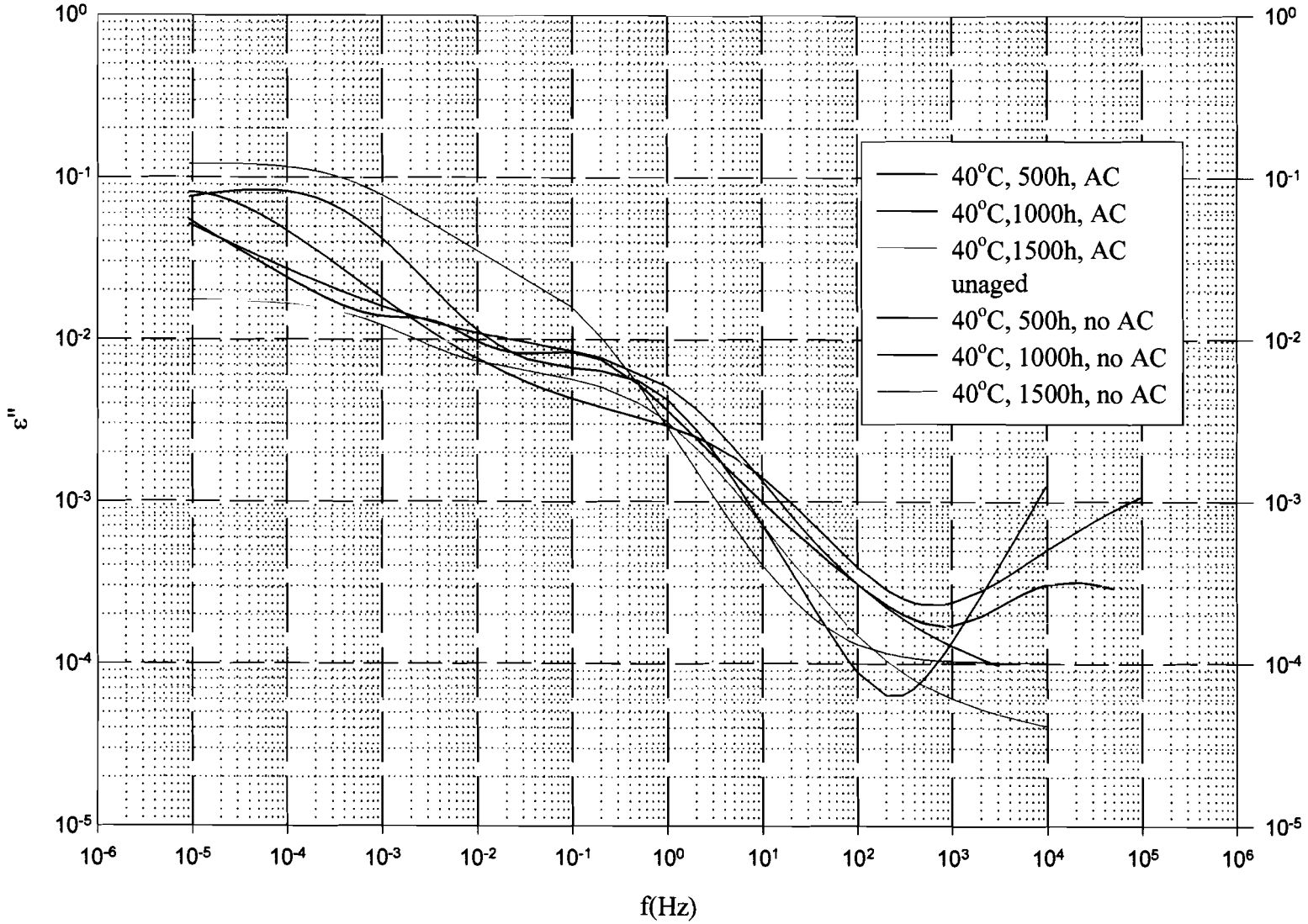

Figure 7.15 Dielectric spectra at 30 °C of LDPE for samples aged electrically (AC – 6 kV/mm, 50 Hz) and thermally (no AC) at 40 °C in a 1M solution of NaCl for different ageing time.

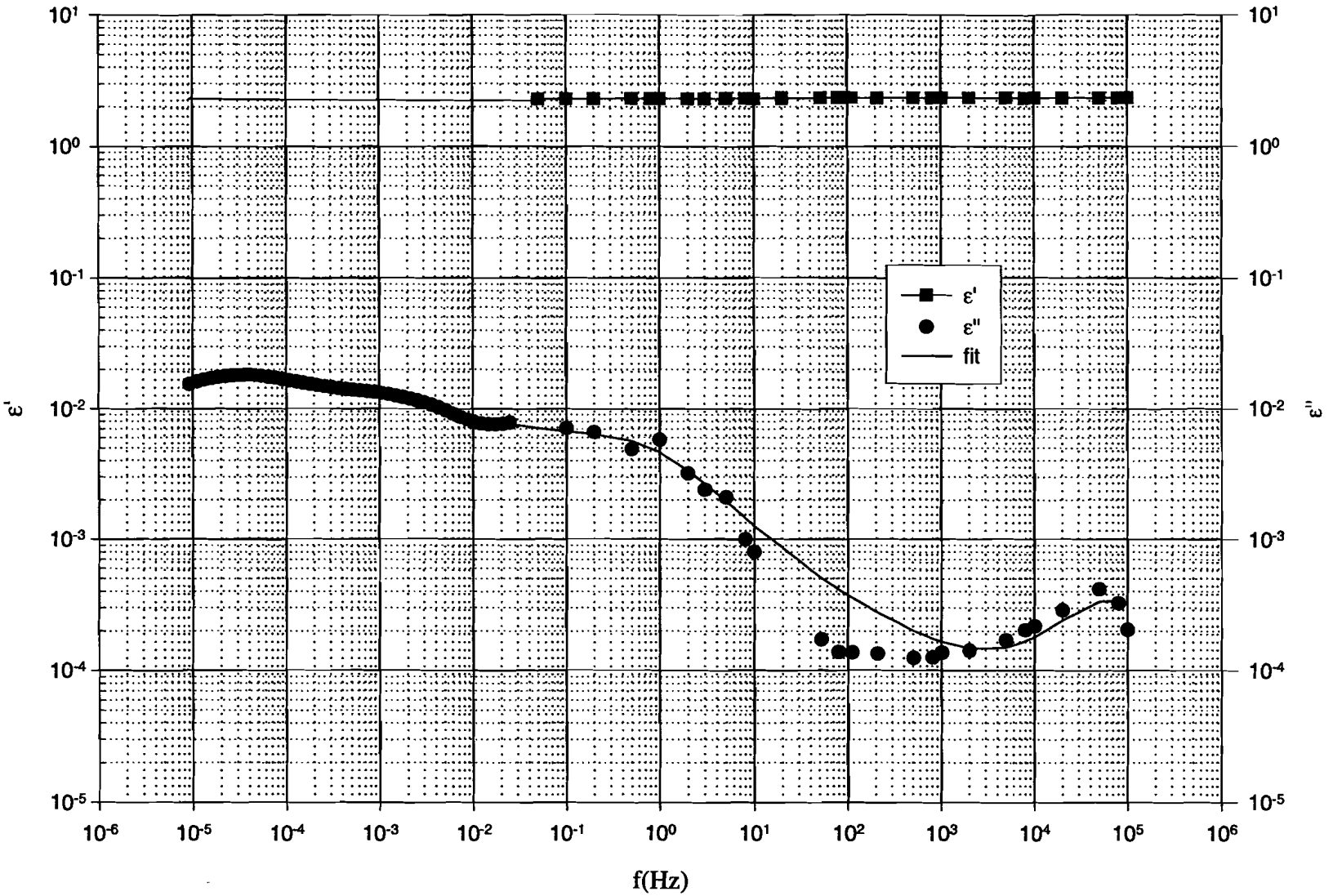

Figure 7.16 - Dielectric spectrum at 30 °C of LDPE unaged sample.

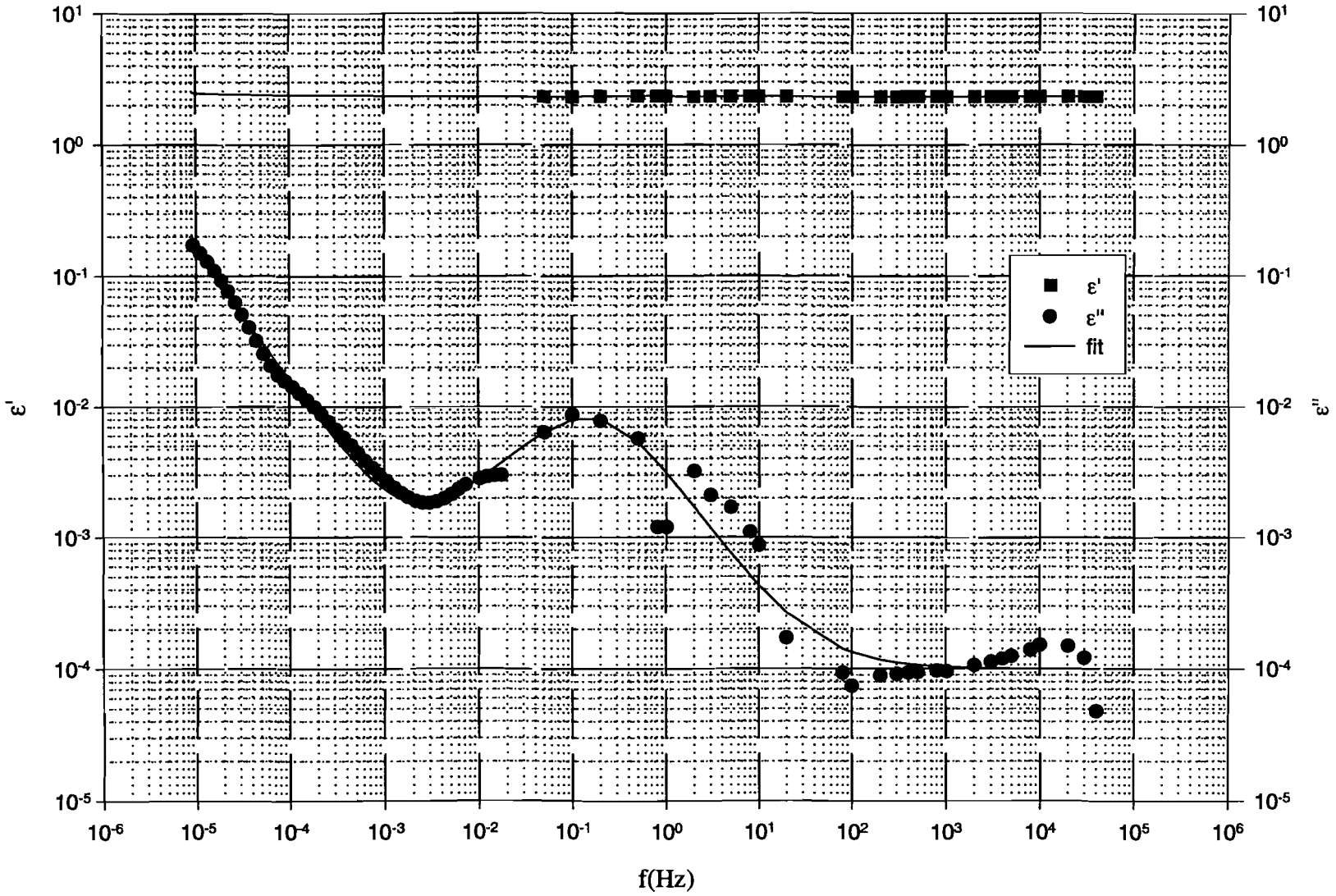

Figure 7.17 - Dielectric spectrum at 30 °C of LDPE of an electrically aged sample (AC, 6 kV/mm, 50 Hz, 1500 h, RT, 1M NaCl).

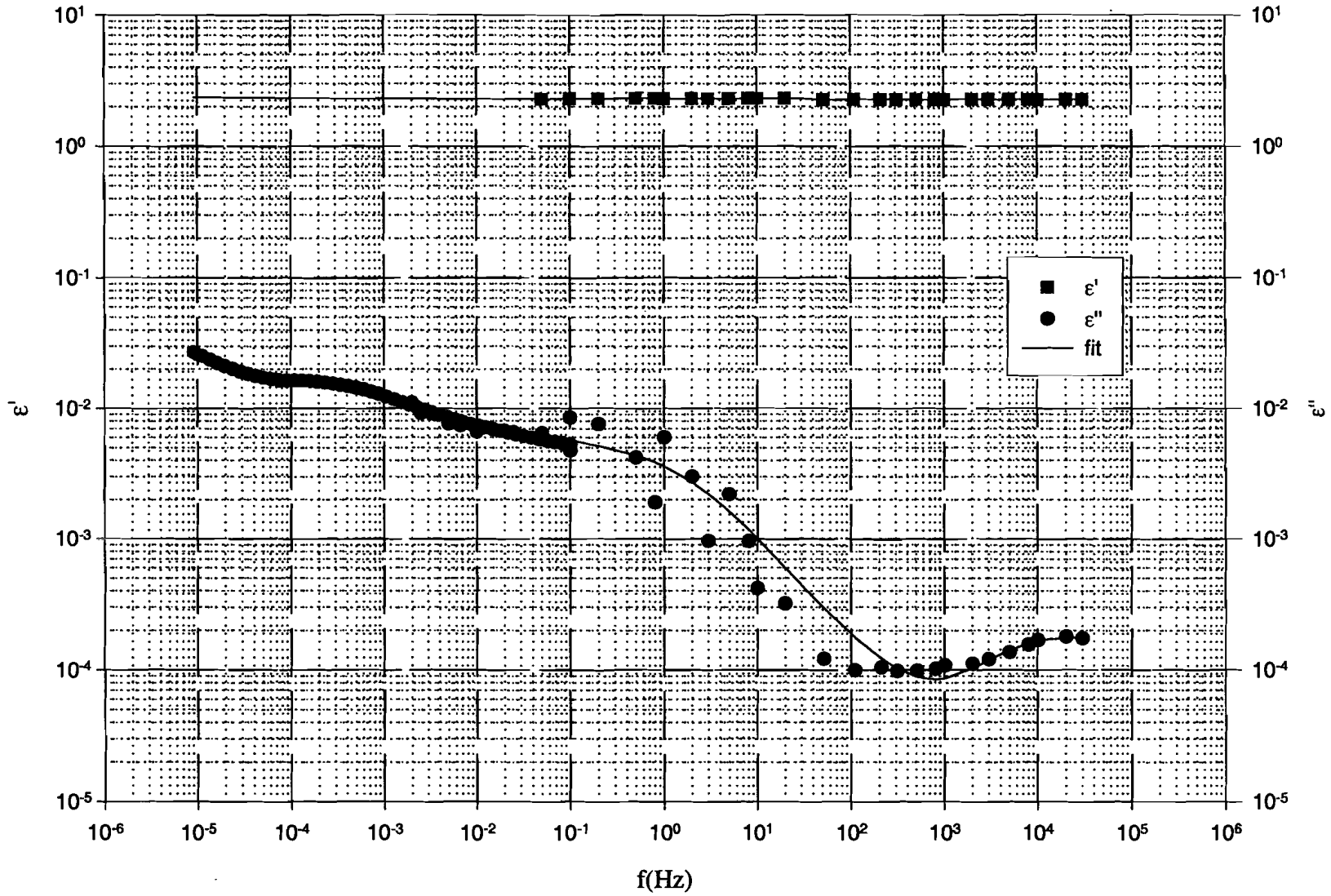

Figure 7.18 - Dielectric spectrum at 30 °C of LDPE of an electrically aged sample (AC, 6 kV/mm, 50 Hz, 1500 h, 35 °C, 1M NaCl).

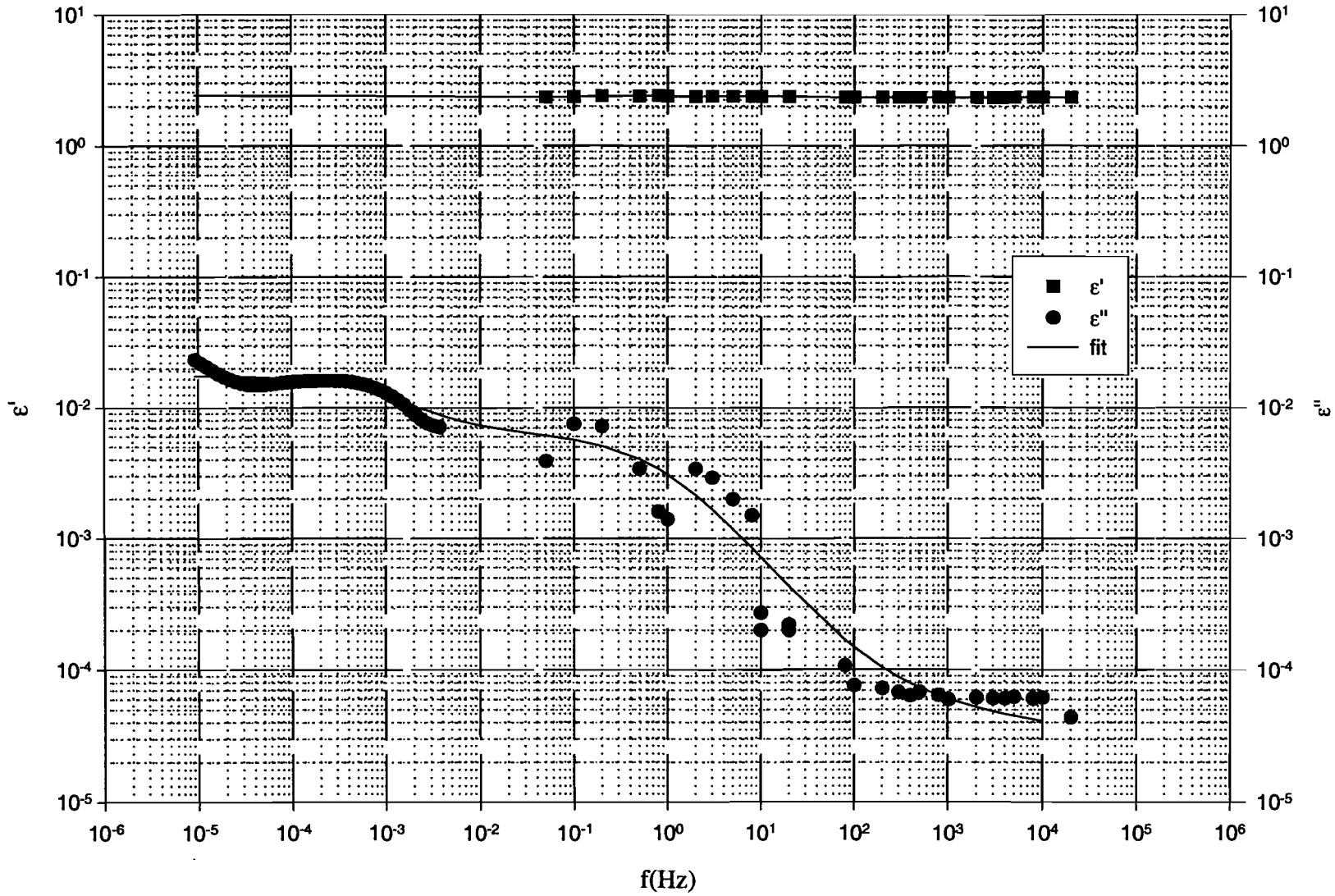

Figure 7.19 - Dielectric spectrum at 30 °C of LDPE of an electrically aged sample (AC, 6 kV/mm, 50 Hz, 1500 h, 40 °C, 1M NaCl).

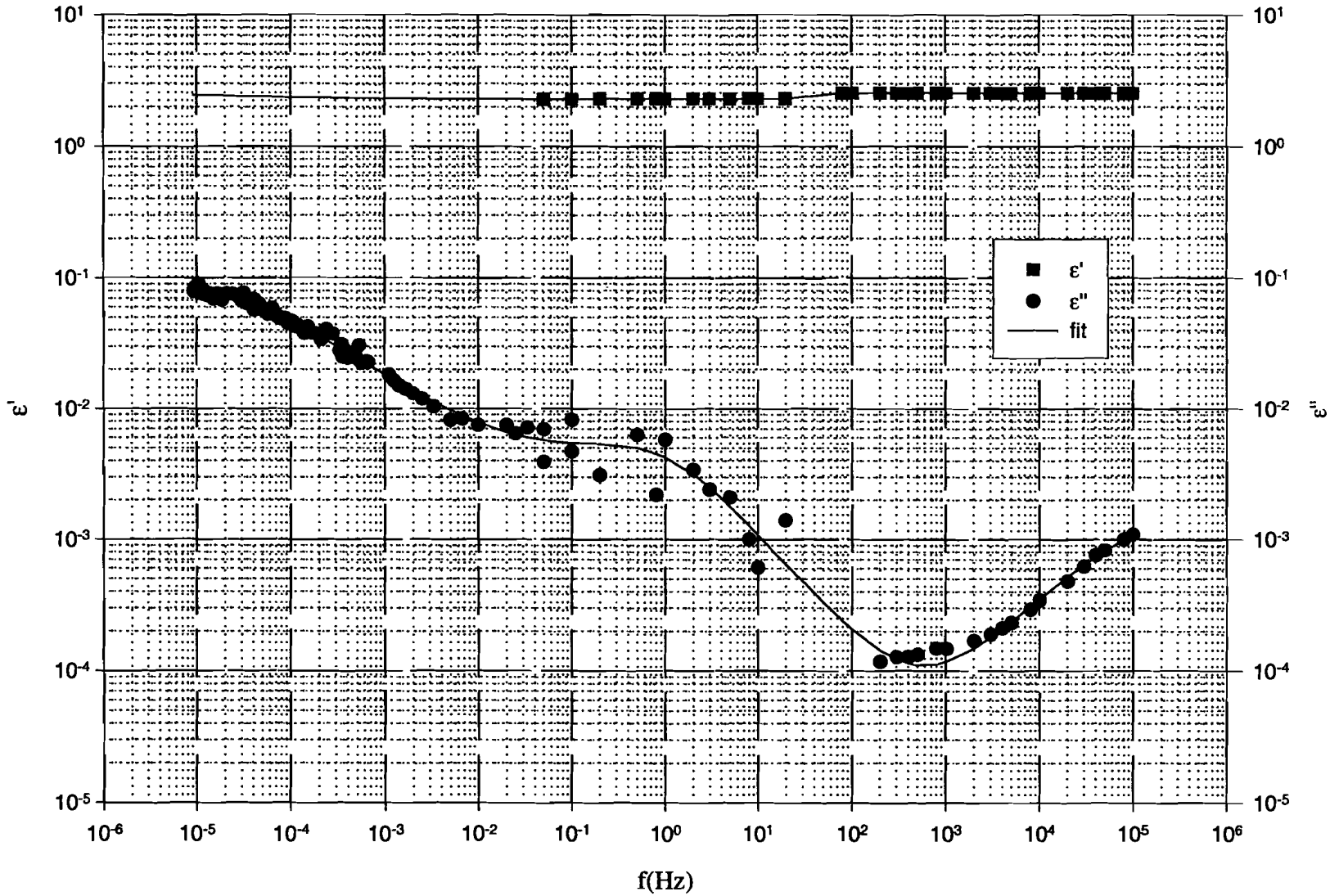

Figure 7.20 - Dielectric spectrum at 30 °C of LDPE of an electrically aged sample (AC, 6 kV/mm, 50 Hz, 1000 h, 40 °C, 1M NaCl).

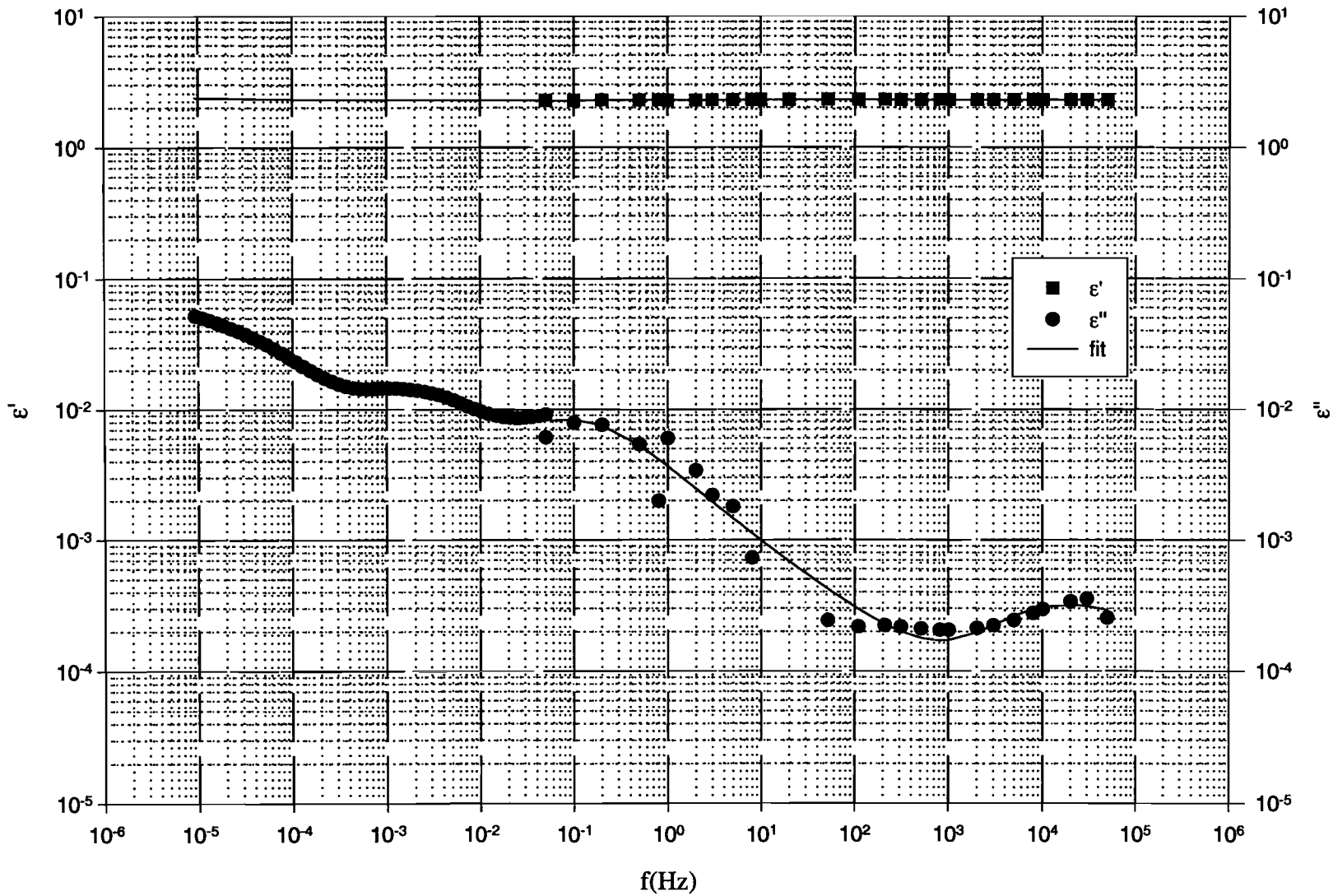

Figure 7.21 - Dielectric spectrum at 30 °C of LDPE of an electrically aged sample (AC, 6 kV/mm, 50 Hz, 500 h, 40 °C, 1M NaCl).

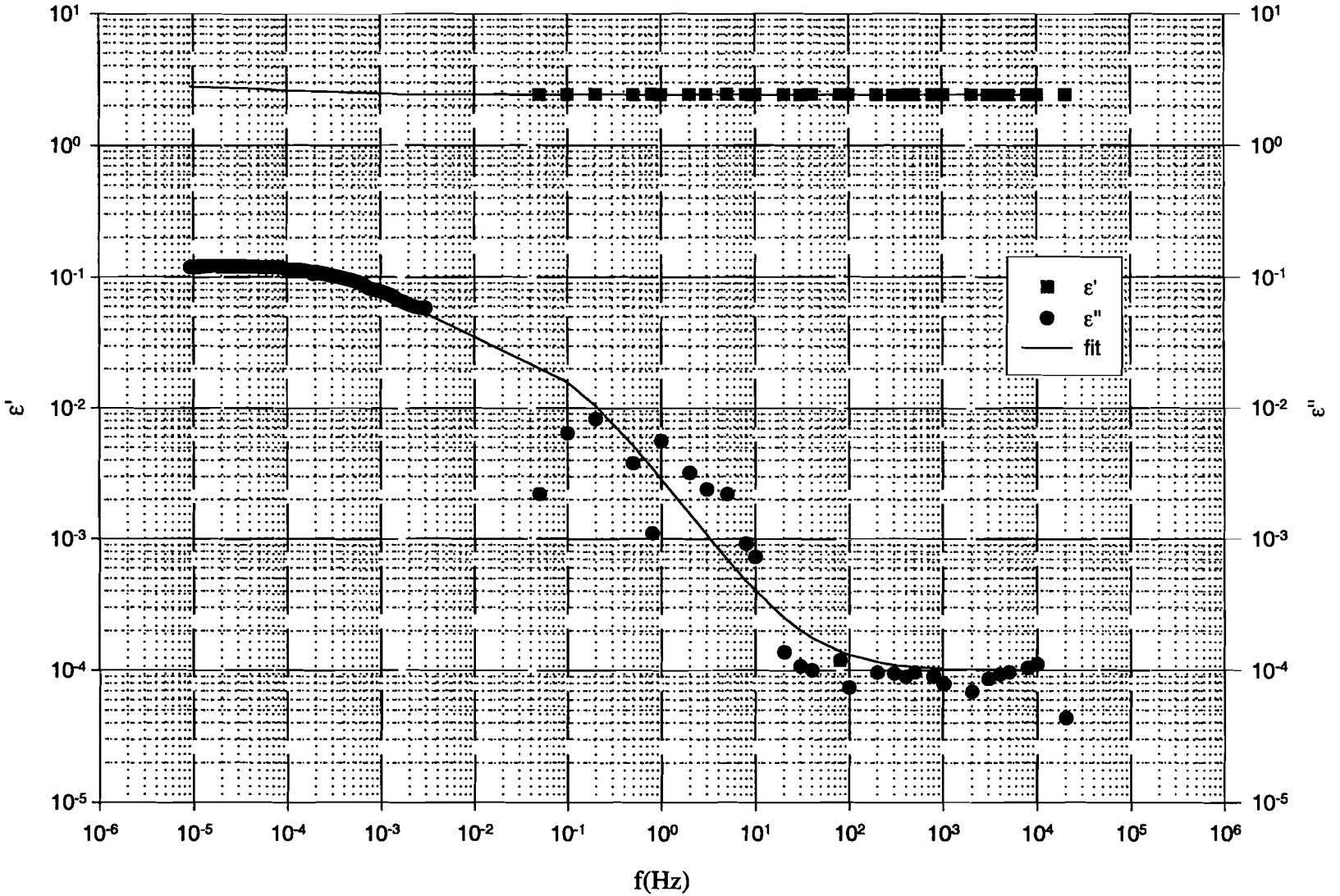

Figure 7.22 – Dielectric spectrum at 30 °C of LDPE of a thermally aged sample (no AC, 1500 h, 40 °C, 1M NaCl).

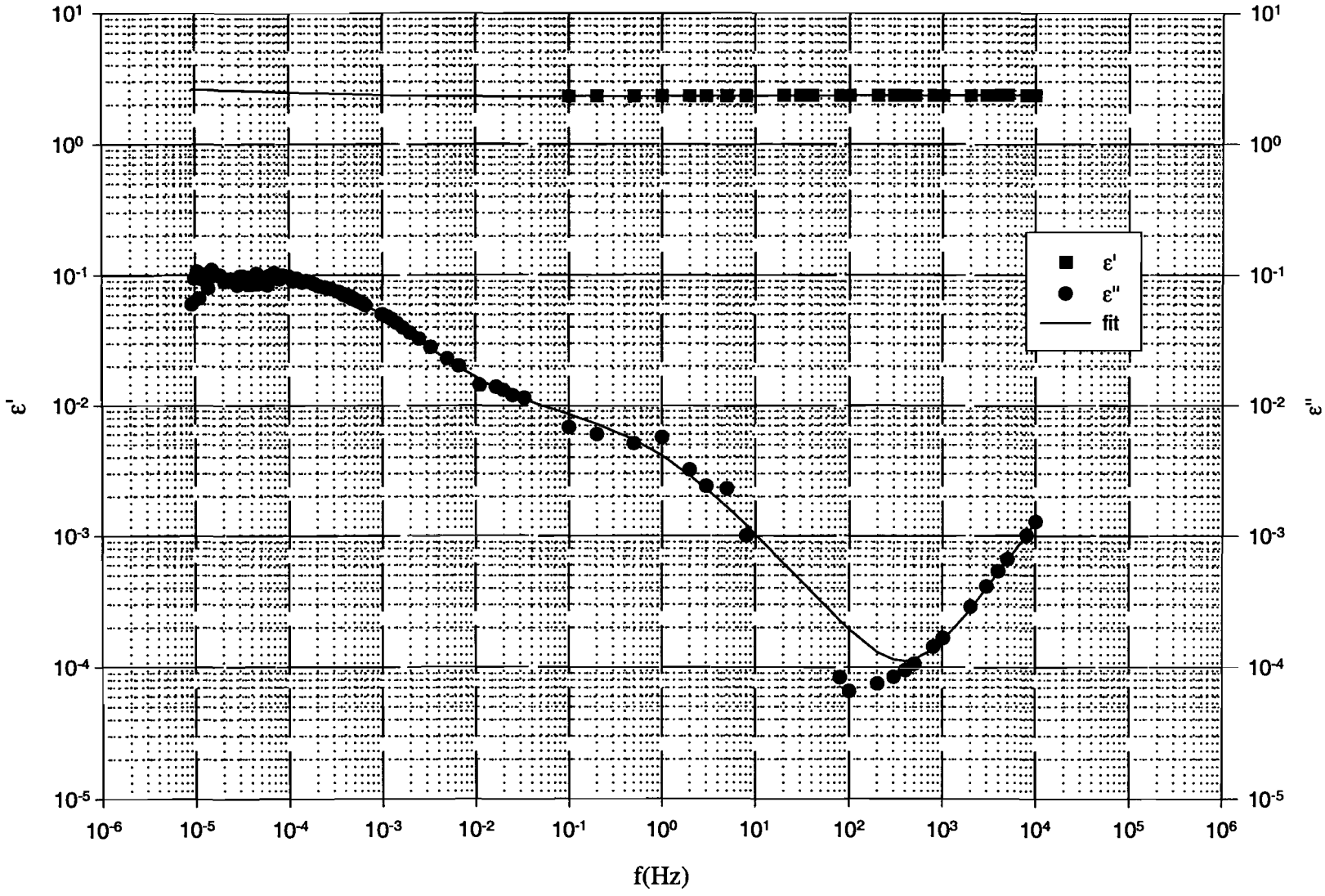

Figure 7.23 – Dielectric spectrum at 30 °C of LDPE of a thermally aged sample (no AC, 1000 h, 40 °C, 1M NaCl).

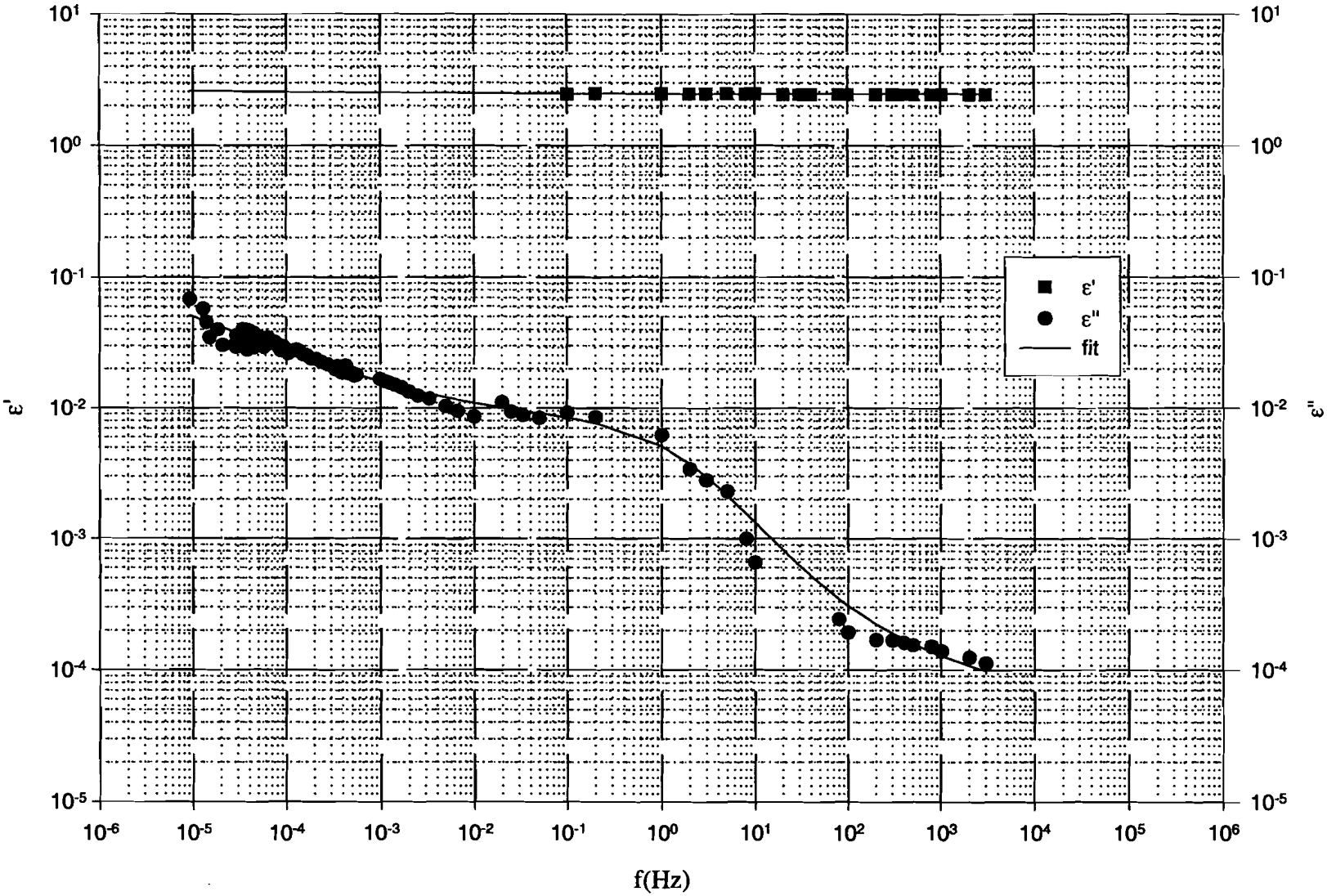

Figure 7.24 – Dielectric spectrum at 30 °C of LDPE of a thermally aged sample (no AC, 500 h, 40 °C, 1M NaCl).

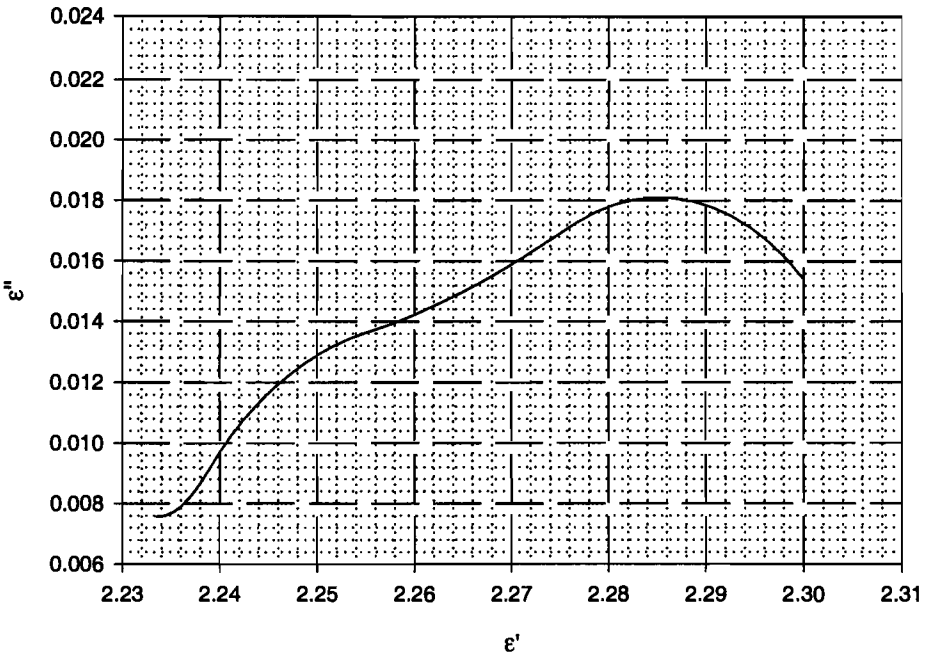

Figure 7.25 – Cole-Cole plot for unaged LDPE (for the LF region).

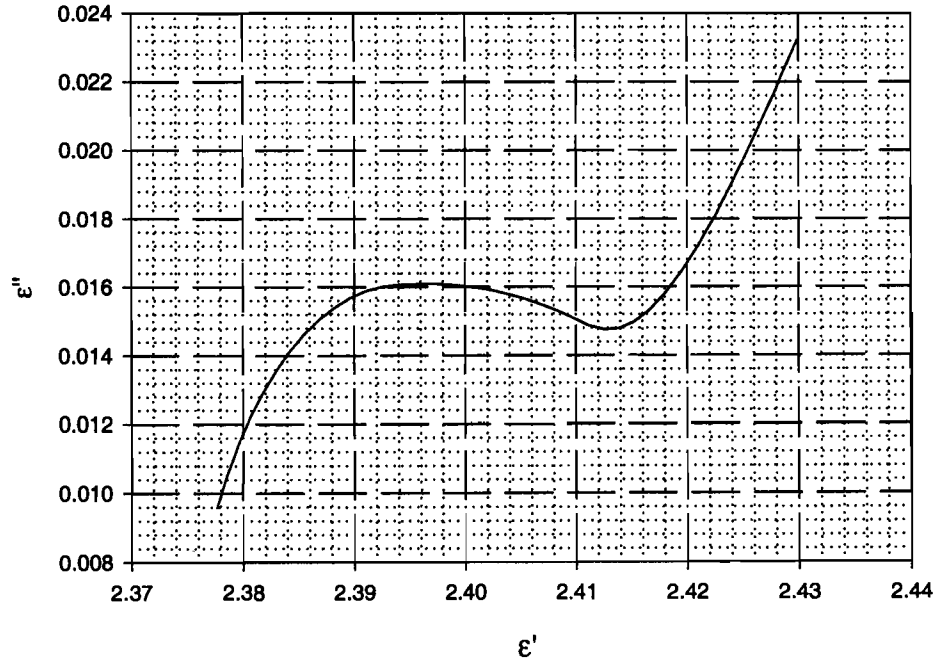

Figure 7.26– Cole-Cole plot for electrically aged LDPE (only for the LF region), 6kV/mm, 50Hz, 1500h, 40°C, 1M NaCl.

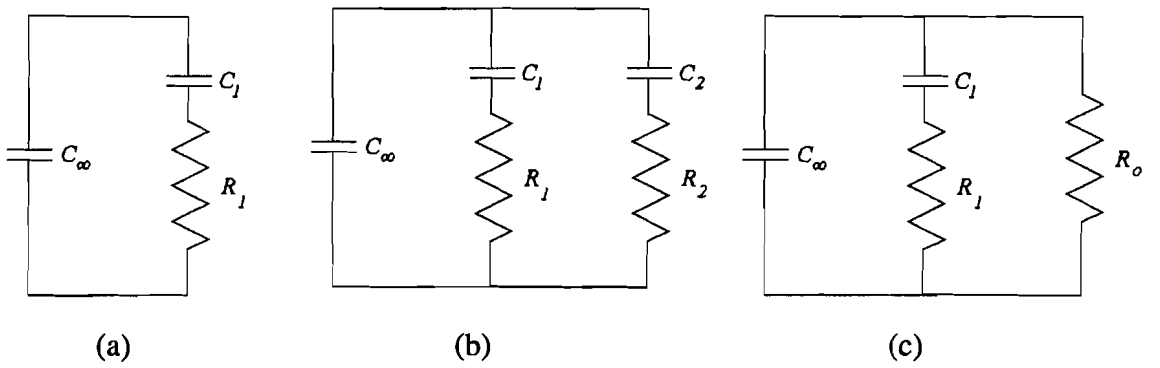

(a) (b) (c)

Figure 7.27 – Equivalent circuits for (a) unaged sample and electrically aged sample 6kV/mm, 50Hz, 1500h, 40°C, 1M NaCl: (b) with two low frequency peaks and (c) with a low frequency peak and DC conductivity.

7.3 Isothermal charge and discharge currents and non-isothermal discharge currents

As was stated previously (see 6.4) a combined measuring procedure was recently developed for PTFE by Neagu et al. [Neagu01] and was applied to polyethylene for the first time in this work. Primarily it was necessary to find the best conditions to perform the experiments in order to obtain results that were both reproducible and possible to analyse. The parameters that can be varied for charging and discharging (ICC and IDC) are the temperature (T_i), the DC field magnitude (E) and the charge/discharge times' ratio (t_c / t_d). In FTSDC the heating rate (β) is the parameter that can be changed[64]. Furthermore the final discharge (FIDC) times (t_{fd}) has to be long enough to ensure an almost complete discharge of the sample so that no residual charge remains on the sample. Careful choice of all these parameters leads to consistent and reproducible information about space charge trapping.

Figure 7.28 shows the ICC and IDC results for one of the runs performed on a thermally aged LDPE sample (at 40 °C for 1500h in 1M NaCl aqueous solution). Corresponding to fast processes the first ten seconds were not considered in the analysis of the results. As stated in 7.2.1 the results are in agreement with the experimental data from other authors [Das Gupta78].

The isothermal and non-isothermal spectra of polyethylene above RT have been widely studied however results have been difficult to reproduce and analyse [Wintle83,99]. Polyethylene is a highly insulating polymer and trapping of space charge can occur in deep traps with very long relaxation times. If care is not taken to fully discharge the sample after

[64] However in this set of experiments the value was kept constant at 1°C/min as stated in the preceding chapter.

each run of an experiment a residual charge remains and influences the results of the next run. This makes the FIDC step fundamental to control the experimental conditions and achieve reproducibility. It is possible that the ICC and IDC measurement are not influenced by the remnant charge and nevertheless the non-isothermal step is highly affected. Figure 7.29 shows the TSDC spectra of two different runs done on the same sample under exactly the same conditions and as can be observed reproducibility is quite good. The previous FIDC for each one was of the order of 10^7 s (more than a day).

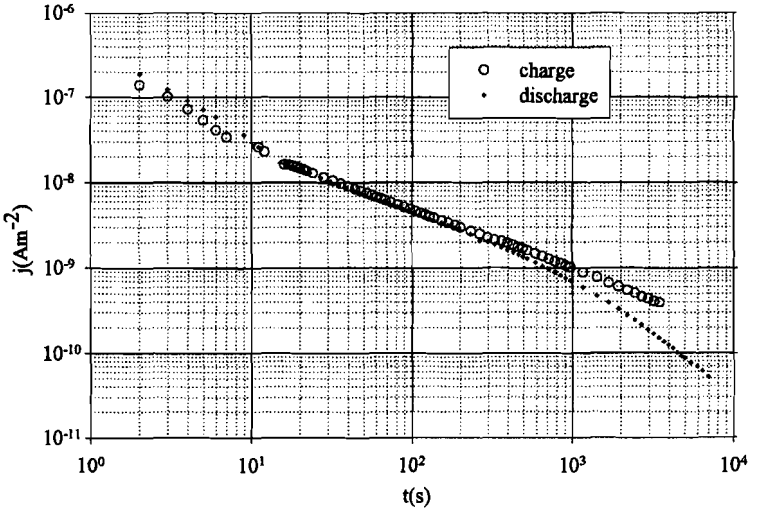

Figure 7.28– ICC and IDC results for the same run (thermally aged sample at 40 °C in 1M NaCl for 1500 h and charging/discharging conditions are: T_i = 30 °C, E = 2 kV/mm and t_c / t_d = 1h/2h).

7.3.1 Influence of charging/discharging conditions on reproducibility and analysis

First it was necessary to investigate the charge/discharge conditions in order to analyse trapping and detrapping (particularly activation energies and relaxation times). Figures 7.30 to 7.36 show a complete set of results of measurements performed at different charging/discharging conditions for thermally aged LDPE (same ageing conditions as in Figures 7.28 and 7.29). In general for polyethylene in the range of temperatures (0 to 90 °C) a dipolar transition is expected corresponding to β or α_a relaxation, near 0 °C, and at higher temperature α or α_c (as the DSC results on unaged LDPE point to, see 7.1.4). These transitions are the result of the reorientation of the carbonyl dipoles in, respectively, the amorphous and the crystalline regions of the polymer (see 2.2.4 and 4.10). However no peak corresponding to these relaxations is visible in any of the non-isothermal measurements

(FTSDC) and instead a very broad peak is present in most of the FTSDC spectra (which indicates a space charge origin, as it will be seen below).

The influence of the charging/discharging parameters on the results will be analysed separately. The effect of the charging/discharging temperature (T_i) is presented in Figure 7.30. ICC and IDC (Figure 7.30-a) and b), respectively) results show the expected increase in amplitude with temperature, though no meaningful change in slope is perceived. For FTSDC (Figure 7.30-c) the maximum of the broad peak varies, if T_i increases so do the peak maxima. Also the noise seems to increase with increasing T_i. If FIDC[65] (Figure 7.30-d) is also studied, it is clear that the higher T_i would result in longer times for this step in order for the residual charge to disappear (more charge is placed in deeper traps for higher T_i).

The influence of the amplitude of the DC charging field (E) is shown in Figures 7.31 and 7.32. For ICC (Figure 7.31-a) and IDC (Figure 7.31-b) the currents are linearly dependent on the applied field but for FTSDC (Figure 7.31-c) there is no linear behaviour. This is more clearly seen by plotting j/E as in Figure 7.32 where a threshold is perceptible at 3 kV/mm.

Space charge phenomena seem to dominate the response as is confirmed by the fact that the FTSDC peak is very broad, the non-linear behaviour with the field amplitude and the presence of the peak well above the charging temperature. For example if T_i = 2 °C the peak maxima is above 40 °C while dipolar peaks are not expected more than 20 °C above the charging/poling temperature [Fischer76]. Vanderschueren [Vanderschueren79] is more specific stating that one or more peaks can appear at temperatures much higher than the charging temperature when there are injected carriers deeply trapped. Also comparing ICC and IDC (Figure 7.28) it is observed that the two currents are not mirror images of each other which can also be attributed to trapped space charge [Das Gupta76, Wintle83].

To reveal the information on (de)trapping characteristics (activation energies and relaxation times) the charge/discharge times are very important (Figure 7.33). The differences are mainly appearing in FTSDC and FIDC as can be seen in Figure 7.33-c) and d). In the ICC plot (Figure 7.33-a) the data is very similar for all the runs shown except for that represented by the solid line, which has a higher current density. This data corresponds to one of the first runs done (run 3 on Table 6.1) and also follows a run (run 1) with a very long charging time (27h). If the previous FIDC had not lasted for long enough time an important amount of residual charge would remain in the sample and the measured values would be higher. One

[65] The current was recorded until the apparatus limit was reached but sometimes the FIDC step would proceed for even longer times.

must also point out in the ICC plot, the start of the steady state regime represented by the dotted line which corresponds to the longer charging time (3h), in agreement with the results of Das Gupta et al. [Das Gupta78]. For this run it is observed noise that may be related to inhomogeneities in the conducting path at the onset of the DC conductivity. The data from run 3 (solid line), referred to before shows also noise that can have the same origin. On the other hand, the IDC curves (Figure 7.33-b) are very similar when the charging time was the same (1h) regardless of the previous history of each run. However when this time is increased (dotted line data results from 3h charging time) there is a higher current density for the last part of the curve (above 10^3 s) that can be attributed to the presence of more charges in traps with longer relaxation times.

In the FTSDC data (Figure 7.33-c) the influence of the ratio t_c/t_d is clearly seen. For instance, too long discharge times results in an almost flat spectrum where only the high temperature peak[66] is visible (dashed line corresponding to t_d = 21h). Longer charging times enhance the high temperature peak with loss of definition of the peaks at lower temperature (comparing the dotted line, t_c/t_d = 3h/3h, with the others).

The importance of the full charging/discharging and ageing history of the sample is revealed by the differences between the data represented by the solid line (run 3 already mentioned above) and the dashed/dotted line (run 8) which have similar charging/discharging parameters but different thermograms. The most obvious differences are the higher current density for run 3 along with the presence of a peak at 85°C which has almost vanished for run 8.

Finally the FIDC graphs (Figure 7.33-d) are determined by the presence of a residual charge which, also influences mainly the high temperature part of the FTSDC plots. The FIDC density currents recorded are very low because space charge is uniformly distributed in the sample [Lança01, Neagu01a, van Turnhout80]. The presence of this undetected uniformly distributed charge will be revealed (influencing the reproducibility and the analyses) in the FTSDC data of the next run [Neagu01a]. For this residual charge to disappear almost completely the final discharge has to proceed beyond the time needed to reach the measuring limit of the setup. For LDPE under the experimental conditions described in this work this discharging time has to be more than 1 day.

[66] Above 80 °C and corresponding to the longest relaxation times.

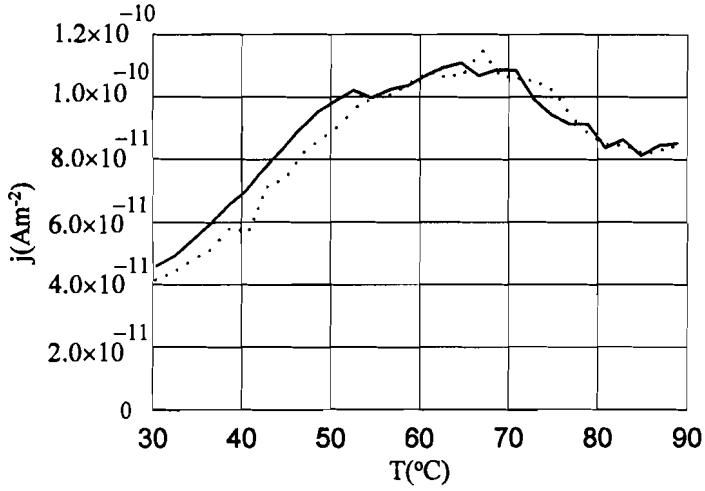

Figure 7.29 – FTSDC for two different runs in the same thermally aged LDPE sample with the same charging/discharging conditions (T_i = 30 °C, E = 2 kV/mm, t_c/t_d = 1h/2h).

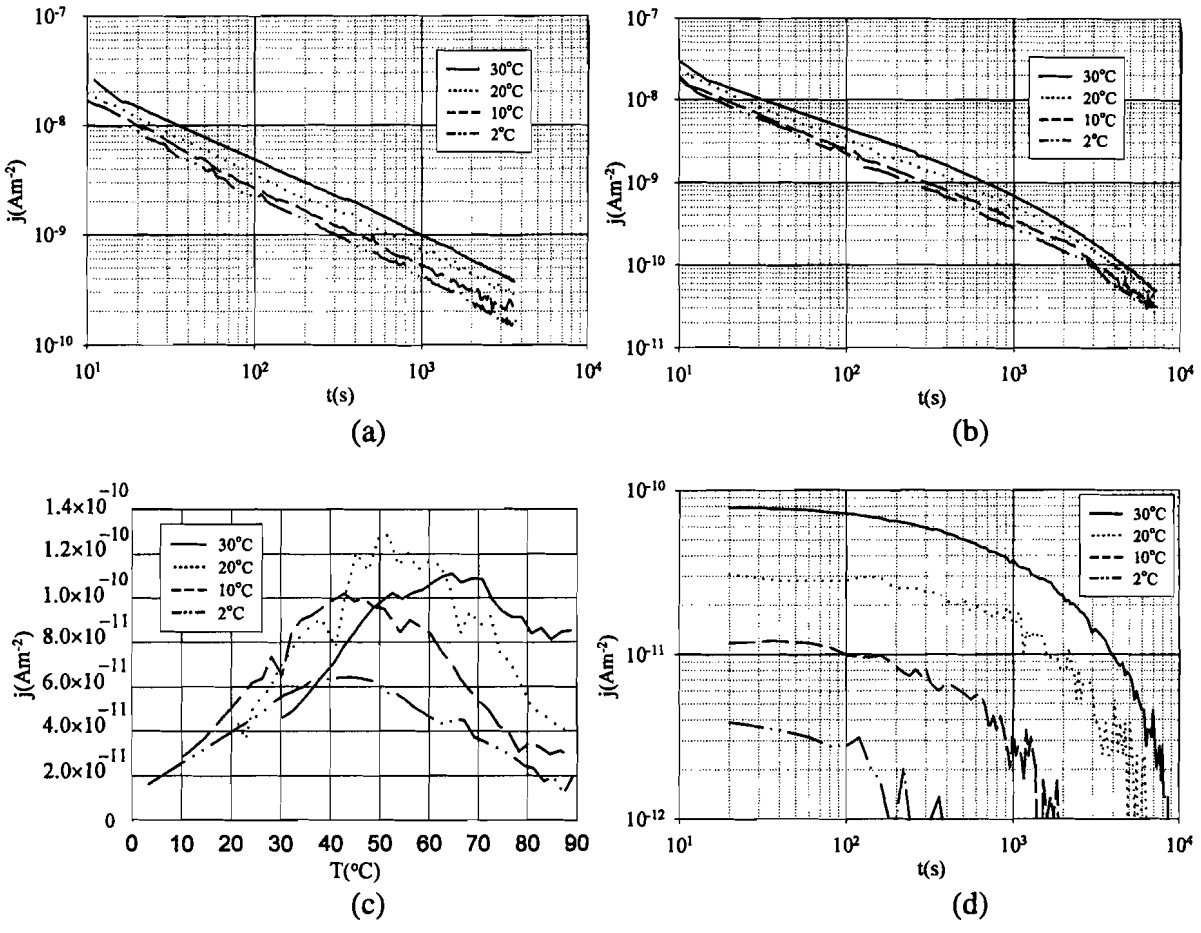

Figure 7.30 – LDPE thermally aged sample results for different charging/discharging temperatures (charging/discharging conditions: E = 2 kV/mm, t_c/t_d = 1h/2h and T_i = 30, 20, 10 and 2 °C). (a) ICC; (b) IDC; (c) FTSDC and (d) FIDC.

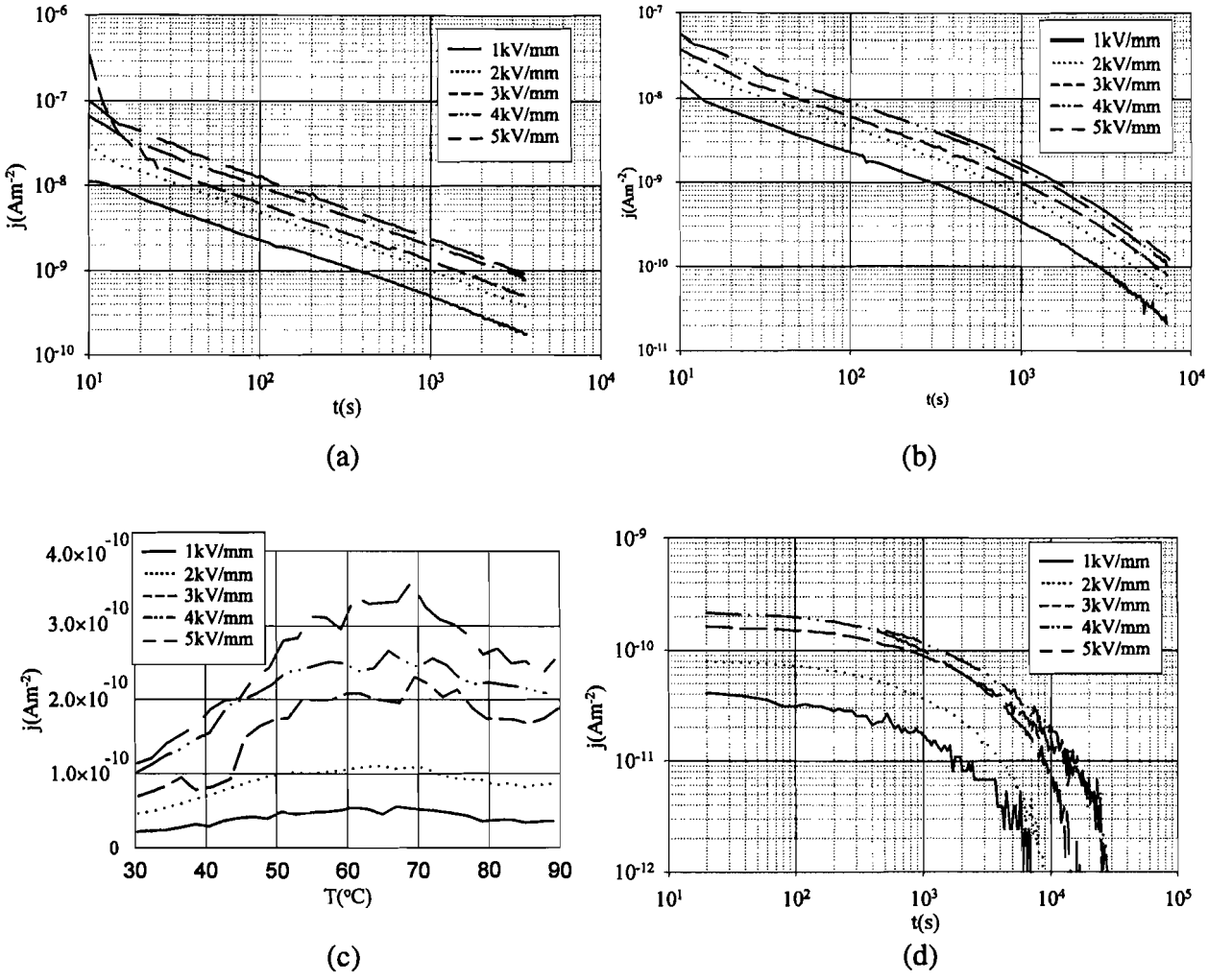

Figure 7.31 – LDPE thermally aged sample results for different charging fields (charging/discharging conditions: T_i = 30 °C, t_c/t_d = 1h/2h and E = 1, 2, 3, 4 and 5 kV/mm). (a) ICC; (b) IDC; (c) FTSDC and (d) FIDC.

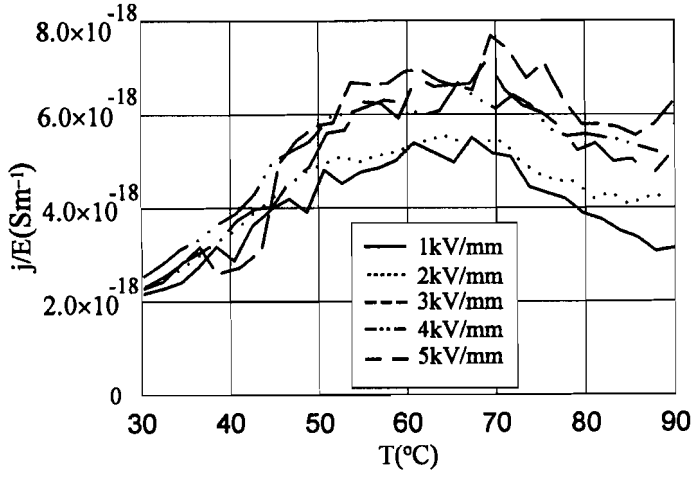

Figure 7.32 – FTSDC plot showing j/E (same conditions as in Figure 7.31). The presence of a threshold between 2 and 3 kV/mm is visible.

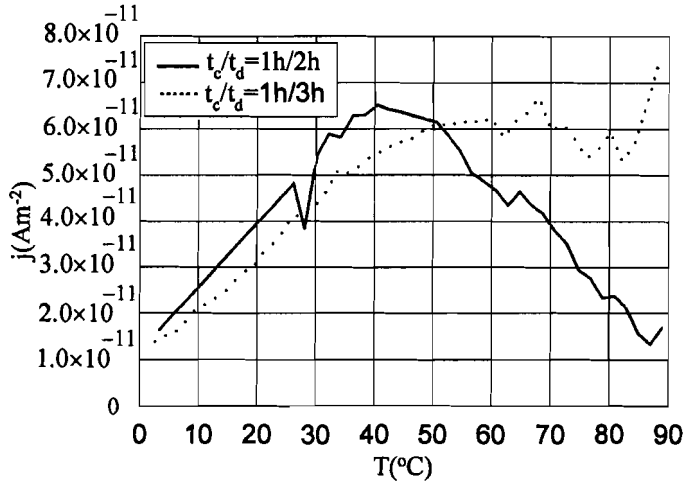

Figure 7.36 – FTSDC spectra of a LDPE thermally aged sample results for different charge/discharge times' ratios (charging/discharging conditions: T_i = 30 °C, E = 2 kV/mm, t_c/t_d = 1h/2h and 1h/3h).

For the same temperature (2 °C), Figure 7.36 shows the influence of t_c/t_d with the lower temperature broad peak maximum being shifted for longer discharge times. More noticeable is the influence of the residual charge, since the run represented by the dotted line had a FIDC step shorter than a day, while for the solid line results the final discharge time was almost 2 days. This charge partially masks the lower temperature peak and does not allow comparison of the amplitudes of the peaks for the different t_c/t_d. Nevertheless it is possible to observe a shift around 15 to 20 °C in the maximum peak temperature (peak maximum for the solid line data is ≅ 40 – 45 °C while for the dotted line data it is ≅ 50 – 60 °C). When a longer t_d is chosen the charge appearing in the thermogram has longer relaxation times because it remains trapped for longer time.

7.3.2 Results and discussion

So far the main analysis concerned the influence of the experimental parameters on the reproducibility and subsequent data interpretation. Now a more detailed analysis of the results will be made in order to understand and obtain some quantitative information concerning the physical processes involved, for thermally aged and electrically aged polyethylene.

The isothermal current data were fitted in order to obtain relaxation times (considering a sum of exponential decay functions). Moreover the total charge was calculated for all four steps of a run and from these values the zero field plane of the charge centroid and mobilities could be obtained.

The charge centroid position can be calculated from the ratio between total charge released during the whole discharge processes ($Q_d = Q_{IDC} + Q_{FTSDC} + Q_{FIDC}$) and the total charge accumulated during the charging process ($Q_c = Q_{ICC}$). The zero field plane of the charge centroid, x, is calculated from [Neagu01a]:

$$x = \left(1 - \left|\frac{Q_d}{Q_c}\right|\right) d \tag{7.3}$$

where d is the sample thickness.

7.3.2.1 Unaged LDPE

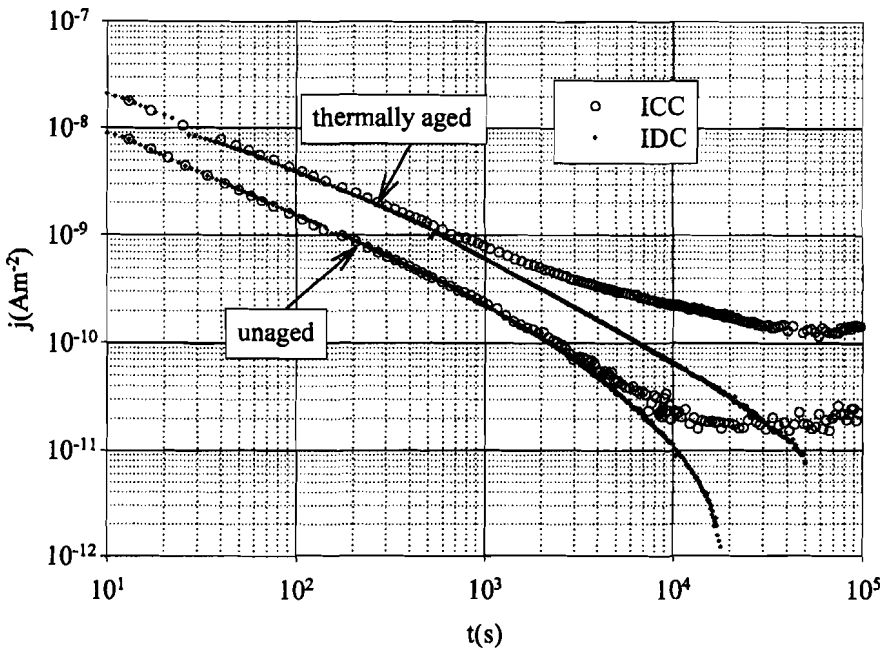

Figure 7.37 – Comparing charge and discharge currents for thermally aged (in 1M NaCl solution at 40°C for 1500h) and unaged LDPE with T_i = 30°C, E = 2 kV/mm.

Attempts were made to apply this procedure to unaged LDPE, however it proved to be very difficult to obtain reproducible results for the FTSDC step. Comparative results between unaged and thermally aged samples are shown for ICC, Figure 7.37) and FIDC (Figure 7.38). Relatively higher current values are recorded for the thermally aged LDPE especially at longer times indicating the presence of much less mobile charges in the virgin polymer. This is also easily seen in the FIDC data where the presence of charge in traps with longer relaxation times is dominant in the aged polymer because it is observed that the unaged

polyethylene current reaches the measuring limit in a much shorter time. Also this current is much smaller and very noisy meaning that very few charges are deposited in deep traps. The problems encountered for the unaged samples results can be due to the surface charge that is deposited during films preparation and which was detected by surface potential measurements (see 7.1.5).

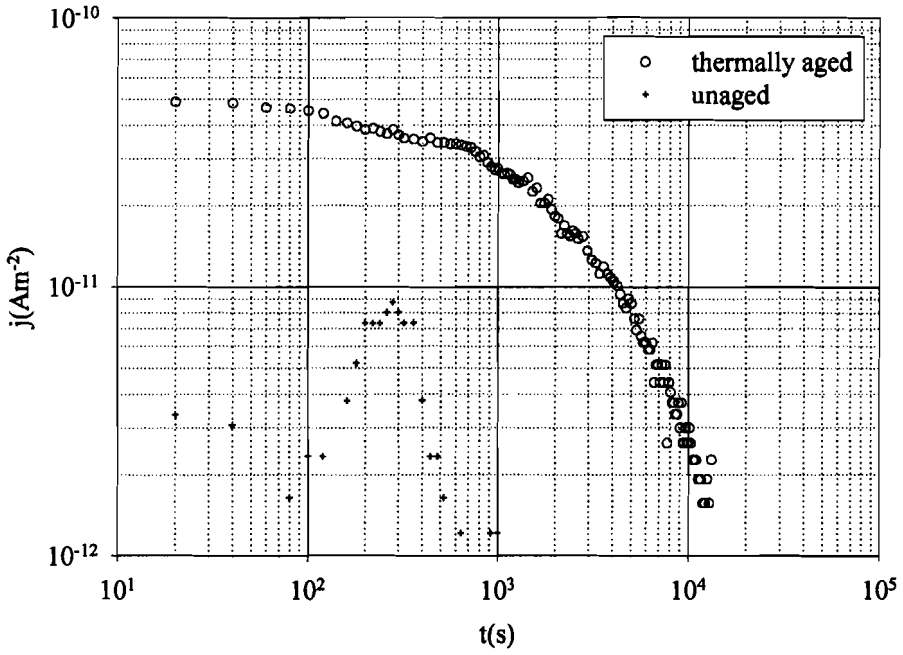

Figure 7.38 – Comparing final discharge currents for thermally aged (in 1 M NaCl solution at 40 °C for 1500h) and unaged LDPE with T_i = 30°C, E = 2 kV/mm.

7.3.2.2 Thermally aged LDPE

Results for thermally aged LDPE are presented in Figures 7.29 to 7.36 and in Tables 7.5 to 7.9. For ICC three different relaxation times were obtained the longest one near 1h (3600s) but usually between 2000 s and 3000 s. Four relaxation times are found for IDC with the longest up to 5000 s while the usual value is near 3000 s. For FIDC data only one or two different relaxation times were found. From comparison of the percentages in brackets, that correspond, respectively, to the ratio between Q_{IDC}/Q_{ICC} and Q_d/Q_{ICC} [67], it is evident that at the end of the IDC step there is still charge in the sample and it only becomes almost completely discharged at the end of the FIDC step. This, again, proves the importance of this last step. The values found for the mobilities span from 6×10^{-17} to 6×10^{-15} $m^2V^{-1}s^{-1}$ and are of

[67] Results in brackets in columns 6 and 8, respectively, in Tables 7.5 to 7.8.

similar order of magnitude to those found in the literature[68] [Wintle70, Fischer78, Pélissou88, Hwangbo98]. It is also found that the charge that remains longer in the sample penetrates very little in the bulk staying near the surface (maximum charge centroid value is around $0.14d \cong$ 30 μm and the minimum one below our measurement range, resulting in zero for the charge centroid and the mobility) as is expected from the literature [Wintle72, Seggern81]. As stated above, space charge seems to be the dominant process and, owing to the long duration of the IDC step when compared with usual TSDC techniques, the charge released during FTSDC and FIDC is related to charge that is (de)trapped in traps with longer relaxation times and also in deeper traps. Under this assumption it is reasonable to assume a hopping mechanism for charge transport [Neagu01a].

In Table 7.5 the influence of charging/discharging temperature on the total charge, charge centroid (x) and mobility is presented (see also Figure 7.30). Evident in the ICC and IDC of all the runs is the decrease of total charge with decreasing temperature. The same is true for the charge centroid position and mobility except at the lowest temperature (2°C) which exhibits a considerable increase. At 10 °C a zero value was found meaning that the charge remains mostly at the surface or very near the surface. As was mentioned above (see 2.2.4 and 4.11) the β or α_a (glass transition) peak is found near 0 °C while the α or α_c peak lies well above 0 °C. At both transitions there are important structural changes that would result in the creation and destruction of traps, so measurements at T_i = 10 °C would be in an intermediate zone where fewer traps would exist. If the temperature is lowered the influence of the α_a transition would start to be felt, while advancing towards higher temperatures it would be the influence of the other transition to appear (reflected also in the broad peak seen in the FTSDC at 40 – 50 °C).

The effect of the DC applied field used to charge the sample is presented in Figures 7.31 and 7.32 and the results for the total charge and mobilities are in Table 7.6. The total charge increases with increasing field for ICC, IDC and FTSDC. For FIDC the same dependence is observed except for the higher field (5 kV/mm). In terms of x the charge penetrates more into the sample for the lower field (1 kV/mm) and attains a minimum at 3kV/mm, increasing first (between 3 and 4 kV/mm) and then more or less stabilising for the highest field amplitudes (the mobility follows the same trend). Considering a trapping/detrapping process it seems that initially as the field is increased deeper and deeper traps are being filled. This corresponds to a

[68] It must be pointed out that it is difficult to find values in literature matching similar experimental conditions (temperature, field, etc.). Also sometimes it is not clearly stated what are the exact experimental conditions.

smaller penetration into the sample since deeper traps are expected to be located nearer the surface [Wintle70, Seggern81]. From a certain field value (the threshold of 3 kV/mm also observed in the FTSDC graph of Figure 7.32) the available traps seem to be filled and the charge is free to move further inside the material. Moreover this charge has gained more energy supplied by the higher electrical field and will move faster, thus an increase in mobility is observed. More charge accumulates until it is enough to give rise to a screening effect which stops the charge from moving further inwards and x and the mobility values become more or less constant [Hwangbo98, Montanari01].

The importance of a careful choice of charging/discharging times has been discussed above and it is seen in Figure 7.33 and Table 7.7. For the only run where it is possible to discern the onset of a steady state (corresponding to the longest charging time, t_c/t_d = 3h/3h) it was possible to estimate a value for the DC conductivity, $\sigma_o = 2.4 \times 10^{-16}$ Sm^{-1}, which is in good agreement with the literature [Pélissou88]. In this run, charge had more time to penetrate into the bulk and it exhibits the highest value for the charge centroid position but not for the mobility (see Table 7.7). On the other hand the run with the longest discharging time, t_c / t_d = 1h/21h, is that which has one of the smallest value for $x = 0.01\ d$. As can be seen, most of the charge has left the sample by the end of IDC (97%) and at the end of FIDC only the charge trapped in deeper traps (near to the surface) remains. It is interesting to notice that for the aforementioned runs 3 and 8 (first and last data rows in Table 7.7) the charge centroids and mobilities are the same, even if they show different amounts of charge as a consequence of the their different histories.

The results in Table 7.8 refer to the influence of the field when the charging/discharging temperature is $\cong$ 2 °C . Similarly to T_i = 30 °C (Table 7.6) there is a significant decrease in the values of the charge centroid position and the mobility, between E = 2 kV/mm and 4 kV/mm. Moreover, for the highest field, it was not possible to calculate these values as they lie in the limit of the apparatus resolution.

The broad peak around 50 °C was observed in the TSC spectra obtained by Fukuzawa et al. [Fukuzawa99] in an experiment using needle electrodes. These authors also calculated the penetration of the charge by thermally stimulated surface potential measurements and as expected from needle electrodes the charge penetrated more than in our experiment. Kim et al. [Kim01] have also found a similar peak in the TSC of γ-irradiated LDPE that was related to space charge, and another peak at 90 °C. FTSDC studies were carried out firstly by

calculating the activation energies using the initial rise method [Vanderschueren79, Turnhout80]. Results for the thermally aged LDPE are presented in the last column of Table 7.5 to 7.8. It is difficult to obtain consistent data since this peak is composed of individual peaks and their relative amplitude is also dependent on the experimental conditions of each run. It should be noted that the low values found are similar to some in the literature [Seggern81].

Individual peaks can sometimes be perceived as a shoulder or a small peak superimposed on the resulting broad peak (see, for instance, Figure 7.33-c). For some selected runs peak decomposition was attempted using an improvement of the method of Neagu et al. [Neagu01b] and taking space charge to be at the origin of the peaks.

In Table 7.9 the first three columns show the data for the broad peak (T_{max} is the peak temperature maximum, j_{max} the current density at the peak maximum and E_a the activation energy calculated by the initial rise method). Choosing a higher charging temperature shifts the FTSDC peak towards higher temperature and also increases the current. The activation energy obtained by the initial rise method is also larger for higher T_i if the data in this table only are considered. As was mentioned above there seems to be no clear relation between the activation energy calculated by this method and the charging temperature (see Table 7.5). A fit done by decomposing the spectra into individual peaks can be seen in Table 7.9 (T_{mi} is the peak temperature maximum, E_{ai} is the activation energy, σ_{oi} the space charge density at T_i and τ_{eq} the relaxation times at T_{mi}). Since the peaks are not well resolved, the peak temperatures estimated have errors and they should be accepted with some caution. As was noted the high temperature peak (above 80 °C) may appear or not, depending mostly on FIDC total time and consequently on whether discharge of the sample is almost complete[69]. However the presence of this peak strongly affects the analysis of the lower temperature broad peak. This broad peak located around 40 °C to 70 °C[70] can be decomposed into at least two peaks. Usually in this region when the fitting is done considering just one peak the correlation is not so good as when two or more peaks are included. In the literature the presence of many peaks has been reported in the thermally stimulated spectra of polyethylene above RT, at positions around 35 °C to 65 °C and attributed to space charge but for different mechanisms [Sawa73&74, Kao79, Mizutani80, Dorlanne82]. Part of this range is a consequence of the poor control of experimental conditions and the difficulty of analysis for high insulating polymers.

[69]But also on the ageing history of the sample (see 7.3.2.3)

[70] Depending on the charging/discharging conditions.

Analysing the thermograms obtained in this work for the charging temperature T_i = 2 °C a decomposition was possible into three individual peaks appearing roughly at 35 °C, 45 °C and 65 °C (and, when appearing, a high temperature peak at 85 °C). For T_i = 30 °C the values found (50 °C, 60 °C, 70 °C) are shifted to higher temperatures. The low temperature peak does not appear because the thermogram starts at 30 °C. The choice of these fitting temperatures was supported by some additional experimental data and also by values found in the literature. Some runs were done without charging the sample, just cooling or heating the sample produced sharp peaks at temperatures close to those selected (45 °C, 65 °C and 85 °C) and detected mostly during cooling. However in the temperature range of the lowest peak (35 °C) no sharp peak was observed during either cooling or heating. Because these peaks are very sharp it is expected that they result from structural changes. Moreover peaks at similar temperatures were reported by other authors, such as Kobayashi et al. [Kobayashi79], who found simultaneously the same three lower temperature peaks. It is interesting to notice that, even if the experiment was done using elongated LDPE, some of the conditions were similar (charging at a lower temperature (15 °C) and then heating using a heating rate of 1 °C/min and the charge/discharge time ratio (t_c / t_d = 1h/2h)). Kobayashi attributed the first two peaks to structural changes (cavities) in the interface crystalline/amorphous caused by melting and recrystallisation. Blake et al. [Blake74] also found a peak at 35°C temperature in γ-irradiated HDPE which was attributed to trapped electrons.

Some authors have also found another peak very close at 40 °C [Mizutani80, Seggern81], which, according to the errors can be related either to the 35 °C or the 45°C peaks. According to these authors this peak is due to electronic traps of chemical origin (chemical impurities, oxidation products[71], broken chains, etc.). Kao et al. [Kao79] have related the peak at 45 °C to traps that can be either in the surface or the bulk of the polymer. Sawa et al. [Sawa73&74] attribute a peak at 50°C to space charge detrapping caused by the onset of molecular motion of the crystallites.

Values for the relaxation times (τ_{eq}) at T_{mi} are presented in Table 7.9 and also for the activation energies (E_{ai}), lying between 0.11 and 1.55 eV. The activation energies found by Sawa et al. [Sawa74] (and obtained by two different methods) are higher than ours. In the present work the values found are: 35 °C: 0.11 to 0.48 eV, 45 °C and 50 °C: 0.21 to 0.80 eV. Nonetheless von Seggern [Seggern81] has found values (0.15eV) closer to ours.

[71] Such as C=O and vinyl bonds.

The peak at 65 °C is usually attributed to electron traps. Kobayashi et al. [Kobayashi79] consider a peak at 60 °C occurring in the crystalline region while von Seggern [Seggern81] attributes it to chemical defects (as for the peak at 40 °C). Dorlanne et al. [Dorlanne82] have found a similar peak in AC stressed LDPE with E_a = 1.35 eV, which is higher than the values estimated in Table 7.9 (65 °C and 70 °C: 0.39 to 0.60 eV). Finally the high temperature peak has also been reported in the literature, however the temperature maximum encountered spreads from 85 °C [Sawa73&74, Dorlanne82], 95 °C [Kao79] to near the melting point at 110 °C [Nakamura77, Seggern81], just to quote a few authors. Its activation energy changes from 0.87 to 1.85 eV just for the same authors. Nevertheless the values obtained in our experiments (1.34 to 1.55 eV) agree well with some found in literature [Sawa74, Kao79, Seggern81, Dorlanne82].

In summary, the peaks in the region above room temperature are attributed to space charges trapped most probably in electron traps. The broad peak close to 40 °C to 60 °C is the superposition of two or three individual peaks and it is due to modifications caused in trap states by the changes in the amorphous/crystalline interface (melt/recystallization, onset of molecular motion of crystallites). This may be related to the α_c transition (glass transition for the crystalline region). The origin of the traps themselves can be either structural (such as cavities) or chemical defects. These traps are shallower than the ones seen above 80 °C and distributed deeper in the bulk resulting in higher mobilities. The high temperature peak has a strong dependence on the FIDC step and corresponds to the deeper traps (with longer relaxation times) and closer to the surface. Since it is near the melting temperature it must be due to changes resulting from the onset of melting. The origin of the traps is probably similar in nature to the more shallow ones but no conclusive evidence is yet available.

Table 7.5 – Thermally aged LDPE relaxation times, total charge, charge centroid, mobility and activation energy (by the initial rise method) for the broad peak in FTSDC calculated from the same data as in Figure 7.30 (change with the charging/discharging temperature for a charging field of 2 kV/mm).

Charging/ discharging conditions	**ICC** τ(s)	**IDC** τ(s)	**FIDC** τ(s)	**ICC** Q (10^{-9}C)	**IDC** Q (10^{-9}C)	**FTSDC** Q (10^{-9}C)	**FIDC** Q (10^{-9}C)	**Charge centroid***	**Mobility** ($10^{-16}m^2V^{-1}s^{-1}$)	**FTSDC** E_a(eV) (initial rise)
E=2 kV/mm T_i= *30°C* t_c/t_d=1h/2h t_{fd}=14h30	τ_1=27 τ_2=300 τ_3=3820	τ_1=14 τ_2=81 τ_3=500 τ_4=2960	τ_1=400 τ_2=2430	3.37	–2.77 (82%)	–0.28	–0.11 (94%)	0.06d	17	0.31
E=2 kV/mm T_i=*20°C* t_c/t_d= 1h/2h t_{fd}=14h	τ_1=18 τ_2=150 τ_3=2140	τ_1=10 τ_2=67 τ_3=500 τ_4=3150	τ_1=95 τ_2=2740	2.47	–2.06 (83%)	–0.29	–0.04 (97%)	0.03d	8.3	0.43
E= 2kV/mm T_i=*10°C* t_c/t_d=1h/2h t_{fd}=42h	τ_1=16 τ_2=150 τ_3=2190	τ_1=10 τ_2=67 τ_3=500 τ_4=3150	τ_1=383 τ_2=1000	1.85	–1.53 (83%)	–0.27	–0.07 (≅100%)	0	0	0.34
E=2 kV/mm T_i=*3°C* t_c/t_d=1h/2h t_{fd}=22h	τ_1=18 τ_2=138 τ_3=2075	τ_1=10 τ_2=58 τ_3=500 τ_4=4000	Very noisy, Difficult to fit	1.51	–1.26 (79%)	–0.16	–0.01 (95%)	0.05d	14	0.22

**d* is the sample thickness (around 200 μm)

Table 7.6 – Thermally aged LDPE relaxation times, total charge, charge centroid, mobility and activation energy (by the initial rise method) for the broad peak in FTSDC calculated from the same data as in Figure 7.31 (change with the charging field for a charging/discharging temperature of 30 °C).

Charging/ Discharging conditions	**ICC** τ(s)	**IDC** τ(s)	**FIDC** τ(s)	**ICC** Q (10^{-9}C)	**IDC** Q (10^{-9}C)	**FTSDC** Q((10^{-9}C)	**FIDC** Q (10^{-9}C)	**Charge centroid***	**Mobility** ($10^{-16}m^2V^{-1}s^{-1}$)	**FTSDC** E_a(eV) (initial rise)
E=1 kV/mm T_i=30°C t_c/t_d=1h,/2h t_{fd}=18h	τ_1=16 τ_2=200 τ_3=2650	τ_1=10 τ_2=65 τ_3=500 τ_4=3215	τ_1=720 τ_2=4000	1.67	–1.32 (79%)	–0.12	–0.05 (89%)	0.11*d*	61	0.37
E=2 kV/mm T_i= 30°C t_c/t_d=1h/2h t_{fd}=14h30	τ_1=27 τ_2=300 τ_3=3820	τ_1=14s; τ_2=81s; τ_3=500s; τ_4=2960s	τ_1=400 τ_2=2430	3.37	–2.77 (82%)	–0.28	–0.11 (94%)	0.06*d*	17	0.31
E=3 kV/mm T_i=30°C t_c/t_d=1h/2h t_{fd}=24h	τ_1=60 τ_2=400 τ_3=2850	τ_1=10 τ_2=79 τ_3=500 τ_4=2960	τ_1=93 τ_2=6730	4.87	–3.92 (80%)	–0.48	–0.46 (99.8%)	0.02*d*	0.6	0.43
E=4kV/mm T_i=30°C t_c/t_d=1h/2h t_{fd}=28h	τ_1=18 τ_2=200 τ_3=2570	τ_1=12 τ_2=74 τ_3=500 τ_4=3230	τ_1=850 τ_2=6150	6.90	–5.64 (82%)	–0.64	–0.59 (>99.5%)	0.05*d*	0.7	0.32
E=5 kV/mm T_i=30°C t_c/t_d=1h/2h t_{fd}=62h	τ_1=19 τ_2=200 τ_3=2790	τ_1=500 τ_2=3300 (from 360s)	τ_1=705 τ_2=3950	8.43	–7.32 (87%)	–0.76	–0.30 (99.4%)	0.06*d*	0.7	0.39

**d* is the sample thickness (around 200 μm)

Table 7.7 – Thermally aged LDPE relaxation times, total charge, charge centroid, mobility and activation energy (by the initial rise method) for the broad peak in FTSDC calculated from the same data as in Figure 7.33 (change with t_c/t_d for a charging field of 2kV/mm at a charging/dicharging temperature of 30 °C).

Charging/ Discharging conditions	**ICC τ(s)**	**IDC τ(s)**	**FIDC τ(s)**	**ICC *Q* (10^{-9}C)**	**IDC *Q* (10^{-9}C)**	**FTSDC *Q* (10^{-9}C)**	**FIDC *Q* (10^{-9}C)**	**Charge centroid***	**Mobility ($10^{-16}m^2V^{-1}s^{-1}$)**	**FTSDC E_a(eV) (initial rise)**
E=2 kV/mm T_i =30°C ***t_c/t_d=1h/2h*** t_{fd}=19h	τ_1= 20 τ_2= 180 τ_3=2200	τ_1=14 τ_2=90 τ_3=500 τ_4=5000	τ_1=620 τ_2=3050	4.3	–3.4 (79%)	–0.38	–0.26 (94%)	0.06d	17	0.34
E=2kV/mm T_i=30°C ***t_c/t_d=3h/3h*** t_{fd}=40h	**σ_o=2.4×10^{-16}Sm^{-1}** τ_1=22 τ_2=140 τ_3=1350	τ_1=18 τ_2=86 τ_3=500 τ_4=4840	τ_1=620 τ_2=3530	5.8	–4.0 (69%)	–0.51	–0.48 (86%)	0.14d	13	0.43
E=2kV/mm T_i=30°C ***t_c/t_d=1h/21h*** t_{fd}=8h	τ_1=25 τ_2= 230 τ_3=3560	τ_1=14 τ_2=70 τ_3=460 τ_4=3600	τ_2=1430 (from 3600)	3.4	–3.3 (97%)	–0.02	–0.03 (99%)	0.01d	2.8	—
E=2kV/mm T_i=30°C ***t_c/t_d=1h/2h*** t_{fd}=15h	τ_1=27 τ_2=300 τ_3=3800	τ_1=14 τ_2=80 τ_3=500 τ_4=2950	τ_1=400 τ_2=2430	3.37	–2.77 (82%)	–0.28	–0.11 (94%)	0.06d	17	0.31

*d is the sample thickness (around 200 μm)

Table 7.8 – Thermally aged LDPE relaxation times, total charge, charge centroid, mobility and activation energy (by the initial rise method) for the broad peak in FTSDC calculated from the same data as Figure 7.34 (change with the charging field for a charging/discharging temperature of 2 °C).

Charging/ Discharging conditions	**ICC** τ(s)	**IDC** τ(s)	**FIDC** τ(s)	**ICC** Q (10^{-9}C)	**IDC** Q (10^{-9}C)	**FTSDC** Q (10^{-9}C)	**FIDC** Q (10^{-9}C)	**Charge centroid***	**Mobility** ($10^{-16}m^2V^{-1}s^{-1}$)	**FTSDC** E_a(eV) (initial rise)
E=2 kV/mm T_i= 3°C t_c/t_d=1h/2h t_{fd}=22h	τ_1=18 τ_2=138 τ_3=2075	τ_1=10 τ_2=58 τ_3=500 τ_4=4000	Very noisy, Difficult to fit	1.51	–1.26 (79%)	–0.28	–0.01 (>95%)	0.05*d*	14	0.22
E=4kV/mm T_i=2°C t_c/t_d=1h/2h t_{fd}=19h	τ_1=25 τ_2=200 τ_3=2500	τ_1=16 τ_2=80 τ_3=500 τ_4=3570	τ_1=191 τ_2=3380	2.79	–2.63 (94%)	–0.43	–0.17 (>100%)	0	0	0.21

**d* is the sample thickness (around 200 μm)

Table 7.9 – Peak decomposition of the broad FTSDC peak situated at 50 °C to 60 °C for some selected runs presented previously for the thermally aged polyethylene.

Charging and discharging conditions	T_{max} (°C)	j_{max} (10^{-11} Am^{-2})	E_a(eV) (initial rise)	T_{mi} (°C)	E_{ai} (eV)	σ_{oi} ($10^{-8}Cm^{-2}$)	$\tau_{eq}(T_{mi})$ (10^2s)	Comments
E = 2kV/mm T_i = 30°C ***t_c/t_d = 3h/3h*** t_{fd} = 40h	70	21	0.43	50 65 70 85	0.21 0.60 0.62 1.55	3.3 40 8.5 82	25 10 9.9 4.4	Same data as in Figure 7.33 and Table 7.7
E = 2 kV/mm T_i = 30°C t_c/t_d = 1h/2h t_{fd} = 15h	60	11	0.31	50 65	0.80 0.39	1.7 39	6.8 15	Same data as in Figure 7.33 and Table 7.7.
E = 2 kV/mm T_i = 3°C t_c/t_d = 1h/2h t_{fd} = 22h	40	6.5	0.22	35 45 65	0.48 0.59 0.52	7.6 5.6 10	10 8.9 11	Same data as in Figure 7.34, Figure 7.35 and Table 7.8.
E = 4kV/mm T_i = 2°C t_c/t_d = 1h/2h t_{fd} = 19h	45	17	0.21	35 45 65 85	0.11 0.38 0.42 1.46	29 42 9.7 15	44 14 14 6.7	Same data as in Figure 7.34, Figure 7.35 and Table 7.8.

7.3.2.3 Electrically aged LDPE

The electrically aged polymer was studied using the previous knowledge acquired during the study of the thermally aged LDPE. Accordingly the charging/discharging temperature, T_i, more often used was 2 °C because it is the one that allows a clearer differentiation of the three individual peaks present in the complex FTSDC broad peak (maximum at 40 ° to 50 °C). Moreover, suitable discharge of the sample during FIDC allowed us to eliminate the higher temperature peak (85 °C) and to be able to obtain the other peak without overlapping. Furthermore if a higher T_i is chosen the first peak (around 35 °C) will not be completely seen in the FTSDC spectrum because the initial rise of the broad peak will not appear.

Current data for different charging fields can be seen in Figure 7.39. But before investigating the field dependence it is interesting to see in more detail the differences between runs 3 and 30 (marked, respectively, (i) and (ii)) that share the same charging/discharging conditions (except for FIDC duration) but were done at different stages of the complete experiment. As

the numbers indicate run 3 was one of the first performed and run 30 one of the last ones (as can be seen in Table 6.3)[72]. Starting to analyse the ICC and IDC steps (Figure 7.39 – a) and b)) it is observed that run 3 (i) always has an higher current value than run 30 (ii), a difference that is more clearly seen in Figure 7.41-a). The relaxation times obtained for these two runs (Table 7.10) are similar for ICC[73] while the longest relaxation time in IDC (τ_4) is four times higher for run 3 than for run 30. The thermogram represented in Figure 7.39-c) and more specifically in Figure 7.41-b) show further the differences between the initial and final conditions of the AC aged sample, respectively, at the beginning and ending of the experiment. The final discharge current also reveals a noticeable variation between the two runs, the time needed for the current in (ii) to fall below the resolution limit is of the order of 10^3 s while for (i) is about four times longer. This is reflected in the calculation of relaxation times, for the former it was only possible to obtain a single relaxation time while for the later two times were estimated from the fitting and, besides, τ_2 is relatively large when compared with the value for other runs done under similar conditions. It should be remarked that it is not a reproducibility problem since Figure 7.43 that presents two different runs done under the same conditions (run 6 and 10) show a very good reproducibility. The observed differences can be better understood if the peak in the FTSDC spectra is decomposed in three individual peaks (as it will be seen below).

Before doing so, the influence of charging field has to be studied since the value of the field will cause different activation of deeper or shallower traps. While ICC and IDC results show an almost linear behaviour with the field (Figure 7.39-a) and b)). In the FTSDC plots (Figures 7.39 and 7.40) the non-linear behaviour is clearly seen. Therefore the behaviour of the AC aged sample with the DC field is similar to the thermally aged polymer. The non-linearity indicates a space charge trapping and detrapping mechanism (the same arguments presented in 7.3.1 are also valid in this case). A more detailed analysis of Figure 7.40 shows that run 3 has a different response. If the other data in the figure (excluding run 3) only is considered the peak position and shape do not seem to change much with the applied field. Also there is a decrease of current with decreasing field (see also Figure 7.39-c)). The FTSDC plot corresponding to run 3 was the first one performed after charging. The previous runs

[72] The elapsed time between the two runs was more than a month.

[73] Calculated considering a small value of DC conductivity (σ_o) plus the 3 different relaxations times (and run 3 has a higher σ_o than run 30). This σ_o cannot be considered a DC conductivity since no onset of the steady state regime is noticed in the ICC graph.

consisted only of the FTSDC step with no field applied to the sample. The presence of a shoulder at around 60 °C is observed also in the thermogram of run 3, which is only seen so clearly in the following runs when the applied field is 4 kV/mm. The relevance of the differences between run 3 and the other presented will be discussed below.

The estimation of relaxation times, total charge, charge centroid position, mobility and activation energies were done following the same procedure as presented above for the thermally aged sample and the results can be seen in Table 7.10. In the ICC three different relaxation times were calculated. Their values are around 10^3s for the longest relaxation time (τ_3) in the ICC. For run 3 (i) it was necessary to consider an extra fitting parameter corresponding to a DC conductivity (σ_o). For the discharge current (IDC) four different relaxation times were estimated and there is a relatively wide variation for τ_4 (10^3 to 6×10^3 s), which was not observed in the ICC (τ_3). The difference between runs 3 (i) and 30 (ii) is already stated above. It appears to be a tendency of the relaxation times to increase with increasing field although this is not completely clear. For the FIDC it was not possible to calculate the second relaxation time in run 30 because the current dropped very quickly below the equipment resolution. This means that most of the charge remaining after FTSDC is in traps with relaxation times shorter than those for the other runs presented in Table 7.10 (and also seen in the graph of Figure 7.40-d)). This is especially interesting if a comparison is made with run 3. For this run a relatively long relaxation time (τ_2) was found when compared with the run performed at a charging field of 3 kV/mm (see 1st and 2nd data rows in Table 7.10). The run with charging field of 3 kV/mm has $\tau_2 = 3\times10^3$ s, while for a charging field of 4 kV/mm τ_2 has increased three times (higher than for run 3).

The total charge measured in all four steps of a run (ICC, IDC, FTSDC and FIDC) decreases with decreasing field. This variation is better seen in the ICC and IDC steps.

The variation of the centroid position and mobility with the charging field is better observed if instead of run 3 (i) we consider run 30 (ii) and leads to a similar variation with the field as for the thermally aged polyethylene. Run 3 has a much lower mobility than run 30 pointing to more space charge remaining in deeper traps.

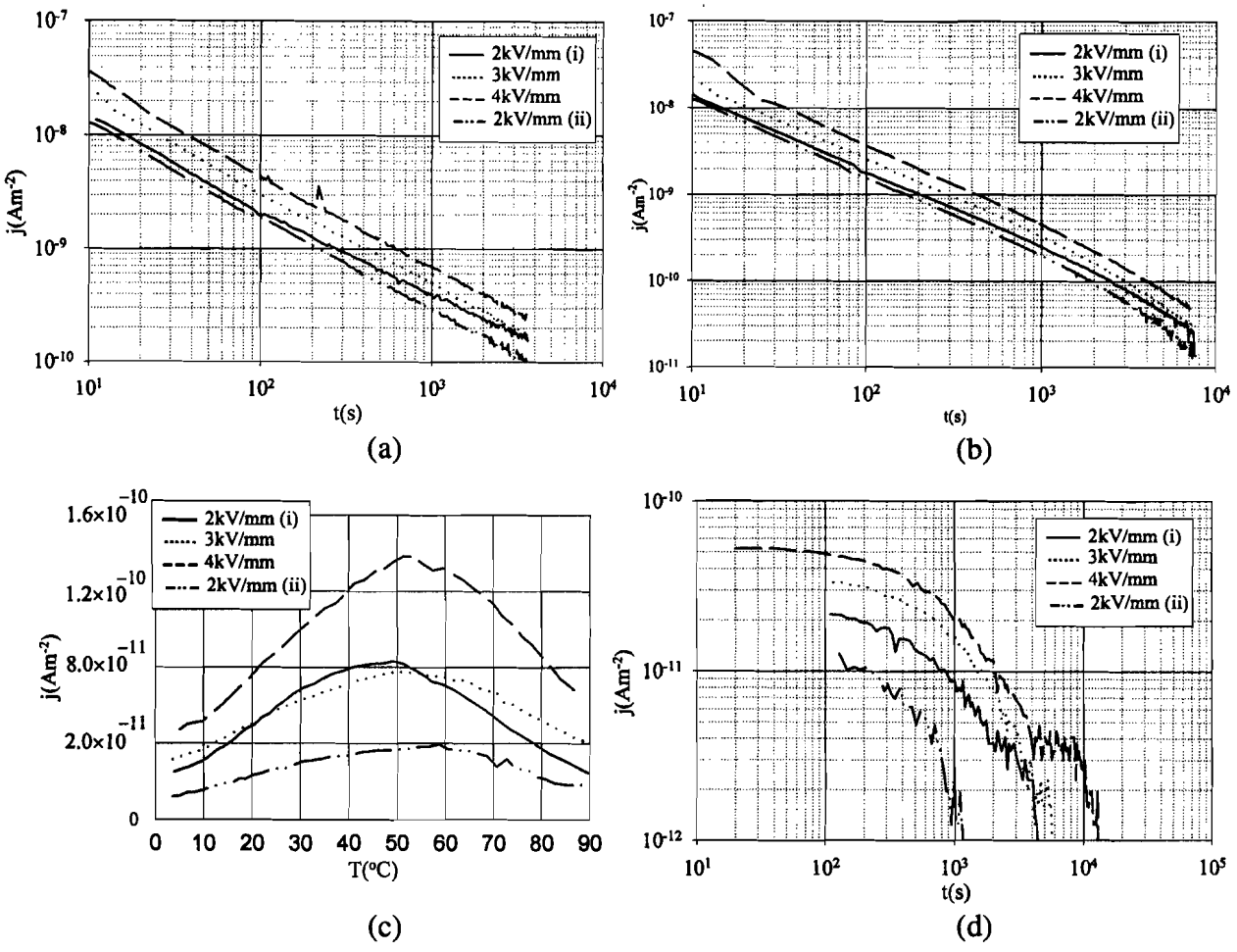

Figure 7.39 – LDPE electrically aged sample results for different charging fields (charging/discharging conditions: $T_i = 2°C$, $t_c/t_d = 1h/2h$ and $E = 2, 3$ & 4 kV/mm). (i) and (ii) are runs made under the same conditions but run 3 (i) – was one of the first runs made while run 30 (ii) – was one of the last ones. (a) ICC; (b) IDC; (c) FTSDC and (d) FIDC.

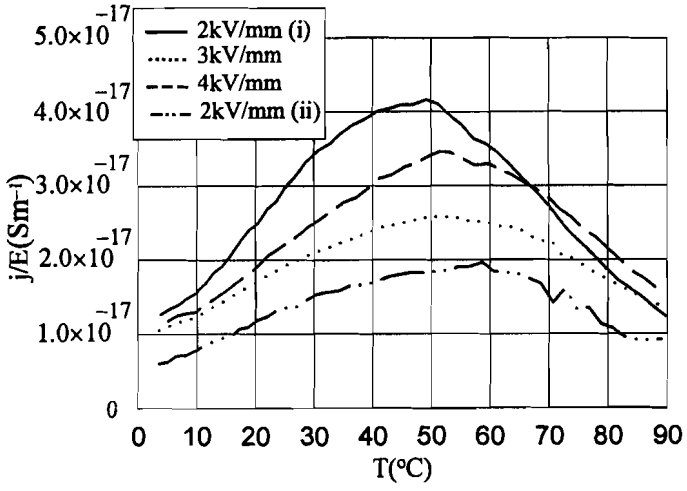

Figure 7.40 – FTSDC plot showing *j/E* (same conditions as in Figure 7.39).

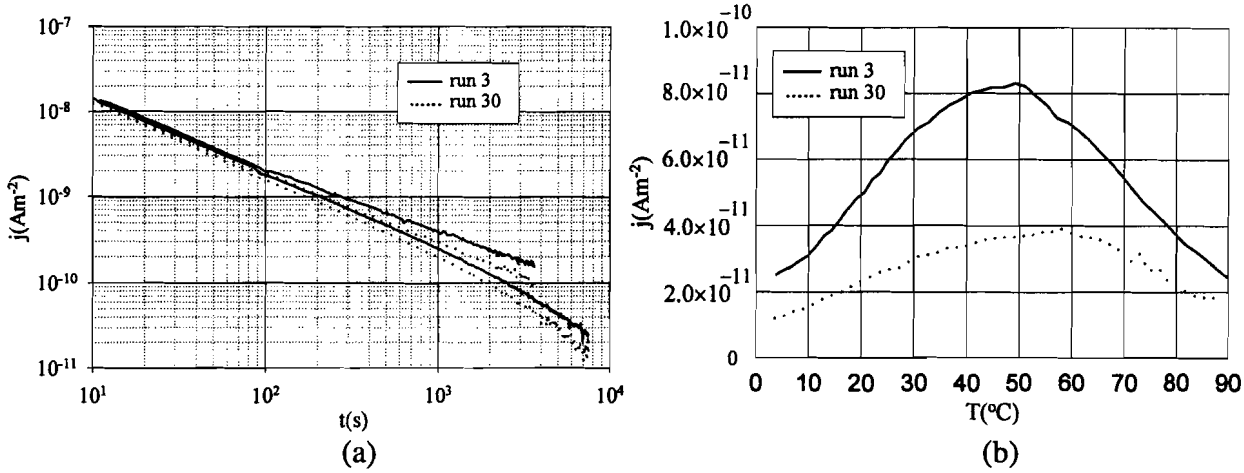

Figure 7.41 – FTSDC for two different runs in the same electrically aged LDPE sample with the same conditions (T_i = 2°C, E = 2 kV/mm, t_c/t_d = 1h/2h – corresponding to run 3 (i) and run 30 (ii) in Figure 7.39). (a) ICC & IDC and (b) FTSDC.

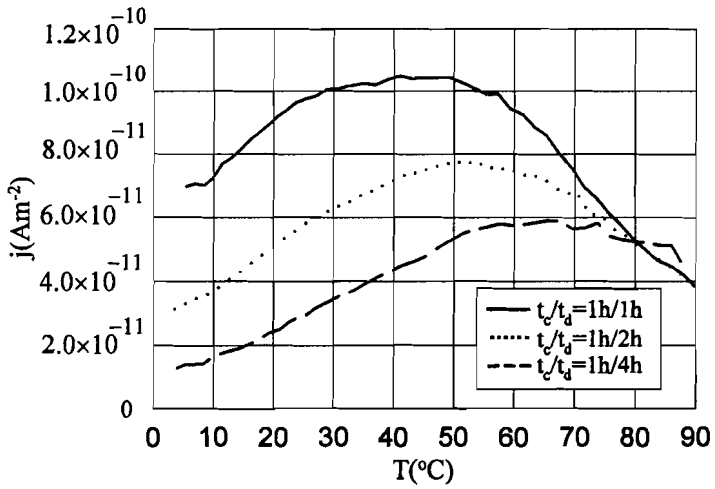

Figure 7.42 – FTSDC spectra of a LDPE electrically aged sample results for different charge/discharge times' ratios (conditions: T_i = 2 °C, E = 3 kV/mm, t_c/t_d = 1h/1h, 1h/2h & 1h/4h).

Activation energies calculated by the initial rise method, as above for the thermally aged polymer, do not show any meaningful change as the field is varied.

In Figure 7.42 the influence of the charge/discharge time ratios can be very clearly seen, with the peak temperature shifting towards higher temperatures with increasing IDC time. In the temperature range of the FTSDC step, a consistent analysis of the data requires well-defined peaks (even if a broad peak cannot be avoided by this procedure). This means that the full

peak (rising, maximum and fall) should be covered in the interval of temperatures of FTSDC step (T_i to 90 °C).

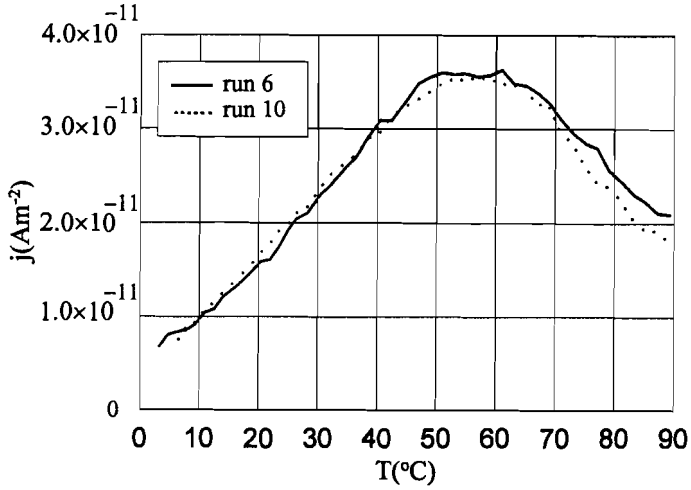

Figure 7.43 – FTSDC for two different runs in the same electrically aged LDPE sample with the same charging/discharging conditions (T_i = 2 °C, E = 2 kV/mm, t_c/t_d = 1h/4h).

As was done for the thermally aged LDPE, for some selected runs the FTSDC spectra were decomposed into individual peaks and the results are presented in Table 7.11. The values chosen for the peak temperatures (35 °C, 45 °C and 65 °C) are the same as that used in the decomposition of the FTSDC of the thermally aged polyethylene (for the reasons stated above).

The first three columns of Table 7.11 show results for the broad peak. The peak's maximum temperature is around 50 °C and run 3 (i) is the only one with a slightly lower value. This difference will be reflected in the decomposition results that have proved to be very important to understand the changes with AC ageing and also during the course of the successive experimental runs. Basically the relevance of the three individual peaks varies during this experiment. The form in which the results are presented in Table 7.11 corresponds, to run 3 (i), run 16, run 5 and run 30 (ii) respectively as can be seen in Table 6.3. The peak at 45 °C is the one that suffers more changes. Its highest magnitude is for run 3 (i), decreases for run 5 (which has a higher charging field) and it almost disappears for runs 16 and 30. Analysis of the FTSDC results from other runs (not included in this Table) also reveals this behaviour. It seems that the charge giving rise to the 45 °C peak (by detrapping) has not been replaced by the DC process. So it is reasonable to assume that it was trapped during the previous history of the sample, meaning that it is mostly a consequence of the AC ageing process. One possibility is the presence of chemical traps created during the AC electrical ageing, that can be ions that also have diffused in during the same process. These ions can also constitute

trapping centres for carriers and, at the same time, recombination centres. Initially the ions would trap the carriers and there would be a peak in the FTSDC spectrum. But if these ions can diffuse and/or recombine with carriers injected by the DC process this would result in both a decrease of the current and the disappearance of the corresponding peak in the course of the combined experiment.

Comparing the results obtained for the AC electrically aged and thermally aged samples is not easy. The main difference observed is in the current values, which are usually higher for the thermally aged polymer. This can be understood if recombination is more important and/or if the number of traps is higher and the traps have longer relaxation times in the electrically aged polyethylene. It is possible also that the AC aged material is a more open structure with more and/or enlarged cavities (as the presence of water trees suggests) allowing an easier path to carriers and thus facilitating diffusion and recombination. This diffusion would not be seen in the results for the mobility because the traps would remain more or less at the same depth in the material. Furthermore in the thermally aged LDPE it appears that the individual peak at 45 °C does not vanish so easily as in the AC aged samples. Furthermore if the relative amplitudes of the peak currents at 35 °C and 65 °C are compared, it is seen that the higher temperature peak is more important in the AC aged than in the thermally aged LDPE. As a consequence the complex peak temperature would be shifted towards higher temperatures (see Tables 7.9 and 7.11). This also points to more charges deposited in traps with longer relaxation times.

Table 7.10 – Electrically aged LDPE relaxation times, total charge, charge centroid, mobility and activation energy (by the initial rise method) for the broad peak in FTSDC calculated from the same data as Figure 7.39 (change with the charging field for a charging/discharging temperature of 2 °C).

Charging/ Discharging conditions	**ICC** τ(s)	**IDC** τ(s)	**FIDC** τ(s)	**ICC** Q (10^{-9}C)	**IDC** Q (10^{-9}C)	**FTSDC** Q (10^{-9}C)	**FIDC** Q (10^{-9}C)	**Charge centroid***	**Mobility** ($10^{-16}m^2V^{-1}s^{-1}$)	**FTSDC** E_a(eV) **(initial rise)**
E* = 2 kV/mm** T_i = 2°C T_c/t_d = 1h,/2h t_{fd} = 61h ***(i)	τ_1 = 11 τ_2 = 66 τ_3 = 800	τ_1 = 12 τ_2 = 80 τ_3 = 710 τ_4 = 1000	τ_1 = 690 τ_2 = 5430	1.44	–1.14 (79%)	–0.26	–0.03 (99%)	0.01*d*	2.8	0.29
***E* = 3 kV/mm** T_i = 2°C t_c/t_d = 1h/2h t_{fd} = 21h	τ_1 = 12 τ_2 = 115 τ_3 = 850	τ_1 = 12 τ_2 = 68 τ_3 = 550 τ_4 = 3700	τ_1 = 750 τ_2 = 3000	1.90	–1.47 (77%)	–0.28	–0.04 (94%)	0.06*d*	11	0.19
***E* = 4kV/mm** T_i = 2°C t_c/t_d = 1h/2h t_{fd} = 14h	τ_1 = 10 τ_2 = 100 τ_3 = 1200	τ_1 = 12 τ_2 = 115 τ_3 = 915 τ_4 = 6000	τ_1 = 880 τ_2 = 9150	2.70	–2.29 (84%)	–0.45	–0.08 (>100%)	0	0	0.23
E* = 2 kV/mm** T_i = 2°C t_c/t_d = 1h/2h t_{fd} = 22h ***(ii)	τ_1 = 11 τ_2 = 82 τ_3 = 1000	τ_1 = 10 τ_2 = 61 τ_3 = 500 τ_4 = 4200	τ_1 = 490	1.13	–0.93 (82%)	–0.12	–0.005 (94%)	0.07*d*	19	0.39

**d* is the sample thickness (around 200 μm)

Table 7.11 – Peak decomposition of the broad FTSDC peak situated at 45 °C to 50 °C for some selected runs presented previously for the electrically aged polyethylene.

Charging and discharging conditions	T_{max} (°C)	J_{max} (10^{-11} Am^{-2})	E_a(eV) (initial rise)	T_{mi} (°C)	E_{ai} (eV)	σ_{oi} ($10^{-8}Cm^{-2}$)	$\tau_{eq}(T_{mi})$ (10^2s)	Comments
E = 2 kV/mm				35	0.45	5.0	11	Same data
T_i = 2°C	45	8.0	0.29	45	0.39	14	14	as in Figure
t_c/t_d = 1h/2h				65	0.33	15	18	7.37 and
t_{fd} = 61h ***(i)***								Table 7.10.
E = 3 kV/mm				35	0.29	14	17	Same data
T_i = 2°C	50	7.5	0.19	45	0.10	0.1	-	as in Figure
t_c/t_d = 1h/2h				65	0.35	24	17	7.37 and
t_{fd} = 21h								Table 7.10.
E = 4 kV/mm				35	0.29	10	17	Same data
T_i = 2°C	50	14	0.23	50	0.47	10	12	as in Figure
t_c/t_d =1h/2h				65	0.30	4.2	18	7.37 and
t_{fd} =14h								Table 7.10.
E = 2 kV/mm				35	0.32	6.0	15	Same data
T_i = 2°C	50	3.8	0.22	45	0.39	1.6	14	as in Figure
t_c/t_d = 1h/2h				65	0.46	9.0	13	7.37 and
t_{fd} = - ***(ii)***								Table 7.10.

7.4 Pulsed electroacoustic space charge profile measurements (PEA)

In Figure 7.44 are seen the results of PEA measurements made on unaged LDPE. Immediately after the DC voltage application a negative charge can be observed in the bulk of the sample (Figure 7.44-a)). After two hours, homocharge has accumulate near the cathode and spreads until the middle of the sample. At the anode only a very small amount of homocharge is observed and it remains close to the surface. In studies of space charge in LDPE by the PEA method both hetero- and homocharge formation have been reported [Aida97, Suh96]. The sign of the charge is related to sample preparation conditions and to the presence (and concentration) of low molecular species [Lee97] and short chains [Suh96]. Also the effect of moisture content was studied by Aida et al. [Aida97] with the sample becoming more conductive at higher moisture content. Homocharge is expected when there is injection of carriers from the electrodes (enhanced by an increase in moisture). A low concentration of short PE chains (mainly carbonyl groups) also leads to homocharge. According to Suh et al. [Suh96] when a press moulding process is used, the carbonyl groups can originate not in oxidation within the sample but be deposited from the backing film (PET films were used in this work (6.1) and see also 7.1.5 for effects of surface charge deposition during sample preparation). The same authors did not detect any oxidation in samples pressed at a

temperature up to 180 °C (the samples were pressed at a temperature ≤140 °C, as was stated in 6.1).

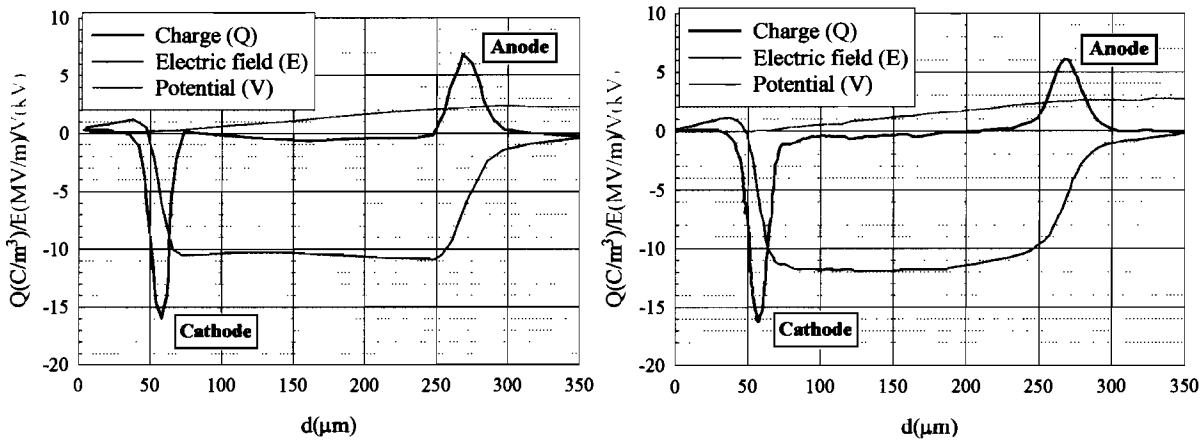

Figure 7.44 – Space charge profile of an unaged LDPE sample (measurement conditions: +2.5 kV_{DC}, pulse +400V, 5 ns, immediately after DC voltage application (a) and 2h later (b)).

For thermally aged LDPE, immediately after the application of the DC field, a negative charge is also observed in the bulk and mostly near the anode but disappearing near the cathode (see Figure 7.45-a). After 2h the situation was similar and consequently the charge distribution is very stable (Figure 7.45-b)). If the amount of space charges is compared with that in the unaged sample it is observed that the amount of charge in the bulk is higher for the aged sample meaning that more charge is present in this case (see also the electric field profile). As stated above (7.2), diffusion of impurities during thermal ageing is due mainly to the immersion in solution (enhanced by the temperature). In the dielectric spectroscopy results it an increase in the height of the low frequency peak without significant shift of the maximum frequency (see 7.2) is seen suggesting just an increase in the number of trapped carriers but no creation of new traps. Moreover oxidation is not likely to be important since in the FTIR results no oxidation was found for thermally aged polyethylene (see 7.7.1). In the thermally aged sample most of the charge is trapped to an extent that does not displace over 2h.

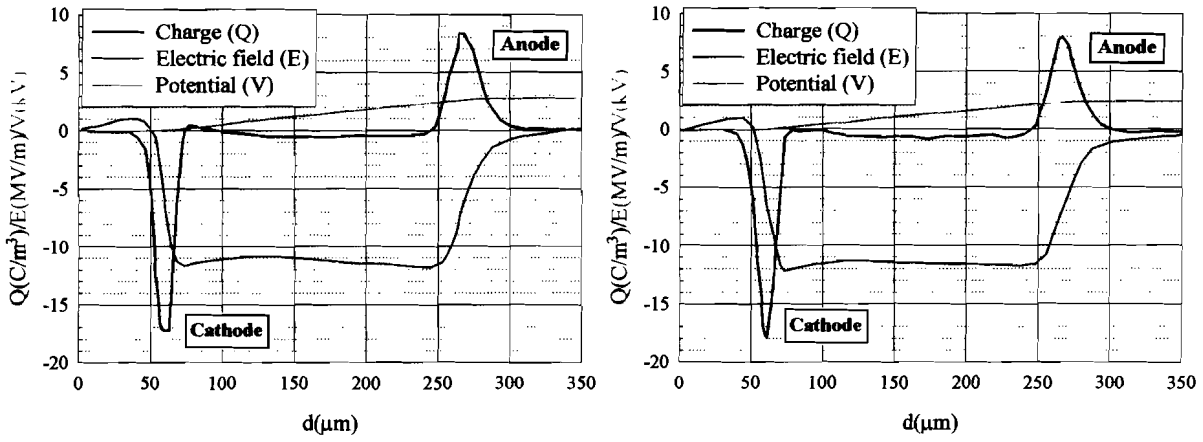

Figure 7.45 – Space charge profile of thermally aged LDPE sample (thermal ageing conditions: 50 °C in 1 M NaCl for 1500 h; measurement conditions: +2.5 kV_{DC}, pulse +400V, 5 ns, immediately after DC voltage application (a) and 2h later (b)).

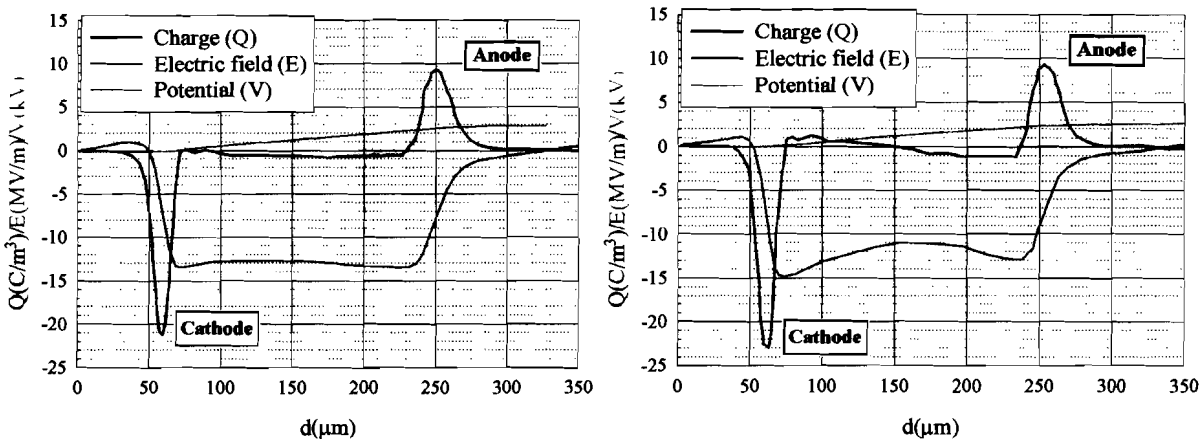

Figure 7.46 – Space charge profile of a dried (in air at RT) water treed LDPE sample (electrical ageing conditions: 6 kV/mm, 50 Hz at 50 °C in 1 M NaCl for 1500 h; measurement conditions: +2.5 kV_{DC}, pulse +400V, 5 ns, immediately after DC voltage application (a) and 2h later (b)).

The results for electrically aged LDPE (with water trees) were obtained under two different sets of conditions. In the first case the sample is dried and the water trees are not visible (the sample dries after AC ageing by being kept in air at RT). In the second case the same sample is wetted by immersion in distilled water during 24h at RT and the water trees are rewet, becoming visible to the naked eye.

For the dry sample the PEA measurement done immediately after switching on the DC voltage, seen in Figure 7.46-a), is very similar to the result obtained before for the thermally aged sample, however the amount of space charge is higher (the mirror charges at the electrodes are larger). As can be seen in Figure 7.46-b), after two hours the observed space charge profile has changed. Now heterocharge is seen near both electrodes, with more charge near the anode (negative). The appearance of heterocharge can be due to charge separation by diffusion. The model of Ross et al. [Ross92&98] discussed in 5.1.5 suggested that the walls of the microcavities that form water trees are polar (as a result of chain scission and oxidation products), attracting charges that remain trapped (ions and electrons). It is possible that the field helps to release the trapped charges that can then diffuse to the electrode of opposite sign. To confirm this hypothesis it would be interesting to see the progress of the charge profile after short-circuiting the sample [Ohki98][74]. As was stated in 7.3.2.3, water treed PE has a more open structure than the non-treed polymer (both unaged and thermally aged), which would greatly enhance the diffusion. Katsuta et al. [Katsuta99] found a value for the DC conductivity of wet water trees of the order of 10^{-9} Sm^{-1} (for untreed LDPE the value is of the order of 10^{-16} Sm^{-1} [Pélissou88]). Ohki et al. [Ohki98] measured a conductivity one order of magnitude higher (10^{-8} Sm^{-1}), which is around 500 times that measured for dry water trees. The increase in conductivity is demonstrated when the results in Figures 7.46 and 7.47 are compared (the wet polymer has, roughly a water content of 1000 ppm). The wet sample immediately after the application of the DC voltage, homocharge is already observed (Figure 7.47-a)) that has travelled through the wet water trees. The conductivity in wet water trees is expected to be a few times higher than in the untreed material [Toyoda01, Ohki98, Katsuta99]. After 1h of DC field application a small positive space charge peak is seen (Figure 7.47-b)) and likewise after 2h (Figure 7.47-c). The charge is of the same sign as the electrode where the water trees start [Li96&97]. This peak is produced by interfacial polarisation caused by the difference in conductivity between treed and untreed regions [Li97][75]. By comparing between space charge profiles obtained by PEA using a small diameter electrode (1mm) in water treed PE aged in NaCl, Ohki et al. [Ohki98] concluded that the wide peak observed is the result of a distribution of water tree lengths. Consequently the

[74] When these experiments were done, it was not possible to calculate the charge profile if no voltage was applied.

[75] Based on this hypothesis a Maxwell-Wagner-Sillars model was used to estimate the permittivity of water treed PE [Nakamura02].

results seen in Figure 7.47 reveal an asymmetry in the two surfaces of the LDPE films with one side more prone to the inception of water trees (anode). This agrees with the results of optical microscopy (7.1.1) and AFM (7.1.3) discussed above for the unaged polymer, which show differences between the two disc surfaces.

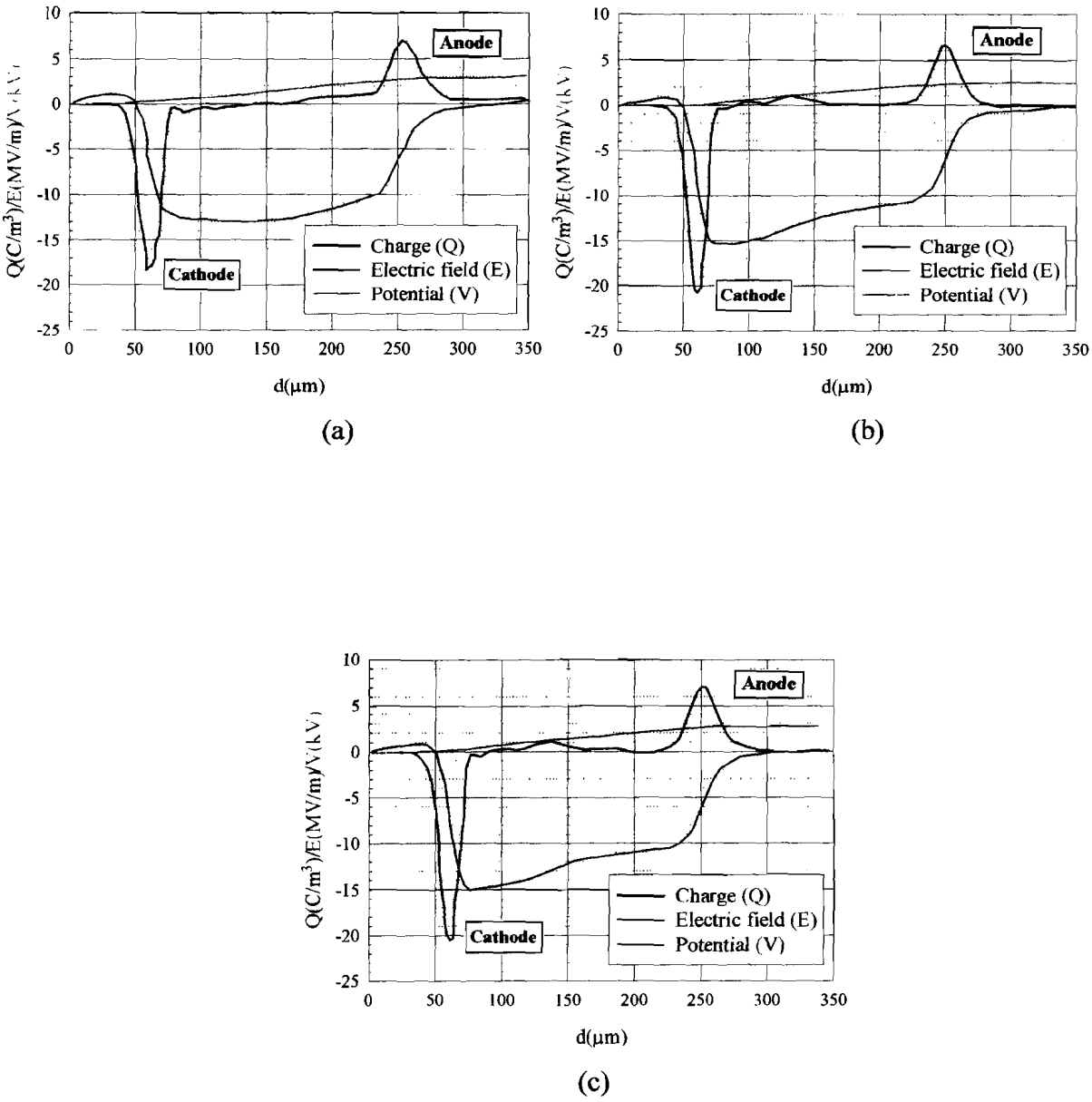

Figure 7.47 – Space charge profile of a water treed LDPE sample after immersion in distilled water for approximately 24h (electrical ageing conditions: 6 kV/mm, 50 Hz at 50 °C in 1 M NaCl for 1500 h; measurement conditions: +2.5 kV_{DC}, pulse +400V, 5 ns, immediately after DC voltage application (a), 1h after (b) and 2h after (c)).

7.5 Methylene blue dyed samples and counting of water trees

As was stated in 6.6 methylene blue dyeing was the technique chosen to render the trees permanently visible. This was mostly done to samples intended to be used for the estimation of the fractal dimension and also for counting the number and size diameter of the trees. In Figure 7.48 dyed water trees can be seen arranged in a "ring", this structure appears when there are air bubbles on the ageing surface. The photograph shows the surface of the disc shaped samples as tree growth is observed in the direction perpendicular to the applied field. Figure 7.49 shows a cut from a microtomed sample and the photograph shows a plane perpendicular to the planar surface of the film revealing the growth of the tree parallel to the electric field direction. The non-uniformity of the sample is apparent in (a) by the way the tree has taken the dye.

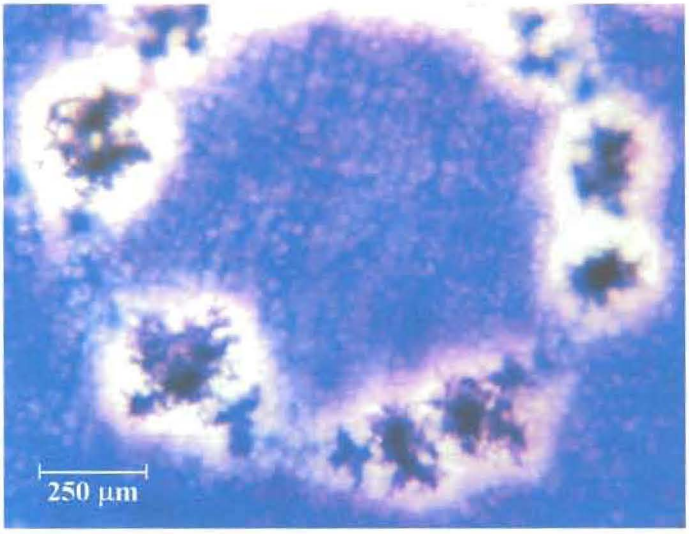

Figure 7.48 – Water trees in a methylene blue dyed LDPE sample (parallel to the film surface[76]). Ring formation results from the presence of air bubbles on the sample surface during ageing (water trees grow at this new interface where the local field is higher).

Counting is a very time consuming process and was done just to see how efficient the sandblasting of the samples was in order to increase the density and size of water trees. Counting was performed for too limited a number of samples to have a valid statistical analysis, and only some preliminary results were obtained.

[76] And perpendicular to the applied field, as discussed before in 6.7.

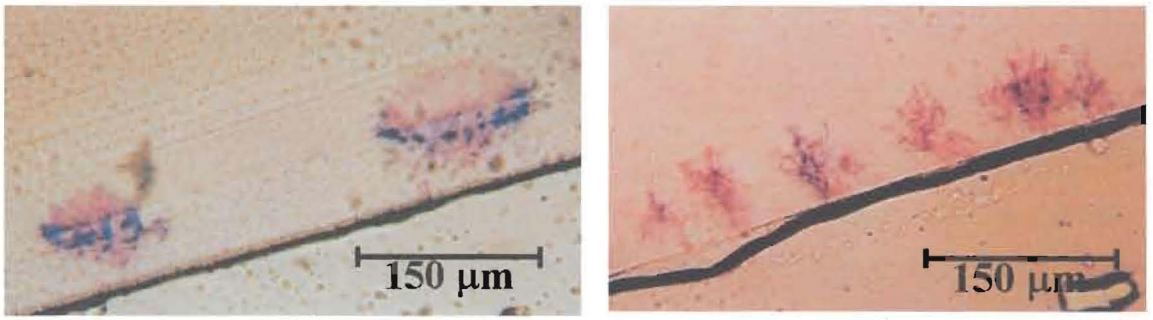

(a) (b)

Figure 7.49 -Details of water trees (perpendicular to the film surface[77]) in a microtomed aged LDPE sample of thickness 1 mm (the water trees are methylene blue dyed and the dark lines are the sample surface).

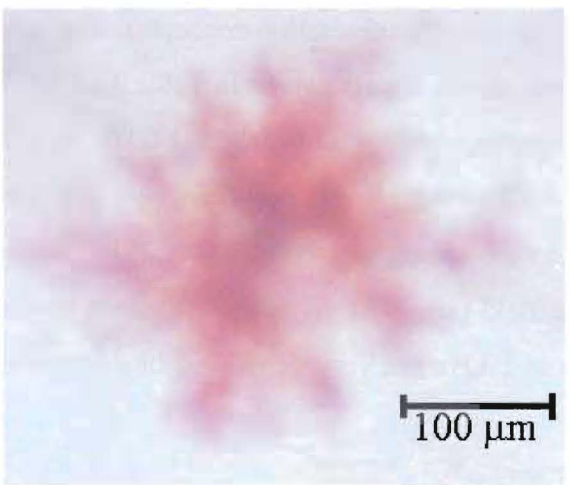

Figure 7.50 – Water tree grown in disc shaped LDPE aged at 1 kHz (Lisbon set). Photograph shows a water tree growing perpendicular to the electric field direction, ⊥.

A value of the order of 10 to 15 water trees per mm^2 was found for sandblasted samples (electrically aged at 6 kV/mm, 50 Hz at 40 °C in 1 M NaCl solution for around 600h until breakdown). If the samples were not sandblasted the density would be 5 to 10 times lower. It is interesting to note that no important difference exists in the diameter of the largest water tree (≅ 600 and ≅ 450 µm for sandblasted and not-sandblasted samples, respectively). This seems to imply that sandblasting provides initiation sites and consequently increases significantly the number of water trees but does not change much the growth rate. Of course more data is needed to have a conclusive result.

[77] And parallel to the applied field, as seen before in 6.7.

7.6 Fractal analysis of water trees

7.6.1 Results

a) Methylene blue dyed water trees

For the two sets of samples used:

The first set corresponds to LDPE samples aged at the University of Leicester by Houlgreave et al. [Houlgreave92]. Samples were aged under an electric field varying from 5 to 8 kV/mm and for two different frequencies 50 Hz and 1.16 kHz (see also [Fothergill93]). The aqueous solution was 0.05M NaCl and the ageing temperature (31±4) °C. As can be seen in Figure 6.10 and 6.12, respectively, some of the photographs show growth along the direction perpendicular to the applied field, ⊥, and others parallel to the field, // (microtomed samples). For results see Table 7.12. The algorithm used by *fd3* also calculates higher order fractal dimensions (see Appendix B for multifractality concepts): the so-called information and correlation dimensions. These results are also given in Table 7.12[78].

The second set of LDPE samples were aged in Lisbon (FCT/UNL). The ageing electric field amplitude varied between 3.5 and 6.5 kV/mm and the frequency was 1.0 kHz. The aqueous solution was 0.1M NaCl and the ageing temperature (50±2) °C. All images were obtained in the direction parallel to the field (see Figure 7.50). Results are presented in Table 7.13. The images of the trees grown at 1 kHz are very dense and bush like (as can be seen in Figure 7.50).

b) SEM images

A study was made to compare different regions of the image. Parts of the background (showing no trees) and of trees (well into a highly damaged area or at the edges of the tree) were studied. No image treatment was applied. The results of the 3-D analysis are given in Table 7.14.

[78] Unity was added to the computed results-according to equation (6.6).

Table 7.12 - Results for the estimation of multifractal dimensions (Leicester samples) (solution 0.05M NaCl at (31±4)°C)

Sample	Position	Freq (Hz)	E (kV/mm)	Ageing time (h)	Capacity dimension[79]	Information dimension	Correlation dimension
1	//	50	8	800	2.79±0.03	2.84	2.88
2	//	50	8	800	2.85±0.04	2.87	2.86
3	//	50	8	100	2.81±0.06	2.84	2.84
4	⊥	50	8	800	2.84±0.04	2.87	2.89
5	⊥	50	5	1000	2.86±0.02	2.89	2.89
6	//	1.16k	5	1200	2.86±0.03	2.91	2.91
7	//	1.16k	5	950	2.78±0.02	2.86	2.89
8	//	1.16k	5	950	2.74±0.02	2.86	2.88
9	//	1.16k	5	950	2.86±0.03	2.90	2.90
10	⊥	1.16k	5	950	2.85±0.03	2.90	2.90

Table 7.13 - Results for the fractal (capacity) dimension of water trees grown in LDPE (Lisbon Samples) (Frequency 1.0 kHz; solution 0.1M NaCl at (50±2) °C)[80]

Sample	E(kV/mm)	Ageing time(h)	Fractal dimension
1	5.5 3.3	31h00 21h00	2.85 ± 0.01
2	3.5	33h30	2.88 ± 0.02
3	3.5	33h30	2.84 ± 0.02
4	6.5	49h00	2.88 ± 0.01

[79] The errors shown result from the least square fitting of the box-counting algorithm. They are not the "true" errors.

[80] Sample 1 was aged for two different periods applying different voltages to the electrodes. Samples 2 and 3 are photographs of different trees from the same LDPE disk.

Table 7.14 - SEM Images (3D analysis)

Image	Detail	Dimension	Notes
1	All	2.32	
	Tree	2.54	Well inside a damaged area
	Tree edge	2.5	Belongs to the tree edge
	Tree edge	2.32	Maybe more background than the previous one
	Background	2.32	
2	All	2.5	
	Tree	2.51	
	Tree	2.53	Inside the tree
	Tree edge	2.58	
	Background	2.44	
3	All	2.3	
	Tree	2.2	
	Tree edge	2.32	
	Background	2.26	
4	All	2.40	
	Tree	2.54	
	Tree	2.58	Highly damaged area
	Tree	2.44	Less damaged area than the previous one
	Background	2.39	
5	All	2.4	
	Tree	2.35	
	Tree	2.50	Less background than the previous one
	Tree	2.55	Less background than the other two
	Background	2.29	

7.6.2 Discussion

From the set of results presented above, the fractal dimension of water trees seems to be very close to 3. Inspection of the photographs shows that this result was to be expected since the water trees are quite dense structures (especially when compared with electrical trees [Kudo98]). In [Dissado92] (see pages 92 to 94) it is shown that if the water tree grows by the

addition of elementary volume units, with each addition being added sequentially in a defined time, then the tree length, L, is given by,

$$L^{d_f} \propto t, \tag{7.4}$$

where t is the ageing time. The experimental data for water trees grown in similar stressing geometries to those used here, analysed in [Dissado92], indicate a value of $D_{WT} = 3$, though the gradients of the log $(L)^3$ – log (t) plot could equally well fit a fractal dimension between 2.80 and 2.85 as found here. The fractal dimension, as found by direct measurements, therefore appears to be consistent with that deduced from the water tree growth law. A brief analysis of our data seems to bear out no relevant difference between the estimated values of D_{WT} for samples aged under different experimental conditions (temperature, ageing time field amplitude, and frequency). It is interesting to note that water trees with different physical appearance such as those grown at 50 Hz and 1.16 kHz (Figures 6.10 and 6.11) have similar values of fractal dimension (capacity, information and correlation).

For images perpendicular to the field, no significant difference is observed between the Leicester and Lisbon samples. The images parallel to the field seem to have on average slightly lower fractal dimension than the ones perpendicular to the field. Parallel images were microtomed and correspond to thin slices (less than 20 μm). When the photographs are made from uncut samples (200μm up to a few mm thick) the projection is denser and all the tree is projected (images perpendicular to the field). For the cut samples (parallel to the field), only the part of the tree present in that slice is projected so each photograph could be associated with a section of the tree. The resulting image is not so dense and the estimated fractal dimension would be smaller. Also since Equation (6.6) is expected to be valid for sections, the value calculated from those images can be a better estimation of the water tree's true fractal dimension. While an upper bound had to be chosen for the projected images, the different values observed can reflect this approximation. Probably instead of adding 1, a value slightly smaller would be a better approach to the real fractal dimension. The value found for electrical trees was 0.7 to 0.8 [Kudo98]. However it must be noted that electrical trees are connected tubes while water trees are structures that include cavities as well as very fine connections. So it would be expected that water trees would fill space more efficiently than electrical trees. Also the water treeing time dependence indicates that growth is almost space filling. Therefore the estimated values are consistent with what is expected for water trees. Since we are dealing with an upper bound, any value of the fractal dimension below 3 indicates that the water tree is a fractal structure.

For the SEM images conclusions seem to point to lower values of the fractal dimension for the background and the regions of higher damage in the tree. This seems to result from the greater uniformity in these areas when compared to the tree edges.

In the NMR determination of pore size in water treed LDPE (see 7.7.2 and [Judenstein00]), samples electrically aged under similar laboratory conditions (ageing temperature 40 °C) but for different ageing times showed the same pore size. This points to a minimum size of damage in the form of water filled pores and cavities in water trees, with just their number increasing with ageing time. In the case of water trees we can take the damage to be the amount of pores and cavities produced within the water tree, and since these are filled with aqueous salt solution their mass will be the mass of the water within the tree. We can assume that the water trees are composed of small units (the pores of size 2.5 nm, as obtained in 7.7.2). The fractal tree will be composed of these elementary units and a damage density, ρ_t, defined by [Lança01]

$$M_t = \rho_t L^{d_t} \ell^{3-d_t} \tag{7.5}$$

where M_t is the total mass of the tree (given by the water content) and ℓ is the size of the elementary units. Up to now the water tree length has been used as a measure of the tree tendency to cause dielectric breakdown. However it is not known if breakdown is more or less likely to occur in a tree of shorter length but denser damage than in one that it is longer but less dense. If the damage density is the important parameter, than one must be able to estimate ρ_t. The intercept of log (M) with the log (L) = 0 axis on these plots therefore gives a measure which is proportional to $\rho_t(\ell)^{3-d_t}$. This value cannot be obtained directly but a proportional quantity can be estimated from the intercept with the y-axis in the log (L) vs. log (ε)[81] plot. This graph is the same that was used in the box counting algorithm to estimate the fractal dimension (Appendix B). So a further step would be to find the intercept that would be proportional to the damage density if ℓ and d_t can be assumed as constant. This is particularly the case with the methylene blue stained trees analysed here since they all have approximately the same value of d_t.

It should be noted that neither of the two types of image studied shows the true structure of the tree. In the literature the effect of dyeing has been discussed (see [Ross90]). It is known

[81] ε is the diameter of the set used to cover the fractal object (for a two-dimensional embbeded space the set can be a circle of radius ε, a square of side ε, etc.). For details see Appendix B.

that the staining process does not result in a chemical reaction, but in the enlargement of the microvoids and connecting pathways. SEM techniques always involve etching of the surface to be observed and so microvoids will be enlarged by this technique also. It is likely that this enlargement does not modify the fractal dimension, it may, however, increase the size of the elementary volume, namely, by increasing ℓ.

7.7 Chemical changes in aged polyethtylene

7.7.1 FTIR studies: results and discussion

As stated in 6.8 both LDPE (electrically and thermally) and XLPE (electrically) aged and unaged samples were analysed using FTIR. The total transmitance spectra obtained for both types of polyethylene can be seen in Figure 7.51. The main difference consists in a peak at 1720 cm^{-1} related to acetophenone (a by-product of crosslinking). To check for the presence of oxidation products specific spectra intervals were analysed in more detail, specially the range 1500 cm^{-1} to 1900 cm^{-1}. Using an optical microscope, areas with water trees and breakdown channels were identified in electrically aged samples. In order to compare oxidation products unaged samples and also regions with no special feature in aged samples were analysed. Since concentration changes were expected to be small (and μ-FTIR was not available) the IR beam was carefully aimed at the selected regions in each sample. Different regions were used in the same sample and the results averaged. Thermal ageing was studied to a lesser extent by following a similar procedure.

7.7.1.1 Results

a) LDPE

In water-treed regions a band at 1720 cm^{-1} associated with the carbonyl group (C=O) appears (see Figure 7.52). This group can reveal the presence of carboxylic acids, ketones, aldehydes or esters. Carboxylic acids are immediately ruled out since ageing occurs in a solution of NaCl and the acids are easily transformed into salts (showing a characteristic band at 1590 cm^{-1}). Furthermore the ester carbonyl group appears at 1740 cm^{-1} not at 1720 cm^{-1}. Therefore, based on the modified Kema model (5.1.5 and [Xu94]), probably the main entities responsible for the 1720 cm^{-1} band are ketones formed during water tree propagation. Calculation of the ratio peak absorbance/thickness (by the base line method [Zichy72]) has not given any relation for different ageing conditions. Using Beer's law [Zichy72] and an extinction coefficient for the carbonyl group of 300 $dm^3mol^{-1}cm^{-1}$ [Garton87], the

concentrations for unaged and electrically aged samples can be approximately calculated. An increase is found in the carbonyl concentration of 15-25% for electrically aged samples relative to unaged ones. These values are higher than those (≈15%) obtained by [Garton87]. Appearing in the spectrum and less enhanced than the 1720 cm^{-1} band are the ones at 1640 cm^{-1} and 1590 cm^{-1}. The former is representative of carbon double bonds (C=C) [82] arising from chain scission. The later corresponds to carboxylate ions (this one is not observed in all samples). Finally the amplitude of a band related to the flexion vibrations of CH_3 terminal end groups (1385 cm^{-1}) is decreased, suggesting that the number of ramifications is reduced, which could be attributed to chain scission at vulnerable sites such as the branching points.

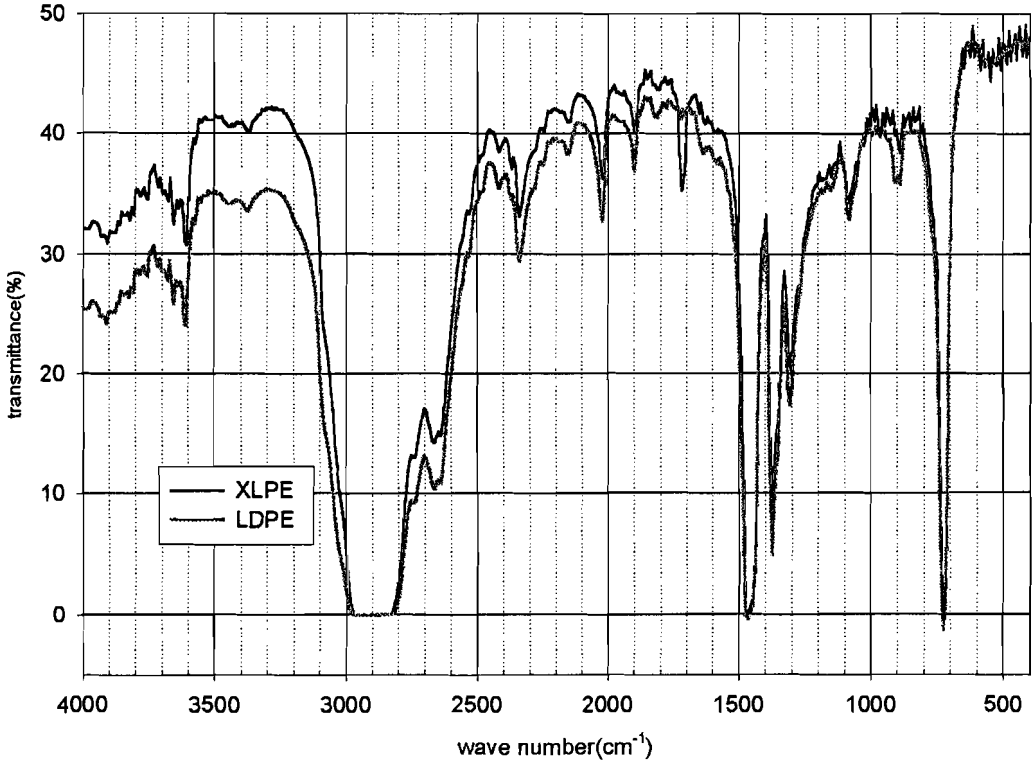

Figure 7.51 – LDPE and XLPE FTIR spectra.

LDPE samples thermally aged in solution but without any electric field were also analysed. The only difference relative to the unaged films is the enhancement of a band at 1740 cm^{-1} showing the existence of anti-oxidants (esters) in the original films (see Figure 7.53). The more common anti-oxidants used for polyethylene have a S–S bond that breaks with temperature producing esters. Samples undergoing thermal treatment (60 °C for 120h) also showed some increase in the number of C=O groups even if they were not in solution and no

[82] This wave number also corresponds to a characteristic band of water . However it should be noted that the samples were dried in an excicator prior to measurements and the presence of water has been greatly reduced.

field was applied. X Ray analyses of these samples revealed an increase in crystallinity (see 7.1.6).

Figure 7.52 – LDPE spectra in the wave number region [1500, 1900] $cm^{-1}$of a water treed region in electrically aged (6 kV/mm, 50 Hz, 1M NaCl, RT, 500h) and unaged samples.

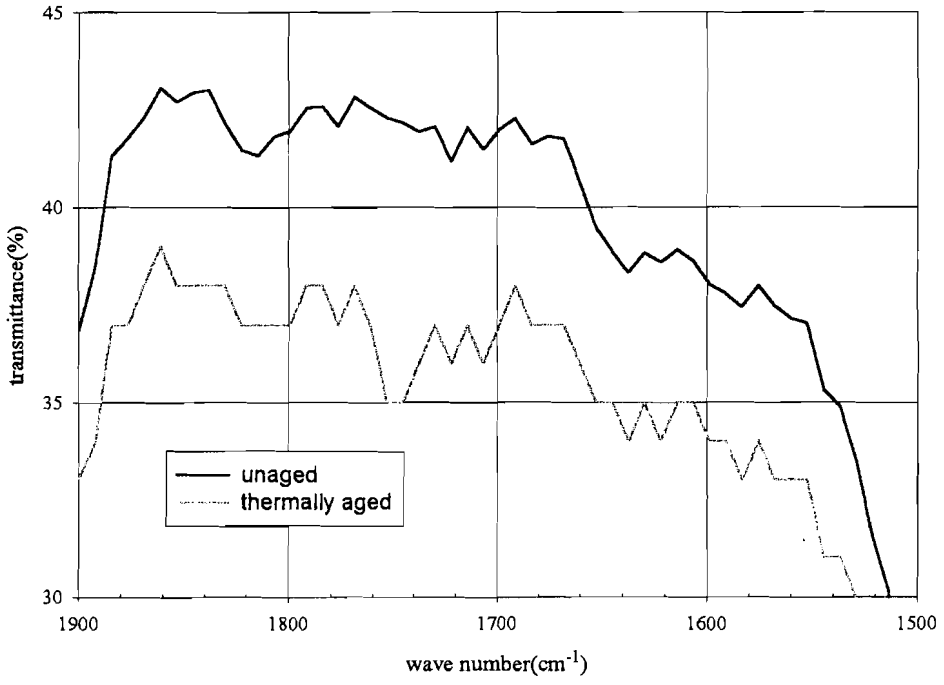

Figure 7.53 – LDPE spectra of unaged and thermally aged in 1M NaCl aqueous solution samples.

b) XLPE

The study of XLPE was more difficult due to the presence of cross-linking by-products and anti-oxidants appearing at the same wave number as some of the expected oxidation products. Acetophenone resulting from the curing process of dicumyl peroxide has a characteristic band at 1720 cm^{-1}, as can be seen in Figure 7.54. Unfortunately it will hide the presence of some oxidation products. All aged samples show lower concentrations of acetophenone which is known to diffuse out with time [Ross98]. This was also observed for the MF peak of the dielectric loss spectra (see 7.2). The main difference between aged and unaged samples is the presence of the 1740 cm^{-1} band of C=O of esters of anti-oxidants. Moreover the anti-oxidants will tend to diffuse to the water treed regions [Ross98] becoming part of the trees. The concentration is higher for samples aged at 50 °C than at lower temperatures in agreement with increased diffusion at higher temperatures. The concentration of C=C bonds (1640 cm^{-1}) is also increased. This band has two companion bands in the region 800-1000 cm^{-1}. These are observed, however, with no increase for aged films. For both LDPE and XLPE a decrease in the absorption at 1305 and 1385 cm^{-1} was seen corresponding to a reduction of the chain ramification.

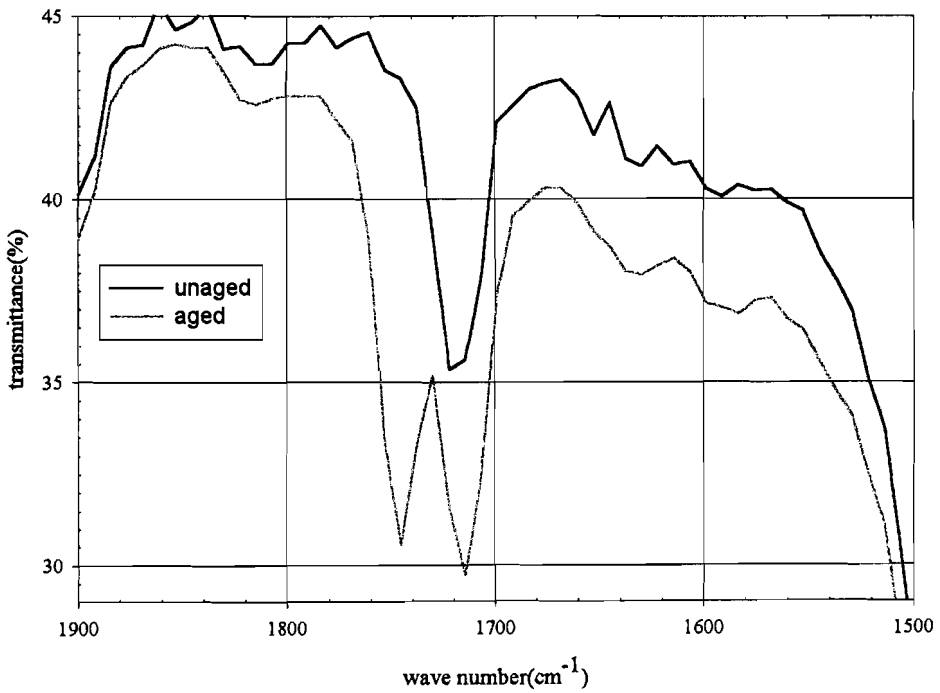

Figure 7.54 – XLPE spectra of unaged and electrically aged samples. The differences observed were attributed to the carbonyl group of esters present in the antioxidants.

Wet samples (soaked in distilled water for 24h) showed an enhancement of the characteristic frequencies of water, at 1640 cm^{-1} and 3380 cm^{-1}. The latter is linked to hydrogen bonds.

7.7.1.2 Discussion

For XLPE, because of interference from acetophenone the only result detected is an increase in the number of C=C. Even the presence of anti-oxidants in the water trees renders the detection of oxidation products in the tree itself more difficult but it can show that hydrophilic tracks must have been created by oxidation. Analysis of wet samples also shows the existence of these hydrophilic tracks dragging water into the trees. Thermal treatments can cause an increase in the number of carbonyl groups resulting from thermal oxidation.

For water trees in LDPE the more important results are the appearance of ketones (1720 cm^{-1}), carboxylate ions (1590 cm^{-1}) and an increase in the number of C=C (1640 cm^{-1} band). According to the Kema model [Ross92, 98] carboxylate ions are the most common product of oxidation in water trees. Yet as Ross emphasises, the model was developed for service aged cables. Specimens aged using accelerated laboratory techniques do not show this higher carboxylate concentration. Furthermore our samples (accelerated aged) do not show such high values as expected from the Kema model. Ketones seem to be the most important oxidation product. It is possible that the samples in this work are not aged enough, i.e., step *e)* of the model did not progress totally. Nevertheless oxidation and chain scission has occurred for water tree formation and growth. No satisfactory oxidation model has been developed for laboratory aged samples. Under accelerated conditions it is not known exactly what mechanism is responsible for the predominance of ketones over carboxylates.
Possible causes are: *(i)* When a combination of oxidation and diffusion occurs the main products are carboxylates. However, it should also be noticed that in pure oxidation the concentration of carboxylates is small compared with other oxidation products. Consequently if the ageing time is shorter, diffusion could play a less important role in the oxidation process. For service-aged cables the ageing time is much longer and the influence of diffusion would be more relevant resulting in a higher concentration of carboxylates and *(ii)* if there is too much diffusion then appears an excess of ions resulting, according to [Dissado92], in more terminal oxidation products and a lower concentration of carboxylates than in service ageing.

7.7.2 NMR studies: results and discussion

As reported in 5.1 the morphology of water trees seems to be microvoids in the micrometer range. Depending on the stress conditions (electric field applied) these voids will be either connected or disconnected. Even if disconnected the structure can be water filled, confirming

that there is diffusion between the microvoids. The existence of very small paths (or tracks or pores) has been suggested [Shaw84 and Ross98].

From the NMR[82] analysis of aged and virgin samples soaked in heavy water for 2 days the size of these pores could be obtained [Judenstein00]. After 800 scans the virgin sample revealed no NMR signal while the aged ones yielded a signal after 300 scans. The water content in the aged specimens is at least 500 times that of the unaged one. A weight fraction of $c = 6x10^{-4}$ was obtained for a 900h aged sample.

The NMR signal was recorded for temperature scans. On increasing the temperature at 260 K there is an abrupt drop in the signal. When decreasing, the temperature a change in the signal is recorded at 240K. The hysteresis observed rules out the possibility of a glass transition. Moreover the glass transition of water lies in the 140K region and its hysteresis is very weak. Instead this behaviour is typical of water crystallisation in confined systems. Using the Thompson and Brun equations (see [Judenstein00]) the dimension of the small pores containing the confined water can be obtained. Comparing with the results for porous glass, whose water content is much higher, a value of 2.5±0.5 nm was estimated. This value did not change with ageing time.

As stated in 5.1.1, for water trees composed of non-connected microvoids, controversy still remains. The results of this NMR study indicates that aged polymer possesses very small structures (pores) in the nanometer range. This agrees with TEM results [Ross98]. The shape of these structures is still unknown and also if they are or are not part of the treed regions. Still they could constitute a likely path for water and ions found in the voids of micrometer dimension.

In order to allow water ingress, the pore surfaces must be hydrophilic. These pores could already exist in the virgin polymer but have hydrophobic walls. Or they could have been created during ageing by oxidation. In either situation electro-oxidation must occur during polymeric electrical ageing (confirmed also by FTIR analysis). It is not certain if the microvoids are just enlarged pores by further oxidation and/or even cracking.

[82] This work was carried out in collaboration with J. Rault´s group.

7.8 Breakdown statistics – results and discussion

The Weibull probability plots can be seen in Figures 7.55 to 7.58 for the different ageing temperatures. The estimated parameters according to the White technique are presented in Table 7.15

Table 7.15 – Estimated parameters (shape and characteristic time)[83] obtained using the White method [White69, Montanari98] for the different ageing temperatures (also the % of censored data is shown).

	a	τ_W(h)	% of censored data
RT	0.88	1110	36
35°C	1.00	1920	51
40°C	1.40	1950	49
50°C	1.17	1440	42

For all the ageing temperatures investigated the shape parameter is relatively close to unity implying that the breakdown mechanisms are not significantly different. Also a is not very different from unity which agrees with Hill et al. [Hill83, 83a].

The lowest value for both the shape parameter and the characteristic time (that is near 1000h) is obtained for samples aged at room temperature. Moreover a is less than unity (even if not very different). The presence of a conditioning process and also the existence of pre-breakdown processes restraining one another are common in this situation [Dissado92]. An example of this kind of mechanisms is tree growth. It should be noticed that samples were aged with no temperature control. Consequently during ageing the samples were subjected both to temperature changes from day to night but also from daily changes over the full period of ageing[84]. Another set of samples was aged at 25°C (with temperature control). However their number is small and the bias in the estimated parameters would be higher than for those analysed [Ross96].

[83] Bias in the estimated parameters is not expected to be large according to the study by Ross [Ross96].

[84] It is helpful to recall that the samples were immersed in the solution so that changes are not so large as if they were kept in air.

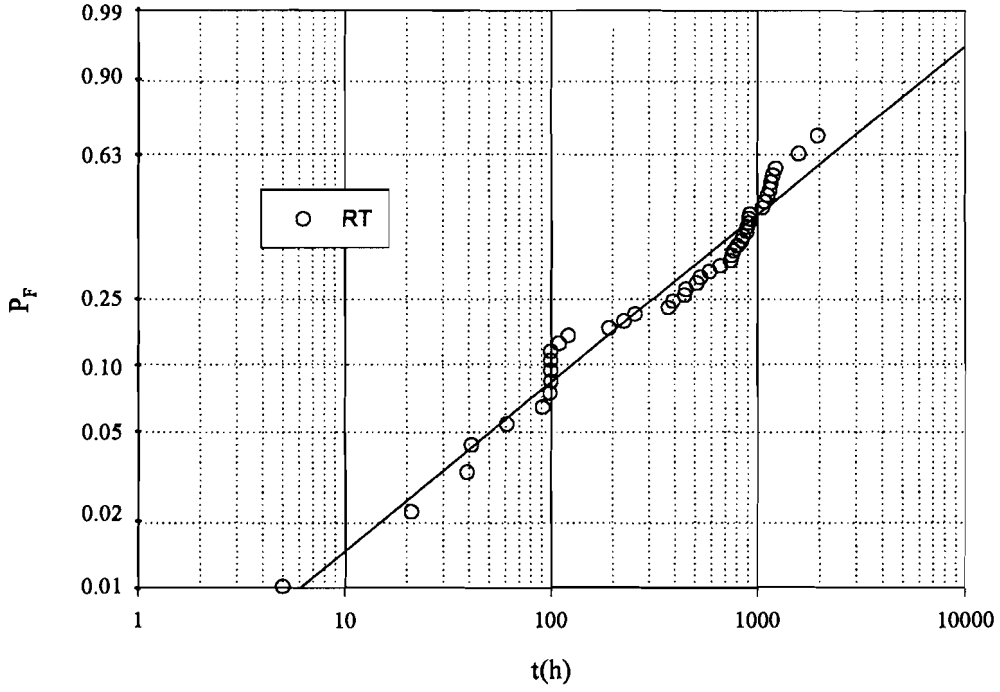

Figure 7.55 – Weibull probability plot of the breakdown times for samples aged at room temperature. The full line is the fit using the White technique.

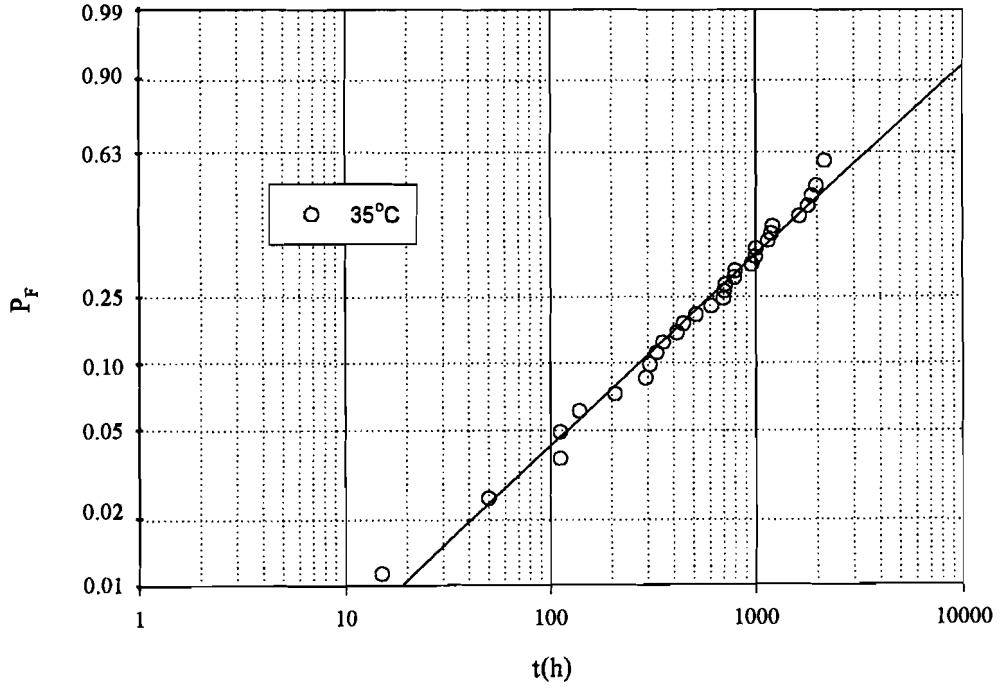

Figure 7.56 - Weibull probability plot of the breakdown times for samples aged at 35°C. Shown is the fit using the White technique (full line).

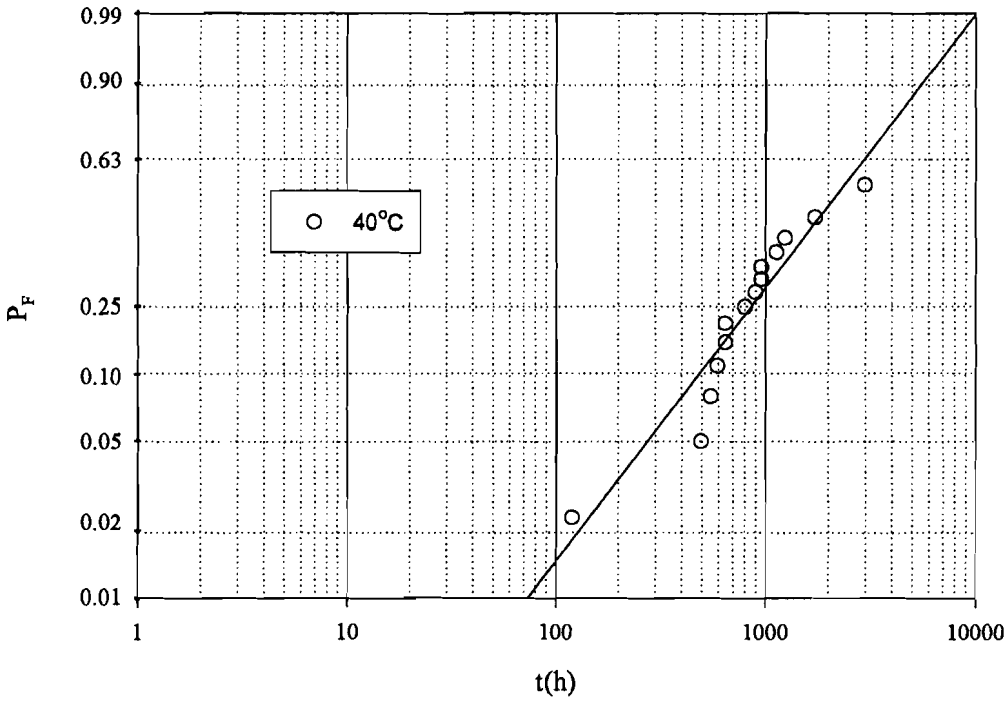

Figure 7.57 - Weibull probability plot of the breakdown times for samples aged at 40°C. The full line is the fit using the White technique.

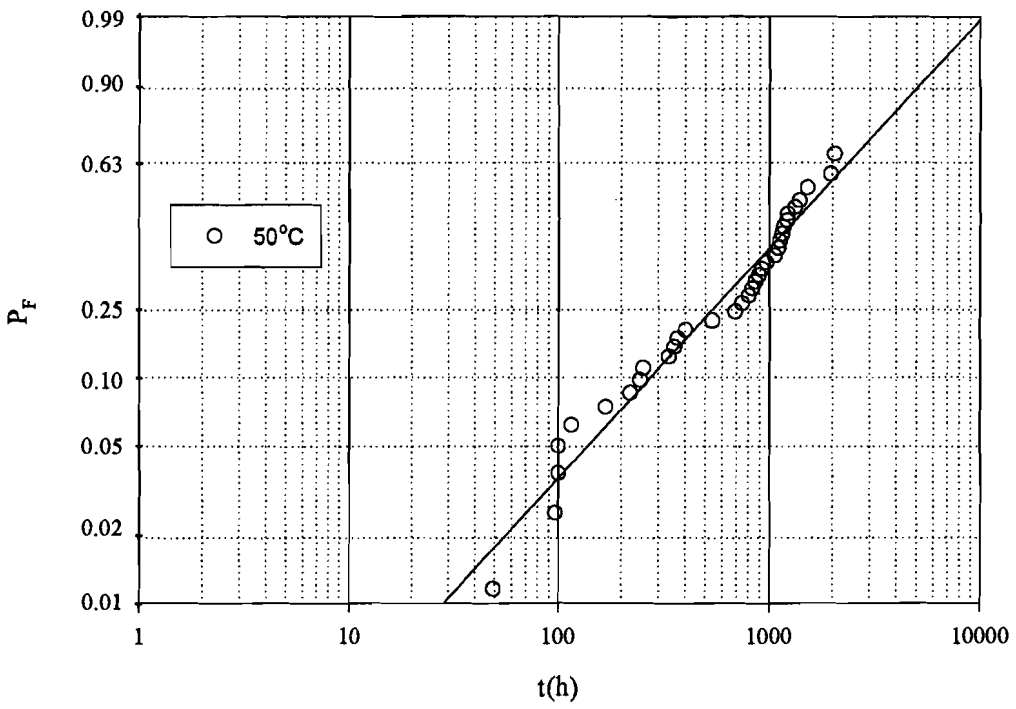

Figure 7.58 – Weibull probability plot of the breakdown times for samples aged at 50°C. Shown is the fit using the White technique (full line).

Table 7.16 – Time (h) at which a given percentage of samples will have failed (calculated from the cumulative distribution function).

% of failed samples	RT	35°C	40°C	50°C
10	85	200	392	210
20	200	425	670	400
30	342	680	935	600
40	515	980	1210	810
50	730	1330	1500	1055
60	1005	1760	1830	1335
70	1370	2315	2225	1685
80	1910	3100	2740	2160
90	2875	4440	3535	2935
95	3885	5785	4265	3670
99	6345	8910	5790	5300
99.9	10080	13390	7730	7490

Interestingly, for the samples aged at 35 °C is the value found for a (1.00). This value corresponds to an exponential, which results from breakdown processes independent of each other and the system has no memory of previous stressing [Dissado92]. The characteristic time is near 2000h and one of the longest found.

The samples aged at 40 °C gave rise to the largest value of the shape parameter (1.40) and also the longest characteristic time (near 2000h) slightly higher than that of 35 °C. Nevertheless the number of samples studied is smaller than at other temperatures giving rise to larger errors in estimated parameters.

Finally the 50°C aged samples show a decrease in both a and τ_W when compared with the increasing tendency with temperature observed previously. In 7.3 peaks were observed around this temperature which once more could indicate some changes occurring in the polymer.

A good way to compare different ageing temperatures is to look at Table 7.16, where the time (in hours) at which a given percentage of samples will have failed is shown. For instance the time corresponding to failure of 90% of the 50 °C aged samples is 2935h, the shortest time for any ageing temperature.

In Table 7.16 two rows are underlined in order to compare the relative breakdown times corresponding to failures percentages of 30 % and 95 %. The two ageing temperatures with shortest characteristic times to breakdown are always RT and 50 °C, but at 30% the samples more prone to fail are aged at RT, while at 95% the situation is reversed and the samples aged at 50 °C will have a higher breakdown probability. A similar trend is seen for the longest times found, which always corresponds to ageing at 35 °C and 40 °C. At a failure rate of 30 % the samples that suffer less breakdown are those aged at 40 °C while at 95 % it is the ones aged at 35 °C. This change in behaviour occurs at 70% failure rate.

As was stated in 7.2, ageing seems to occur due to the competition between two processes, oxidation and carrier diffusion. Oxidation will have an optimum temperature, unlike diffusion, which increases with increasing temperature. At higher temperatures, when diffusion becomes more important, the enhancement of the local electric field by the presence of more carriers raises the probability of breakdown. When oxidation (which can cause water treeing) is high enough it may retard the occurrence of breakdown. For treeing, according to Dissado et al. [Dissado92] as time advances and the defect (tree) grows the local field at the tip is reduced and, as a consequence, also the hazard rate.

The shorter characteristic time found for room temperature as compared to 35°C and 40°C aged samples, could be explained if the oxidation process was not progressing at a high enough rate to compensate the increase in local field due to carrier diffusion. It can also result from the charge that is deposited during sample preparation (as was shown in 7.1.5) essentially accumulating at defects in the surface and which diffuses slower at lower temperature.

In conclusion, the samples aged at intermediate temperatures (40°C and even more at 35°C) are the least prone to fail as a consequence of the competition between the oxidation and diffusion processes. This is in agreement with the results from other measurements reported above.

Chapter 8. Conclusions

We shall not cease from exploration
And the end of all our exploring
Will be to arrive where we started
And know the place for the first time.
T.S. Elliot

8.1 Conclusions

Hot-pressed moulded disc-shaped polyethylene samples of low density (LDPE) and crosslinked (XLPE) polyethylene were prepared and aged (electrical and/or thermal) varying electric field amplitude and frequency, temperature and concentration of the immersing NaCl aqueous solution. Some experimental techniques have been used to characterise differences in unaged, thermal and electrical aged samples. It is suggested that the more important physical mechanisms contributing to ageing are diffusion and oxidation enhanced by temperature and electric field for the samples aged under the experimental conditions here presented.

Oxidation and diffusion are two competing processes with different behaviours with temperature. While oxidation has an optimal temperature for which maximum rate is expected, diffusion increases with rise of temperature. For electrical field amplitude and frequency it is known that an increase of both or either of them always increases ageing[85]. However in this work most of the times a single amplitude (6 kV/mm) and a single frequency (50 Hz) were used.

One of the major features to notice is the overall conclusion by the different characterisation techniques used that point to the important combined role of oxidation and diffusion. This is manifested in dielectric relaxation spectroscopy (DRS) and combined isothermal and non-isothermal currents measurements (FTSDC) by the presence of space charges in new deeper traps. These new traps were assigned to electroxidation (including chain scission) which is only meaningful when the ageing is electrical (or more correctly thermoelectrical). Space charge presence is also observed in PEA experiments. The relative low fields used for

[85] At least for the frequency range used in this work.

electrical ageing do not support damage due only to electromechanical stresses. Furthermore FTIR measurements show the presence of oxidation products.

The possibility of relating samples aged under similar conditions (electrode geometry, aqueous solution, time) with and without applied field (which have been referred as electrical and thermal ageing) has not been much explored in the past. However it reveals to be important to understand the changes brought to ageing by an alternate electric field.

The new combined procedure joining usual isothermal and non-isothermal currents measurements (FTSDC) allowed for the first time to access the importance of the control of experimental conditions. It made also possible to confirm the presence of new traps and the diffusion of charges (probably ions) that only occurred during the AC ageing and not the DC charging step of FTSDC. These results together with the DRS are bulk measurements pointing to the importance of space charge in ageing.

The estimation of the fractal dimension of water trees was also made for the first time with results that point to same underlying physical mechanism at the microvoid level. Fractal estimation of SEM microphotographs at the namometer scale is not conclusive about the mechanism because of the limited experimental conditions. However NMR studies of the pore dimension also point to the presence of the same process regardless of ageing temperature and time. PEA measurements of water treed LDPE have showed that wet water trees are more conductive than the untreed regions of the polymer thus contributing to bring space charge (eletrons and ions) into the material and enhancing the probability of failure.

FTIR and the statistical treatment of breakdown allow finding a limited relation between localised changes and bulk changes of the aged specimens. Once more combined oxidation and diffusion effects are seen for electrically aged specimens. The results from the application of Weibull statistics to the available data of samples that have suffered breakdown shows the importance of manufacturing on initial failure. On the other hand, the temperature dependence of diffusion and oxidation is perceived with the samples aged at room temperature being the more prone to initial breakdown.

If we report ourselves to the quotation of Shaw and Shaw in the introduction and keep in mind the main conclusions, it is necessary to mention the importance of sample conditioning prior to age in order to understand better the changes brought either by thermal and/or electrical ageing.

8.2 Future work

The DRS measurements were restricted to a single temperature, so it would be important to be able to performed these measurements at different temperatures. It should be noted that it is only possible to use each sample once, since the time domain measurement bring changes to the sample (as FTSDC showed).

It would be also useful to make these measurements in XLPE samples (for instance DRS and FTSDC, etc.).

Estimation of total damage in water trees can be important to find out if size is the determinant measure of indirect danger to the insulation or just the type of mechanism (which is related to the fractal dimension).

If possible it would be interesting to apply Dissado-Mazzanti-Montanari model (see 5.4) for the influence of space charge in electrical ageing to water trees taking into account water trees inception times and the electro-mechano-chemical models.

References

[Abdolall82] K. Abdolall, H.E. Orton, M.W Reynolds, B.D. Robert, "Some physicochemical aspects of water trees", Annual Report CEIDP, pp. 604-614, 1982.

[Aida97] F. Aida, S. Wang, M. Fujita, G. Tanimoto, Y. Fujiwara, "Study of the mechanism of space charge formation in polyethylene", J. Electrostatics, vol. 42, pp. 3-15, 1997.

[Alison98] J.M. Alison, "The pulsed electro-acoustic method for the measurement of the dynamic space charge profile within insulators", in *Space charge in solid dielectrics*, edt. J.C. Fothergill and L.A. Dissado, Dielectric Society, Leicester, pp. 93-121, 1998.

[Alison98a] J.M. Alison, "A high field pulsed electro-acoustic apparatus for space charge and external circuit current measurement within solid insulators", Meas. Sci. Technol., vol. 9, pp. 1737-1750, 1998.

[Ashcraft76] C.R. Ashcraft, R.H. Boyd, "A dielectric study of molecular relaxation in oxidized and chlorinated polyethylenes", J. Poly. Sci., vol. 14, pp. 2153-2193, 1976.

[Bamji91] S.S. Bamji, A.T. Bulinski, A.T. Densley, M. Matsuki, "Degradation mechanism at XLPE/Semicon Interface Subjected to High Electrical Stress", IEEE Trans. Elect. Ins., 26(2), pp 278-284, 1991.

[Barrie66] I.T. Barrie, K.A. Buckingham, W. Reddish, "Dielectric properties of polyethyne for submarine telephone cables", Proc. IEE, 113(11), 1849-1854, 1966.

[Bartnikas83] R. Bartnikas, R.M. Eichhorn (edts), *Engineering dielectrics vol IIA-Electrical properties of solid insulating materials: molecular structure and electrical behavior*, ASTM Special Technical Pub 783, ASTM Pub Philadelphia, 1983.

[Billmeyer84] F.W. Billmeyer jr., *Textbook in polymer science*, 3rd edt., Wiley and Sons, New York, 1984.

[Blaise01] G. Blaise, "Charge localization and transport in disordered dielectric materials", J. Electrostatics, vol. 50, pp. 69-89, 2001.

[Blake74] A.E. Blake, A. Charlesby, K.J. Randle, "Simultaneous thermoluminescence and thermally stimulated current in polyethylene", J. Phys. D: Appl. Phys., vol. 7, pp. 759-770, 1974.

[Blythe79] A.R. Blythe, *Electrical properties of polymers*, Cambridge Univ. Press, New York, 1979.

[Boyd85a] R.H. Boyd, "Relaxation process in crystalline polymers: experimental behaviour – a review", Polymer, vol. 26, pp. 323-345, 1985.

[Boyd85b] R.H. Boyd, "Relaxation process in crystalline polymers: molecular interpretation – a review", Polymer, vol. 26, pp. 1123-1133, 1985.

[Boyd97] R.H. Boyd, F. Liu, "Dielectric spectroscopy of semicrystalline polymers", in *Dielectric spectroscopy of polymers – fundamentals and applications*, edt. J.P. Rundt, J.J. Fitzgerald, American Chemical Society, Washington, 1997.

[Brooks99] N.W. Brooks, M. Ghazali, R.A. Duckett, A.P. Unwin, I.M. Ward, "Effects of morphology on the yield stress of polyethylene", Polymer, vol. 40, pp. 821-825, 1999.

[Bulinski98] A.T. Bulinski, J.-P. Crine, B. Noirhomme, R.J. Densley, S. Bamji, "Polymer oxidation and water treeing", IEEE Trans. Diel. and Elect. Ins., vol. 5(4), pp. 558-570, 1998.

[Cole41] K.S. Cole, R.H. Cole, "Dispersion and absorption in dielectrics – I – alternating currents characteristics", J. Chem. Phys, vol. 9, pp. 341-351, 1941.

[Crine98] J.-P. Crine, "Electrical, chemical and mechanical processes in water treeing", IEEE Trans Diel. & Elect. Ins., vol. 5(5), pp. 681-694, 1998

[Crine00] J.-P. Crine, "When Taguchi meets water treeing", IEEE Ins. Mag., vol 16(3), pp.13-18, 2000.

[Cross84] J.D. Cross, J.Y. Koo, "Some observations on the structure of water trees", IEEE Trans. Elect. Ins., vol. 19(4), pp.303-306, 1984.

[Cullity78] B.D. Cullity, *Elements of X-ray diffraction*, Addison-Wesley, Inc., Reading, 1978.

[Daniel67] V.V. Daniel, *Dielectric relaxation*, Academic Press, London, 1967.

[Das Gupta75] D.K. Das Gupta, T. Noon, "Some spectroscopic and optical methods to characterise trap sites in polyethylene", Inst. Phys. Conf. Ser., n. 27, pp. 122-129, 1975.

[Das Gupta76] D.K. Das Gupta, K.J. Joyner, "On the nature of absorption currents in polyethylene terephtalate (PET)", J. Phys D: Appl. Phys, vol. 9, pp. 829-839, 1976.

[Das Gupta78] D.K. Das Gupta, R.S. Brockley, "A study of 'absorption currents' in low-density polyethylene", J. Phys D: Appl. Phys, vol. 11, pp. 955-962, 1978.

[Das Gupta90] D.K. Das Gupta, A. Svatik, A.T. Bulinski, R.J. Densley, S. Bamji, D.J. Carlsson, "On the nature of AC field aging of cross-linked polyethylene using liquid electrodes", J. Phys. D: Appl. Phys., vol. 23, 1990.

[Das Gupta92] D.K. Das Gupta, "Electrical properties of surfaces of polymeric insulators", IEEE Trans Elect. Ins., vol. 27(5), pp. 909-923, 1992.

[Das Gupta94] D.K. Das Gupta, "Polyethylene: structure, morphology, molecular motion and dielectric behavior", IEEE Elect. Ins. Mag., vol. 10(3), pp. 5-15, 1994.

[Das Gupta97] D.K. Das Gupta, "Conduction mechanisms and high-field effects in synthetic insulating polymers", IEEE Trans Diel. & Elect. Ins., vol. 4(2), pp. 149-156, 1997.

[Das Gupta99] D.K. Das Gupta, P.C.N. Scarpa, "Modelling of dielectric relaxation spectra of polymers in the condensed phase", Elect. Ins. Mag., 15(2), 23-32, 1999.

[David95] E. David, "Comparison between experimental results and fractal growth model for electrical treeing in polyethylene", In Conf. Proc. 5th Int. Conf. on Solid Dielectrics, pp. 199-203, 1995.

[Davidson51] D.W. Davidson, R.H. Cole, "Dielectric relaxation in glycerol, propylene glycol and n-propanol", J. Chem. Phys., vol. 19, pp. 1484-1490, 1951.

[Delhalle74] J. Delhalle, J.M. Andre, S. Delhalle, J.J. Pireaux, R. Caudano, J.J. Verbist, "Electronic structure of polyethylene: theory and ESCA", J. Chem. Phys., vol. 60(2), pp. 595-600, 1974.

[Dias96] C.J. Dias, "Determination of relaxation frequencies based on experimental relaxional data", Phys. Rev. B, 53(21), pp. 14212-14222, 1996

[Dissado83] L.A. Dissado, R.M Hill, "A cluster approach to the structure of imperfect materials and their relaxation spectroscopy", Proc. Roy. Soc. Lond. A, vol. 390, pp 131-180, 1983.

[Dissado84] L.A. Dissado, R.M. Hill, "Anomalous low-frequency dispersion", J.Chem. Soc. Faraday Trans. 2, 80, pp. 291-319, 1984.

[Dissado89] L.A. Dissado, R.M. Hill, "The fractal nature of the cluster model dielectric response functions", J. Appl. Phys., 66(6), pp. 2511-2524, 1989.

[Dissado92] L.A. Dissado, J.C. Fothergill, *Electrical Degradation and Breakdown in Polymers*, IEE P. Peregrinus, London, 1992.

[Dissado95] L.A. Dissado, G. Mazzanti, G.C. Montanari, "The incorporation of space charge degradation in the life model for electrical insulating materials", IEEE Trans Diel. & Elect. Ins., vol. 2(6), pp. 11-471158, 1995.

[Dissado97] L.A. Dissado, G. Mazzanti, G.C. Montanari, "The role of space charges in electrical aging of insulating materials", IEEE Trans Diel. & Elect. Ins., vol. 4(5), pp. 496-506, 1997.

[Dissado97a] L.A. Dissado, S.J. Dodd, J.V. Champion, P.I. Williams, J.M. Alison, "Propagation of electrical tree structure in solid polymeric insulation", IEEE Trans Diel. & Elect. Ins., vol. 4(3), pp. 259-279, 1997.

[Dissado01] L.A. Dissado, G. Mazzanti, G.C. Montanari, "Elemental strain and trapped space charge in thermoelectrical aging of insulating materials: Part 1: Elemental strain under thermo-electrical-mechanical stress", IEEE Trans Diel. & Elect. Ins., vol. 8(6), pp. 959-965, 2001.

[Dorlanne82] O. Dorlanne, S. Sapieha, M.R. Wertheimer, A. Yelon, "Thermally stimulated discharge of polyethylene following AC stress", IEEE Trans. Elect. Ins., vol. 17(3), pp. 199-202, 1982.

[Fan96] Z.H. Fan, N. Yoshimura, "The influence of crystalline morphology on the growth of water trees in PE", IEEE Trans. Diel. Elect. Ins., vol. 3(6), pp. 849-858, 1996.

[Feder88] J. Feder, *Fractals*, Plenum Press, New York, 1988.

[Fischer76] P. Fischer, P. Röhl, "Thermally stimulated and isothermal depolarization currents in low-density polyethylene", J. Pol. Sci., 14, pp 531-542, 1976.

[Fischer76a] P. Fischer, P. Röhl, "Relaxation time spectrum of dipolar reorientation in low-density polyethylene", J. Pol. Sci., 14, pp 543-554, 1976.

[Fischer78] P. Fischer, "Electrical conduction in polyolefins", J. Electrostatics, vol. 4, pp.149-173, 1978.

[Fothergill93] J.C. Fothergill, "Assessing the life of polymeric power cables", Technical Report, Univ. of Leicester, 1993.

[Fukuzawa99] M. Fukuzawa, M. Iwamoto, "TSC measurements of space charge in low-density PE under a needle-plane electrode system", IEEE Trans. Diel. Elect. Ins., vol. 6(6), pp. 858-863, 1999.

[Garton87] A. Garton, S. Bamji, A. Bulinsky, J. Densley, "Oxidation and water tree formation in service-aged XLPE cable insulation", IEEE tans. Elect. Ins., vol. 22(4), pp. 405-412, 1987.

[Goodfellow00] Goodfellow Ltd., "Goodfellow CD-ROM Catalogue", Ermine Business Park, Huntingdon, PE 296WR, UK, 2000.

[Graff94] M.S. Graff, R.H. Boyd, "A dielectric study of molecular relaxation in linear polyehtylene", Polymer, vol. 35, pp 1797-1801, 1994.

[Grassberg83] P. Grassberg, "Generalized dimensions of strange attractors", Phys. Lett. A, vol 97, pp 227-230, 1983.

[Hall89] C. Hall, *Polymeric materials*, 2nd ed., Macmillan, London, 1989.

[Hamon52] B.V. Hamon, "An approximate method for deducing dielectric loss factor from direct measurements", Proc. IEE, 99(IV), 151-155, 1952.

[Haralick92] R.M. Haralick, L.G. Shapiro, "Glossary of computer terms", Pattern recognition, 24(1), 69-93, 1992.

[Havriliak66] S. Havriliak, S. Negami, "A complex plane analysis of α-dispersion in some polymer systems", J. Polymer Sci. – Pt. C, vol. 14, pp. 99-117, 1966

[Henkel85] H.J. Henkel, N. Müller, "Additive zur Inhibierung van wasserbäumchen in polyolefinen für kabelisolierungen", Electrotechnische Gesellschaft Fachberichte, vol. 16, pp. 132-134, 1985.

[Hedvig77] P. Hedvig, *Dielectric spectroscopy of polymers*, Adam Hilger, Bristol, 1977.

[Hilczer86] B. Hilczer, J. Malecki, *Electrets*, Elsevier, Warsaw, 1986

[Hill83] R.M. Hill and L.A. Dissado, "Theoretical basis for the statistics of dielectric breakdown", J. Phys. C: Solid State Phys., vol. 16, pp. 2145-2156, 1983

[Hill83a] R.M. Hill and L.A. Dissado, "Examination of the statistics of dielectric breakdown", J. Phys. C: Solid State Phys., vol. 16, pp. 4447-4468, 1983

[Höhne96] G. Höhne, W. Hemminger, H.-J. Flammersheim, *Differential scanning calorimetry*, Springer, Berlin, 1996.

[Hou90] X.J. Hou, R. Gilmore, G.B. Mindlin, H. Solari, "An efficient algorithm for fast O(N*ln(N)) box-counting", Physics Letters A, vol. 151, pp. 43-46, 1990.

[Houlgreave92] J.A. Houlgreave, A. Eccles, J.C. Fothergill, "Characterization of water treeing and the use of frequency acceleration techniques", In Conf. Proc. 6th Int. Conf. on Dielectric Materials, Measurements and Applications, 492-495, 1992.

[Huang94] Q. Huang, J.R. Lorch, R.C. Dubes, "Can the fractal dimension of images be measured?", Pattern Recognition, 27, 339-349, 1994.

[Hwangbo98] S. Hwangbo, Y. Koon, S. Jeon, M. Han, "Direct correlation between space charge and conduction characteristics of low density polyethylene at various temperatures", Jpn. J. Appl. Phys., vol. 37, pp. 4419-4427, 1998.

[Jacquelin97] J. Jacquelin, "Inference of sampling on Weibull parameter estimation", IEEE Trans. Diel. Elect. Ins., vol. 3(6), pp. 809-816, 1996.

[Jeroense97] M. Jeroense, "Charges and discharges in HVDC cables, in particular in mass-impregnated HVDC cables", PhD thesis, Delft University Press, 1997.

[Johnson70] N.L. Johnson, S. Kotz, *Continuous univariate distributions-1*, John Wiley&Sons, New York, 1970.

[Jonscher83] A.K. Jonscher, *Dielectric relaxation in solids*, Chelsea Dielectrics Press Ltd, London, 1983.

[Jonscher92] A.K. Jonscher, "The universal dielectric response and its physical significance", IEEE Trans. Elect. Ins., vol. 27, pp. 407-423, 1992.

[Jonscher97] A.K. Jonscher, "Dielectric relaxation with dipolar screening", J. Mat. Sci., vol. 32, pp 6409-6414, 1997.

[Jonscher99] A.K. Jonscher, "Dielectric relaxation in solids", J. Phys. D: Appl. Phys., vol. 32, pp R57-R70, 1999.

[Jonscher99a] A.K. Jonscher, "Low-loss dielectrics", J. Mat. Sci., vol. 34, pp 3071-3082, 1999.

[Jonscher01] A.K. Jonscher, "Limiting losses in dielectrics", IEEE Trans. Diel. Elect. Ins., vol. 8, pp. 345-351, 2001

[Judenstein00] P. Judenstein, M.C. Lança, J. Marat-Mendes, J. Rault, "Pore dimension of water trees in PE: NMR studies", Polymer, vol. 41, pp. 8151-8154, 2000.

[Ieda84] M. Ieda, "Electrical conduction and carrier traps in polymeric materials", IEEE Trans. Elect. Ins., vol. 19(3), pp. 162-178, 1984.

[Kao79] K.J. Kao, S.S. Bamji, M.M. Perlman, "Thermally stimulated discharge current study of surface charge release in polyethylene by corona-generated excited molecules, and the crossover phenomenon", J. Appl. Phys., vol 50(12), pp.8181-8185, 1979.

[Katsuta99] G. Tatsuta, A. Toya, Y. Li, M. Okashita, F. Aida, Y. Ebinuma, Y. Okhi, "Experimental investigation on the cause of harmfulness of blue water tree to XLPE cable insulation", IEEE Trans. Diel. Elect. Ins., vol. 6(6), pp. 887-891, 1999.

[Kim01] K.Y. Kim, B.H. Ryu, D.J. Byun, S.M. Shin, "Thermally stimulated current study in γ-ray irradiated low density polyethylene", Eur. Polymer J., vol 37(5), pp. 1061-1064, 2001.

[King93] J.A. King, M: Grundmeyer, D. Stepp, D. Hugo, "Water tree morphology", IEEE Trans. Elect. Ins., vol. 28, pp. 415-419, 1993.

[Kobayashi79] S. Kobayashi, K. Yahagi, "Thermally stimulated current in elongated low-density polyethylene film", Jpn. J. Appl. Phys., vol. 18(2), pp. 261-268, 1979.

[Kudo98] K. Kudo, "Fractal analysis of electrical trees", IEEE Trans Diel. & Elect. Ins., vol 5, pp. 713-727, 1998.

[Lança96] M.C. Lança, L.A. Dissado, "An estimate of the fractal dimension of water trees" In 7th Int. Conf. on Dielectric Materials, Measurements and Applications, pp. 214-219, Bath, UK, 1996.

[Lança01] M.C. Lança, L.A. Dissado, J.N. Marat-Mendes, "The fractal analysis of water trees: an estimate of the fractal dimension", IEEE Trans. Diel. Elect. Ins., vol. 8(5), pp. 838-844, 2001.

[Lança02] M.C. Lança, E.R. Neagu, J.N. Marat-Mendes, "Combined isothermal and non-isothermal current measurements applied to space charge studies in low-density polyethylene", J. Phys. D: Appl. Phys., vol. 35, pp. L29-L32, 2002

[Lee97] S.H. Lee, J-K. Park, C.R. Lee, K.S. Suh, "The effect of low-molecular-weight species on space charge and conduction in LDPE". IEEE Trans Diel. & Elect. Ins., vol 4(4), pp. 425-432, 1997.

[Li94] Y. Li, M. Yasuda, T. Takada, "Pulsed electroacoustic method for measurement of charge accumulation in solid dielectrics", IEEE Trans. Diel. Elect. Ins., vol. 1(2), pp. 188-195, 1994.

[Li96] Y. Li, J. Kawai, Y. Ebinuma, Y. Imaizumi, K. Suzuki, Y. Tanaka, "Three-dimensional space charge distribution in water tree tip using the pulsed electroacoustic method", Proc. of the 9th Int. Conf. on Dielectrics, ISE9, Shangai, pp. 217-221, 1996.

[Li97] Y. Li, J. Kawai, Y. Ebinuma, Y. Fujiwara, Y. Okhi, Y. Tanaka, T. Takada, "Space charge behavior under ac voltage in water-treed PE observed by the PEA method", IEEE Trans. Diel. Elect. Ins., vol. 4(1), pp. 52-57, 1997.

[Liebovitch90] L.S. Liebovitch, T. Toth, "A fast algorithm to determine the fractal dimension by box-counting", Physics Letters A, vol. 141, pp. 386-390, 1990.

[Maeno88] T. Maeno, T. Futami, H. Kushibe, T. Takada, M.C. Cooke, "Measurement of spatial charge distribution in thick dielectrics using the pulsed electroacoustic method", IEEE Trans. Elect. Ins., vol. 23(3), pp.433-439, 1988.

[Mandelbrot67] B.B. Mandelbrot, "How long is the coast of Britain? Statistical self-similarity and fractalional dimension", Science, vol. 155, pp. 636-638, 1967.

[Mandelbrot75] B.B. Mandelbrot, *Les objects fractal, forme, hasard et dimension*, Flammarion, Paris, 1975.

[Mandelbrot82] B.B. Mandelbrot, *The fractal geometry of nature*, Freeman & Comp, New York, 1982.

[Maxwell91] J.C. Maxwell, *A treatise on electricity and magnetism*, Dover, New York, 3rd ed., 1891.

[Mayoux97] C. Mayoux, "Aging of polymeric insulating materials in power cables", IEEE Trans. Diel. Elect. Ins., vol. 4(6), pp. 665-673, 1997.

[Mazzanti99] G. Mazzanti, G.C. Montanari, L.A. Dissado, "A space charge life model for AC electrical aging of polymers", IEEE Trans Diel. & Elect. Ins., vol. 6(6), pp. 864-875, 1999.

[Mazzanti01] G. Mazzanti, G.C. Montanari, L.A. Dissado, "Elemental strain and trapped space charge in thermoelectrical aging of insulating materials: Part 2: Life modeling", IEEE Trans Diel. & Elect. Ins., vol. 8(6), pp. 966-971, 2001.

[McCrum67] N.G. McCrum, B.E. Read, G. Williams, *Anelastic and dielectric effects in polymeric solids*, Dover, New York, 1967

[McLachlan99] D.S. McLachlan and M.B. Heaney, "Complex ac conductivity of a carbon black composite as a function of frequency, composition and temperature", Phys. Rev. B, vol. 60(18), pp. 12746-12751, 1999.

[Meyer83] C.T. Meyer, "Water absorption during water treeing", IEEE Trans. Elect. Ins., vol. 18(1), pp. 28-31, 1983.

[Mizutani80] T. Mizutani, T. Tsukahara, M. Ieda, "Thermally-stimulated currents in oxidized low-density polyethylene", Jpn. J. Appl. Phys., vol. 19(11), pp. 2095-2098, 1980.

[Montanari97] G.C. Montanari, G. Mazzanti, M. Cacciari, J.C. Fothergill, "In search of convenient techniques reducing bias in the estimation of Weibull parameters for uncensored tests", IEEE Trans. Diel. Elect. Ins., vol. 4(3), pp. 306-313, 1997.

[Montanari97a] G.C. Montanari, G. Mazzanti, M. Cacciari, J.C. Fothergill, "Optimum estimators for the Weibull distribution from censored test data (singly-censored tests)", IEEE Trans. Diel. Elect. Ins., vol. 4(4), pp. 462-469, 1997.

[Montanari98] G.C. Montanari, G. Mazzanti, M. Cacciari, J.C. Fothergill, "Optimum estimators for the Weibull distribution from censored test data (progressively-censored tests)", IEEE Trans. Diel. Elect. Ins., vol. 5(2), pp. 157-163, 1998.

[Montanari01] G.C. Montanari, G. Mazzanti, F. Palmieri, A. Motori, G. Perego, S. Serra, "Space-charge trapping and conduction in LDPE, HDPE and XLPE", J. Phys. D: Appl. Phys., vol. 34, pp. 2902-2911, 2001.

[Moreau93] E. Moreau, C. Mayoux, C. Laurent, A. Boudet, "The structural characteristics of water trees in power cables and laboratorial specimens", IEEE Trans. Elect. Ins., vol. 28, pp.54-64, 1993.

[Mott40] N.F. Mott, R.W. Gurney, *Electronic process in ionic crystals*, Oxford Univ. Press, New York, 1st edt., 1940.)

[Nakamura77] S. Nakamura, G. Sawa, M. Ieda, "Anomalous luminescence from oxidized PE in high-temperature region", J. Appl. Phys., vol. 48(8), pp. 3626-3627, 1977.

[Nakamura02] S. Nakamura, T. Ozaki, N. Ito, J. Kawai, "Change of dielectric property with water-treed region", IEEE Trans. Diel. Elect. Ins., vol. 9(3), pp. 329-334, 2002.

[Nath89] R. Nath, M.M. Perlman, "Effects of crystallinity on charge storage in polypropylene and polyethylene", IEEE Trans. Elect. Ins., vol. 24(3), pp.409-412, 1989.

[Neagu99] E.R. Neagu, J.N. Marat Mendes, R.M. Neagu, D.K. Das Gupta, "Nonisothermal and isothermal discharging currents in polyethylene terephtalate at elevated temperatures", J. Appl. Phys, vol. 85(4), pp. 2330-2336, 1999.

[Neagu01] E.R. Neagu, J.N. Marat Mendes, "Combined isothermal and non-isothermal techniques to analyze charge trapping and stability in insulating materials", Jpn. J. Appl. Phys., vol. 40, pp. L1160-L1162, 2001.

[Neagu01a] E.R. Neagu, R.M. Neagu, "On the nature of the origin of the isothermal and non-isothermal current released from dielectric materials", Thin Solid Films, vol. 384, pp. 15-22, 2001.

[Neagu01b] R.M. Neagu, E.R. Neagu, I.M. Kalogeras, A. Vassilikou-Dova, "Evaluation of the dielectric parameters from TSDC spectra: application to polymeric systems", Mat. Res. Innovat., vol. 4, pp. 15-25, 2001.

[Nichols54] J.B. Nichols,"X-ray and infrared studies on the extent of crystallisation of polymers", vol. 25, pp. 840-847, 1954.

[Niemeyer84] L. Niemeyer, L. Pietronero, H.J. Wiesman, "Fractal dimension of dielectric breakdown", Phys. Rev. Lett., vol. 52, pp. 1033-1036, 1984.

[Niklasson87] G.A. Niklasson, "Fractal aspects of the dielectric response of charge carriers in disordered materials", J. Appl. Phys., vol. 62(7), pp. R1-R14, 1987.

[Noon73] T. Noon, "Some spectroscopic and optical methods to characterise trap sites in polyethylene", MSc thesis, Univ. of Wales (Bangor), 1973.

[Ohki98] Y. Okhi, Y. Ebinuma, S. Katakai, "Space charge formation in water-treed insulation", IEEE Trans. Diel. Elect. Ins., vol. 5(5), pp. 707-712, 1998.

[Olley92] R.H. Olley, D.C. Basset, A.S. Vaughan, V.A.A. Banks, P.B. McAllister, S.M. Moody, "Delineating water trees in cross-linked polyethylene: a new technique", J. Mat. Sci., vol. 27, pp. 5192-5198, 1992.

[Olley95] R.H. Olley, A.S. Vaughan, D.C. Basset, S.M. Moody, "Electron microscopy of water trees in XLPE", Proc of the 5th International Conference on Conduction and Breakdown in Solid Dielectrics, ICSD'95, Leicester, pp. 676-680, 1995.

[Papir71] Y.S. Papir and E. Baer, "New relaxation phenomena in linear polyethylene at cryogenic temperatures", J. Appl. Phys, vol. 42(12), pp. 4667-4674, 1971.

[Pélissou88] S. Pélissou, H. St-Onge, M.R. Wertheimer, "Electrical conduction of polyethylene below and above its melting point", IEEE Trans. Elect. Ins., vol. 23(3), pp. 325-333, 1988.

[Phillips83] P.J. Phillips, "Morphology and molecular structure of polymers and their dielectric behavior", in *Engineering dielectrics vol IIA-Electrical properties of solid insulating materials: molecular structure and electrical behavior*, edt. R. Bartnikas, R.M. Eichhorn, ASTM Special Technical Pub 783, ASTM Pub, Philadelphia, 1983.

[Rosen93] S.L. Rosen, *Fundamental principles of polymeric materials*, John Wiley & Sons, inc., New York, 2nd edt., 1993.

[Ross89] R. Ross, W.S.M. Geurts, J.J. Smit, J.H. Van der Maas, E.T.G. Lutz, Kema Sci. & Tech. Rep., Vol. 7(6), pp. 357-364, 1989.

[Ross90] R. Ross, "Composition, structure and growth of water trees in polyethylene", Kema Sci. & Tech. Rep., Vol. 8(4), pp. 209-271, 1990.

[Ross92] R. Ross, "Composition and growth of water trees in XLPE", IEEE Trans. Elect. Ins., vol. 27, n. 3, pp 519-531, 1992.

[Ross98] R. Ross, "Inception and propagation mechanisms of water treeing", IEEE Trans. Diel. Elect. Ins., vol. 5, n. 5, pp 660-680, 1998.

[Sakamoto02] W.K. Sakamoto, D.J. Perez, D.K. Das Gupta, "On the characterisation of electrically stressed polyethylene before and after chemical treatment", J. Mat. Sci., vol. 37, pp. 1295-1300, 2002.

[Sawa73] G. Sawa, M. Kawade, M. Ieda, "Field-assisted trapping in polyethylene", J. Appl. Phys., vol. 44(12), pp. 5397-5398, 1973.

[Sawa74] G. Sawa, M. Kawade, M. Ieda, "Thermally stimulated current from polyethylene in high temperature region", Jpn. J. Appl. Phys., vol. 13(10), pp. 1547-1553, 1974.

[Scarpa95] P.C.N. Scarpa, "Polarisation and dielectric behaviour of AC aged polyethylene", PhD thesis, Univ. of Wales (Bangor), 1995.

[Schönhals97] A. Schönhals, "Dielectric properties of amorphous polymers", in *Dielectric spectroscopy of polymers-fundamentals and applications*, edt. J.P. Rundt, J.J. Fitzgerald, American Chemical Society, Washington, 1997.

[Seggern81] H. von Seggern, "Detection of surface and bulk traps", J. Appl. Phys, vol. 52(6), pp. 4087-4089, 1981.

[Shaw84] M.T. Shaw, S.H. Shaw, "Water treeing in solid dielectrics", IEEE Trans. Electrical Insulation, vol. 19(5), pp. 419-452, 1984.

[Shinozaki91] D.M. Shinozaki, P.C. Cheng, S. Haridoss, R. Mitchell, A. Fenster, "Three-dimensional optical microscopy of water trees in polyethylene", J- Mat. Sci., vol. 26, pp. 6151-6160, 1991.

[Stanley88] H.E. Stanley, P. Meakin, "Multifractal phenomena in physics and chemistry", Nature, vol 335, pp 405-409, 1988.

[Steennis90] E.F. Steenis, F.H. Kreuger, "Water treeing in polyethylene cables", IEEE Trans. Elect. Ins., vol. 25(5), pp. 989-1028, 1990.

[Stepp96] D. Stepp, J.A. King, J. Worrall, A. Thompson, D.E. Cooper, "High-resolution study of water trees grown in silver nitrate solution", IEEE Trans. Diel. Elec. Ins., vol. 3, pp.392-398, 1996.

[Suh96] K.S. Suh, J.H. Koo, S.H. Lee, J.K. Park, T. Takada, "Effect of sample preparation conditions and short chains on space charge formation in LDPE", IEEE Trans. Diel. Elec. Ins., vol. 3(2), pp. 153-160, 1996.

[Taylor71] D.M. Taylor, T.J. Lewis, "Electrical conduction in polyethylene terephtalate and polyethylene films", J. Phys. D: Appl. Phys., vol. 4, pp. 1346-1357, 1971.

[Teyssedre97] G. Teyssedre, S. Mezghani, A. Bernes. C. Lacabanne, "Thermally stimulated currents of polymers", in *Dielectric spectroscopy of polymers-fundamentals and applications*, edt. J.P. Rundt, J.J. Fitzgerald, American Chemical Society, Washington, 1997.

[Toyoda01] T. Toyoda, S. Mukai, Y. Okhi, Y. Li, T. Maeno, "stimation of conductivity and permittivity in PE from space charge distribution measurements", IEEE Trans. Diel. Elect. Ins., vol. 8(1), pp. 111-116, 2001.

[Turnhout80] J. Turnhout, "Thermally stimulated discharge of electrets" in *Electrets*, edt by G.M. Sessler, Sringler-Verlag, Berlin, 1980.

[Vanderschueren79] J. Vanderschueren, J. Gasiot, "Field-induced thermally stimulated currents", in *Thermally stimulated relaxation in solids*, edt. P.Bräunlich, Springler-Verlag, Berlin, 1979.

[Watson95] P.K. Watson, "The transport and trapping of electrons in polymers", IEEE Trans. Diel. Elect. Ins., vol. 2(5), pp. 915-924, 1995.

[Weibull51] W. Weibull, "A statistical distribution function of wide applicability", J. Appl. Mech., vol. 18, pp. 293-297, 1951.

[Weron91] K. Weron, "A probabilistic mechanism hidden behind the universal power law for dielectric relaxation: general relaxation equation", J. Phys: Condens. Matter, vol. 3, pp. 9151-9162, 1991.

[Weron93] K. Weron, A. Jurlewicz, "Two forms of self-similarity as a fundamental feature of the power law dielectric response", ", J. Phys A: Math. Gen., vol. 26, pp. 395-410, 1993.

[Weron01] K. Weron, A. Jurlewicz, A.K. Jonscher, "Energy criterion in interacting cluster systems", vol. 8, pp. 345-351, 2001.

[Wiesman86] H.J. Wiesman, H.R. Zeller, "A fractal model for dielectric breakdown and prebreakdown in solid dielectrics", J. Appl. Phys., vol. 60, pp. 1770-1773, 1986.

[Williams97] G. Williams, "Theory of dielectric properties", in *Dielectric spectroscopy of polymers-fundamentals and applications*, edt. J.P. Rundt, J.J. Fitzgerald, American Chemical Society, Washington, 1997.

[Williams70] G. Williams, D.C. Watts, "Non-symmetrical dielectric relaxation behavior arising from a simple empirical decay function", Trans. Far. Soc., vol. 66, pp. 80-85, 1970.

[Wintle70] H.J. Wintle, "Decay of static electrification by conduction processes in polyethylene", J. Appl. Phys., vol. 41(10), pp. 4004-4007, 1970.

[Wintle72] H.J. Wintle, "Surface decay in insulators with nonconstant mobility and deep trapping", J. Appl. Phys., vol. 43(7), pp. 2927-2930, 1972.

[Wintle73] H.J. Wintle, "Absorption current, dielectric constant and dielectric loss by tunnelling mechanism", J. Appl. Phys., vol. 44(6), pp. 2514-2519, 1973.

[Wintle83] H.J. Wintle, "Conduction processes in polymers" in *Engineering dielectrics vol IIA-Electrical properties of solid insulating materials: molecular structure and electrical behavior*, edt. R. Bartnikas, R.M. Eichhorn, ASTM Special Technical Pub 783, ASTM Pub, Philadelphia, 1983.

[Wintle85] H.J. Wintle, S. Kurylowicz, "Edge corrections for strip disc capacitors", IEEE Trans. Inst. Meas., IM-34(1), 41-47, 1985.

[Wintle99] H.J. Wintle, "Charge motion and trapping in insulators", IEEE Trans. Diel. Elect. Ins., vol. 6(1), pp. 1-10, 1999.

[White69] J.S. White, "The moments of log-Weibull order statistics", Technometrics, vol. 11(2), pp. 373-386, 1969.

[Wood72] M.H. Wood, M. Barber, I.H. Hillier, J.M. Thomas, "Experimental and theoretical study of the valence band of polyethylene", J. Chem. Phys., vol. 56(4), pp. 1788-1789, 1972.

[Xu94] J.J. Xu, S.A. Boggs, "The chemical nature of water treeing: theories and evidence", IEEE Elect. Ins. Mag., vol. 10, n. 5, pp 29-37, 1994.

[Zeller87] H.R. Zeller, "Thermodynamics of water treeing", IEEE Trans. Elect. Ins., vol. 22(6), pp. 677-681, 1987.

[Zeller91] H.R. Zeller, "Noninsulating properties of insulating materials", in Proc. Conf. CEIDP, pp. 19-47, 1991.

[Zichy72] V.J.I. Zichy, "Quantitative infrared analysis of polymeric materials", in *Laboratory methods in infrared spectroscopy*, edt. R.G.J. Miller, B.C. Stace, 2nd edt., Heyden&Son, Ltd., London, 1972.

Appendix A. Siemens Procedure for dyeing with Methylene Blue

Procedure described by Shaw&Shaw [Shaw84])

Preparation of a methylene blue dye solution:

1. 6g of methylene blue (microscopy quality [a] and 0.5 g of Na_2CO_3 (analysis quality, anhydrous) are introduced into a 250 ml glass beaker and then topped up with distilled water to 200 ml.

2. The dye solution is heated to (70±2.5) °C with stirring (magnetic agitator) and kept at this temperature for 4h while the stirring is continued.

3. At the end of the 4h, the dye solution is not yet ready for use but has to be maintained at 70°C for a few hours (through thermostatic control) before it is used for the first time. Therefore the covered beaker shall be placed in a heating cabinet preheated inside to 70°C. A residence time should not be less than 20h as otherwise a granular deposition of dye may form on the thin cut PE sections. A residence time of 20h can be considered as an optimum.

Use of methylene blue dye solution

1. The thin cut sections should always be touched with gloves (e.g. vinyl gloves). Touching the thin cut sections directly with the fingers may have the consequence that the contacted areas do not take up as much dye.

2. Each time before it is used, the dye solution shall be stirred (with a magnetic agitator) for not less than 15 min at 70°C while the beaker is kept covered with a film.

3. Subsequently the thin cut sections shall be immersed in the dye solution [b]. The beaker containing the sections shall be covered again and placed in a heating cabinet pre-heated to 70°C. Experience has shown that the optimum residence time is normally 5h.

4. At the end of the residence time the thin cut sections shall be removed from the dye solution and rinsed with warm water for preliminary cleaning. Following this the thin cut sections shall be placed in ethanol for a few minutes and then be wiped thorougly with a paper tissue impregnated with ethanol.

By this treatment the surfaces of the thin cut sections shall be cleaned of any dye residues [c].

By experience the dye solution can be re-used and kept at room temperature for later use.

Hints for handling methylene blue

The label on the tin makes it clear that methylene blue is detrimental to health, in particular when ingested. This chemical substance, however, is not listed as a detrimental material, but when handling methylene blue, general laboratory precuations are to heed.

In case any dye solution gets into the eyes, these should be washed immediately.

Notes:

[a] Quality of methylene blue is extremely important. Impure dye produces agglomerations in the dyed specimen.

[b] Sections must be kept separated from each other.

[c] Dye tends to exude as sections are cooled.

Appendix B. Fractal geometry

Fractal from the Latin fractus
(irregular, broken, fractured).
B. B. Mandelbrot

The paper published by B. Mandelbrot in 1967 [Mandelbrot67] introduced the fractal geometry. In 1975 it was the first time that Mandelbrot used the term *fractal* [Mandelbrot75]. But it was his book published in 1982 [Mandelbrot82] that made well known the concept of *fractal objects*.

Today fractals are useful in many branches of science and when the other approaches fail. This appendix does not intend to describe the concepts of fractal geometry. It is only a very brief review of terms.

a) Fractal object and fractal dimension

One of the features of a fractal is the *fractal dimension* (a non-integer value corresponds to a fractal while an integer one to a non-fractal object). For instance a line has dimension 1, a square dimension 2 and a cube dimension 3, a fractal embedded in a 3-dimensional Euclidean space will have a fractal dimension between 2 and 3 (for example a tree). The classical example of Mandelbrot is the length of the coast of Britain [Mandelbrot67]. If a coastline was a polygonal line its length would be uniquely determined regardless of the precision of the ruler used to measure it. If the finest division of a ruler is 1 cm or 1 nm the measurement results would be exactly the same. However a coastline is sinuous, curved, it bends and winds so if we use the step of a man or the step of an ant the end results will give different values (see Figure A.1). The coastline is a fractal object not a polygonal line. This implies that it is too complex to be considered a one-dimensional object but it is not a two-dimensional area. For a line, area, volume or hypervolume the dimension is given by

$$L(\varepsilon) \propto \varepsilon^{D}, \tag{B.1}$$

where ε is the measurement unit[86] and D is the euclidean dimension (1 for a line, 2 for an area, 3 for a solid, etc.).

---

[86] For the coastline it can be a segment with fixed length (the finest division of the ruler) and the length is just the sum of all the measurement units needs to cover the line.

For a fractal object the value of D can be a fractional number and it is called the fractal dimension (the coastline dimension is a fractional number between 1 and 2). The definition in Equation (A.1) generalised for the fractal object is called the Hausdorff-Besicovitch dimension [Mandelbrot82] and there are other definitions of fractal dimension as it will be seen below (where D, an integer number, is replaced by D_f, a real number).

Figure A.1 – A coastline is a self-similar fractal object. In the figure is an example, part of the coastline of the Norway [Feder88]. The number of squares and therefore the value of the length are dependent on the size of the squares.

An important property of a fractal is *self-similarity* which means that zooming at the coastline using different scales we always see similar features. The small turns and bends are similar to the larger scale ones, as if each small part of the object is just a small scale copy of the whole fractal object. So the self-similar fractal object has an internal homothety.

The dimension calculated in this work for the water trees in 6.7 and 7.6 (using a box-counting algorithm) is the *capacity dimension*. The capacity dimension of a fractal object is a real number

$$D_f = -\lim_{\varepsilon \to o^+} \frac{\log N}{\log \varepsilon}, \tag{B.2}$$

where N is the minimum number of sets[88] of diameter less than or equal to ε needed to cover the all object (if the limit exists). A relatively easy to implement algorithm was developed based on this definition. The *box counting algorithm* uses different size sets (for instance, squares or cubes for an embedded 2 or 3 dimensional Euclidean space) to cover the fractal object under study and calculates the slope of the log-log plot of the number of sets vs. ε. The slope is equal to the fractal dimension.

b) Multifractals

When a fractal set is not a simple fractal but it is composed of sub-fractal sets with different scaling (fractal) characteristics it is called a *multifractal* [Feder88]. This concept was, once again, introduce first by B. Mandelbrot (see, per example, [Mandelbrot82]), applied to the study of turbulence and, according to Feder [Feder88], it is many times related to the study of a distribution of a physical or other quantities in a geometric support. Multifractality has been applied to the study of DLA (diffusion limited aggregation) and other growth phenomena including viscous fingers [Stanley88]. Since water treeing is a growth process it is most probable that a multifractal study can also be used.

An important definition to characterise multifractal is the generalised dimensions introduced by Grassberger [Grassberg83]. As it is well known, when the box-counting method is used to calculate the fractal dimension, the fractal object is covered with boxes of size ε. The box is counted if at least one point of the fractal is in the box. However a box can contain more than one point. If the number of points in each box was also counted, a probability distribution (like a density distribution) could be defined characterised by its moments [Stanley88]

$$Z(q) = \sum_i n(\mu_i)\mu_i^q, \tag{B.3}$$

where q is an integer ($-\infty < q < +\infty$), $n(\mu_i)$ is the number of boxes with fraction of points $\mu_i = \frac{N_i}{N_t}$ (N_i is number of points in box i and N_t is the total number of points). This fraction can be associated to an occupation probability.

The generalised dimensions are defined by

[88] In a embbeded space of dimension 2 the set can be a square of side ε, a circle of radius ε, etc.

$$D_q = \frac{1}{q-1}\lim_{\varepsilon \to o} \frac{\log \sum_i N(q,\varepsilon)}{\log \varepsilon}, \tag{B.4}$$

$N(q,\varepsilon) = \sum_i \mu_i^q$ is the weighted number of occupied boxes.

The generalised dimensions calculated in this work are:

For $q = 0$, $N(q,\varepsilon)$ is just the total number of occupied boxes and $D_0 = D_f$.*(capacity dimension)*.

For $q = 1$, D_1 is called the *information dimension* because $N(q,\varepsilon)$ is the analogous the Shannon information entropy. It quantifies the non-uniformity of the point distribution.

For $q = 2$, D_2 is the *correlation dimension* (a measure of the distance between pairs of points).

This formalism can be treated in similarity with the thermodynamic formalism since $Z(q)$ is analogous to the thermodynamic partition function. An exponent $\alpha(q)$ is defined characterising the singularities of fractal set. A $f(\alpha)$ function is related to these exponents:

$$\begin{aligned} f(\alpha) &= q\alpha(q) + \tau(q) \\ \alpha(q) &= \frac{d}{dq}\tau(q) \end{aligned} \tag{B.5}$$

these two equations represent a Legendre transform. Comparing with the thermodynamic formalism $\tau(q)$ is similar to the energy and $f(\alpha)$ to the entropy [Stanley88].

Appendix C. Published papers

The more representative published papers are:

- P. Judenstein, M.C. Lança, J. Marat-Mendes, J. Rault, "Pore dimension of water trees in PE: NMR studies", Polymer, vol. 41, pp. 8151-8154, 2000.
- M.C. Lança, L.A. Dissado, J.N. Marat-Mendes, "The fractal analysis of water trees: an estimate of the fractal dimension", IEEE Trans. Diel. Elect. Ins., vol. 8(5), pp. 838-844, 2001.
- M.C. Lança, E.R. Neagu, J.N. Marat-Mendes, "Combined isothermal and non-isothermal current measurements applied to space charge studies in low-density polyethylene", J. Phys. D: Appl. Phys., vol. 35, pp. L29-L32, 2002.
- J. Mateo, M.C. Lança, J.N. Marat-Mendes, "Infrared spectroscopy studies of aged polymeric insulators", Advanced Materials Forum I, Key Eng. Mat., vol. 230-232, edt. T. Vieira, pp. 384-387, 2002.
- M.C. Lança, C.J. Dias, D.K. Das Gupta, J. Marat-Mendes, "Dielectric properties of electrically aged low density polyethylene", Advanced Materials Forum I, Key Eng. Mat., vol. 230-232, edt. T. Vieira, pp. 396-399, 2002..
- M.C. Lança, E.R. Naeagu, J.N. Marat-Mendes, "Studies of space charge in electrically aged low density polyethylene", in Proceedings of the 11th International Symposium on Electrets (ISE11), edt R.J. Fleming, pp 19-22, IEEE, Monash (Australia) ,2002.
- M.C. Lança, E.R. Naeagu, R.M. Neagu, C.J. Dias, J.N. Marat-Mendes, "Space charge studies in LDPE using combined isothermal and non-isothermal current measurements", submitted for publication in IEEE Trans. On Diel. Elect. Ins.

:LSEVIER

Polymer 41 (2000) 8151–8154

polymer

www.elsevier.nl/locate/polymer

Polymer Communication

Pore dimension of water trees in PE: NMR studies

P. Judeinstein[a], M. Carmo Lanca[b], J. Marat-Mendes[b], J. Rault[c,*]

[a]*RMN en milieu Orienté, ESA 8074, Bat.410, Université Paris-Sud, Orsay 91405, France*
[b]*Seccao de Fisica Aplicada, Univeresidade Nova de Lisboa 2825, Monte de Caparica, Portugal*
[c]*Laboratoire de Physique des Solides, Université Paris-Sud, Bat 510, CNRS, Orsay 91405, France*

Received 28 February 2000; Received in revised form 4 April 2000; accepted 7 April 2000

ıstract

In PE films aged under electric field the crystallisation of water (and melting of ice) has been studied by quadrupolar NMR, this technique ows one to determine the concentration of water as low as 10^{-4}. It is shown that the pore dimensions of the tracks forming the water trees of : order of 2.5 nm, are independent of the ageing time. The mobility of water in these water trees and in porous glass, of similar pore nensions, are compared. © 2000 Elsevier Science Ltd. All rights reserved.

ywords: Pore dimension; Water trees; Polyethylene films

Introduction

Insulating polymers have been widely used in power bles. The most common material used in high and :dium voltage cables is polyethylene. Under service nditions electrical ageing of the insulation is inevitable d may in the long run give rise to costly cable failure. At : first stage of ageing water treeing may occur. Even if it is t a direct cause of dielectric rupture their presence consid- ıbly reduces the breakdown voltage. Water trees appear as sh structures filled with water with a length ranging from μm to about 1 mm, they are composed of disconnected res (also called tracks) of diameter in the nanometer ıge. However, up to now, there is no non-destructive :hnique for measuring the lateral dimension of such croscopic tracks. The track surface is hydrophilic allow- ; diffusion of water (and other polar species, such as ions). :eption of water trees starts in the presence of an aqueous lution (with ions) and an alternate high electric field. ıdies have shown the influence of many factors in the :eption and growth of water trees such as temperature, :hanical stress, type and concentration of ionic salts, plied electric field (frequency and amplitude), polymer ɔrphology and composition, etc. Due to the complex :hanisms involved in the nucleation and propagation of ıter trees in polymer insulators, conflicting results have en reported; models involving electromechanical and electrochemical processes are still under development [1–5]. The aim of this paper is to show that quadrupolar NMR gives information on the amount of water absorbed in these materials and on the size dimension of the tracks created by electrical ageing.

2. Experimental

In this work, low density polyethylene (LDPE) from Borealis, with a density of ≈ 0.92, was aged under an AC electric field (6 kV/mm at 50 Hz) in the presence of an aqueous solution of sodium chloride (1 M) at a constant temperature of 45°C for different time periods (475 and 900 h). Disc shaped samples of ≈ 200 μm thickness and diameter of ≈ 30–35 mm were press-moulded from pellets. Afterwards, the samples were sandblasted in order to increase the number of initiation sites for water trees, and then the amount of water in the aged material. For ageing, a modified Cigré cell [3,4] was used with the aqueous solution acting as electrodes on both sides of the disc shaped samples (planar electrodes), as can be seen in Fig. 1. The aged LDPE samples and the virgin sample (weight: 200 mg) were soaked in heavy water for 2 days. Water in these materials cannot be detected by differential scanning calorimetry (DSC).

NMR experiments on the aged film swollen with D_2O were performed with a Bruker AM250 spectrometer equipped with a 5 mm broad-band probe without field/frequency lock control. The film is rolled in the NMR tube, the magnetic field is perpendicular to the film

Corresponding author.
E-mail address: rault@lps.u-psud.fr (J. Rault).

: S0032-3861(00)00281-0

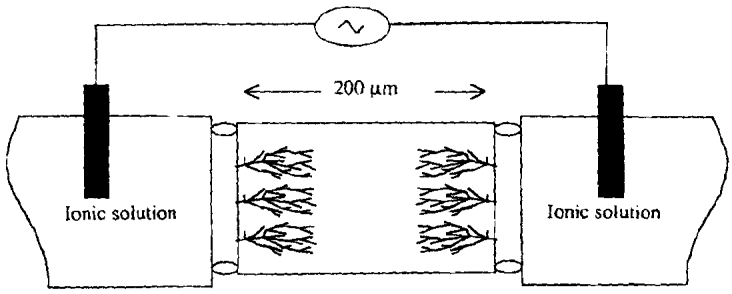

Fig. 1. Electrical ageing set-up for disk shaped LDPE samples with a diameter of 5 cm, the film thickness is 200 μm. Water trees with an average length of 20–50 μm are formed on both sides of the film.

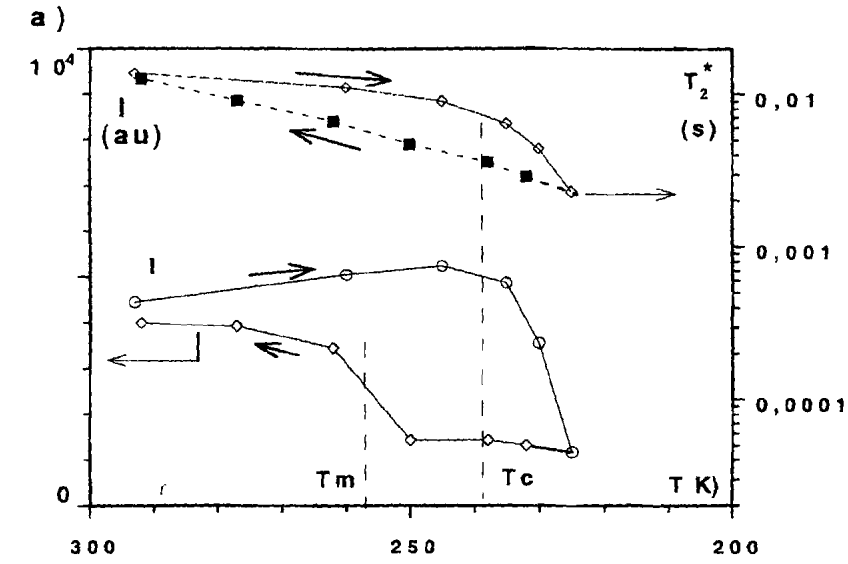

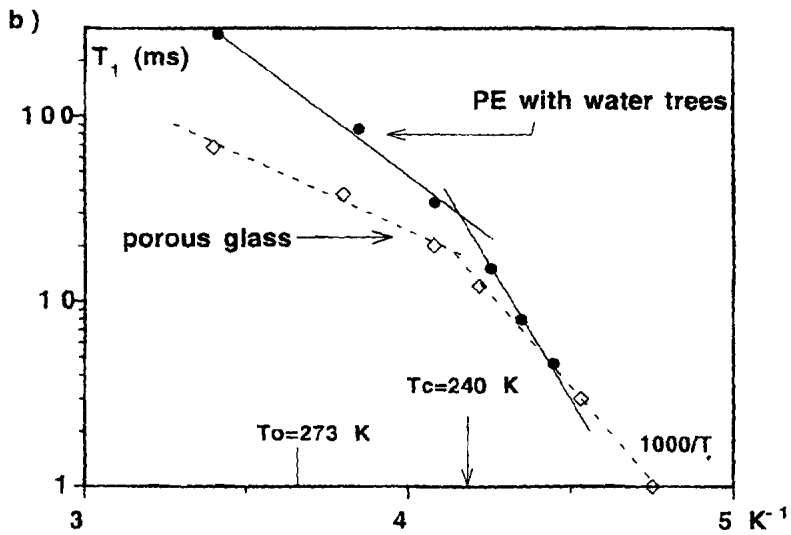

Fig. 2. (a) Evolution of the quadrupolar deuterium NMR signal due to heavy water absorbed in PE water trees: surface area I in arbitrary units and t transversal relaxation time T_2^*. (b) Spin–lattice relaxation time T_1 of heavy water in PE water trees and in silica glass of dimension 2.5 nm, in de temperature.

ckness, that is to say perpendicular to the propagation of : water trees through the sample, during the electrical eing. Temperature was controlled in the range of 210–0 K by a Bruker VT100 system (±1°C regulation). ^2H ectra were recorded at a frequency of 38.376 MHz. The nsients (FID) were obtained using a $\pi/2$ pulse width 4 μs) and a recycle delay of 2 s, 800 transients were ually added to obtain spectra with a good signal-to-ise (S/N) ratio. The FID signals were typically sampled th 4 K real data points over a 10 000 Hz spectral width, l an exponential line broadening of 5 Hz was used (which small compared to the experimental line width). Peak as and line widths were obtained by deconvolution h a single Lorentzian shaped curve. T_1 values were ained by the inversion-recovery method (delay–π–τ–2–acq.)$_n$ using 12 different τ(values to obtain the T_1, lowing standard procedures [6].

Results and discussion

The concentration of water in these films (polymer weight g) has been measured by comparing the NMR integrated nal intensity (peak area after 800 scans) containing uterium water in pores with a standard sample containing imilar amount of heavy water. For an electrical ageing of) h, a weight fraction of $c = 6 \times 10^{-4}$ of water is found. e virgin sample after 8000 scans did not present an NMR nal, so one can estimate that the (mobile) water concen-ion is at least 500 times less than in the aged material. In . 2a, the total intensity I of the NMR peak and the effec-e transversal relaxation time, T_2^*, (deduced from the line dth $w = 1/\pi T_2^*$) as a function of temperature, during cool-and heating experiments is reported. In Fig. 2b a nparison of the T_1 spin–lattice relaxation times of deut-ted water in a PE film with water trees and in porous glass lica Gelsil glass from Geltech company) of pore dimen-n $d = 2.5$ nm is given. These porous glasses have been died by various techniques, in particular by DSC and lectric spectroscopy [7,8]. Between each measurement corresponding time is about 1 h (30 min for thermal uilibrium and 30 min for measurement).

When the temperature is decreasing, at first the total ensity increases: this is the classical Curie law observed bulk water and in porous glass. Near 260 K the signal reases abruptly by a factor of 5, similarly, in the same mperature domain the relaxation time T_2^* decreases. Such ects could be due to the freezing of water as a result of stallisation or to amorphisation passing through the glass nsition at T_g.

When temperature is increasing, at first the signal inten-y is constant and then increases abruptly at 240 K, the dth w of the NMR peak decreases continuously. The portant hysteresis observed in the intensity measurement not be interpreted in terms of a glass transition: the glass nsition of water is about 140 K and the hysteresis of such a transition is generally very weak. The broadening of the glass transition in most compounds is larger (20–30 K) than the width observed here (<10 K). Also, this transition must not be confused with the λ transition observed near 228 K in pure bulk water [9]. These effects must be interpreted in terms of crystallisation; such important hysteresis effects were already observed in porous silica glass [10–13] filled with water and in butyl rubbers containing small pores [13]. In these materials, DSC measurements were possible because the amount of water was large ($c = 0.80$ instead of 10^{-4} in aged PE).

The melting and crystallisation depression temperatures, $\Delta T_m = T_m^0 - T_m$ and $\Delta T_c = T_c^0 - T_c$, of water in porous glass has been measured by various authors [10–14], T_m^0 and T_c^0 being the ice melting and crystallisation temperatures in bulk water. As shown by Neffati [7], the depression ΔT_m of water in various porous glass and polymers containing holes always obeys the same Thompson equation: $\Delta T_m = 49/d$ (d in nm). Brun [10,11] has shown that the crystallisation depression verifies a similar expression: $\Delta T_c = 64.7/(d - 0.6)$, this equation which is the basis of thermoporometry applies only if the cooling rate is lower than 0.6 K/min. In our NMR study, the equivalent cooling rate is of the same order, about 1 K/min.

It is important to note that the melting depression $\Delta T_m = 15 \pm 0.5$ K of ice in PE films, observed by NMR, is of the order of that observed in silica glass of pore dimension $d = 2.5$ nm (Neffati [7]). The crystallisation depression $\Delta T_c = 40$°K observed by this technique gives the same value of 2.2 nm when the Thomson–Brun equation is applied. The same value of ΔT_c is observed in butyl rubbers containing pores of the same dimension filled with water [7,8] One concludes that the sharp transitions observed by NMR in PE containing water trees are due to the first order crystal–liquid transition, confined in very small pores of dimension 2.5 ± 0.5 nm. It is important to remark that the width of the melting transition, less than 10°C, is smaller than the width of the DSC endotherm peak observed in silica glass, 15–20°C. This suggests that the distribution of pore size in aged PE is sharper than that in porous glass.

In Fig. 2b, one notes that after crystallisation at T_c around 240 K for these two types of materials, the spin–lattice relaxation time T_1 decreases more rapidly than before crystallisation. Assuming isotropic reorientation the relaxation rate $1/T_1$ due to quadrupolar interactions is given by: $1/T_1 = (3/8)(e^2qQ/h)^2(1 + \eta^2/3)\tau_c$, where $(e2qQ/h)$ is 2π times the nuclear quadrupole coupling constant in Hz, η is the asymmetry parameter (of the order of 1) and τ_C the reorientational correlation time [6]. It has been found experimentally by Liu et al. [14] that this correlation time varies as $\tau_C \approx 1/T_1 \approx 1/d$ for strong polar liquid interacting with the surface, and as $1/d^2$ for non-polar liquid interacting weakly with the surface. This last scaling law has been theoretically explained by Korb et al. [15]. In porous materials crystallisation of water has mainly two effects on the confinement of water: (a) when ice is formed in the larger pores, the

proportion of small pores filled with liquid water increases; (b) crystallisation cannot lead to ice crystallites matching exactly the surface of the pores (the surface can have a fractal dimension between 2 and 3), therefore some liquid water becomes confined between the pore surface and the crystallites, the larger pores are replaced by small pores during the process of ice formation. These two effects increase the correlation time in the low temperature domain when crystallisation occurs. The $T_1(T)$ curves of water in water trees PE and in silica glass are very similar because crystallisation occurs at the same temperature, at $T_c = 240$ K. The same behaviour is observed in butyl rubbers containing pores of the same dimension [7]. One notes, however, a difference in the values at high temperature: probably this effect could be due to the different interaction of water with the functional groups attached to PE and silica surfaces [16,17].

We have performed similar studies on PE aged during 375 h under the same electric field. The intensity and the line width varies in the same manner as that reported here, therefore the structure of the water trees seem to be very similar during its growth.

4. Conclusions

NMR spectroscopy demonstrates that water crystallises in the small pores formed in PE when submitted to electrical ageing. This property permits one to estimate the dimension, $d = 2.5 \mp 0.5$ nm, of the pores via the Thompson and Brun relations. The accuracy of NMR permits one to measure the mobility and the amount of liquid and crystallisable water in weight fraction as low as 10^{-4}, this accuracy can be easily improved by increasing the amount of material in the NMR tube, and by increasing the NMR frequency and the scan number. The study of different films aged under different ageing times and electric fields show the same trends in the crystallisation temperature of water. Therefore, the dimension of the pores (tracks) are of the same order: this indicates that during the growth of water trees, new canals (or pores) are formed and there is no thickening of the pores previously formed at the beginning of the process (Fig. 1). Ice formations in PE containing water trees and in silica glass of pore are very similar; the hydrophilic character of silica glass is due to the OH groups attached to the surface, it is also well known that the surfaces of pores in PE contain various polar groups due to the oxidation during electrical ageing [5]. One emphasises however, that in polymers some additional effects could occur: the electrical treatment produces polar groups grafted on the surface of the pores and certainly with a certain thickness, also some chains are disrupted; so the interface should not be considered as sharp but continuous with a gradient of density of polar groups concentration and, therefore, of mechanical properties. These effects should also have an influence on the dynamics of confined water.

Acknowledgements

The authors would like to thank Dr J. Houlgreave and his co-workers for kindly lending some modified Cigré cells, Borealis for the LDPE pellets and Mr F. Pedroso of BICC-Celcat (Portugal). We also want to thank Drs Apekis, Neffati and Dias for stimulating discussions.

References

[1] Dissado LA, Forthergill JC. Electrical degradation and breakdown in polymers. London: Peter Peregrinus, 1992.
[2] Dissado LA, Forthergill JC, editors. Space charge in solid dielectric Leicester: The Dielectric Society, 1998.
[3] Ross R. IEEE Trans Dielect El 1998;5:660.
[4] Fothergill JC, Eccles A, Houlgreave JA, Dissaldo LA. IEEE Proc A 1993;140(5):397.
[5] Moreau E, Boudet A, Mayou C, Laurent C, Wright M. J Mater Sci 1991;28:161–9.
[6] Harris RK. Nuclear magnetic resonance. London: Pitman, 1983.
[7] Neffati R. PhD thesis. Université d'Orsay, France, 1999.
[8] Pissis P, Laudat J, Kyritsis A. J Non-Cryst Solids 1994;171:201.
[9] Lang EW, Lüdermann HD. Angew Chem Int Ed Engl 1982;21:315.
[10] Brun M, Lallemand A, Quison JF, Eyrauld C. Thermochim Acta 1971;21:59.
[11] Brun M. Thesis. Lyon, France, 1973.
[12] Henda YP. Phys Chem 1992;96:8594.
[13] Neffati R, Apekis L, Rault J. J Therm Anal 1998;V54:741.
[14] Liu G, Li Y, Jonas J. J Chem Phys 1991;95:6892.
[15] Korb JP, Xu S, Jonas J. J Chem Phys 1993;98:2411.
[16] Arndt M, Kremer F. Mater Res Soc Symp Proc 1995;366:259.
[17] Streck C, Mel'nichenko Y, Richert R. Phys Rev B 1996;53:5341.

The Fractal Analysis of Water Trees

An Estimate of the Fractal Dimension

M. Carmo Lança, J. N. Marat-Mendes

Departamento de Ciência dos Materiais
Seccá de Fisica Aplicada (CENIMAT)
Faculdade de Ciências e Tecnologia
Universidade Nova de Lisboa, Portugal

and L. A. Dissado

Department of Engineering
University of Leicester, UK

ABSTRACT

Water trees result from ac electrical aging of the polymeric insulation of medium and HV power cables in a humid or wet environment. As suggested by their name, they arise from penetration of water in the polymer. Visual observation with the help of an optical microscope shows tree (bush) type structures. This suggests that water trees might be fractal objects. Calculation of the fractal dimension from experimental samples may confirm the fractal characteristics and also give information on the damage caused to the polymer. In this work images of water trees taken under the optical microscope, dyed by methylene blue and etched for scanning electron microscopy (SEM), were studied in order to estimate the fractal dimension using a box-counting algorithm. The photographs, made using an optical microscope (scale of 100 μm), of the dyed samples were obtained from laboratory-aged low-density polyethylene (LDPE) specimens using accelerated techniques. Different field amplitude and frequency and also time of aging were used and the dimension values were compared. SEM images resulting from aged cross-linked polyethylene (XLPE) cables revealed a structure at a different scale (~ 3 μm). Each photograph was analyzed to compare regions with and without water trees.

1 INTRODUCTION

SINCE the late 1950's polymers have been used widely as insulation for power cables. In medium and HV power cables, low density polyethylene (LDPE) initially was used, but more recently crosslinked polyethylene (XLPE) has become the most common insulating material. In the early stage of electrical aging of PE (and other polymers) water treeing may occur. This phenomenon has been known for the last thirty years (for reviews, see [1, 2]). In the presence of an aqueous salt solution and under an ac high electric field, inception and growth of the water trees occur. Their presence facilitates the initiation of electrical treeing and lowers the breakdown strength, giving rise in the long run to costly cable failure. They appear as bush structures containing water, with a length ranging from ~ 10 μm to ~ 1 mm. Water treeing is a complicated process, and reproducible results are difficult to obtain due to the many parameters controlling it (temperature, electric field amplitude and frequency, polymer composition and morphology, type and concentration of ionic salts, mechanical stress, *etc.* [2]). Experimental evidence, either from laboratory aged samples or service aged cables, points to a complex electromechanical-chemical mechanism. Over the last few years some progress has been made in finding a theoretical model for water tree inception and growth [3].

Their ramified visual aspect has the appearance of fractal characteristics (see Figure 1). Studying the fractal characteristics of water trees may help gain some quantitative information leading to a better understanding of the underlying mechanisms. One of the features characterizing a fractal is the fractal dimension [4]. Calculation of this parameter can help to confirm the fractal character of the trees and also quantify the amount of damage caused to the polymer. In order to estimate the fractal dimension, some kind of permanent recording of the appearance of the water trees needs to be carried out. Different kinds of experimental images can be obtained. In this work two different types were analyzed, corresponding to water tree damage at two different scales (~ 200 μm and ~ 5 μm) and different characteristic structures can be seen as will be emphasized in Section 3:

1. One of the most common processes is dyeing the sample using methylene blue [5]. Trees are then observed using an optical microscope coupled to a photographic camera [6, 7]. Samples of LDPE, laboratory-aged

1070-9878/1/ $3.00 © 2001 IEEE

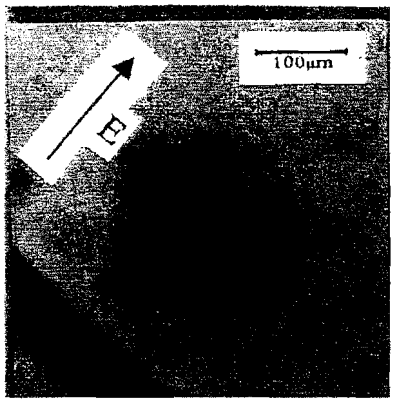

Figure 1. Water tree grown (bush-like) in LDPE aged at 50 Hz. Photograph showing a water tree growing along the electric field direction (courtesy of Houlgreave and coworkers).

at different electric fields (amplitude and frequency), and temperature were analyzed.

2. Images obtained using SEM. Samples came from laboratory-aged 11 kV, XLPE cable cores [8, 9].

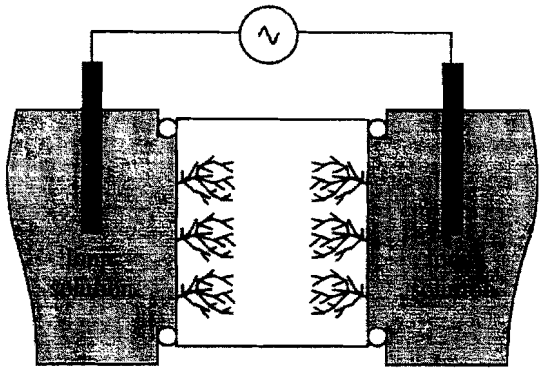

Figure 2. Schematic representation of the modified Cigré cell used in the Leicester and Lisbon experiments.

The images must be digitized and need to undergo an image treatment process (*e.g.*, reducing the image noise) before any calculation can be done. Since the authors had no knowledge of previous work on the fractal dimension of experimental water trees, a preliminary study had to be carried out in order to find the best possible method. Since the image treatment can influence the estimated value strongly, special care has to be taken with the method used. For (1) a simple thresholding technique was chosen after some testing, images resulting from SEM were not treated. Also, there are different definitions of fractal dimension, in this work the capacity dimension was chosen and numerical calculations were done using a box-counting algorithm [4]. Water trees are three-dimensional objects and photographic images are two-dimensional. As a first approach the fractal dimension was considered to be the computed dimension +1.

Results for different aging conditions will be presented and compared using images from (1). The aim of the study of the SEM images is to find differences in microstructures that could help to determine the relevance of shape and density of damage.

2 PRODUCTION OF WATER TREES AND THEIR IMAGES

2.1 METHYLENE BLUE DYED WATER TREES IMAGES

Water trees were produced in the laboratory using accelerated techniques. Some of the samples were aged at Leicester University [6, 10] and others at Lisbon [7, 11]. Both of them used press molded LDPE disc-shaped samples and a modified Cigré aging cell (developed by Houlgreave [6]) with NaCl solution acting as electrodes on both surfaces (see Figure 2 for a schematic representation). The cells were immersed in an oil bath kept at constant temperature. Applied fields varied from 3.0 to 11 kV/mm and frequency from 50 Hz to 3 kHz. To render the trees permanently visible the discs were dyed with methylene blue, using the technique described in Shaw *et al.* [5]. Photographs were obtained by coupling an optical microscope with a photographic camera (enlarged ($\simeq$100× or 400×). Photographs are then digitized and an image process treatment is applied (see Section 3). Figures 1 and 3 show typical examples of trees grown at different frequencies. The trees are bushlike if grown at 50 Hz while at 1.16 kHz they present the shape of viscous fingers. Photographs were taken along two different directions, one perpendicular and the other parallel (the disk-shaped samples were microtomed after aging) to the electric aging field. The difference between images along the direction of the applied field (parallel $\|$) and perpendicular ($\perp$) can be seen in Figures 1 and 4, respectively.

2.2 SCANNING ELECTRON MICROSCOPY IMAGES OF THE WATER TREES

As was stated previously, samples from laboratory-aged 11 kV XLPE cable cores were investigated also (for details see [8, 9]). A special etching technique was developed by Olley *et al.* [8], which is suitable for SEM analysis of water trees. Special care was put into sample preparation, because some procedures tend to destroy the connecting pathways. As shown in Figure 5, SEM allows the microstructure of the trees to be seen (order of magnitude down to ~ 5 μm). For the calculations some of the original photographs appearing in [9] were used. Like the photographs of the methylene-blue dyed samples they too were digitized.

3 IMAGE PROCESSING AND ESTIMATION OF THE FRACTAL DIMENSION

A digitized image has to undergo a treatment process chosen according to the purpose for which the image is to be used. In the present work we want to estimate the fractal dimension of the object represented in the image. We need to be able to distinguish the object from the surrounding background. In real images it is not easy to distinguish between object borders and other important features and characterize correctly which parts belong or do not belong to the water tree. A large number of image treatment techniques have been developed and it can

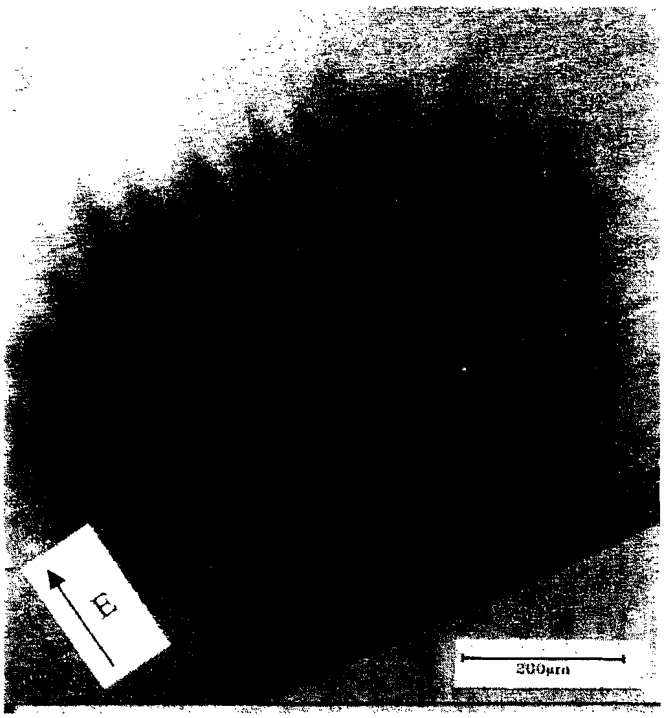

Figure 3. Water tree grown (viscous finger) in LDPE aged at 1.16 kHz. Photograph showing a water tree growing along the electric field direction, (courtesy of Houlgreave and coworkers).

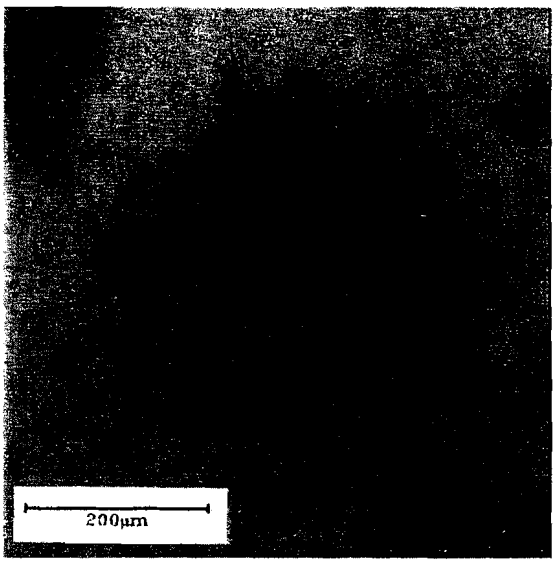

Figure 4. Water tree grown in disc shaped LDPE aged at 50 Hz. Photograph showing a water tree growing perpendicular to the electric field direction, ⊥ (courtesy of Houlgreave and coworkers).

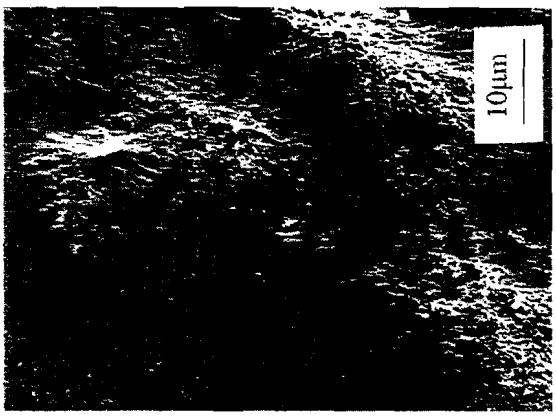

Figure 5. SEM image of water trees grown in XLPE cables (after Olley *et al.* [9]).

ɔe a difficult task to know which to apply to our specific problem. It is important to note that image treatment can influence the calculated value of the dimension. This is especially the case if the fractal dimension lies very near the Euclidean dimension in which the object is embedded.

3.1 METHYLENE BLUE DYED WATER TREES

These photographs are either the result of the projection in a two-dimensional space of the 3D structure, or the sectioning of the same 3D structure of the water tree. According to Mandelbrot [4] if the section is non-empty, for most fractals it can be considered

$$D_W = D_c + 1 \quad (1)$$

where D_W is the fractal dimension of the 3D water tree and D_c is the estimated fractal dimension of the 2D image (see Section 5.4 of [1] for a definition of fractal dimension as obtained from 2D projections). Kudo [12] has studied for electrical trees the relation of fractal dimensions estimated for the 2D projection and for the real 3D tree. If the structure is not very dense (fractal dimension <2) the projection has the same dimension as the parent tree. Both bush type electrical trees and water trees are very dense. Their projections can have a dimension of 2 (filling space completely), but the real tree dimension could actually be any value between 2 and 3. The real (3D) electrical tree dimension has been estimated by sectioning and reconstruction of the whole tree from the sections. Kudo [12] shows that for electrical trees with projected fractal dimension $\lesssim 1.65$, the projected and sectioning fractal dimensions are the same. However, when the projected fractal dimension is >1.65, the sectioning fractal dimension is increasingly higher than the projection, by a value that approaches 0.7 to 0.8 for the most dense trees. When a substantial fraction of the structure is filled it can have a much larger value of the fractal dimension than the projection (because of the obscured structure).

However, Equation (1) will be used for projections also. The addition of 1 to the projected dimension gives an upper bound. Water trees have projected structures that have a large part of the field filled in. It would therefore be expected for them to have a fractal dimension well above that of the projection, with d_p+1 being an upper bound, and d_p+0.7 possibly being a lower bound.

The aim of the image treatment is to find an image where we know undoubtedly what is part of the water tree and what is part of the background. Usually a binary image is created and for each point, *e.g.* value 0 corresponds to background and value 1 to the tree. Three dif-

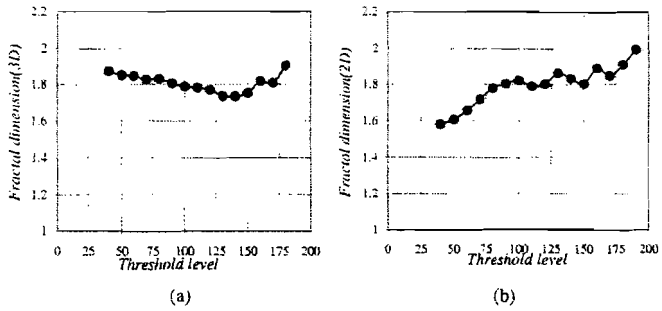

(a) (b)

Figure 6. Graph (a) shows the plot of the pseudo-fractal dimension (3D) with the threshold level (a minimum appears between threshold levels 130 to 140). From graph (b) the 2D fractal dimension (D_c) is obtained by choosing the value corresponding to the same threshold level of the minimum in (a). The fractal dimension of the 3D water tree is calculated as $D_c + 1$.

ferent processes were tried but only the last one gave acceptable and reproducible results. When the original image objects have well defined boundaries, good contrast and also a good resolution, a histogram of the distribution of colors or grey-tones shows sharp peaks. If this happens it is easy to distinguish between background and water trees, and with a simple threshold filter, it is then possible to get a binary image. For the images used, the peaks were not well defined and a more complex method had to be applied as will be explained later on. There are several different ways to define fractal dimension, as was stated before. In this work the capacity dimension is calculated using the box-counting numerical implementation. The algorithm used was introduced by Liebovitch and Toth [13] and improved by Hou *et al.* [14]. The computer implementation f_{d3} performed the calculations (f_{d3} is a shareware computer program based on the box-counting algorithm and developed by Sarraile and Di Falco). A normalization of coordinates was undertaken, considering the maximum value of all the coordinates to imply no change in the aspect ratio. A series of thresholds were performed on the same image (varying from totally white to totally black binary images). For each of the threshold images a fractal dimension was calculated. First for a 2D space (2D fractal dimension D_2) and then for a 3D space (3D fractal dimension D_3) where the third dimension was the grey-tone or color-level. A plot of D_3 *vs.* threshold level was made. D_3 starts with a value near 2, decreases and starts to increase until it again reaches 2. So there is a minimum (looking at the images it corresponds to the threshold level value at which the tree-like shape starts to be 'lost' in these plots). The minimum value of D_3 is thus the smallest fractal dimension for which the tree structure is retained. In Figure 6 the typical graphs for the 3D and 2D *vs.* threshold level are presented. In Figure 6(a), the minimum can be seen and for the same threshold level the corresponding fractal dimension is obtained from Figure 6(b). However, this minimum can be very difficult to determine, and for some tree images are impossible. But for those where the minimum is defined, the fractal dimension can be calculated.

There are problems associated with the calculation of the fractal dimension from experimental objects. In the results presented here no particular study was made of the influence of image treatment in the calculated values (in Lança and Dissado [11] the influence of resolution was studied briefly).

Table 1. Results for capacity dimension estimation (Leicester samples). results obtained from the application of the algorithm to the 2D images and applying Equation (1). The shown error limits result from the least square fitting of the box-counting algorithm. They are not the 'real' errors.

Sample	Position	f Hz	E kV/mm	Aging h	Capacity dimension
1	∥	50	8	800	2.79±0.03
2	∥	50	8	800	2.85±0.04
3	∥	50	8	100	2.81±0.06
4	⊥	50	8	800	2.84±0.04
5	⊥	50	5	1000	2.86±0.02
6	∥	1160	5	1200	2.86±0.03
7	∥	1160	5	950	2.78±0.02
8	∥	1160	5	950	2.74±0.02
9	∥	1160	5	950	2.86±0.03
10	⊥	1160	5	950	2.85±0.03

3.2 SEM IMAGES

The available SEM images of the water trees are black and white photographs (see Figure 5). They are not 2D projections but result from a planar cut in the polymer. In the digitized images the grey tone of each point can be related to the relief in the polymer surface. As a first attempt to estimate the fractal dimension a pseudo-fractal dimension was calculated. A three-dimensional space was considered by taking the third dimension as the grey tone. This dimension does not represent a true fractal dimension for the Euclidean (physical) space where the water tree grows.

4 RESULTS

4.1 METHYLENE BLUE DYED WATER TREES

For the two sets of samples used:

1. The first set corresponds to LDPE samples aged at the University of Leicester by Houlgreave *et al.* [6]. Samples were aged under an electric field varying from 5 to 8 kV/mm and for two different frequencies, 50 Hz and 1.16 kHz (see also [10]). The aqueous solution was 0.05 M NaCl and aging temperature (31±4)℃. As can be seen in Figures 1 and 4, respectively, some of the photographs show growth along the direction perpendicular to the applied field, ⊥ (samples were microtomed), and the others parallel to the field, ∥. For results see Table 1. The algorithm used by f_{d3} also calculates higher order fractal dimensions (see the Appendix for the term multifractality): the so-called information and correlation dimensions. These results are given in Table 2 (Equation (1) was also used).
2. The second set of LDPE samples were aged in Lisbon (FCT/UNL). The aging electric field amplitude varied between 3.5 and 6.5 kV/mm and the frequency was 1.0 kHz. The aqueous solution was 0.1 M NaCl and aging temperature (50±2)℃. All images were obtained in the direction parallel to the field (see Figure 7). Results are presented in Table 3. The images of the trees grown at 1 kHz are very dense and bushlike (as can be seen in Figure 7).

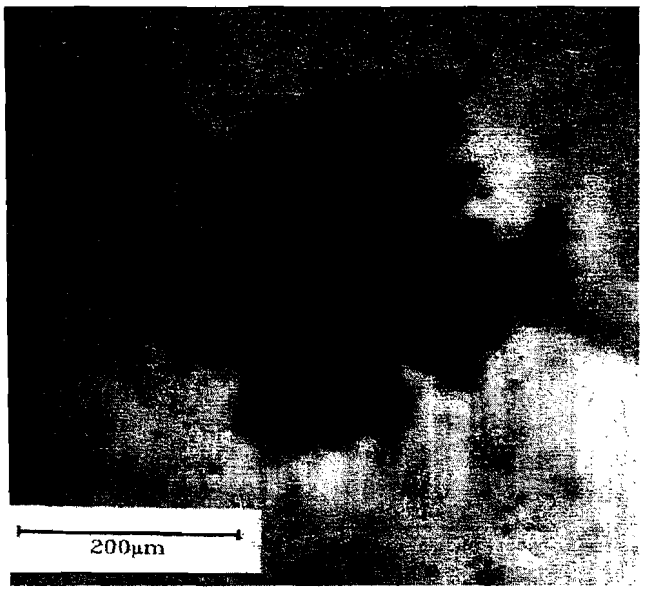

Figure 7. Water tree grown in disc shaped LDPE aged at 1 kHz (Lisbon set). Photograph showing a water tree growing perpendicularly to the electric field direction, ⊥.

Table 2. Multifractal analysis (same images as Table 1).

Sample	Information dimension	Correlation dimension
1	2.84	2.88
2	2.87	2.86
3	2.84	2.84
4	2.87	2.89
5	2.89	2.89
6	2.91	2.91
7	2.86	2.89
8	2.86	2.88
9	2.90	2.90
10	2.90	2.90

4.2 SEM IMAGES

A study was made to compare different regions of the image. Parts he background (showing no trees) and of trees (well into a highly ıaged area or at the edges of the tree) were studied. No image treatıt was applied. The results of the 3D analysis are given in Table 4.

5 DISCUSSION

From the set of results in Section 4.1 (methylene blue dyed sam-) the fractal dimension of water trees seems to be very close to 3. ɔection of the photographs shows that this result is expected since water trees are quite dense structures (specially when compared h electrical trees [12]). In [1] (see pages 92 to 94) it is shown that if water tree grows by the addition of elementary volume units, with ı addition being added sequentially in a defined time, then the tree ɜth L is given by

$$L^{d_f} \propto t \tag{2}$$

ɜre t is the aging time and d_f the fractal dimension of the tree (see tion 5.4 of [1] and Equation (3) below for a definition). The experimental data for water trees grown in similar stressing geometries to those used here, analyzed in [1], indicate a value of d_f=3, though the gradients of the $\log(L)^3 - \log t$ plot could equally well fit a fractal dimension of between 2.8 and 2.85 as found here. The fractal dimension, as found by direct measurements, therefore appears to be consistent with that deduced from the water tree growth law. A brief analysis of our data seems to indicate no relevant difference between the estimated values of d_f for samples aged under different experimental conditions (temperature, aging time field amplitude, and frequency). It is interesting to note that water trees with different physical aspects such as the those grown at 50 Hz and 1.16 kHz (Figures 1 and 3) have similar values of fractal dimension (capacity, information and correlation).

For images perpendicular to the field, no significant difference is observed between the Leicester and Lisbon samples, Sections 4.1 (a) and 4.1 (b). The images parallel to the field seem to have on average slightly lower values for the fractal dimension than the ones perpendicular to the field. Parallel images were microtomed and found to correspond to thin slices (<20 μm). When the photographs are made from un-cut samples (≈200 μm to a ≈2 mm thick) the projection is denser and

Table 3. Results of the fractal dimension for water trees grown in LDPE (Lisbon Samples), results obtained from the application of the algorithm to the 2D images and applying Equation (1). Sample 1 was aged for two different periods, applying different voltages to the electrodes. Samples 2 and 3 are different trees photographed from the same LDPE disk. (Frequency 1.0 kHz; solution 0.1 M NaCl at 50°C).

Sample	E kV/mm	Aging h	Capacity dimension
1	5.5	31:00	
	3.3	21:00	2.85±0.01
2	3.5	33:25	2.88±0.02
3	3.5	33:25	2.84±0.02
4	6.5	48:50	2.88±0.01

Table 4. SEM Images (3D analysis).

Image	Detail	Dimension	Notes
1	All	2.32	
	Tree	2.54	Well inside a damaged area
	Tree edge	2.5	Belongs to the tree edge
	Tree edge	2.32	More background than the previous
	Background	2.32	
2	All	2.5	
	Tree	2.51	
	Tree	2.53	Inside the tree
	Tree edge	2.58	
	Background	2.44	
3	All	2.3	
	Tree	2.2	
	Tree edge	2.32	
	Background	2.26	
4	All	2.40	
	Tree	2.54	
	Tree	2.58	Highly damaged area
	Tree	2.44	Less damaged area than the previous
	Background	2.39	
5	All	2.4	
	Tree	2.35	
	Tree	2.50	Less background than the previous
	Tree	2.55	Less background than the other two
	Background	2.29	

the entire tree is projected (images perpendicular to the field). For the cut samples (parallel to the field) only the part of the tree present in that slice is projected so they could be associated to sections of the tree. The resulting image is not so dense and the estimated fractal dimension would be smaller. Also since Equation (1) is expected to be valid for sections, the value calculated from those images can be a better estimation of the water tree real fractal dimension. While an upper bound had to be chosen for the projected images the different values observed can reflect this approximation. Probably instead of adding 1, a value slightly smaller would be a better approach to the real fractal dimension. The value found for electrical trees was 0.7 to 0.8 (Kudo [12]). However it must be noted that electrical trees are connected tubes while water trees are structures that include cavities as well as very fine connections. So it would be expected that water trees would exhibit a higher percentage of space filling than electrical trees. Also the water treeing time dependence indicates that growth is almost space filling. Therefore the estimated values are consistent with what is expected for water trees. Since we are dealing with an upper bound, any value of the fractal dimension <3 indicates that the water tree is a fractal structure.

For the SEM images conclusions seem to point to lower values of the fractal dimension for the background and the regions of higher damage in the tree. This seems to result from the higher uniformity in these areas, when compared to the tree edges.

It is interesting to refer to a recent NMR determination of pore size in water treed LDPE [15]. Samples electrically aged under similar laboratory conditions (aging temperature was 40℃), but for different aging times, showed the same pore size, 2.5± 0.5 nm. This points to a minimum size of damage in the form of water filled pores and cavities in water trees, with just their number increasing with aging time. The question of the damage density now arises. In Euclidean objects, the density is defined easily as the mass per unit volume. For fractals, the density depends upon the size of the object over which it is measured. For example, the mass of the fractal object (of dimension d_f) contained within the box of volume L^3 is proportional to L^{d_f}, the density of the object is thus proportional to L^{d_f-3}, and hence decreases as its overall size increases. In the case of water trees we can take the damage to be the amount of pores and cavities produced within the water tree, and since these are filled with aqueous salt solution their mass will be the mass of the water within the tree. Since the fractal structure cannot be maintained to infinitely small sizes, we can assume that the damage per unit volume is constant (*i.e.* the damage is uniform) for an elementary box of size l_e which contains a mass M_e. The elementary size l_e must be larger than the pore size, 2.5 nm. The fractal structure will thus be constructed from these elementary boxes of uniform density and the mass M_L contained within a box of size L will be given by the number of boxes multiplied by the mass per box, *i.e.*

$$M_L = M_e \left(\frac{L}{l_e}\right)^{d_f} \tag{3}$$

Equation (3) can be rewritten as

$$M_L = \frac{M_e}{l_e^3} L^{d_f} l_e^{3-d_f} = \rho_e L^{d_f} l_e^{3-d_f} \tag{4}$$

where ρ_e is the damage density in the elementary volume. M_e should be in kg but it is obvious that the object cannot be weighed, so a measure proportional to the mass is used instead (it also applies to other physical quantities). Since the structure is a fractal constructed from elementary volumes, the density on all size scales is scale-related to ρ_e, which therefore defines a characteristic measure of the damage density throughout the water tree. The quantities that we have used to estimate the fractal dimension of the water tree are measures of the water content (Section 4.1) or damage (Section 4.2) in the tree. They are therefore proportional to M_L. The fractal dimension is obtained effectively from the gradient of a plot of $\log(M_L)$ as a function of $\log(L)$. The intercept of $\log(M_L)$ with the $\log(L)$=0 axis on these plots therefore gives a measure which is proportional to $\rho_e(l_e)^{3-d_f}$. In order to obtain a quantitative value for ρ_e it would be necessary to determine the value of both l_e and the proportionality between the observed quantity and the mass of water. A qualitative measure suitable for comparison of ρ_e within a particular set of measurements can be made, however, using the value of the intercept and a reasonable guess for l_e. SEM and the NMR results indicate that 2.5 nm<l_e<1 μm. If it is assumed that the value of l_e is a material property, and remains essentially unchanged with the other experimental conditions, a qualitative estimate of the variation of damage density can be obtained just by comparing the intercept.

This is particularly the case with the methylene-blue stained trees analyzed here since they have essentially the same value of d_f. The damage density is not a quantity that has received much attention in the investigation of water trees, though it can be imagined that it could be of major importance [1]. The length of water trees is usually taken to be a measure of their propensity to induce breakdown [1, 2], but if water tree retardant materials reduce the length of the water trees at the expense of a higher damage density, is this really an improvement? Do long trees grown in service have more damage density than shorter trees, and is this why they are more dangerous? The damage density can be expected to influence the conductivity of the tree, and hence of the electric field enhancement generated by the tree [16, 17]. It should be noted however, that higher conductivity does not necessarily mean more field enhancement around the tree, because its shape also may be influenced by the damage density, and this will be a factor in determining the electric stress generated. A difference in ρ_e may serve to explain why water trees grown at high frequency, that are known to grow faster than those at power frequency [6], still have the same fractal dimension. This could be accommodated if the damage densities were to be less at higher frequencies.

It should be noted that neither of the two types of image studied shows the true structure of the tree. In the literature the effect of dyeing has been discussed (see Ross [18]). It is known that the staining process does not result in a chemical reaction, but the microvoids and connecting pathways have been enlarged. SEM techniques always involve etching of the surface to be observed and so microvoids will be enlarged by this technique also. It is likely that this enlargement does not modify the fractal dimension. It may, however, increase the size of the elementary volume, namely l_e.

6 CONCLUSIONS

WATER trees are fractal objects with a dimension ~ 2.85 on the macroscopic scale and ~ 2.55 on the microscopic scale. These values are in agreement with deductions from the time dependence of the

ater tree length. Also the measured fractal dimensions are consistent ith diffusion limited aggregation models [19] for fractal structures, it this does not imply that this process is involved in their formation.

7 APPENDIX

When a fractal set is not a simple fractal but is composed of subıctal sets with different scaling (fractal) characteristics, it is called a ıultifractal' [20]. This concept was introduced first by B. Mandelbrot], applied to the study of turbulence and, according to Feder [20], is often related to the study of a distribution of a physical or other ıantities in a geometric support. Multifractality has been applied to ə study of diffusion limited aggregation (DLA) and other growth phe-ımena including viscous fingers [21]. Since water treeing is a growth ocess it is most probable that a multifractal study can be applied also.

An important definition to characterize a multifractal is the generzed dimension introduced by Grassberger [22]. As is well known, ıen the box-counting method is used to calculate the fractal dimen-ın, the fractal object is covered with boxes of size δ. The box is ınted if at least one of the points of the fractal is in the box. However ıox may contain more than one point. If the number of points in each x were counted also, a probability distribution could be defined (like lensity distribution) in terms of moments [21]

$$Z(q) = \sum_i n(\mu_i)\mu_i^q \qquad -\infty < q < +\infty \tag{5}$$

ıere $Z(q)$ is the moment of order q, q is an integer, $n(\mu_i)$ is the mber of boxes with a fraction of points

$$\mu_i = \frac{N_i}{N_t} \tag{6}$$

; is number of points in box i and N_t the total number of points. This ction can be associated to an occupation probability. The generalized nensions D_q, are defined by

$$D_q = \frac{1}{q-1} \lim_{\delta \to 0} \frac{\log \sum_i N(q,\delta)}{\log \delta} \tag{7}$$

$(q,\delta) = \sum_i \mu_i^q$ is the weighted number of occupied boxes of size

The generalized dimensions calculated in this work are:

1. For q=0, $N(q,\delta)$ is just the total number of occupied boxes and $D_0 = d_f$ (capacity dimension).
2. For q=1, D_1 is called the information dimension because $N(q,\delta)$ is analogous of the Shannon information entropy. It quantifies the non-uniformity of the point distribution.
3. For q=2, D_2 is the correlation dimension (a measure of the distance between pairs of points).

This formalism can be treated similarly to the thermodynamic for-ılism, since $Z(q)$ is analogous to the thermodynamic partition func-n. An exponent $\alpha(q)$ is defined characterizing the singularities of ə fractal set. A Legendre transform defines a function, $f(\alpha)$

$$\begin{aligned} f(\alpha) &= q\alpha(q) - \tau(q) \\ \alpha(q) &= \frac{d\tau(q)}{dq} \end{aligned} \tag{8}$$

ıere $\tau(q)$ is related to the generalized dimension by $\tau(q) = (q - D_q$. Comparing with the thermodynamic formalism $\tau(q)$ is similar the energy and $f(\alpha)$ to the entropy [21].

ACKNOWLEDGMENT

The authors would like to thank J. Houlgreave for the original photographs of methylene blue dyed water trees and A. Vaughan for making available the previously published photographs of SEM images of water trees. Would also like to thank Borealis for supplying the LDPE pellets and BICC-Celcat, specially Mr. F. Pedroso. Furthermore, the Lisbon group is grateful to J. Houlgreave and coworkers for gently lending some modified Cigré cells.

REFERENCES

[1] L. A. Dissado and J. C. Fothergill, *Electrical Degradation and Breakdown in Polymers*, IEE P. Peregrinus, London, 1992.

[2] E. F. Steenis and F. H. Kreuger, "Water treeing in polyethylene power cables", IEEE Trans. Electrical Insulation, Vol. 25, pp. 989–1028, 1990.

[3] R. Ross, "Inception and propagation mechanisms of water treeing", IEEE Trans. Dielectrics and Electrical Insulation, Vol. 5, pp. 660–680, 1998.

[4] B. B. Mandelbrot, *The fractal geometry of nature*, Freeman & Comp, New York, 1982.

[5] M. T. Shaw and S. H. Shaw, "Water treeing in solid dielectrics", IEEE Trans. Electrical Insulation, Vol. 12, pp. 383–388, 1977.

[6] J. Houlgreave, A. Eccles and J. C. Fothergill, "Characterization of water trees and the use of frequency acceleration techniques", Proc of the 6th International Conference on Dielectric Materials, Measurements and Applications, DMMA'92, Manchester, pp. 492–495, 1992.

[7] M. Carmo Lança, L. Dissado, J. Marat Mendes and D. K. Das Gupta, "Water trees growth and fractal analysis", Proc of the International Conference on Dielectrics and Insulation, ICDI-97, Budapest, pp. 297–300, 1997.

[8] R. H. Olley, D. C. Basset, A. S. Vaughan, V. A. A. Banks, P. B. McAllister and S. M. Moody, "Delineating water trees in cross-linked polyethylene: a new technique", Journal of Materials Science, Vol. 27, pp. 5192–5198, 1992.

[9] R. H. Olley, A. S. Vaughan, dc Basset and S. M. Moody, "Electron microscopy of water trees in XLPE", Proc of the 5th International Conference on Conduction and Breakdown in Solid Dielectrics, ICSD'95, Leicester, pp. 676–680, 1995.

[10] J. C. Fothergill, *Assessing the life of polymeric power cables*, Univ. of Leicester, Technical Report, 1993.

[11] M. Carmo Lança and L. Dissado, "An estimate of the fractal dimension of water trees", In 7th Int. Conf. on Dielectric Materials, Measurements and Applications, pp. 214–219, Bath, UK, 1996.

[12] K. Kudo, "Fractal analysis of electrical trees", IEEE Trans Diel. & EI, Vol. 5, pp. 713–727, 1998.

[13] L. S. Liebovitch and T. Toth, "A fast algorithm to determine the fractal dimension by box-counting", Physics Letters A, Vol. 141, pp. 386–390, 1990.

[14] X. J. Hou, R. Gilmore, G. B. Mindlin and H. Solari, "An efficient algorithm for fast O (N*ln (N)) box-counting", Physics Letters A, Vol. 151, pp. 43–46, 1990.

[15] P. Judeinstein, M. Carmo Lança, J. N. Marat Mendes and J. Rault, "Pore dimension of water trees in PE: NMR studies", Polymer, Vol. 41, no. 22, pp. 8151–8154, 2000

[16] Y. Li, J. Kawai, Y. Ebinuma, Y. Fujiwara, Y. Okhi, Y. Tanaka and T. Takada, "Space charge behavior under ac voltage in Water-treed PE observed by the PEA method", IEEE Trans Diel. & EI, Vol. 4, pp. 52–57, 1997.

[17] I. Radu, M. Acedo, P. Notingher, F. Frutos and J. C. Filippini, "A study on the dependence of water tree permittivity with time", Ann. Rep. CEIDP, pp. 762–765, 1996.

[18] R. Ross, "Comparing, structure and growth for water trees in polyethylene", Kema Scientific & Technical Reports, Vol. 8, no. 4, pp. 209–271, 1990.

[19] S. Satpathy, *Fractals in Physics*, eds L. Pietronero, and E Tosatti, North Holland, Amsterdam, pp. 173–176, 1986.

[20] J. Feder, *Fractals*, Plenum Press, New York, 1988.

[21] H. E. Stanley and P. Meakin, "Multifractal phenomena in physics and chemistry", Nature, Vol. 335, pp. 405–409, 1988.

[22] P. Grassberg, "Generalized dimensions of strange attractors", Phys. Lett. A, Vol. 97, pp. 227–230, 1983.

Manuscript was received on 29 August 2000, in final form 21 April 2001.

INSTITUTE OF PHYSICS PUBLISHING JOURNAL OF PHYSICS D: APPLIED PHYSICS
J. Phys. D: Appl. Phys. 35 (2002) L29–L32 PII: S0022-3727(02)31700-5

RAPID COMMUNICATION

Combined isothermal and non-isothermal current measurements applied to space charge studies in low-density polyethylene

M Carmo Lança, Eugen R Neagu and José N Marat-Mendes

Departamento de Ciência dos Materiais, CENIMAT, Faculdade de Ciências e Tecnologia, Universidade Nova de Lisboa, 2829-516 Caparica, Portugal

Received 7 December 2001
Published 2 April 2002
Online at stacks.iop.org/JPhysD/35/L29

Abstract
A new experimental procedure combining usual isothermal DC charging and discharging with non-isothermal current measurements has been recently proposed. It is mainly suitable for very high insulating polymers and it was successfully applied to the study of space charge trapping and transport in low-density polyethylene. The analysis of the isothermal currents revealed the presence of different traps whose characteristic (de)trapping times can be deduced. The isothermal procedures allowed the selective charging of the sample. By choosing the charging field and the ratio of charge/discharge times, non-isothermal analysis permitted the differentiation of three or four peaks (at ≈50°C, ≈65°C, ≈70°C and ≈85°C) associated with charge detrapping from surface or near-surface (<20 μm) traps. These traps have activation energies between 0.21 and 1.54 eV. The mobility at 30°C is around 5×10^{-16} m^2 V^{-1} s^{-1}. Samples had to be conditioned before each experiment in order to obtain reproducible results.

1. Introduction

Experiments concerning space charge (SC) trapping such as the thermally stimulated discharge currents (TSDC) method do not take into account the long time needed for trapping and detrapping of charge in good insulators. Without taking these long times into consideration, results become difficult to reproduce and interpret. Also, individual isothermal measurements of charge and discharge currents are unable to reveal consistent information on SC trapping and transport. Moreover, after any experiment involving sample charging, it is possible that a residual SC still remains even if the measured discharge current is very low. In consequence, for highly insulating polymers the mechanisms of charge transport and trapping cannot be investigated properly by a single (isothermal or non-isothermal) measurement.

A new technique combining isothermal DC charging and discharging with non-isothermal measurements has been recently proposed [1]. First the sample is isothermally charged and discharged. The isothermal charge current (ICC) and the isothermal discharge current (IDC) are recorded and analysed. A careful selection of charge and discharge conditions (field, temperature and ratio of charge and discharge times) allows the distinct features of SC traps (activation energy, relaxation times) to appear as peaks in the following non-isothermal current measurement. During this step of the experiment, the sample is heated at a constant rate b. This is the final thermally stimulated discharge current (FTSDC) technique [2, 3]. SC is still trapped in the sample at the end of FTSDC experiments, but it is not detected in usual measurements. For the SC to vanish completely, it is necessary to keep the sample at the final temperature of FTSDC for some time. This is the last step of the experiment during which the final isothermal discharge current (FIDC) is monitored to ensure characterization of the traps and almost complete discharge of the sample [2, 4]. In this way the sample is conditioned so that prior history does not influence the next measurement impairing reproducibility and interpretation of results.

Polyethylene is one of the best insulating polymeric materials and many attempts have been made to study SC.

However, methods relying on individual measurements of either isothermal or non-isothermal currents have produced results that are difficult to interpret and reproduce [5]. In this paper, results obtained for low-density polyethylene (LDPE) using the new combined technique are presented. Analysis of ICC and IDC showed the presence of different relaxation processes and the corresponding relaxation times were estimated. Based on a judicious selection of charging and discharging parameters (selective charging), it was possible to distinguish the presence of different peaks. Activation energies W were calculated using the initial-rise method [6] and/or by fitting the experimental data with an analytical expression for the current.

2. Experimental

Films of 200 μm thickness from Borealis LDPE pellets almost additive free were obtained by press moulding. Samples were thermally aged in 1 M NaCl solution at 40°C for 1500 h. After ageing Al electrodes with diameters of 33 mm were vacuum deposited on both surfaces of the sample. The experimental setup for electrical measurements was presented elsewhere [7]. Figure 1 schematically presents the measuring procedure. In order to study SC transport and trapping in the polymer, the first step was to perform a selective isothermal charging of the material. Under vacuum, a DC field E was isothermally applied for time t_1, followed by a discharge at the same temperature during time t_2. Both ICC and IDC were registered. By choosing field strength, temperature and ratio of charging and discharging times, the sample was selectively charged. Consequently, at the end of the selective charging the stored charge is trapped below a certain energy level and at a mean depth into the material. During FTSDC, the sample was heated at a low constant rate b. Finally, the polyethylene had to be kept at the final temperature of FTSDC for a long time (t_4). This is the FIDC, which allowed correct analysis of the SC stored in the sample during selective charging and ensured that no SC remained trapped at the end, i.e. after t_4. Without performing this last step, the following set of experiments would be drastically influenced by the remnant charge in the polymer.

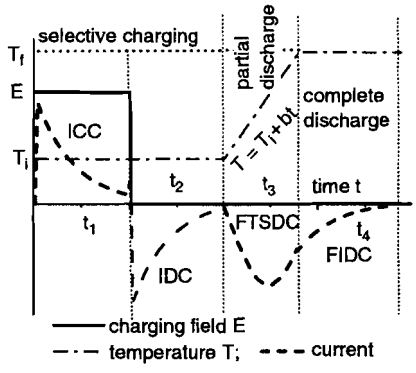

Figure 1. Experimental procedure used to analyse SC in thermally aged LDPE. The four steps are schematically represented showing electric field, temperature and current. Selective charging corresponds to isothermal charging and discharging. Partial discharge proceeds during FTSDC. Almost complete discharge is only achieved during FIDC.

3. Results and discussion

Results for typical measurements covering the four stages of each run can be seen in figures 2–5. The same charging temperature (30°C), electric field (2 MV m^{-1}) and heating rate (1°C min^{-1}) were used in all measurements. The currents from the ICC step are presented in figure 2. The charging time was 3 h for run (b) and 1 h for runs (a), (c) and (d). No important differences are visible for the recorded currents (b–d), showing the very good reproducibility of the measurements. However, current (a) exhibits a slightly higher value. This is a consequence of the previous charging history of the sample. During the previous run, the charging period was 27 h and non-controlled remnant charge affects the charging current in (a). A transition to the steady-state current is observed only at times longer than 1 h, i.e. for (b) where the charging time reaches 3 h, and in spite of the current being noisy the beginning of the steady state is clearly visible (as it was also observed before [8]). The observed noise can be related to inhomogeneities in the conducting paths at the onset of the DC conductivity. Noise of the same origin is also observed in the last part of curve (a). Since the sample is more conductive, the DC onset will occur at shorter time. By fitting the data for curve (b) in figure 2, the relaxation times and DC conductivity were obtained. The value for conductivity was $\sigma_0 = 1.6 \times 10^{-16}$ S m^{-1}, which is in good agreement with the expected value [9].

Figure 3 presents the discharge currents that followed the charging processes seen in figure 2. Initially, all discharge currents are very similar, indicating that the results are well reproducible. However, looking at longer times (near 10^4 s), curve (b) has a higher value for the discharge current. This is related with the longest charge time (see figure 2). It is clear from the analysis of the curves in figures 2 and 3 that three or four relaxation processes are present, the number observed depending on both charging and discharging times, temperature (T) and electric field (E). The values of relaxation times for curves (b) and (c) in figure 3 are presented in table 1. It must be noted that they do not exceed 1 h. The graph insert in figure 3 represents the fit done for current (c) considering four

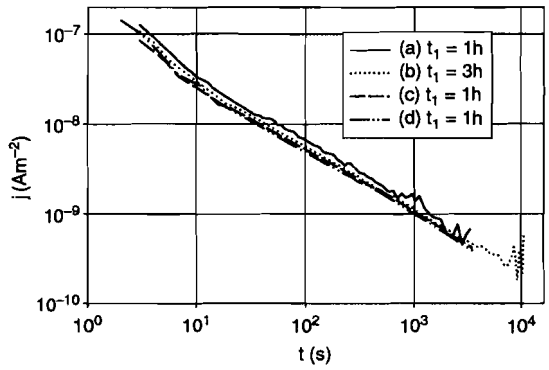

Figure 2. ICC results for measurements made in vacuum at 30°C with an applied DC field of 2 MV m^{-1}. For 3 h (b) charging the beginning of the DC conductive regime is seen.

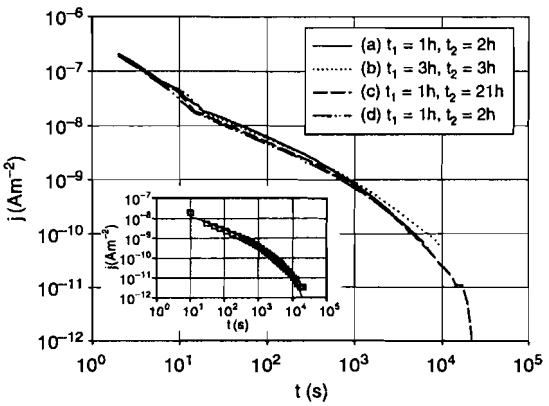

Figure 3. IDC measurements obtained after the corresponding charging currents reported in figure 2 (same symbols are used). The insert shows the fitting made for data represented by line (c) considering four relaxation times.

Table 1. Relaxation times obtained from IDC curves (b) and (c) in figure 3.

Run	τ_1 (s)	τ_2 (s)	τ_3 (s)	τ_4 (s)
(b)	18	86	500	3500
(c)	14	70	460	3600

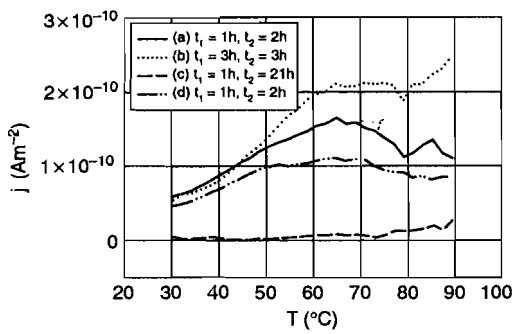

Figure 4. FTSDC for different selective charging conditions measured after the corresponding discharging currents reported in figure 3. The influence of different ratios of charging/discharging times is observed.

relaxation times. The first 10 s were not considered because they can be attributed to fast processes.

Figure 4 presents the FTSDC current where four more or less well-shaped peaks are observed. These peaks can be related to the four relaxation processes found in (dis)charge currents. Using the ratio of charge/discharge times, which makes it easier to better observe some peaks, the influence of selective charging is perceived. For instance, in run (a) there is a shoulder (≈55°C) while for run (d) this shoulder becomes a peak. Run (c) has a very long discharge time (t_2 = 21 h), so the current is very low and near the resolution limit of the experimental setup and only the high-temperature peak appears. The influence of the previous history is again visible in run (a), showing (i) a higher current value and (ii) an unexpected high increase of the current at high temperature for an applied field of 2 MV m^{-1}. Table 2 shows the activation

Table 2. Activation energies (determined by the initial-rise method) and released charge (Q) for FTSDC (figure 4).

Run	W (eV)	Q (10^{-10} C)
(a)	0.34	3.7
(b)	0.45	4.9
(d)	0.35	2.6

Table 3. Activation energies for run (b) in figure 4 resulting from the decomposition of the FTSDC spectrum in four peaks.

W (eV)	0.21	0.60	0.62	1.54

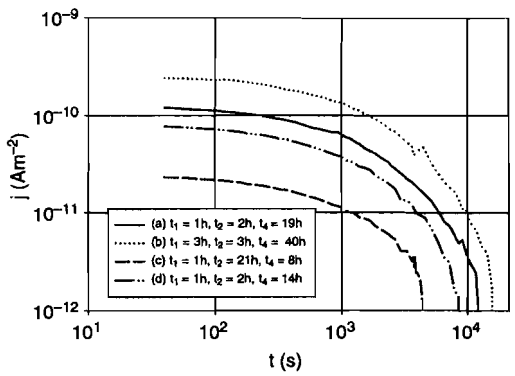

Figure 5. FIDC results obtained after the corresponding FTSDC reported in figure 4. The FIDC temperature is the same as the final temperature of FTSDC.

energy calculated by the initial-rise method [6] and the total charge. Table 3 presents the activation energies obtained from the decomposition in four elementary peaks of the thermogram (b) in figure 4. The values for W agree with others in the literature: 0.15 eV [10], 1.4–1.5 eV [11, 12], 0.4–0.6 eV [10] and 1.2–1.3 eV [11, 12] for peaks at ≈40°C, ≈50°C, ≈60°C and ≈85°C, respectively. Spectra are due to SC detrapping because: (i) the dependence of the current with the electric field is non-linear (not shown here); (ii) peak maxima appear at a higher temperature compared to the charging temperature with $T_m - T_c > 20$°C, where T_m is the maximum temperature of the peak and T_c is the charging temperature (contrary to what is usually found in thermal sampling for dipolar peaks [12] where $T_m - T_c \leqslant 20$°C); (iii) almost complete discharge occurs as t_2 increases (as can be seen for curve (c) in figure 4); and (iv) long time effects associated with SC still exist in the sample for intermediate values of t_4 even if the discharging current is very low at this time. An additional confirmation is obtained during cooling when sharp peaks for similar temperatures as the ones during heating are observed. Other authors found peaks at identical temperatures, but usually in each experiment not more than two are seen [10–12]. Most likely, these peaks can be attributed to structural changes [14]. The remnant charge from previous charging processes strongly influences the high-temperature behaviour including the peak around 85°C. The presence of this charge can also be observed in FIDC (see figure 5) that was recorded until the limit resolution of the experimental setup was reached (electrometer Keithley 6517A). At this stage the current is very low, not because

Table 4. Relaxation times and charge released during FIDC (figure 5).

Run	τ_1 (s)	τ_2 (s)	Q (10^{-10} C)
(a)	620	3060	2.4
(b)	620	3530	4.8
(d)	700	3150	2.2

there is no SC in the sample but because SC is now more or less uniform through the sample [4, 13]. For FIDC in figure 5, two relaxation times at $\approx$10 min and less than 1 h are found (see table 4). The higher value of τ_2 for curve (b) shows that by increasing t_1 the charge becomes more stable (in good agreement with the largest value of the high-temperature current (b) in figure 4). After 1 day there is still some charge (uniformly distributed) in the sample [4], and only after 2 days will it become efficiently discharged. The important conclusion is that only after this procedure will the results become reproducible. The total charge in the non-isothermal experiments is of the same order of magnitude as the one released during FIDC (see tables 2 and 4). In this way, the FIDC step becomes relevant and essential by allowing (i) us to know about SC stability (quantified by the values of the relaxation times at high temperature) and (ii) the sample to discharge completely.

Simple calculation of the ratio between charge released in IDC, Q_d, and ICC, Q_c, in run (b) gives $Q_d/Q_c = 0.74$, while the ratio of released charge during all discharge processes, Q_1, and charging, Q_c, is $Q_1/Q_c = 0.9$ (where $Q_1 = Q_d + Q_{TC} + Q_{FD}$ and Q_d is the total charge released during IDC, Q_{TC} during FTSDC and Q_{FD} during FIDC).

The zero field plane of the charge centroid, x, can be obtained from the following equation [4]:

$$|Q_1| = \left(1 - \frac{x}{L}\right) Q_c,$$

where L is the sample thickness. For runs (b) and (d), with different charging times, the values of $0.1L$ and $0.01L$, respectively, were found for x. This implies that the carriers are not penetrating linearly with charging time, which can be attributed to the remnant SC near the electrodes. This charge enhances a non-uniform local field and gives rise to a field activated mobility [14]. If this mobility (μ) is calculated for run (d), the value obtained is 2.8×10^{-16} m^2 V^{-1} s^{-1}, while for run (b) it is 9.2×10^{-16} m^2 V^{-1} s^{-1}. The order of magnitude for μ is in good agreement with the literature [9, 14, 15].

Up to now, nothing has been said about the sign of the carriers. As is well known, this is a matter of some discussion. According to Lewis [16], the gap energy of polyethylene is about 8.8 eV, and Rhoderick [17] states that the work function of Al is 4.3 eV. Consequently, the band diagram at metal–dielectric contact is favourable to electron injection from an Al cathode into LDPE. On the other hand, hole injection from the Al anode into LDPE is very unlikely. Also it is known that most of the polymers charge negatively when in contact with metals [16]. However, to completely clarify this matter some further experiments are under consideration. Work is also in progress for virgin samples.

4. Conclusions

The combined method permitted us to find the conditions under which the presented measurements for LDPE become reproducible and the subsequent analyses are consistent. Selective charging can distinguish particular peaks allowing the decomposition of the FTSDC spectra in elementary peaks and the separation of the contribution of the relaxation processes to the ICC and the IDC. In this way, useful information about traps such as relaxation times and activation energies was obtained. By determining the total charge stored in the sample, it was possible to estimate the charge centroid and the mobility. For the given conditions, the charge is trapped in a narrow sheet (<20 μm) near the injecting cathode.

Acknowledgments

The authors are very grateful to Borealis for supplying the LDPE pellets and to INVOTAN for a research grant.

References

[1] Neagu E R and Marat-Mendes J N 2001 *Japan. J. Appl. Phys.* **40** L1160–2
[2] Neagu E R, Marat-Mendes J N, Neagu R M and Das-Gupta D K 1999 *J. Appl. Phys* **85** 2330–6
[3] Neagu E R and Neagu R M 2000 *Thin Solid Films* **358** 283–91
[4] Neagu E R and Neagu R M 2001 *Thin Solid Films* **384** 15–22
[5] Wintle H J 1983 *Engineering Dielectrics* vol IIA, ed R Bartnikas (New Jersey: Bound Brooks) pp 239–354
[6] Garlick G F K and Gibson A F 1948 *Proc. Phys. Soc.* **60** 574–8
[7] Neagu E R and Neagu R M 1994 *Phys. Status Solidi* A **144** 429–38
[8] Das-Gupta D K and Brockley R S 1978 *J. Phys. D: Appl. Phys.* **11** 955–62
[9] Pélissou S, St-Onge H and Wertheimer M R 1988 *IEEE Trans. Elect. Ins.* **23** 325–33
[10] von Seggern H 1981 *J. Appl. Phys.* **52** 4086–9
[11] Sawa G, Kawade M and Ieda M 1973 *J. Appl. Phys.* **44** 5397–8
[12] Sawa G, Kawade M, Lee D C and Ieda M 1974 *Japan. J. Appl. Phys.* **13** 1547–53
[13] van Turnhout J 1980 *Electrets, Topics in Applied Physics* vol 33, ed G M Sessler (Berlin: Springer) pp 81–215
[14] Fischer P 1977 *J. Electrostatics* **4** 149–73
[15] Hwangbo S, Kwon Y, Jeon S and Han M 1998 *Japan. J. Appl. Phys.* **37** 4419–27
[16] Lewis T J 1990 *J. Phys. D: Appl. Phys.* **23** 1469–78
[17] Rhoderick E H 1978 *Metal–Semiconductor Contacts* (Oxford: Clarendon) p 53

Key Engineering Materials Vols. 230-232 (2002) pp. 384-387

Infrared Spectroscopy Studies of Aged Polymeric Insulators

J. Mateo, M. Carmo Lança and J. Marat-Mendes

Departamento de Ciência dos Materiais, , Secção de Materiais Electroactivos (CENIMAT),
Faculdade de Ciências e Tecnologia, Universidade Nova de Lisboa,
PT-2825-114 Caparica, Portugal

Keywords: Dielectric Breakdown, Electrical Ageing, FTIR, Oxidation, Polyethylene

Abstract. Thin films of low density polyethylene (LDPE) and crosslinked polyethylene (XLPE) were aged under an AC electric field while kept in sodium chloride aqueous solution. After aging the samples showed water trees (localized damaged with the appearance of hydrophilic ramified structures whose size ranges from a few microns to 1 mm). Some of the samples suffered dielectric breakdown showing small channels (1-2 mm diameter) crossing the film and sometimes also signs of carbonization. In order to identify the oxidation mechanisms contributing to aging, FTIR was used to analyze both unaged and aged specimens. Comparing between unaged and aged LDPE an increase in the FTIR spectrum for bands at 1720 cm^{-1}, 1640cm^{-1} and 1590cm^{-1} was visible for the aged samples. The first region corresponds to carbonyl groups (C=O bonds) resulting from oxidation (most probably ketones). While the second one is related to carbon double bonds formed due to chain scission. Finally the third one is due to carboxylates. For the XLPE the analysis is more difficult. Besides aging it needs to be taken into account the by-products of crosslinking that will tend also to diffuse out with time. The main effect of aging is an increase in the concentration of 1640 cm^{-1} band (C=C bonds). For the water treed regions dry and wet samples were compared. In the wet ones the absorbance is larger for the 3380cm^{-1} exhibiting, as expected, water absorption in the water treed regions (hydrophilic characteristics were increased).

Introduction

Medium and high voltage power cables are using as insulator polymers such as cross-linked polyethylene. The presence of a high electric field causes electrical ageing in the polymer. In the long run it may produce *dielectric breakdown* with subsequent cable failure. Detection and replacement of the damage part of the cable is always highly costly.

Previous to breakdown the aging process is already occurring. The phenomenon of *water treeing* appears in this early stage [1,2]. A water tree consists of water filled microcavities enlarged either by oxidation or cracking. They are due to the combined action of electric field (ac) and aqueous solution. By themselves water trees do not destroy the insulator characteristic of the polyethylene, yet they reduce the breakdown strength and can be the initiation sites for more dangerous aging phenomena (such as electrical trees). Theoretical models for water treeing point to a complex mechanism involving electro-mechano-chemical processes [3,4]. Possible oxidation reactions have been proposed over the years, see for example Dissado et al. [1]

Researchers have detected evidence of oxidation in water trees. Comparing water treed regions with unaged polymer it was observed an increase in carbonyl groups (C=O) concentration [5]. Also a reduction in oxidative stability was noticed [5]. Laboratory ageing experiments where sodium and copper ionic solutions were used showed the greater rate of water tree growth in the presence of copper ions [5]. According to Ross [3] the most common oxidation products are carboxylates (COO^-), along with aldehydes, ketones and carboxylic acids. The kind of products are very dependent on aging conditions, for instance there are significant differences between laboratory and field aged specimens. The former showing higher contents of carboxylates than the later.

FTIR and, specially, micro-FTIR and other techniques [5] have been used to study oxidation in water trees. A model was developed by the Kema group [6] dividing the polyolefins oxidation related to water treeing in five steps:

a) Water electrolysis
Results in oxidative agents: hydrogen peroxide, oxygen and radicals;

b) Initial degradation of the polyolefin
the electric field + transition metal ions catalyze the oxidative degradation of the polymeric chain originating very reactive free radicals.
These radicals react with oxidants giving peroxides or peroxide radicals;

c) Degradation catalyzed by metal ions
The presence of peroxides and their radicals diminish the neighboring carbon bond strength. Alkoxy radicals are formed by breaking the O-O bond (by the presence of the electric field + metal ions);

d) Breakdown of chains resulting in ketones and carboxylate ions
Alkoxy radicals can enhance the breakdown of C-C bonds producing ketones, chain breakdown and radicals;

e) Conversion of ketones to carboxylate ions
The high concentration of carboxylate ions found on the water trees suggests that ketones are converted to carboxylate ions.

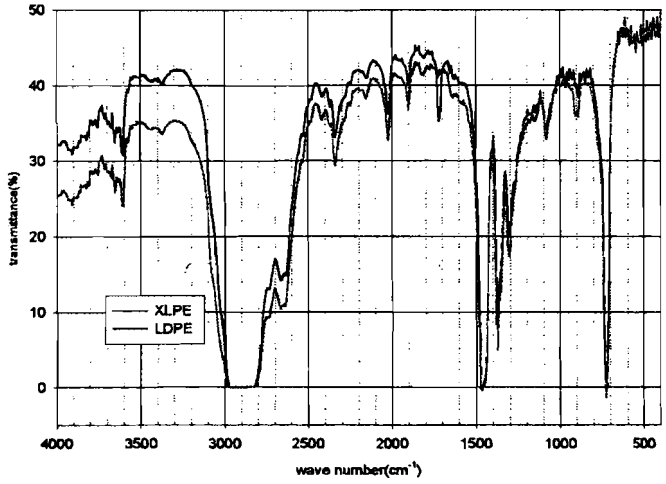

Figure 1 – LDPE and XLPE spectra (main difference the band of acetophenone).

Experimental setup

Sample preparation and electrical aging - Films of LDPE and XLPE were hot press-molded. XLPE crosslinking was achieved by using dycumil peroxide. Samples of LDPE and XLPE were aged in the laboratory under an AC electric field. Disc shaped samples of $\cong 200\mu m$ thickness and diameter of $\cong$ 30-35mm were press-moulded from pellets. The basic configuration of a modified Cigré cell developed by Houlgreave et al [6,7] was chosen (for details [8]). The cells were immersed in an insulator oil bath. The aqueous solution acted as electrodes on both sides of the disc shaped samples (planar electrodes). The samples were aged at an applied AC field of 6kV/mm at 50Hz, at three different constant temperatures of room temperature (RT), 35°C and 50 °C. The aqueous solution was of sodium chloride 1M and the ageing time varied from 250h up to a maximum of 1000h. For each ageing time the field was applied to all of the samples except to a reference one which was kept in solution with no field applied.

FTIR measurements- A BioRad-FTS 165 was used to obtain the FTIR spectra. Both unaged and aged samples of LDPE and XLPE were analyzed prior and after aging. For aged samples showing both water trees and breakdown channels the spectra were obtained for different regions (p. ex., water-treed region).

Results and discussion

The total transmitance spectra obtained for both LDPE and XLPE samples can be observed in fig. 1. The main difference between these two spectra is a peak in the 1720 cm^{-1} related to acetophenone (a by-product of crosslinking). To look for the oxidation products distinct spectra intervals were analyzed in more detail, specially the region 1500 cm^{-1} to 1900 cm^{-1}.

For LDPE, comparison is made between aged (water treed regions) and unaged samples. Sometimes also areas showing no water trees or breakdown in aged samples were also compared. In water-treed regions a band at 1720 cm^{-1} associated with the carbonyl group (C=O) appears (see figure 2). This group can reveal the presence of carboxylic acids, ketones, aldehydes or esters. Carboxylic acids are transformed in salts (characteristic band at 1590 cm^{-1}) and esters carbonyl group shows at 1740 cm^{-1}. Based on Kema model the more probable responsible for the 1720 cm^{-1} are ketones formed during water tree propagation. Calculation of the ratio absorbance/thickness (by the base line method) has not showed any relation with different aging conditions. Less enhanced than the 1720cm^{-1} band, 1640cm^{-1} and 1590 cm^{-1} bands appear in the water spectrum. The former is representative of carbon double bonds (C=C) originated by chain scission. The later corresponds to carboxylate ions (this one is not observed for all the samples). Finally a band related to the CH_3 terminal end groups (1385 cm^{-1}) is increased. Suggesting that the number of ramifications decrease most probably due to chain scission.

For LDPE, samples aged in solution but without any electric field were also analyzed. The only difference between the unaged films is the enhancement of a band at 1745 cm^{-1} showing the existence of anti-oxidants in the original films. Samples undergoing thermal treatment (60°C for 120h) also showed some increase in the number of C=O groups even if they were not in solution and no field was applied. Analyses of these samples with X Rays showed an increase in crystallinity.

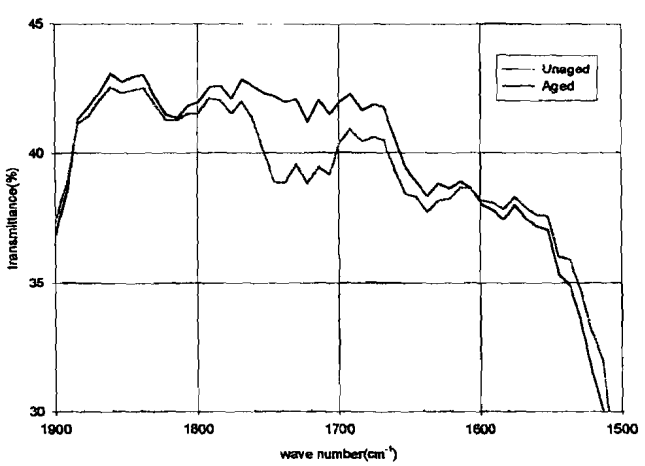

Figure 2 – LDPE spectra of aged and unaged samples in the region [1500, 1900]cm^{-1}.

The study of XLPE was more difficult due to the presence of cross-linking by-products and anti-oxidants. Acetophenone resulting from the curing process of dycumil peroxide has a characteristic band at 1720 cm^{-1}, as can be seen in fig. 1. Unfortunately it will hide the presence of some oxidation products. All aged samples show less concentration of acetophenone who is known to diffuse out with time [3]. The main difference between aged and unaged samples is the presence of the 1740 cm^{-1} band of C=O of esters of anti-oxidants. Moreover the anti-oxidants will tend to

diffuse to the water treed regions [3] becoming part of the trees. Concentration is higher for samples aged at 50°C than at lower temperatures agreeing with increased diffusion with temperature. The concentration of C=C bonds (1640 cm^{-1}) is also increased. This band has two companion bands in the region 800-1000 cm^{-1}. These are observed however with no increase for aged films. Both for LDPE and XLPE a decrease in the absorption at 1305 and 1385 cm^{-1} was seen corresponding to a reduction of the chain ramification.

Wet samples (soaked in distilled water for 24h) showed an enhancement of the characteristic frequencies of water, at 1640 cm^{-1} and 3380 cm^{-1}. The later is linked to hydrogen bonds.

Conclusions

The more important conclusion for water trees in LDPE is the appearance of ketones (1720 cm^{-1}), carfboxylate ions (1590 cm^{-1}) and an increase of C=C (1640 cm^{-1} band). According to Kema model (Ross[3]) carboxylate ions are the most common product of oxidation in water trees. Yet our samples do not show such higher values as Ross states. Ketones seem to be the most important oxidation product. Most probably the samples in this work are not enough aged, i.e., step *e)* of the model has not progressed totally or aging conditions (other than aging time) do not favor conversion of ketones to carboxylates. Nevertheless oxidation and chain scission has occurred for water tree formation and growth. About XLPE interferences from acetophenone limit the conclusion to the increase of number of C=C. Even the presence of anti-oxidants in the water trees renders more difficult the detection of oxidation products in the tree itself but it can show that hydrophilic tracks must have been created by oxidation. The analysis of wet samples also shows the existence of these hydrophilic tracks dragging the water into the trees. Thermal treatment can cause increase in the number of carbonyl groups.

Acknowledgments

The authors would like to thank Borealis for the LDPE pellets and to Mr. F. Pedroso of BICC-Celcat.

References

[1] L.A. Dissado and J.C. Fothergill: *Electrical Degradation and Breakdown in Polymers* (IEE P. Peregrinus, 1st edition, London, 1992).

[2] E.F. Steenis and F.H. Kreuger: IEEE Trans. Elec. Ins, Vol. 25(1990),pp. 989ff.

[3] R. Ross: IEEE Trans. Diel. Elec. Ins., Vol. 5(1998), pp. 660ff.

[4] J.-P. Crine:IEEE Trans. Diel. Elect. Ins., Vol. 5 (1998), pp. 558ff.

[5] R. Ross: Kema Sci. & Tech. Rep., Vol. 8(1990), pp. 209ff.

[6] J.J. Xu and S.A. Boggs: IEEE Elect. Ins. Mag., Vol 10 (1994), pp. 18ff.

[7] J.C. Fothergill, *Assessing the life of polymeric power cables* (Technical Report, Univ. of Leicester, 1993).

[8] M. Carmo Lança, C. J. Dias, D.K. Das Gupta, J. Marat-Mendes: Materials Science Forum (in press).

Key Engineering Materials Vols. 230-232 (2002) pp. 396-399

Dielectric Properties of Electrically Aged Low Density Polyethylene

M. Carmo Lança[1], C.J. Dias[1], D.K. Das Gupta[2] and J. Marat-Mendes[1]

[1] Departamento de Ciência dos Materiais, , Secção de Materiais Electroactivos (CENIMAT), Faculdade de Ciências e Tecnologia, Universidade Nova de Lisboa, PT-2825-114 Caparica, Portugal

[2] School of Informatics, University of Wales, Bangor, Gwynedd LL57 1UT, UK

Keywords: Dielectric Constant, Electrical Ageing, Insulating Polymers, Space Charges

Abstract. Low density polyethylene (LDPE) films kept in a sodium chloride aqueous solution, were aged under a high AC electrical field. The films were prepared from press moulding of LDPE pellets with small amounts of antioxidants. The dielectric spectra at 30 °C in the range of 10^{-5} Hz to 10^{5} Hz were obtained prior and after ageing. Three different experimental techniques were used to obtain the full spectrum. For the low frequency (LF) region (10^{-5} Hz to 10^{-1} Hz) the time domain technique was used (charge and discharge currents were also measured). The measuring device used for the 10^{-1} Hz to 10^{1} Hz medium frequency (MF) region was a lock-in amplifier. While for the high frequency (HF), 10^{-1} Hz to 10^{5} Hz, RLC bridge measurements were performed. Differences can be seen between aged and unaged PE. The region showing less changes with ageing is the MF region where the peak of the unaged samples seems to become less defined with ageing time. This peak is probably due to additives and impurities (such as antioxidants) that will tend to slowly diffuse out with time. The LF peak is a broad peak related to localised space charge injection driven by the electric field. This peak increases in an earlier stage of ageing decreasing afterwards possibly when the polymer becomes more conductive. Finally the HF shows the beginning of a peak due to γ and β transitions. The later is related to dipolar rotation of carbonyl groups in amorphous polymer regions, while the former is associated to crankshaft motions in the main polymer chain. This peak decreases with ageing disappearing for the most aged samples. This could also be explained if the sample becomes more conductive.

Introduction

High and medium voltage power cables use polymers as insulator. Polyethylene (PE) is one of the most used. The continuous stress caused by the applied electric field together with environmental factors such as humidity, temperature and ionic salt concentrations, lead to electrical aging of the PE [1]. In the long run aging will end cable's life through localized dielectric breakdown. Experiments analyze both aged polymers in service conditions and accelerated ageing in laboratory. From these it is possible to conclude that many parameters contribute to aging. Among these are intensity and frequency of applied electric field, temperature, mechanical stress, type and concentration of ionic salts, polymer morphology and composition. Owing to the complexity, published results have been sometimes conflicting and difficult to reproduce. This shows the importance of a good characterization of sample properties prior and after aging. Different aging phenomena can also occur, for instance water-treeing [1,2], electrical treeing and dielectric breakdown [1].

In the earlier stages of aging the dielectric properties of the material start to change. Studying the dielectric spectra might help to characterize the aging status and may predict remaining cable lifetime. Some recent work [3,4] has investigated the changes in dielectric spectra of low-density polyethylene (LDPE) and cross-linked polyethylene (XLPE). These results show the initial importance of space-charge accumulation, leading to an enhanced conductivity of the polymer with time. If aged for long enough the spectra show a quasi-DC (QDC) process. From these spectra it is also possible to obtain equivalent circuits describing different stages of aging.

Experimental

In this work LDPE films were aged in laboratory and the dielectric spectra characterized prior and after aging.

Sample preparation and aging – From pellets with very low amounts of antioxidant and impurities, disc shaped samples of $\cong 200\mu m$ thickness and diameter of $\cong$ 30-35 mm were press-molded. For the aging cell the basic configuration of a modified Cigré cell developed by Houlgreave et a.l [5] was chosen. The cells were immersed in an insulator oil bath. The aqueous solution acted as electrodes on both sides of the disc shaped samples (planar electrodes). The samples were aged at an applied AC field of 6kV/mm at 50Hz, at four different constant temperatures of room temperature (RT), 35°C, 40°C and 50°C. The aqueous solution was of sodium chloride 1M and the aging time varied from 500h up to a maximum of 1500h.

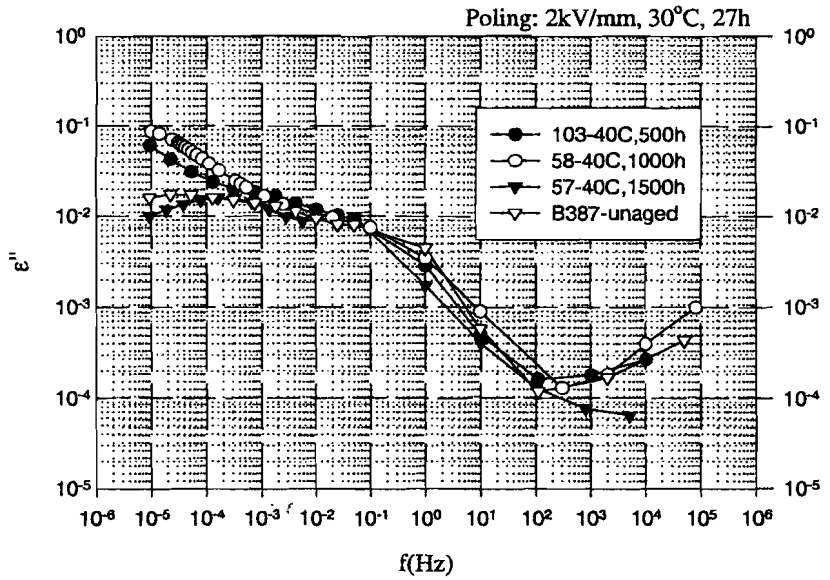

Figure 1 – Dielectric spectra of LDPE samples aged at 40°C for different ageing times.

Dielectric measurements – The dielectric constant was measured at constant temperature (30°C) in vacuum with the frequency varying from 10^{-5}Hz up to 10^{5}Hz. In order to cover this span of frequencies three different measuring techniques were used. In the low frequency region (LF) the complex permittivity was obtained from time domain measurements. The samples were subjected to a DC electric field (2kV/mm) for 27h and the discharge current was recorded for $\approx 10^{4}$s. Using the Hamon approximation [6] the imaginary dielectric constant was calculated and from ε'' the real permittivity could be estimated. For the medium frequency region (MF) spanning from 10^{-1} Hz to 10^{2} Hz, measurements were performed using a lock-in amplifier. From the application of an AC low voltage signal (V) at the measuring frequency both the real and imaginary dielectric constants could be obtained from the direct measurements of the two components of the current. Finally for the high frequency region (HF)-10^{2} Hz to 10^{5} Hz- a RLC General Radio Bridge was used. The dielectric constant was calculated from the measured values of capacitance and conductance.

Results and discussion

Fitting of the experimental data was made using either the Jonscher universal law [7](peaks) or QDC processes [7,8].

These plots are similar to the ones obtained by Scarpa [3] where the polymer also was contaminated by impurities. Isochronal dielectric spectra for linear polyethylene (LPE), slightly

oxidized from Graff and Boyd [9] show dipolar α and β dipolar peaks. The difference between LDPE and oxidized LPE dielectric spectra consists mainly of an increase of α and β peaks intensities. Also measurements of Barrie et al [10] show the presence of loss peaks in the LDPE spectra.

Starting with the LF region , given in fig. 1, for some of the aged samples there seems to be the enhancement of a probable peak whose maximum lies below 10^{-5} Hz (outside the range of measured frequencies). Peaks in this low frequency region are related to the presence of trapped space charge. As can be seen in the 40°C graph, both the unaged and the 1500h aged samples don't present this steep increase of ε'' for lower frequency. Examining the 500h sample it is observed this increase, being even higher for the 1000h samples. In the presence of an electric field space charge is injected with subsequent trapping ending up to give rise to peaks in this range. Specially for the LDPE films and as ageing progresses, initially more charges are trapped in the polymer and will cause an increasing of peak amplitude. With time deeper traps are created and start to be filled resulting in peaks at lower frequency. If aging is carried for long enough time the traps will tend to be filled. New charges in the material will now move more freely and a decrease in the peak amplitude will occur.

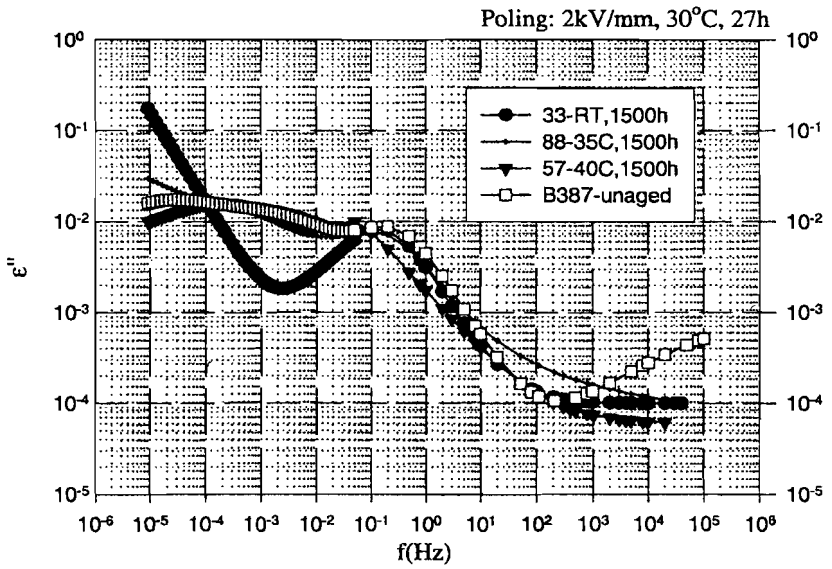

Figure 2 – Dielectric spectra of LDPE samples electrical aged in aqueous solution at diferent temperatures for 1500h.

The peak in the MF range (see figs. 1 and 2) can be attributed to impurities and anti-oxidants present in the material previous to aging. Also a small contribution of the α dipolar peak could be expected. Graff et al. [9] found for measurements at 30°C that the peak frequency should be in the region 1 to 10Hz. On the other hand, it is known that in the LDPE pellets used to prepare the press molded samples were present some anti-oxidants. The press molding process can originate oxidation and bring impurities into the films. These impurities tend to slowly diffuse out [11] with time, so a peak decrease is expected. Looking at the 40°C graphs (fig. 1) a slight decrease can be noted with aging time. It is also expected that this decrease will be more pronounced for higher aging temperatures where diffusion is enhanced (see fig.2). So it seems more probable that the main contribution to this peak will come from the impurities and anti-oxidants. Moreover taking into account that the initial number of carbonyl groups must be very small and also the degree of crystallinity, the contribution of the α transition must be very small.

In the HF region of the spectrum, it is seen for most of the samples the starting of a rise in ε'' as frequency increases. According to Barrie [10] for highly pure LDPE there is a peak above 10^7 Hz (measurements performed at 30°C) that can be attributed to β and γ transitions. This peak generally decreases for the aged samples as can be seen on 40°C and 1500h results. In the 1500h aged samples the peak disappeared. While for the 40°C aged samples, comparing with the unaged sample an increase occurs initially (500h aged and specially for the 1000h aged sample) and no rise appears for the 1500h aged specimens. The initial rise might be do to the crankshaft movements of the γ transition. After long enough time the sample becomes more conductive and the peak will tend to disappear. The decrease can be explained by considering a competitive process between space charge and dipoles. With aging charge moving freely becomes the dominant process.

Conclusions

The main effect of electrical aging seems to be the initial enhancement of the space charge peak and in the γ and β peaks followed by a decrease. The samples analyzed in this work are at a very early stage of aging when compared to the more aged samples of Scarpa (p. ex., 6000h). Contrary to Scarpa results [3] the polymer has not yet become significantly conductive. Even if the films already show the presence of water trees however they are a localized phenomenon and the contribution to bulk properties is still small. The changes in the LF and HF regions for 1500h aged sample seem to indicate that for longer ageing times the samples will become more conductive and may be a QDC regime will appear. The initial effect of aging seems to be the injection of space charge into the polymer.

References

[1] L.A. Dissado and J.C. Fothergill, *Electrical Degradation and Breakdown in Polymers* (IEE P. Peregrinus, 1st edition, London, 1992).

[2] J. Mateo, M. Carmo Lança and J. Marat-Mendes: Sci. Mater. Forum (in press).

[3] P.C.N. Scarpa, *Polarization and dielectric behaviour of AC aged polyethylene* (PhD thesis, Univ. of Wales (Bangor), 1995).

[4] D.K. Das Gupta, P.C.N. Scarpa: Elect. Ins. Mag., Vol. 15(1999), pp. 23ff.

[5] J.A. Houlgreave, A. Eccles, J.C. Fothergill: Proc. 6th Int. Conf. on Dielectric Materials, Measurements and Applications (1992), pp. 492ff.

[6] B.V. Hamon: Proc. IEE, vol. 99 (1952), pp.151ff.

[7] A.K. Jonscher, *Dielectric relaxation in solids* (Chelsea Dielectric Press, London, 1983).

[8] L.A. Dissado and R.M. Hill: J.Chem. Soc. Faraday Trans. 2, vol. 80 (1984), pp. 291ff

[9] M-S. Graff, R.H. Boyd: Polymer, vol. 35 (1994), pp. 1797ff.

[10] I.T. Barrie, K.A. Buckingham and W. Reddish: Proc. IEE, Vol. 113(1966), pp.1849ff.

[11] S.S Bamji, A.T. Bulinski, A.T. Densley, M. Matsuki: IEEE Trans. Elect. Ins., Vol. 26(1991), pp 278ff.

STUDIES OF SPACE CHARGE IN ELECTRICALLY AGED LOW DENSITY POLYETHYLENE

M.C.Lança, E.R.Neagu and J.N.Marat-Mendes
Departamento de Ciências dos Materiais, CENIMAT, Faculdade de Ciências e Tecnologia,
Universidade Nova de Lisboa, 2829-516, Caparica-Portugal

Abstract
Space charge in electrically aged LDPE was studied using a recently developed technique combining isothermal charging and discharging with non-isothermal measurements. Samples were aged in a NaCl aqueous solution at 40°C for 1500h under an AC field of 6MV/m (50Hz). The samples were then isothermally DC charged and discharged (both currents recorded). Next a non-isothermal experiment with constant heating rate was performed. Finally the sample was kept at the highest temperature and the final isothermal discharge current registered. The last step has to be carried on for long time to ensure an almost complete discharge of the remnant charge so that results become reproducible and possible to analyze. Selective charging (careful choice of the field, temperature and the ratio of charging/discharging times) revealed the presence of different trapping sites. From the analysis of the isothermal and non-isothermal data the relaxation times and activation energies could be obtained.

Introduction

Space charge studies of high insulating materials reveal long relaxation times for (de)trapping. Conventional isothermal methods, as DC charging and discharging current measurements, and even non-isothermal methods, as thermally stimulated discharge currents (TSDC), do not consider these long relaxation times. As a consequence the results do not exhibit good reproducibility and are difficult to analyze. Furthermore at the end of each experiment it is possible that space charge is still remnant in the sample even if the measured current is very low. If this remnant charge is not allowed to vanish it will influence following measurements impairing reproducibility.

A new procedure combining isothermal charging and discharging with non-isothermal measurements has been recently developed [1] and successfully applied to thermally aged low density polyethylene [2]. Each run of the procedure comprises of four steps in which the current is monitored: (1) Isothermal charge current (IDC) – the sample is DC charged at constant temperature (T_i) during time t_c;. (2) Isothermal discharge current (IDC) – the sample is discharged at the same constant temperature (T_i) as in (1) during time t_d; (3) Final thermally stimulated discharge current (FTSDC) – the sample is heated at the constant rate (b) from temperature T_i until temperature T_f; (4) Final isothermal discharge current (FIDC) – the sample is maintained at temperature T_f for long enough time (t_f) to ensure almost complete discharge of the sample.

Steps (1) and (2) allow a selective charging of the sample by careful choice of applied electric field strength, temperature T_i and the ratio of charge/discharge times (t_c/t_d). By selectively charging it is possible to separate different space charge traps (possessing different features such as relaxation times and activation energies) that will appear as separated peaks in the following FTSDC spectra [3,4]. Undetected in usual TSDC measurements, at the end of step (3) there is charge trapped in the sample. Step (4) will add further information to characterize the traps besides allowing almost complete discharge of the remnant charge [3,5].

Polyethylene, especially low density polyethylene, is one of the best insulating polymers. Several attempts have been made along the years to study space charge in it. However results are many times difficult to reproduce and difficult to interpret [6]. The above stated procedure has been previously applied to thermally aged LDPE. In this work the same technique was used to study a similar LDPE sample that was electrically aged. The work on thermally and electrically aged samples is the preliminary study to prepare a more detailed analysis of space charge effects on LDPE aging.

Experimental

Films of 200 μm thickness from Borealis LDPE pellets almost additive free were obtained by press moulding. Samples were electrically aged in 1 M NaCl solution at 40 °C for 1500 h under a 6MV/m – 50Hz AC electric field. After aging Al electrodes with diameter of 33 mm were vacuum evaporated on

0-7803-7560-2/02/$17.00 © 2002 IEEE

both surfaces of the sample. The experimental setup for electrical measurements was presented elsewhere [7]. The measurements were made following the four steps procedure described in the introduction. The charging and discharging temperature was 2°C and the applied electric field values were 2, 3 and 4 MV/m. Charging/discharging times ratio varied between 1 and ¼ (corresponding to 1h charging and 1, 2 or 4h discharging time). The FTSDC was performed with a heating rate of 1°C/min and the final temperature was 90°C. The FIDC time was of the order of 1 day (or higher when considered necessary) and recorded until the limit resolution of the setup. If this last step was not performed for a sufficient time it was visible on the next run in FTSDC spectra an additional peak at temperatures near 90°C.

Results and discussion

Typical results for current density are shown in Figures 1 to 6 covering the four steps of each run described above. In Fig. 1 are shown the ICC data for four different runs with charging time 1h (differing in the applied field: (a) and (b) 2MV/m, (c) 3MV/m and (d) 4MV/m). Runs (a) and (b) were performed under the same conditions but at different stages of the experiment. Run (a) was one the first measured while run (b) corresponds to one of the last runs performed on the sample. For runs (b), (c) and (d) the charging currents are more or less parallel with the highest current density corresponding to the highest field. Whereas for run (a) the current is always slightly above the one for run (b) indicating the presence of more space charges. These features are also clearly seen in the IDC plot (Fig. 2). The discharging currents revealed the existence of four relaxation times which vary from 10s to 6000s and the first three (shorter relaxation times) do not change significantly for the different runs analyzed. The longest relaxation time varies from 1000s up to 6000s. Increasing electric field will increase the space charge in traps with longer relaxation (detrapping) times.

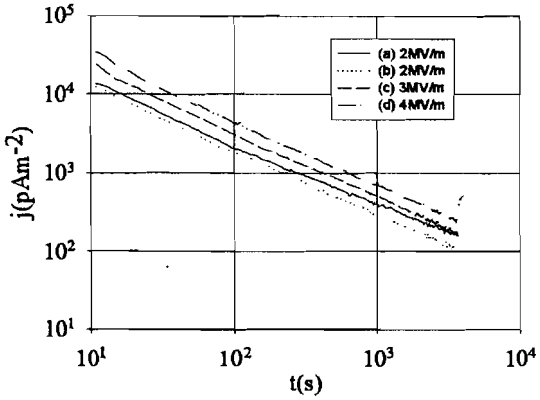

Fig. 1 – ICC plot for different applied fields. Poling conditions were T_f=2°C during 1h.

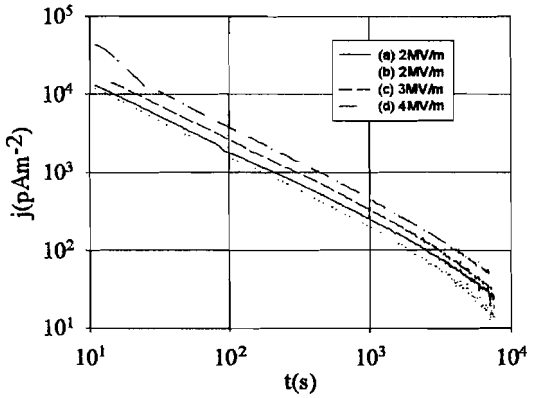

Fig. 2 – IDC plot for the same runs shown in Fig. 1 (discharge time is 2h)

Figure 3 evidences more distinctly the differences between runs (a) and (b) observed during the continuation of the experiment. The solid lines show the charge and discharge currents for run (a) and the dotted ones for run (b). As the experiment proceeds and successive runs are performed on the same sample a conditioning process is occurring and space charge that was present initially in the sample at deeper traps (and resulting from the AC aging process) is released. For run (a) the longest relaxation time is 1000s while for run (b) it has increased around four times. The pre-existing space charge, that was in less deep traps, has been released during the experiment and only the one in deeper traps still remains.

In Fig. 4 are presented the FTSDC obtained for the runs discussed so far (Fig. 1and 2). A very broad complex peak situated near 50°C is visible in all the runs. The comparative behavior for all runs follows the same trends described above with run (a) exhibiting a peak with much higher maximum then run (b) and occurring at lower temperature. As it was already seen in thermally aged samples [2] the peaks are due to space charge detrapping (clearly visible in Fig. 4 since there is a non-linear dependence of the current density with the applied field and the peak maximum temperature, 50°C, being above the poling temperature, 2°C). Initial rise method [8] was used to calculate the values of

activation energies shown in Table 1. These values show no meaningful difference between the different runs. Decomposition of the complex peak in elementary peaks was performed resulting in three relaxation processes with temperature maxima around 30 °C, 45 °C and 65°C and activation energies between 0.30 and 0.45 eV. Peaks at identical temperatures have been found in the literature but usually not more than one or two [2, 9-11].

FIDC is represented in Fig. 5 for the same runs presented previously in Fig. 1, 2 and 4. Here it is also quite clear the influence of the field on the remnant charge that is not only higher but has also longer relaxation times. Once more, run (a) shows a different behavior with a longer relaxation time compared with run (b) revealing the presence of more charges in deeper traps.

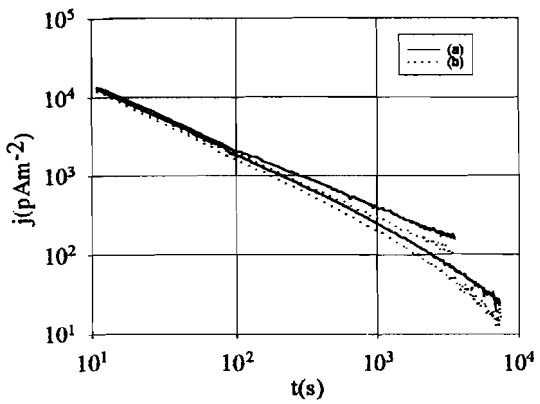

Fig. 3 – ICC and IDC plots for two runs with the same charging and discharging conditions.

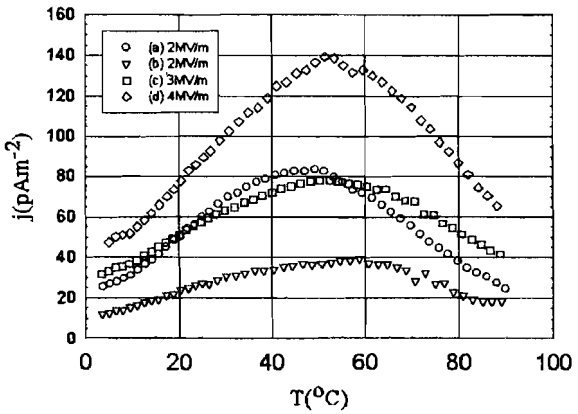

Fig. 4 – FTSDC spectra for the same runs shown in Fig. 1 and 2.

Finally Fig. 6 shows the influence of the ratio charging/discharging time. For the same charging time the longer the discharging time (smaller the ratio) the higher the peak temperature showing that only charges in traps with longer relaxation times have remained in the sample while charges in traps with shorter relaxation times had time to released during IDC.

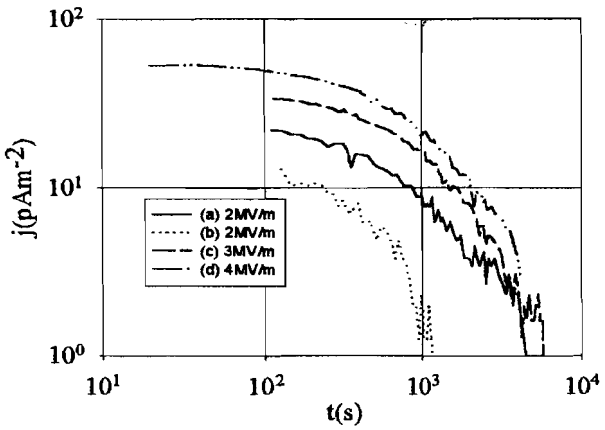

Fig. 5 – FIDC for the same runs presented in previous figures.

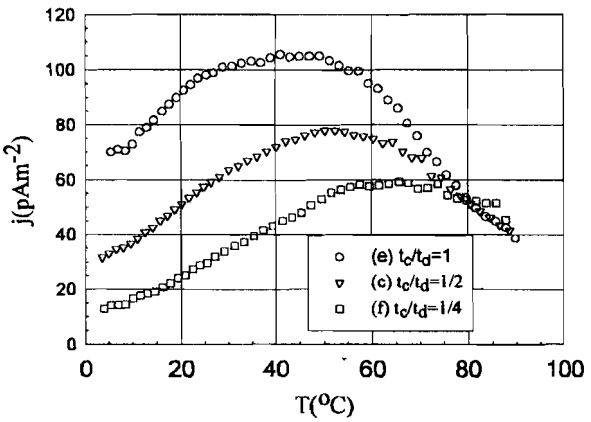

Fig. 6 – FTSDC spectra showing the influence of ratio charging/discharging times on the peak positions (applied field was 3MV/m).

Decomposition in elementary peaks has shown that the middle peak at 45°C is the most important during the first run but rapidly decreases until it almost completely vanishes for the last runs made along the full experiment. There seems to be pre-existing charges resulting from the AC aging process that are initially present but disappear with successive charging and discharging of the sample and which the DC process is not able to replace. These space charge can result from field activated diffusion of charge carriers present in the aging solution and that also can be trapped in new formed traps caused by electro-oxidation. Dielectric relaxation studies [12] and FTIR analyses [13] have, respectively, detected the presence of space charge and oxidation in electrically (AC) aged samples. For the other peaks this is not observed becoming more dominant as the experiment proceeds specially

the peak at higher temperature. Also this peak at 65°C is the one that increases more with increasing field.

For runs (a), (c) and (d) the zero field plane was obtained according to [5] and is, respectively, 0.01L, 0.06L and 0.06L (the sample thickness is L≈200μm). From this result is possible to calculate the mobilities, which are respectively 2.8, 11 and 17 ($\times 10^{-16}$) $m^2V^{-1}s^{-1}$, which are in good agreement with literature [2, 14-16]. As can be seen mobility is field activated increasing with the field. For run (b) the zero field plane had a very small value meaning that the charges remain very near the surface.

The total charge released during FTSDC is presented in Table 1 and it is one order of magnitude lower than the values obtained for ICC and IDC steps and one order of magnitude higher than for FIDC. Even if the total charge released during the final discharge is very small compared with the other three steps it can influence significantly the high temperature spectra of FTSDC even if no effect is detected during DC charging and discharging. Under these circumstance a peak appears around 85°C (that has also been observed in thermally aged samples [2]). Considering runs (b) to (d) it is noticed the influence of the applied field strength resulting in more trapped charge in the sample (as it was also noticed for ICC, IDC and FIDC). Moreover run (a) shows also a higher value than run (b) in agreement with the assumption that the pre-existing amount of space charge results from electrically (AC) aging in solution.

Table 1 – Activation energies determined from the initial rise method and released charge for the runs represented in Fig. 4.

Runs	(a)	(b)	(c)	(d)
E_a(eV)	0.29	0.22	0.28	0.23
Q($\times 10^{-10}$C)	2.6	1.2	1.9	4.5

Conclusions

Electrically aged LDPE space charge trapping can be successfully studied with the combined procedure. Selective charging allows the differentiation of different peaks. Three peaks have been clearly identified and activation energies and maximum temperature calculated. The relaxation processes are not due to dipoles but resulting from space charge. From the charge centroid results the space charge is trapped in a narrow layer (<15μm). For electrically aged LDPE (AC) there seems to be a peak that disappears with the successive DC charging and subsequent discharging processes.

Acknowledgments

The authors are very grateful to Borealis for supplying the LDPE pellets and to INVOTAN for a research grant.

References

[1] E. R. Neagu and J. N. Marat-Mendes, *Jpn. J. Appl. Phys.* **40** (2001) L1160-1162
[2] M. C. Lança, E. R. Neagu and J.N. Marat Mendes, *J. Phys. D: Appl. Phys* **35** (2002) L29-32
[3] E. R. Neagu, J.N. Marat-Mendes, R. M. Neagu D. K. and Das-Gupta, *J. Appl. Phys* **85** (1999) 2330-2336
[4] E. R. Neagu and R. M. Neagu, *Thin Solid Films* **358** (2000) 283-291
[5] E. R. Neagu and R. M. Neagu, *Thin Solid Films* **384** (2001) 15-22
[6] H. J. Wintle, *Engineering Dielectrics* vol IIA, ed. R. Bartnikas, New Jersey, 1983, Ch. 3
[7] E. R. Neagu and R. M. Neagu, *Phys. Status Solidi A* **144** (1994) 429-438
[8] G. F. K. Garlick and A. F. Gibson, *Proc. Phys. Soc. London* **60** (1948) 574-578
[9] H. von Seggern, *J Appl Phys* **52** (1981) 4086-4089
[10] G. Sawa, M. Kawade and M. Ieda, *J Appl Phys* **44** (1973) 5397-5398
[11] G. Sawa, M. Kawade and D.C. Lee and M. Ieda, *Jpn J Appl Phys* **13** (1974) 1547-1553
[12] M. C. Lança, C.J. Dias, D.K. Das Gupta, J.N. Marat Mendes, accepted for publication in *Mater Sci Forum*
[13] J. Mateo, M. C. Lança, J.N. Marat Mendes
[14] S. Pélissou, H. St-Onge and M. R. Wertheimer, *IEEE Trans. Elect. Ins.* **23** (1988) 325 – 333
[15] P. Fischer, *J Electrostatics* **4** (1977) 149-173
[16] S. Hwangbo, Y. Kwon, S. Jeon and M. Han, *Jpn. J. Appl. Phys.* **37** (1998) 4419-4427

Space charge studies in LDPE using combined isothermal and non-isothermal current measurements

M. Carmo Lança, E. R. Neagu, R. M. Neagu, C. J. Dias,

J. N. Marat-Mendes

Departamento de Ciência dos Materiais, Secção de Materiais Electroactivos (CENIMAT)

Faculdade de Ciências e Tecnologia, Universidade Nova de Lisboa

Portugal

D. K. Das Gupta

School of Informatics

University of Wales, Bangor, UK

ABSTRACT

Using a recently developed procedure combining isothermal and non-isothermal current measurements space charge trapping and transport in LDPE was successfully studied. Unaged, thermally and electrically aged samples were investigated. The samples were conditioned before each measurement in order to obtain reproducible results. In the non-isothermal measurements appeared a broad peak (40 °C to 50°C) that was possible to decompose into two or three peaks (35°C, 45 °C and 65°C). At even higher temperature another peak was sometimes present (85 °C) depending on the prior sample conditioning. The space charge is trapped near the surface in deep traps (maximum depth of ≈15 μm). Relaxation times, mobilities and activation energies have been calculated for different charging/discharging conditions. For unaged samples the reproducibility of the results was poor while for the aged polyethylene it was quiet good, meaning that aging helps

conditioning. In the electrically aged LDPE there is a decrease of conductivity and the broad peak of the non-isothermal spectra shows a slight shift towards higher temperatures when compared with the data found in the thermally aged polymer.

1. INTRODUCTION

For high insulating polymers, such as polyethylene, space charge (SC) can remain trapped for very long time (traps have long relaxation times). After an experiment involving sample charging and discharging it is possible that a residual SC remains and can even go undetected in discharging current measurements. However if a non-isothermal experiment, such as thermally stimulated discharge currents (TSDC), is performed the influence of the remnant charge is visible. Consequently usual TSDC measurements are highly affected even if conventional methods for isothermal DC charging and discharging measurements are sometimes unable to reveal the presence of this SC in the sample. Therefore it is difficult to obtain reproducible results if there is not a way to control the remnant SC. Also the analysis of the results are troublesome. For polyethylene, specially low density polyethylene (LDPE), there has been many attempts to understand SC (de)trapping and transport. Single measurements, either isothermal or non-isothermal, have produced results both difficult to reproduce and interpret [1].

To overcome these problems, in this work, a recent developed procedure combining isothermal charging and discharging methods and non-isothermal measurements [2] was used and adapted for LDPE [3, 4]. This combined procedure is an improvement of the FTSDC (final thermally stimulated discharging current) method [5] and will be described in detail in the next section.

2. THE COMBINED ISOTHERMAL AND NON-ISOTHERMAL PROCEDURE

The procedure combines different measurements and this combination allows to ensure almost complete discharge of the sample at the end of a complete run of the experiment. Reproducibility and analysis are achieved by a careful control of the experimental parameters. Each run is time consuming and composed of different steps (see Figure 1):

i) and *ii)* Isothermal DC charging and discharging currents measurement (ICC – isothermal charging current and IDC – isothermal discharging current). The sample is charged while kept at constant temperature (T_i) and a DC field (E) is applied during time t_c and the ICC registered. Then the field is switched off and the sample is short-circuited, discharging during time t_d still at constant temperature T_i and the IDC is recorded. These two steps corresponds to a selective charging of the sample.

iii) Non-isothermal discharging current measurement (FTSDC – final thermally stimulated discharge current) in which the sample is heated at a low constant rate b.

iv) Final isothermal discharging current measurement (FIDC) at the final temperature of *iii)* to allow as much as possible a complete discharge of the sample and the FIDC is registered.

A careful selection of charging and discharging conditions (field strength, temperature and ratio of charging and discharging times) allow distinct features of SC traps (activation energy and relaxation times) to be revealed in the following FTSDC. The FIDC at the final temperature of the FTSDC allows almost complete discharge of the sample. In this way the sample is conditioned so that its prior measurement history does not influence the next measurement impairing reproducibility and interpretation of results. The complete procedure is repeated in each run. Experiments following this full procedure are time consuming (particularly the FIDC step) but are unfortunately unavoidable.

3. EXPERIMENTAL

3.1 Sample preparation and aging

In this work LDPE disk shaped films of approximated 200 μm thick were hot pressed molded from Borealis pellets almost additive free. For aging the useful disc area had a diameter of 35 to 40 mm. The aging configuration used a modified Cigré cell and was presented in [6].

Three different types of samples were used:

A - thermally aged in solution (during 1500h at 40°C in 1M NaCl),

B - electrically aged in solution (applied AC electric field of 6 kV/mm, 50 Hz during 1500h at 40°C in 1M NaCl) presenting water trees and

C - unaged (just hot press molded).

3.2 Combined measurements procedure

The first LDPE samples (type *A*) to be studied following this procedure were also used to establish the best measurement parameters (field, temperature and charging/discharging times ratio) to be used in charging and discharging (selective charging) on the following samples.

The measurement setup has been described elsewhere [7]. For measurements (after aging) Al electrodes with 33 mm diameter were vacuum evaporated on both surfaces of the disk shaped samples. All experiments were performed under rotary pump vacuum.

The method followed was implemented using sample types *A* by a thorough test of the different conditions. For this sample charging and discharging temperatures of 2, 10, 20 and 30 °C were studied. The DC field strength was also investigated and 1 to 5 kV/mm were applied. The influence of the ratio of charging and discharging times was also analyzed. The FTSDC was performed always at a heating rate of 1 °C/min from the charging temperature (T_i) up to 90 °C. This final temperature was kept during long enough time in order to ensure almost complete discharge of the remnant SC after each run (FIDC).

4. RESULTS

As it was stated above the thermally aged LDPE (type *A*) was used to investigate the best conditions to perform the experiment in order to obtain consistent and reproducible information about SC trapping. Previously published results [3] focused mainly on the influence of charging/discharging time ratio (t_c/ t_d) and the influence of the FIDC step was analysed. The effect of charging temperature (T_i) and electric field (E) is presented here. In Figure 2 are shown the currents measured during the four steps of each run for different charging fields for a charging temperature of 30 °C and t_c/ t_d = 1h/2h. The charging (ICC) and discharging (IDC) curves in Figure 2 (a) and (b), respectively, are typical results for LDPE and have a magnitude in good agreement with values found in the literature [8]. Under these measurement conditions it is usual that the FTSDC spectra obtained have a broad peak around 40 to 60 °C, like it is observed in Figure 2 (c). However if the FIDC step has not proceed for long enough time it does not guarantee nearly complete discharge of the remnant charge and another peak around 85 °C appears [3]. As can be also observed in Figure 2 (c) the current is not linearly dependent on the applied electric field contrary to what happens with the ICC and the IDC (Figure 2 (a) and (b)). This response is typical of mechanisms that are SC dominated and not of dipolar origin as it will be discussed in more detail in section 5. The FIDC data (Figure 2 (d) were recorded until setup measurement limit was reached. From the plot it is seen that at higher fields this limit is achieved at longer times. Consequently, it can be concluded that more charges are deposited in traps with longer relaxations times as the charging field is increased.

The effect of charging/discharging temperatures is seen for the FTSDC (a) and the FIDC (b) steps in Figure 3. The peak maxima in the FTSDC plots are shifted towards higher temperatures with the increase of charging temperature. And also the current noise seems to increase with T_i up to 20 °C. In order to make the residual charge vanish it is clear from the

analysis of the FIDC data (Figure 3 (b) that higher T_i results in larger currents and the need for longer discharging times.

While the ICC and the IDC steps can be little affected by a less careful control of the selective charging (as it is described in section 2), the FTSDC is greatly influenced. However a good reproducibility can be obtained for runs performed under the same controlled measurements conditions (see Figure 4).

The non-linear behavior with charging field observed for type *A* samples at T_i = 30 °C is, as expected, also seen when the charging temperature is lower (2 °C in Figure 5). The data represented by the dotted line (4 kV/mm) shows the influence of the remnant charge from the previous run for which the FIDC step was too short. Moreover this high temperature contribution masks partially the lower broader peak making more difficult the analysis of the thermograms. Once more the importance of this last FIDC step is perceived.

The electrically aged LDPE (type *B* samples) was studied using the knowledge acquired during the analysis of thermally aged LDPE (type *A* samples). On Figure 6 FTSDC data for a type *B* sample are shown (charging/discharging conditions are the same used for type *A* data on Figure 5). In agreement with the results found for type *A* samples, also for type *B* there is a non-linear behavior with the applied field. The results marked with (i) and (ii) correspond to two runs that share the same charging/discharging conditions but the results are not reproducible. During the measurement history of this sample the run marked as (i) was one the first ones done while (ii) data corresponds to one of the last runs performed on the same sample (with more than 20 runs in between corresponding to about 40 days). The differences found (higher current and lower maximum peak temperature for (i)) reflect the influence of previous aging history on the films. It should be remarked that it is not a reproducibility problem since others runs made for the same sample following the same measurement conditions show a very good reproducibility.

Finally the attempts made to use this method on unaged LDPE (type *C* samples) revealed to be very difficult to obtain reproducible results for the FTSDC step. However for the ICC and the IDC measurements lower current values were registered for the virgin samples when compared with aged ones. In the FIDC for the unaged polymer the current drops below the measurement range much faster than for the aged LDPE. This indicates that much less charge is deposited in deeper traps in the virgin films.

5. DISCUSSION

From the analysis of the data it is possible to understand the origin of the peaks observed in FTSDC spectra. As it was stated in the previous section the non-linear dependence of the current with the applied field suggests that the peaks are due to SC and not to dipole reorientation. Further evidence is found in the FTSDC spectra since the peak is very broad and its maximum is well above the charging temperature. For example, for T_i = 2 °C the temperature of maxima currents are above 40 °C while dipolar peaks are not expected more than 20 °C above the poling temperature [9]. Vanderschueren et al. [10] more specifically states that one or more peaks can appear at temperatures much higher than the charging temperature when they are due to injected carriers deeply trapped. Also comparing the ICC and the IDC, it is observed that the two currents are not mirror images of each other specially for high fields and long enough t_c, which also can be attributed to trapped SC [1, 11].

An estimation of relaxation times was made for ICC, IDC and FIDC steps for the aged polymer (either thermally or electrically aged). The longest relaxation time found for the IDC stage spans from 1000 s to 6000 s. An increase in the relaxation times is observed when the charging temperature decreases while the change with the field is not significant (if Figure 1 (b) is analyzed no meaningful change in the slopes is seen). In FTSDC the peak position is not much affected by the field amplitude (Figure 1 (c), and Figure 6).

The total charge in each step was calculated and some representative results can be seen in Table 1 for the runs presented in Figure 3. Seen in the ICC and the IDC of all the runs is the decrease of the total charge with decreasing temperature. The ratio Q_{IDC}/Q_{ICC} (third column in Table 1 in %) it is inferior to the one found by adding the contribution from all the discharging processes, Q_d/Q_{ICC} where $Q_d = Q_{IDC} + Q_{FTSDC} + Q_{FIDC}$. Consequently at the end of the IDC step (and even at the end of the FTSDC step) there is still trapped charge remaining in the sample. In this way it is shown the importance of the FIDC step in reproducibility and analysis of the results in high insulating polymers.

The zero field plane of the charge centroid, x, was calculated using the equation in Neagu et al. [12] and from these values the mobility was obtained (see last columns of Table 1). The values found for the mobilities span from 6×10^{-17} to 6×10^{-15} $m^2V^{-1}s^{-1}$ and when compared with the literature are of similar order of magnitude [13 – 16]. The charge centroid position and mobility values decrease with decreasing temperature T_i except for the lowest temperature (2°C) which exhibits a considerable increase. For T_i = 10°C a zero value was found meaning that the charge remains mostly at the surface or very near the surface. As it is known for LDPE, the β or α_a (glass transition) peak is found near 0°C while the α or α_c (glass transition in the crystalline regions) lies well above this temperature [17, 18]. At both transitions there are important structural changes that would result in creation and destruction of traps, so the measurements with T_i=10°C would be in an intermediate zone where less traps would exist. If the temperature is lowered the influence of the α_a transition would start to be felt, while advancing towards higher temperatures it would appear the influence of the α_c transition (which is, also, reflected in the broad peak seen in the FTSDC at 40 – 50°C).

The effect of the DC applied field in the charge centroid and the mobility is presented in Table 2. In terms of x the charge penetrates more in the sample for the lower field (1kV/mm) and attains a minimum at 3kV/mm, increasing first (between 3 and 4 kV/mm) and then

stabilising for the highest field strengths (mobility follows the same trend). Considering a trapping/detrapping process it seems that initially with field increase deeper traps are being filled. This represents a smaller penetration in the sample since deeper traps are expected to be located more near the surface [13, 19]. From a certain field value (3 kV/mm) the available traps seem to be completely occupied and the charge is free to move further in the bulk. Moreover this charge has gained more energy supplied by the higher electrical field and it will move faster so that an increase in mobility is observed with the field strength rise. More charge accumulates until there is enough to produce a screening effect which stops the charge from moving further inside. Therefore x and the mobilities values become approximately constant [16].

The more striking feature of the FTSDC plots is the presence of a broad peak roughly at 40 – 50 °C. The spectra of polyethyelene obtained by Fukuzawa et al. [20], in a TSC experiment using needle electrodes, also shows a broad peak around 50°C. Kim et al. [21] have found a similar peak in TSC of γ-irradiated LDPE that was related to SC (and also another one at 90 °C).

Activation energies were calculated by the initial rise method [10, 22]. Some results for thermally and electrically aged LDPE are presented on Table 3. With this method it is difficult to obtain consistent data since the peak is composed of individual peaks and their relative influence is dependent on the experimental parameters. Nevertheless it should be remarked that the low values found are similar to some in the literature [19].

Individual peaks can sometimes be perceived as a shoulder or a small peak superimposed on the resulting broad peak (see, for instance, Figure 6). For some selected runs, a peak decomposition was attempted using an improvement of the method by Neagu et al. [23] and considering SC as the origin of the peaks.

In Table 3 the first three columns show the data for the broad peak (T_m is the peak temperature maximum, j_m the current density at the peak maximum and E_a the activation energy calculated by the initial rise method). Fittings done by decomposition of the spectra into individual peaks can be seen in the last columns of Table 3 (T_{mi} is the individual peak temperature maximum, E_{ai} the activation energy, Q_{oi} the SC density at T_i and $\tau_{eq}(T_{mi})$ the relaxation times). As it was observed the high temperature peak (above 80°C) may appear or not, depending mostly on the FIDC duration and consequently on the almost complete discharge of the sample. The presence of this peak strongly affects the analysis of the lower temperature broad peak.

In the literature the thermally stimulated spectra of polyethylene above RT report the presence of many peaks at temperatures around 35 °C to 70 °C and attributed to SC but considering different mechanisms [24 – 29]. Part of this range is a consequence of poor control of experimental conditions and the difficulty of analysis for high insulating polymers.

For charging temperature T_i= 2°C it was possible to decompose the thermogram into three (four) individual peaks roughly at 35 °C, 45 °C and 65°C (and, when appearing, a high temperature peak at 85°C). The choice of these temperatures was done supported by some extra experimental data (as heating and cooling the sample without previous charging) and also by values found in the literature. Just by cooling or heating the sample sharp peaks appeared at temperatures close to ones selected (45 °C, 65 °C and 85 °C) and detected mostly during cooling. Because these peaks are very sharp it is expected that they result from structural changes. Also peaks at similar temperatures were reported by other authors, such as Kobayashi et al. [30] that found simultaneously the same three lower temperature peaks. It is interesting to notice that, even if the experiment was done using elongated LDPE, some of the conditions were similar (charging at a lower temperature (15 °C) and then heating using a heating rate of 1°C/min and the charging/discharging times ratio (t_c/t_d = 1h/2h)). Kobayashi

attributed the first two peaks to structural changes (cavities) in the interface crystalline/amorphous motivated by melting and recrystallization. Blake et al. [31] have also found a peak at 35 °C in γ–irradiated HDPE which was attributed to trapped electrons.

Some authors also report another peak very close to 40 °C [19, 27], which can be related either with the 35 °C or the 45 °C peaks. According to these authors this peak is due to electron traps of chemical origin (chemical impurities, oxidation products[1], broken chains, etc.). At 45 °C Kao et al. [26] have related the peak to traps that can be both in the surface and the bulk of the polymer. Sawa et al. [24, 25] attribute a peak at 50°C to SC detrapping caused by the onset of the molecular motion of the crystallites.

The values for relaxation times, $\tau_{eq}(T_{mi})$, are of the order of magnitude expected and can be related to a peak found in dielectric spectroscopy below 10^{-3} Hz [32]. The activation energies found by Sawa et al. [25] (and obtained by two different methods) are higher than the ones calculated in this work (0.11 to 0.48 eV at 35 °C and 0.21 to 0.80 eV at 45 °C and 50 °C). Nonetheless von Seggern [19] has found values (0.15eV) more similar to the ones reported here.

The peak at 65 °C is usually attributed to electron traps. Kobayashi et al. [30] consider a peak at 60 °C occurring in the crystalline region while von Seggern [19] attributes it to chemical defects (as for the peak at 40 °C). Dorlanne et al. [28] has found a similar peak in AC stressed polyethylene. The high temperature peak has also been reported in the literature, however the temperature maximum encountered spreads from 85 °C [24, 25, 28], 95 °C [26] to near the melting point at 110 °C [19, 33], just to quote a few authors. Its activation energy expands from 0.87 to 1.85 eV for the same authors. Nevertheless the values obtained in the work presented here (1.34 to 1.55 eV) agree well with some found in literature [19, 25, 26, 28].

[1] Such as C=O and vinyl bonds.

The electrically aged LDPE (type *B*) was analyzed in a comparable way to the thermally aged polymer. The behavior is relatively similar with the type *A* LDPE, for instance, both FTSDC spectra show a similar broad peak. However if the temperature of the maximum of those peaks are compared there is a slight shift towards higher temperatures for the electrically aged polyethylene, as can be seen in Table 3.

The differences in Figure 6 for the runs (i) and (ii) (already referred above) revealed to be very important to understand the influence of the aging history. As can be observed run (i) has a shoulder around 60 °C, that it is seen as well when the applied field is 4 kV/mm. Also the mobility values showed that run (i) has a much lower mobility than run (ii) suggesting that more SC remains in the sample in deeper traps.

The activation energies calculated by the initial rise method, like above for the thermally aged polymer, do not show any significant change with the field, even for runs (i) and (ii).

As it was done for the thermally aged LDPE for some selected thermograms the FTSDC spectra were decomposed in individual peaks and the results are presented in Table 3. The values chosen for the peaks temperature (35 °C, 45 °C and 65 °C) are the same as the ones used in the decomposition of the FTSDC of the thermally aged polyethylene (for the reasons stated above).

The results for the broad peak, in the first three columns of Table 3, show that the peaks maximum temperature is around 50 °C and run (i) is the only one with a slightly lower value. This difference will be reflected on the decomposition results that have proved to be very important to understand the changes with AC ageing and also during the course of the successive experimental runs. Basically the three individual peaks relevance varies along the measurements. The form in which the results are presented in Table 3 correspond to the chronological order in which the runs were done, with run (i) as one of the firsts and run (ii) one of the last. The peak at 45 °C is the one that suffers more changes during the course of the

experiment. Its higher magnitude is for run (i), decreasing for the next one (which has a higher charging field, 4 kV/mm) and almost disappears for the remaining two (3 kV/mm and (ii)), which seen by the changes in the values of Q_{oi}. Analysis of other FTSDC results (not presented here) also indicate this behavior. It seems that the charge responsible for the 45 °C peak (by detrapping) has not been replaced by the DC charging process. So it seems possible to assume that that the charge was trapped during the previous history of the sample, meaning that it is mostly a consequence of the AC ageing process. One possibility can be the presence of chemical traps created during the AC electrical ageing that can be related to ions which have also diffused in during the same process (it is known that oxidation has occurred during electrical ageing [34]). These ions can act as trapping centres for carriers and/or recombination centres. If these ions can diffuse and/or recombine with carriers injected by the DC process them it would result in both a decrease of current and the gradual disappearance of the corresponding peak in the course of the combined experiment. Furthermore for the thermally aged LDPE it appears that the individual peak at 45 °C does not vanish so easily as for the AC aged samples. The electrically aged material would also be a more open structure facilitating the transport of carriers. This diffusion would not be seen in the results for mobility because the traps would remain more or less at the same depth in the material.

For unaged samples, which are just partially conditioned, the reproducibility is not good. Hence it is possible that the aging process itself acts as conditioning.

5. CONCLUSIONS

The combined isothermal and non-isothermal method allows to obtain reproducible results for LDPE. It was possible to study the FTSDC spectra and to decompose the complex broad peak (around 40 to 50°C). Depending mainly on the FIDC a peak at higher temperature (close to the melting point) can also appear.

In the region above room temperature the peaks found are attributed to trapped SC and most probably to electron traps. The broad peak in the range of 40 °C to 50 °C is the superposition of two or three individual peaks and it is due to modifications caused in the trap states by changes in the amorphous/crystalline interface (melt/recystallization, onset of molecular motion of crystallites). This is likely to be related to the α_c transition (glass transition for the crystalline region). The origin of the traps themselves can be either structural (such as cavities) or chemical defects. The high temperature peak has a strong dependence on the FIDC step and corresponds to the deeper traps (with longer relaxation times) and closer to the surface. Since it is near the melting temperature it must be related to changes resulting from the onset of melting. The origin of the traps is probably similar in nature to the more shallow ones but no conclusive evidence is still available.

Comparing the results obtained for the AC electrically aged and thermally aged samples is not easy. The main difference observed is the current values, which are usually higher in the thermally aged polymer. If the relative amplitudes of peaks current for the 35 °C and 65 °C are compared, it is seen that the higher temperature peak is more important in AC aged than in thermally aged LDPE. As a consequence the complex peak temperature would be shifted towards higher temperatures. These two differences could be understood if recombination was more important and/or if the number of traps was higher and the traps had longer relaxation times in the electrically aged polyethylene. Also it is possible that the AC aged material is a more open structure with more and/or enlarged cavities (such as the water trees presence indicates) allowing an easier path to carriers and thus facilitating diffusion and recombination.

Acknowledgments

The authors would like to thank Borealis for supplying the LDPE pellets and BICC-Celcat-Portugal, specially Mr. F. Pedroso. Furthermore, the authors are grateful to J. Fothergill (Univ. of Leicester, UK) and co-workers for gently lending some modified Cigré cells.

References

[1] H.J. Wintle, *Engineering dielectrics vol IIA-Electrical properties of solid insulating materials: molecular structure and electrical behavior*, ASTM Special Technical Pub 783, ASTM Pub, Philadelphia, 1983, Chapter 3.

[2] E.R. Neagu, J.N. Marat Mendes, "Combined isothermal and non-isothermal techniques to analyze charge trapping and stability in insulating materials", Jpn. J. Appl. Phys., vol. 40, pp. L1160-L1162, 2001.

[3] M.C. Lança, E.R. Neagu, J.N. Marat-Mendes, "Combined isothermal and non-isothermal current measurements applied to space charge studies in low-density polyethylene", J. Phys. D: Appl. Phys., vol. 35, pp. L29-L32, 2002

[4] M.C. Lança, E.R. Neagu, J.N. Marat-Mendes, "Studies of space charge in electrically aged low density polyethyelene", accepted for publication in Proceedings of ISE11, Melbourne, 2002

[5] E.R. Neagu, J.N. Marat Mendes, R.M. Neagu, D.K. Das Gupta, "Nonisothermal and isothermal discharging currents in polyethylene terephtalate at elevated temperatures", J. Appl. Phys, vol. 85(4), pp. 2330-2336, 1999.

[6] M.C. Lança, L.A. Dissado, J.N. Marat-Mendes, "The fractal analysis of water trees: an estimate of the fractal dimension", IEEE Trans. Diel. Elect. Ins., vol. 8(5), pp. 838-844, 2001.

[7] E.R. Neagu, R.M. Neagu, "Analysis of Charging and Discharging Currents in Polyethylene terephthalate", Phys. Status Solidi A, vol. 144, pp. 429-438, 1994

[8] D.K. Das Gupta, R.S. Brockley, "A study of 'absorption currents' in low-density polyethylene", J. Phys D: Appl. Phys, vol. 11, pp. 955-962, 1978.

[9] P. Fischer, P. Röhl, "Thermally stimulated and isothermal depolarization currents in low-density polyethylene", J. Pol. Sci., 14, pp 531-542, 1976.

[10] J. Vanderschueren, J. Gasiot, *"Field-induced thermally stimulated currents"*, in *Thermally stimulated relaxation in solids*, edt. P.Bräunlich, Springler-Verlag, Berlin, 1979.

[11] D.K. Das Gupta, K.J. Joyner, "On the nature of absorption currents in polyethylene terephtalate", J. Phys D: Appl. Phys, vol. 99, pp. 829-839, 1976.

[12] E.R. Neagu, R.M. Neagu, "On the nature of the origin of the isothermal and non-isothermal current released from dielectric materials", Thin Solid Films, vol. 384, pp. 15-22, 2001.

[13] H.J. Wintle, "Decay of static electrification by conduction processes in polyethylene", J. Appl. Phys., vol. 41(10), pp. 4004-4007, 1970.

[14] P. Fischer, "Electrical conduction in polyolefins", J. Electrostatics, vol. 4, pp.149-173, 1978.

[15] S. Pélissou, H. St-Onge, M.R. Wertheimer, "Electrical conduction of polyethylene below and above its melting point", IEEE Trans. Elect. Ins., vol. 23(3), pp. 325-333, 1988.

[16] S. Hwangbo, Y. Koon, S. Jeon, M. Han, "Direct correlation between space charge and conduction characteristics of low density polyethylene at various temperatures", Jpn. J. Appl. Phys., vol. 37, pp. 4419-4427, 1998.

[17] N.G. McCrum, B.E. Read, G. Williams, *Anelastic and dielectric effects in polymeric solids*, Dover, New York, 1967

[18] P. Hedvig, *Dielectric spectroscopy of polymers*, Adam Hilger, Bristol, 1977.

[19] H. von Seggern, "Detection of surface and bulk traps", J. Appl. Phys, vol. 52(6), pp. 4087-4089, 1981.

[20] M. Fukuzawa, M. Iwamoto, "TSC measurements of space charge in low-density PE under a needle-plane electrode system", IEEE Trans. Diel. Elect. Ins., vol. 6(6), pp. 858-863, 1999.

[21] K.Y. Kim, B.H. Ryu, D.J. Byun, S.M. Shin, "Thermally stimulated current study in γ–ray irradiated low density polyethylene", Eur. Polymer J., vol 37(5), pp. 1061-1064, 2001.

[22] J. Turnhout, *"Thermally stimulated discharge of electrets"* in *Electrets*, edt by G.M. Sessler, Sringler-Verlag, Berlin, 1980.

[23] R.M. Neagu, E.R. Neagu, I.M. Kalogeras, A. Vassilikou-Dova, "Evaluation of the dielectric parameters from TSDC spectra: application to polymeric systems", Mat. Res. Innovat., vol. 4, pp. 15-25, 2001.

[24] G. Sawa, M. Kawade, M. Ieda, "Field-assisted trapping in polyethylene", J. Appl. Phys., vol. 44(12), pp. 5397-5398, 1973.

[25] G. Sawa, M. Kawade, M. Ieda, "Thermally stimulated current from polyethylene in high temperature region", Jpn. J. Appl. Phys., vol. 13(10), pp. 1547-1553, 1974.

[26] K.J. Kao, S.S. Bamji, M.M. Perlman, "Thermally stimulated discharge current study of surface charge release in polyethylene by corona-generated excited molecules, and the crossover phenomenon", J. Appl. Phys., vol 50(12), pp. 8181-8185, 1979.

[27] T. Mizutani, T. Tsukahara, M. Ieda, "Thermally-stimulated currents in oxidized low-density polyethylene", Jpn. J. Appl. Phys., vol. 19(11), pp. 2095-2098, 1980.

[28] O. Dorlanne, S. Sapieha, M.R. Wertheimer, A. Yelon, "Thermally stimulated discharge of polyethylene following AC stress", IEEE Trans. Elect. Ins., vol. 17(3), pp. 199-202, 1982.

[29] P.C.N. Scarpa, "Polarisation and dielectric behaviour of AC aged polyethylene", PhD thesis, Univ. of Wales (Bangor), 1995.

[30] S. Kobayashi, K. Yahagi, "Thermally stimulated current in elongated low-density polyethylene film", Jpn. J. Appl. Phys., vol. 18(2), pp. 261-268, 1979.

[31] A.E. Blake, A. Charlesby, K.J. Randle, "Simultaneous thermoluminescence and thermally stimulated current in polyethylene", J. Phys. D: Appl. Phys., vol. 7, pp. 759-770, 1974.

[32] M.C. Lança, C.J. Dias, D.K. Das Gupta, J. Marat-Mendes, "Dielectric properties of electrically aged low density polyethylene", *Advanced Materials Forum I*, Key Eng. Mat., vol. 230-232, edt. T. Vieira, pp. 396-399, 2002.

[33] S. Nakamura, G. Sawa, M. Ieda, "Anomalous luminescence from oxidized PE in high-temperature region", J. Appl. Phys., vol. 48(8), pp. 3626-3627, 1977.

[34] J. Mateo, M.C. Lança, J. Marat-Mendes, "Infrared spectroscopy studies of aged polymeric insulators", *Advanced Materials Forum I*, Key Eng. Mat., vol. 230-232, edt. T. Vieira, pp. 384-387, 2002.

Table of acronyms

Table 1 – Total charge calculated for each of the four stages of a run with different charging/discharging temperature (T_i) for a thermally aged LDPE sample – type A (charging/discharging conditions: E = 2 kV/mm, t_c/t_d = 1h/2h and T_i = 30, 20, 10 & 2 °C).

Table 2 – Charge centroid and mobility for different charging DC electric fields (E) for a thermally aged LDPE sample – type A (charging/discharging conditions: T_i = 30 °C, t_c/t_d = 1h/2h and E = 1 to 5 kV/mm).

Table 3 – FTSDC results for thermally (type A) and electrically (type B) aged LDPE

Figure 1 – Experimental procedure used to analyse space charge in LDPE. The four steps are schematically represented showing electric field, temperature and current. Selective charging corresponds to isothermal charging and discharging (ICC and IDC). Partial discharge proceeds during FTSDC. Almost complete discharge it is only achieved during FIDC (schematics adapted from [3]).

Figure 2 – Thermally aged LDPE (type *A*) results for different charging fields (charging/discharging conditions: T_i = 30 °C, t_c/t_d = 1h/2h and E = 1 to 5 kV/mm). (a) ICC; (b) IDC; (c) FTSDC and (d) FIDC.

Figure 3 – Thermally aged LDPE (type *A*) results for different charge/discharge temperatures (charging/discharging conditions: E = 2 kV/mm, t_c/t_d = 1h/2h and T_i = 30, 20, 10 & 2 °C). (a) FTSDC and (b) FIDC.

Figure 4 – FTSDC for two different runs in the same thermally aged LDPE sample with the same charging/discharging conditions (T_i = 30 °C, E = 2 kV/mm, t_c/t_d = 1h/2h). The reproducibility of the spectra is quite good (it is also dependent on the FIDC's time to be long enough to guarantee an almost complete discharge of the sample).

Figure 5 – FTSDC plot showing *j/E* thermally aged LDPE (type *A*) for different charging fields (charging/discharging conditions: T_i = 2 °C, t_c/t_d = 1h/2h and E = 2 & 4 kV/mm).

Figure 6 – FTSDC plot showing *j/E* of electrically aged LDPE (type *B*) for different charging fields (charging/discharging conditions: T_i=2°C, t_c/t_d=1h/2h and, E=2 to 4 kV/mm). (i) and (ii) are runs made under the same conditions but run (i) – was one of the first runs made while run (ii) – was one of the last ones.

Table of acronyms

PE	polyethylene
LDPE	Low density polyethylene
TSDC	Thermally stimulated discharge currents
ICC	Isothermal charging current
IDC	Isothermal discharging current
FTSDC	Final thermally stimulated discharge current
FIDC	Final isothermal discharging current
SC	Space charge

Table 1 – Total charge calculated for each of the four stages of a run with different charging/discharging temperature (T_i) for a thermally aged LDPE sample – type A (charging/discharging conditions: E = 2 kV/mm, t_c/t_d = 1h/2h and T_i = 30, 20, 10 & 2 °C).

Charging/ discharging conditions	Q_{ICC} (10^{-9}C)	Q_{IDC} (10^{-9}C) ($\%Q_{IDC}/Q_{ICC}$)	Q_{FTSDC} (10^{-9}C)	Q_{FIDC} (10^{-9}C) ($\%Q_d/Q_{ICC}$)	**Charge centroid***	**Mobility** ($10^{-16}m^2V^{-1}s^{-1}$)
E=2 kV/mm T_f= 30°C t_c/t_d=1h/2h t_{fd}=14h30	3.37	–2.77 (82%)	–0.28	–0.11 (94%)	0.06L	17
E=2 kV/mm T_f=20°C t_c/t_d= 1h/2h t_{fd}=14h	2.47	–2.06 (83%)	–0.29	–0.04 (97%)	0.03L	8.3
E= 2kV/mm T_f=10°C t_c/t_d=1h/2h t_{fd}=42h	1.85	–1.53 (83%)	–0.27	–0.07 (≅100%)	0	0
E=2 kV/mm T_f=3°C t_c/t_d=1h/2h t_{fd}=22h	1.51	–1.26 (79%)	–0.16	–0.01 (95%)	0.05L	14

*L is the sample thickness (around 200μm)

Table 2 – Charge centroid and mobility for different charging DC electric fields (E) for a thermally aged LDPE sample – type A (charging/discharging conditions: T_i = 30 °C, t_c/t_d = 1h/2h and E = 1 to 5 kV/mm).

Charging/ Discharging conditions	**Charge centroid***	**Mobility ($10^{-16}m^2V^{-1}s^{-1}$)**
E=1 kV/mm T_f=30°C t_c/t_d=1h,/2h t_{fd}=18h	0.11*L*	61
E=2 kV/mm T_f= 30°C t_c/t_d=1h/2h t_{fd}=14h30	0.06*L*	17
E=3 kV/mm T_f=30°C t_c/t_d=1h/2h t_{fd}=24h	0.02*L*	0.6
E=4kV/mm T_f=30°C t_c/t_d=1h/2h t_{fd}=28h	0.05*L*	0.7
E=5 kV/mm T_f=30°C t_c/t_d=1h/2h t_{fd}=62h	0.06*L*	0.7

**L* is the sample thickness (around 200μm)

Table 3 – FTSDC results for thermally (type A) and electrically (type B) aged LDPE

Sample Ageing	**Charging and discharging conditions**	T_m (°C)	J (10^{-11} Am^{-2})	E_a (initial rise) (eV)	T_{mi} (°C)	E_{ai} (eV)	Q_{oi} (10^{-8}Cm^{-2})	$\tau_{eqi}(T_{mi})$ (10^2s)
Thermal	*E=2 kV/mm* T_f= 3°C t_c/t_d=1h/2h t_{fd}=22h	40	6.5	0.22	35 45 65	0.48 0.59 0.52	7.6 5.6 10	10 8.9 11
Thermal	*E=4kV/mm* T_f=2°C t_c/t_d=1h/2h t_{fd}=19h	45	17	0.21	35 45 65 85	0.11 0.38 0.42 1.46	29 42 9.7 15	44 14 14 6.7
Electrical	*E=2 kV/mm* T_f= 2°C t_c/t_d= 1h/2h t_{fd} = 61h *(i)*	45	8.0	0.29	35 45 65	0.45 0.39 0.33	5.0 14 15	11 14 18
Electrical	*E=4 kV/mm* T_i= 2°C t_c/t_d=1h/2h t_{fd}=14h	50	14	0.23	35 50 65	0.29 0.47 0.30	10 10 4.2	17 12 18
Electrical	*E=3 kV/mm* T_i= 2°C t_c/t_d= 1h/2h t_{fd} = 21h	50	7.5	0.19	35 45 65	0.29 0.10 0.35	14 0.1 24	17 - 17
Electrical	*E=2 kV/mm* T_i= 2°C t_c/t_d= 1h/2h t_{fd} = - *(ii)*	50	3.8	0.22	35 45 65	0.32 0.39 0.46	6.0 1.6 9.0	15 14 13

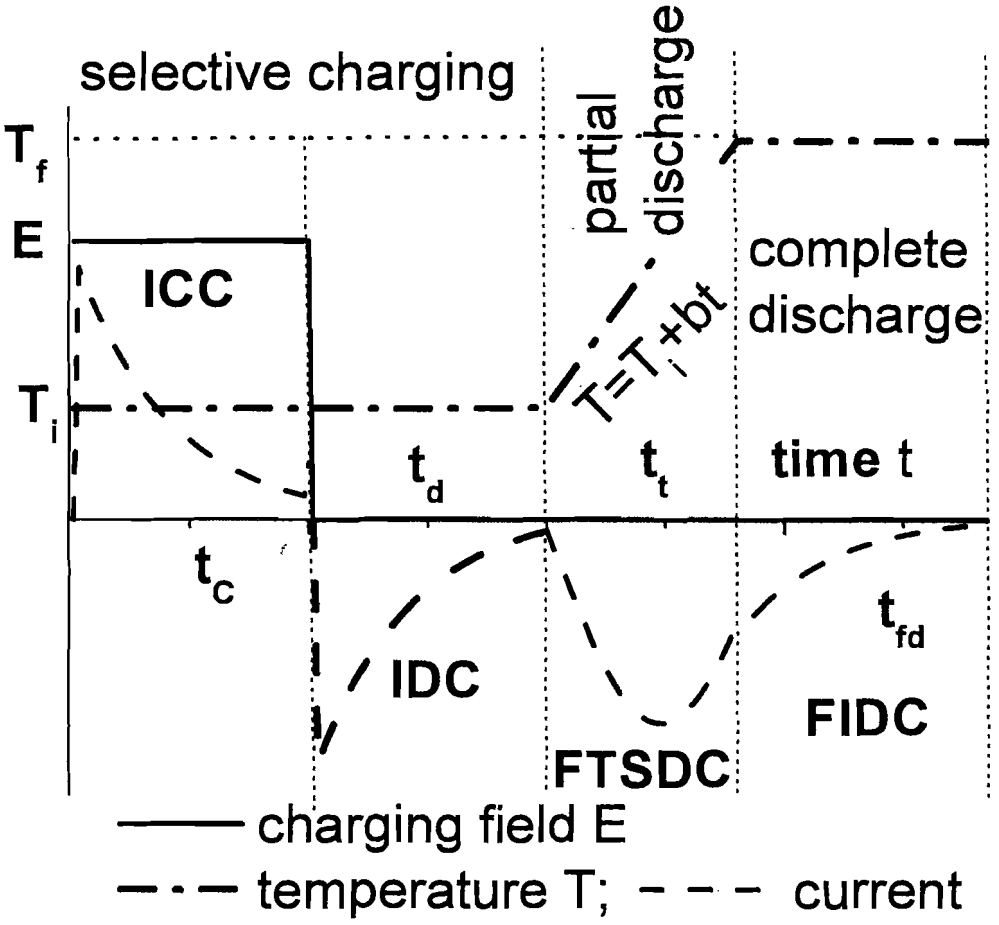

Figure 1 – M. C. Lança

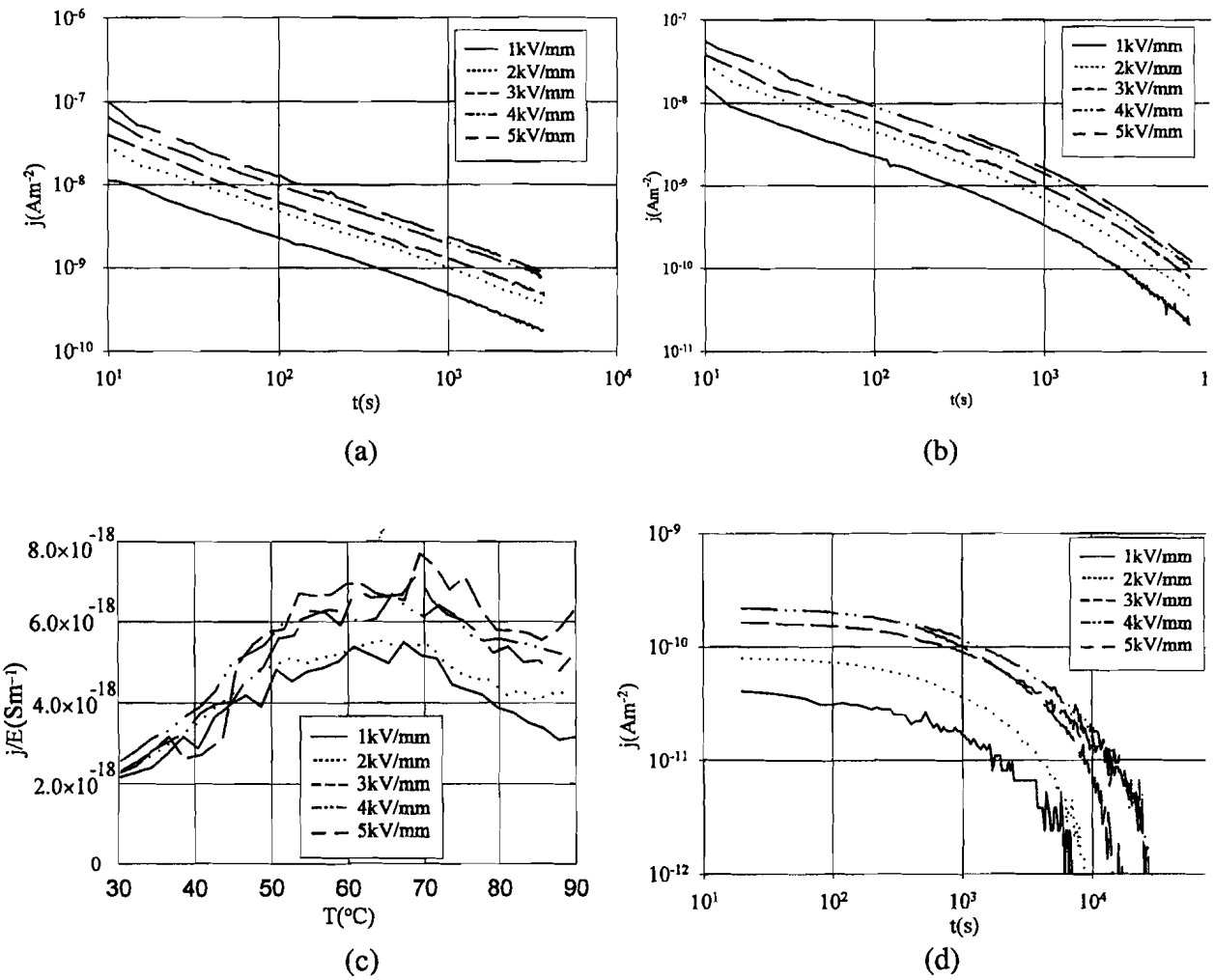

Figure 2 – M. C. Lança

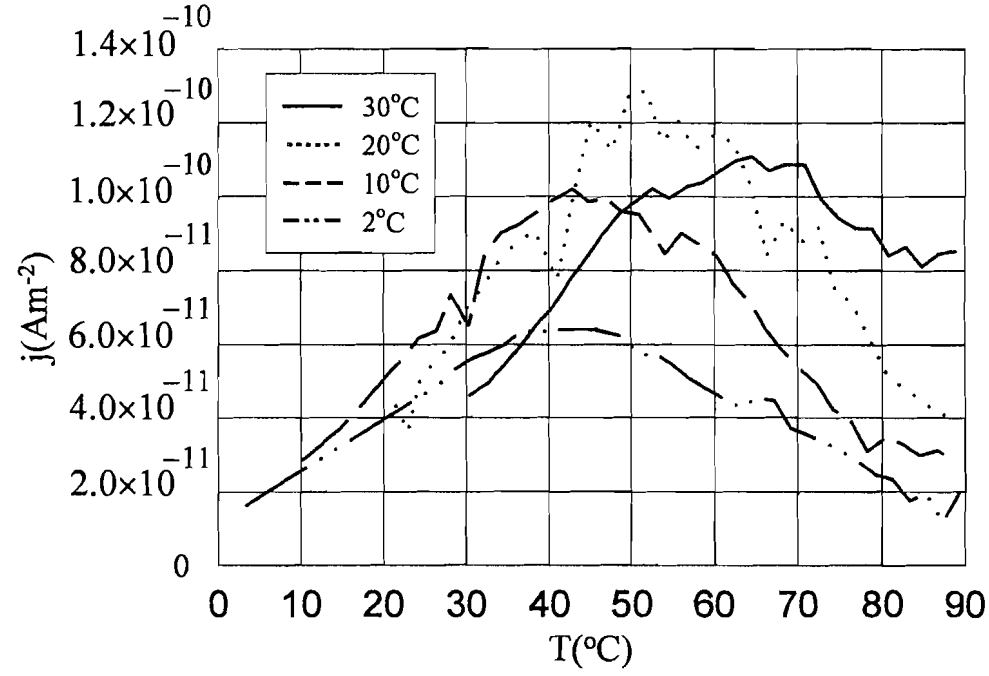
1.4×10⁻¹⁰
1.2×10⁻¹⁰
1.0×10⁻¹⁰
8.0×10⁻¹¹
6.0×10⁻¹¹
4.0×10⁻¹¹
2.0×10⁻¹¹
0
j(Am⁻²)
30°C
20°C
10°C
2°C
0 10 20 30 40 50 60 70 80 90
T(°C)

(a)

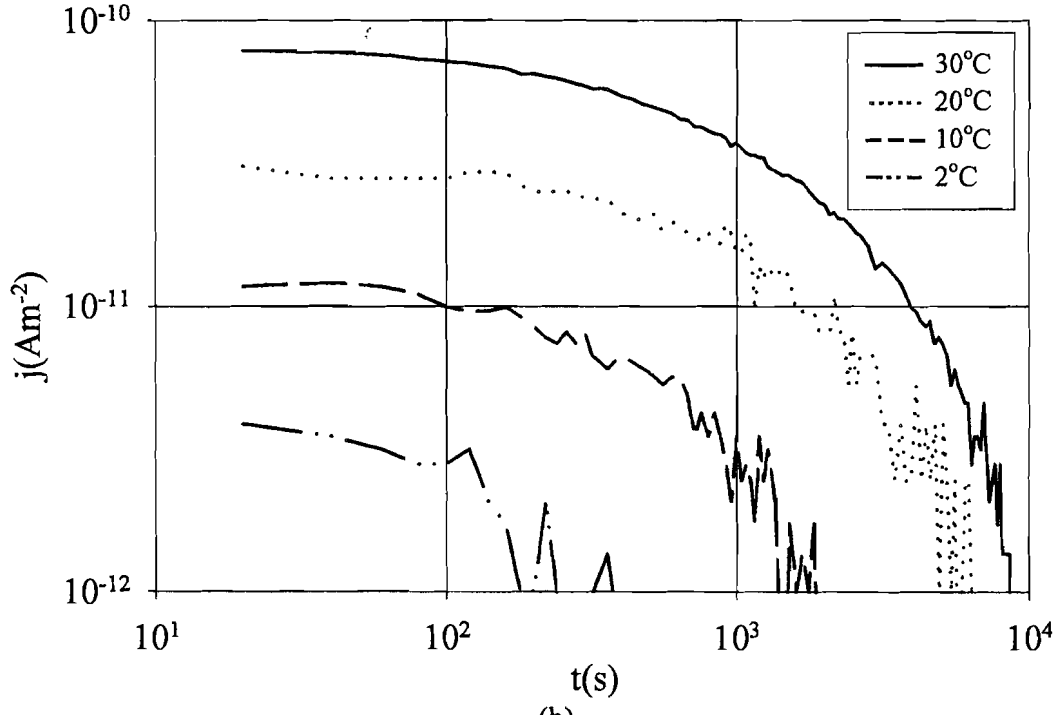
10⁻¹⁰
10⁻¹¹
10⁻¹²
j(Am⁻²)
30°C
20°C
10°C
2°C
10¹
10²
10³
10⁴
t(s)

(b)

Figure 3 – M. C. Lança

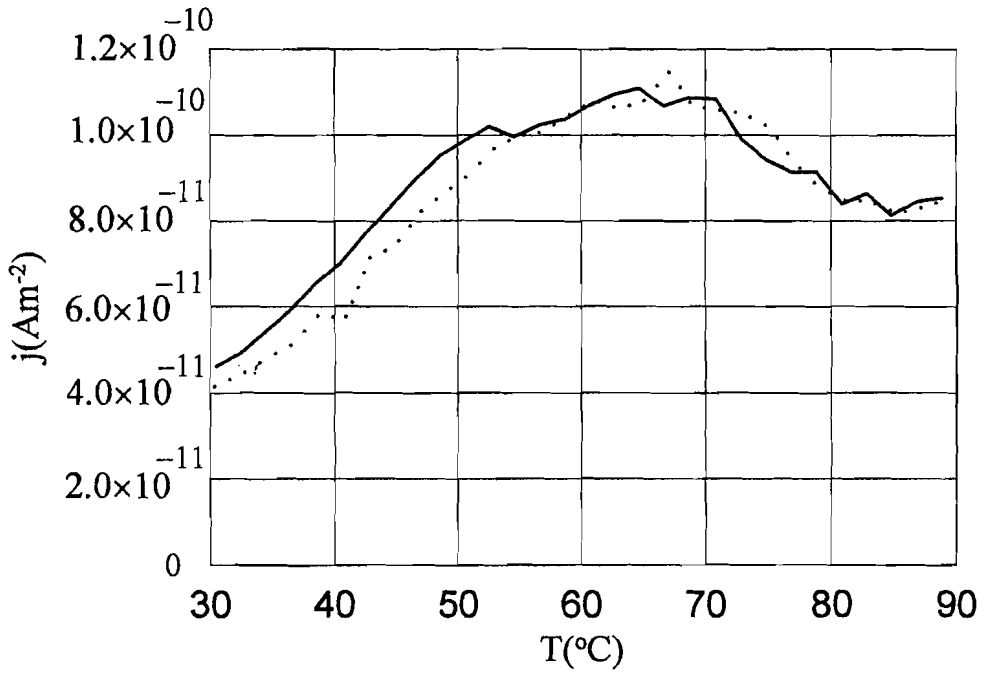

Figure 4 – M. C. Lança

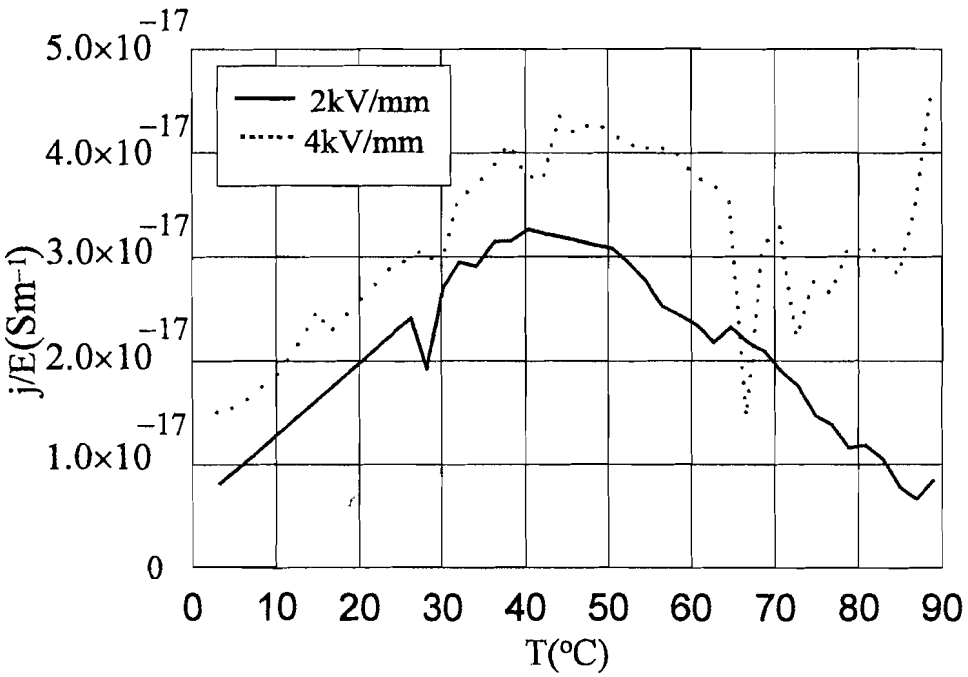

Figure 5 – M. C. Lança

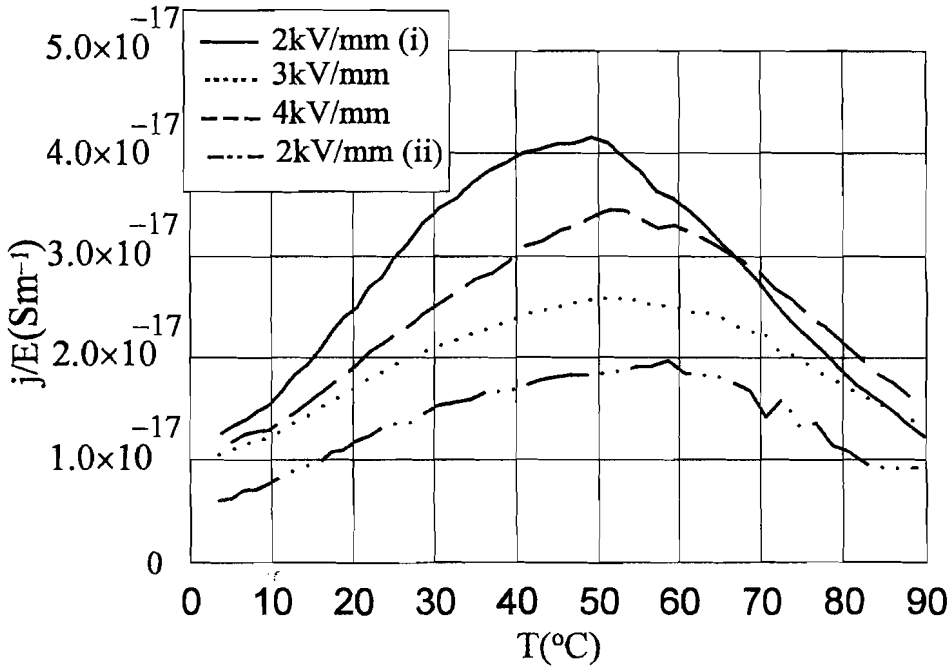

Figure 6 – M. C. Lança